SAPIENZA
UNIVERSITÀ DI ROMA

DOTTORATO DI RICERCA IN ENERGIA E AMBIENTE
PhD Program in ENERGY and ENVIRONMENT

XXXVII Cycle

Thermal-Hydraulic Design and Analysis of the STEAM and Water Loop Facilities to support the development of the EU-DEMO tokamak fusion reactor

PhD Thesis

Scuola di Dottorato in Scienze e Tecnologie per l'Innovazione Industriale
Facoltà di Ingegneria Civile e Industriale
Dipartimento di Ingegneria Astronautica, Elettrica ed Energetica

Alessandra Vannoni

Advisor
Prof. Ing. Fabio Giannetti

Co-Advisor/Tutor
Dr. Ing. Alessandro Del Nevo
Dr. Cristiano Ciurluini

A.A. 2023-2024

(Page intentionally left blank)

SOMMARIO

Il Dipartimento di Ingegneria Astronautica, Elettrica ed Energetica dell'Università Sapienza di Roma e la Divisione di Ingegneria Sperimentale – Dipartimento Nucleare – di ENEA collaborano nell'ambito del progetto EUROfusion. Questo, cofinanziato dal programma EURATOM, ha l'obiettivo di sviluppare il progetto e le tecnologie per la realizzazione di un reattore nucleare a fusione dimostrativo capace di produrre energia elettrica, denominato DEMO. L'Italia gioca un ruolo fondamentale nel consorzio EUROfusion, con l'ENEA, beneficiario principale, e Università, Enti di Ricerca e partner industriali come affiliati.

Una delle sfide tecnologiche più rilevanti per la realizzazione di DEMO riguarda la progettazione e lo sviluppo delle tecnologie del concetto di *breeding blanket Water-Cooled Lithium-Lead* (WCLL). Tale componente ha un ruolo essenziale nella generazione del combustibile (trizio), nell'assorbimento del calore per la produzione di energia e nella protezione delle parti interne del reattore. Il WCLL *breeding blanket* utilizza una miscela di litio e piombo (PbLi) come materiale fertile e acqua pressurizzata nel circuito principale di raffreddamento. In generale, il progetto concettuale del *Balance of Plant* (BoP), sviluppato da ENEA e i suoi partner, prevede la generazione di energia elettrica tramite un ciclo *Rankine*: avremo, quindi, un circuito primario monofase ad alta pressione e alta temperatura che refrigera il WCLL *breeding blanket* e trasferisce la potenza al circuito secondario tramite generatori di vapore dove una turbina genera elettricità.

In questo contesto, ITER rappresenta un passaggio indispensabile verso la realizzazione di DEMO. Questo reattore sperimentale, attualmente in costruzione a Cadarache, in Francia, è progettato per dimostrare la fattibilità scientifica e tecnologica della fusione nucleare. ITER esplorerà aspetti cruciali del confinamento e della stabilità del plasma, producendo una potenza di fusione fino a 500 MW per brevi durate. A differenza di DEMO, che mira a dimostrare la fattibilità economica dei reattori a fusione, ITER non genererà elettricità ma si concentrerà sulla validazione dei regimi operativi e sul collaudo di sistemi chiave in condizioni rilevanti per la fusione, dimostrando la fattibilità tecnologica dei reattori a fusione.

Tra i sistemi fondamentali che verranno testati in ITER vi sono i *Test Blanket Module* (*TBM*), che rivestono un ruolo cruciale nel progresso delle tecnologie necessarie per il breeding blanket di DEMO. Questi moduli sono integrati nella struttura di ITER per valutare le prestazioni di diversi concetti di *breeding blanket*. Il programma *TBM* fornirà dati inestimabili sul trasferimento di calore, sulla resistenza al flusso neutronico e sul recupero del trizio, contribuendo direttamente alla progettazione e all'ottimizzazione di vari concetti, incluso il *breeding blanket* WCLL di DEMO. ITER, quindi, agisce come un ponte tra la ricerca sperimentale sulla fusione e la realizzazione pratica dell'energia da fusione, ponendo le basi per le innovazioni tecnologiche necessarie in DEMO.

Allo stato attuale della conoscenza, un funzionamento continuo a potenza costante non è realizzabile in un reattore a fusione basato sulla tecnologia tokamak. Gli studi di riferimento per DEMO prevedono un funzionamento pulsato, con cicli a piena potenza di 2 ore (detti *pulse*) seguiti da 10 minuti a potenza quasi zero (detti *dwell*). Questa modalità di funzionamento pone sfide nuove e significative per la progettazione, affidabilità e sicurezza del *breeding blanket* e del BoP di DEMO. In particolare, i componenti maggiormente sollecitati da questo funzionamento sono la prima parete, il generatore di vapore e la turbina. Per i primi due, progettazione, analisi e dimostrazione sperimentale di fattibilità e affidabilità sono responsabilità di ENEA e, in parte, l'oggetto dell'attività della presente tesi.

Per affrontare le sfide uniche poste dall'operazione pulsata di DEMO, il generatore di vapore a singolo passaggio (OTSG) è stato scelto per il design del generatore di vapore grazie alla sua minore inerzia termica rispetto ai generatori convenzionali a tubi a U. Questa ridotta inerzia termica, dovuta alla minore massa d'acqua dell'OTSG, gli consente di rispondere in modo più efficace alle rapide fluttuazioni di potenza. Inoltre, l'OTSG beneficia di una vasta validazione in applicazioni nei reattori ad acqua pressurizzata (PWR), dove le condizioni termodinamiche a piena potenza sono comparabili, rafforzando ulteriormente la sua idoneità per DEMO.

L'obiettivo principale è il progetto concettuale della sezione di prova del generatore di vapore di DEMO e della campagna sperimentale per dimostrare la stabilità dei principali parametri termoidraulici durante il funzionamento del componente, nonché le sue prestazioni e l'efficacia della strategia di regolazione adottata. Questo obiettivo ha incluso il raggiungimento di altri significativi traguardi secondari rilevanti per la ricerca e per la crescita professionale, tra cui: 1) il contributo alla progettazione dell'impianto STEAM, acquisendo competenze nella progettazione di sistemi a vapore e nell'uso dei codici di supporto; 2) lo studio dei dispositivi di misura e del loro utilizzo; 3) il supporto, grazie alle simulazioni numerica, alla progettazione dei sistemi di controllo e acquisizione della sezione di prova; 4) il contributo alla progettazione dell'impianto Water Loop; 5) la partecipazione alla stesura delle specifiche tecniche di fornitura degli impianti Water Loop e STEAM; 6) la partecipazione a un grande progetto internazionale, lavorando, presso il Centro Ricerche Brasimone, con la Divisione di Ingegneria Sperimentale di ENEA; 7) il miglioramento delle competenze nel campo della termo-idraulica e nell'uso del codice termoidraulico RELAP5, anche grazie ad un tirocinio di tre mesi presso l'Idaho National Laboratory (INL).

L'attività è stata svolta, contribuendo alla progettazione ed analisi della piattaforma sperimentale W-HYDRA, che include l'impianto Water Loop per le prove sperimentali dei componenti del *breeding blanket* di DEMO e del *TBM* di ITER e l'impianto STEAM per la sperimentazione sul generatore di vapore. Le strutture Water Loop e STEAM affrontano obiettivi complementari nello studio dei componenti dei reattori a fusione, ma, a seguito di analisi di sensitività, i loro circuiti primari sono stati integrati in un unico circuito primario W-HYDRA, con l'obiettivo di ottimizzare il progetto mantenendo le funzionalità distinte delle strutture, riducendo le ridondanze e minimizzando i costi.

In prima istanza, è stata sviluppata la scalatura e il progetto concettuale della sezione di prova del generatore di vapore (i.e. Once Through Steam Generator), per poi studiare la rappresentatività durante il funzionamento operativo di riferimento. Le analisi termoidrauliche effettuate utilizzando il codice RELAP5 hanno convalidato il design e consentito il confronto con la configurazione di riferimento di DEMO. L'obiettivo è stato raggiunto proponendo la campagna sperimentale da eseguire, la strategia di controllo da implementare, il progetto concettuale della sezione di prova (e la specifica di fornitura) e la strumentazione necessaria per il controllo e l'acquisizione dei dati.

Successivamente, l'attività si è focalizzata sulla progettazione e analisi dell'impianto sperimentale STEAM. L'obiettivo è stato assicurare che l'impianto avesse una dinamica di variazione della potenza capace di testare la sezione di prova simulando adeguatamente le variazioni di potenza previste in DEMO. Una criticità nella scelta dell'architettura d'impianto era quella di limitare la potenza assorbita dallo stesso a 4 MW. Sono state, inoltre, condotte analisi numeriche per valutare componenti critici come gli aerotermi e le prestazioni della sezione a bassa pressione del circuito secondario in vari scenari operativi. In conclusione, sono stati studiati scenari incidentali incentrati su guasti delle pompe (ad es., *Loss Of Flow Accident* e *Loss Of Heat Sink*) per studiare la dinamica dell'impianto.

Essendo il circuito primario dell'impianto STEAM interconnesso a quello del Water Loop, lo studio e le analisi hanno riguardato sia il funzionamento ad alta potenza (3.1 MW) che quelle a più bassa potenza (800kW). Nel primo caso la potenza dei riscaldatori elettrici è rimossa attraverso il generatore di vapore mentre nel secondo caso attraverso scambiatori di calore monofase la cui progettazione e regolazione sono state anch'esse oggetto di indagine. Sono state condotte analisi di sensibilità per ottimizzare l'integrazione tra Water Loop e STEAM al fine di ottimizzarne i costi dell'impianto, minimizzando il numero di componenti. La configurazione proposta del Water Loop può testare diverse sezioni di prova, incluso componenti fronte plasma in un ampio range di potenza, di portata, di temperatura e pressione. Le analisi RELAP5 hanno mostrato che è anche possibile effettuare le transizioni *pulse-dwell-pulse* e la simulazione di transitori incidentali.

Anche se STEAM e Water Loop condividono parte del circuito primario, hanno scopi estremamente differenti. STEAM mira a fornire una struttura per analisi a livello di componente, concentrandosi sulla caratterizzazione del mock-up del generatore di vapore in diversi scenari operativi e incidentali. In questo contesto, le analisi svolte hanno supportato la progettazione della facility, garantendo che essa possa replicare le risposte termoidrauliche dell'impianto DEMO in termini di condizioni al contorno in tutti gli scenari considerati, pur non essendo rappresentativa dell'impianto DEMO stesso. Per questo motivo, sono stati implementati sistemi di controllo di tipo proporzionale-integrale per assicurare l'accuratezza e la stabilità delle condizioni al contorno. Di conseguenza, le analisi di sicurezza eseguite per STEAM, come le simulazioni dei transitori, non sono destinate a supportare direttamente la sicurezza del reattore DEMO. Piuttosto, servono come analisi preliminari per garantire il corretto funzionamento della facility stessa. In questa fase, infatti, lo scopo principale di STEAM è dimostrare le prestazioni e l'affidabilità del mock-up del generatore di vapore in condizioni di funzionamento pulsato, mentre altre analisi si concentrano esclusivamente sul supporto al funzionamento della facility.

Al contrario, Water Loop è progettata per condurre analisi a livello di sistema, dove la risposta termoidraulica dell'intero impianto è tanto importante quanto quella della sezione di prova. Per questo motivo, le analisi svolte con Water Loop mirano a supportare gli aspetti di sicurezza del design di ITER, valutando il comportamento integrato del sistema in una varietà di scenari.

Grazie all'attività svolta e ai risultati ottenuti è stata progettata un'attività sperimentale capace di dimostrare la fattibilità di operare un generatore di vapore in funzionamento pulsato; è stata progettata una piattaforma sperimentale capace di testare sezioni di prova di componenti quali generatori di vapore, componenti fronte plasma, o di simulare transitori incidentali; sono state prodotte le specifiche tecniche di fornitura di sistemi e componenti attualmente in costruzione o oggetto di gare di appalto. Pertanto, l'attività di dottorato ha rappresentato un contributo significativo e determinante nella definizione e realizzazione di un'infrastruttura sperimentale unica nel panorama internazionale per qualificare componenti e tecnologie del TBM di ITER, del *breeding blanket* e del BoP di DEMO.

ABSTRACT

The Department of Astronautical, Electrical, and Energy Engineering at Sapienza University of Rome and the Division of Experimental Engineering – Nuclear Department – of ENEA collaborate within the framework of the EUROfusion project. This project, co-funded by the EURATOM program, aims to develop the design and technologies for the realization of a demonstration nuclear fusion reactor capable of producing electrical energy, known as DEMO. Italy plays a fundamental role in the EUROfusion consortium, with ENEA as the main beneficiary, and universities, research institutions, and industrial partners as affiliates.

One of the most significant technological challenges for the realization of DEMO concerns the design and development of the technologies for the *Water-Cooled Lithium-Lead (WCLL) breeding blanket* concept. This component has an essential role in generating fuel (tritium), absorbing heat for energy production, and protecting the internal parts of the reactor. The WCLL *breeding blanke*t adopts a mixture of lithium and lead (PbLi) as fertile material and pressurized water in the primary cooling circuit. The conceptual design of the *Balance of Plant* (BoP), developed by ENEA and its partners, involves the generation of electrical energy through a Rankine cycle: a single-phase, high-pressure, high-temperature primary circuit cools the WCLL *breeding blanket* and transfers power to the secondary circuit via steam generators, where electricity is generated by a turbine.

In this context, ITER represents an indispensable step toward the realization of DEMO. This experimental reactor, currently under construction in Cadarache, France, is designed to demonstrate the scientific and technological feasibility of nuclear fusion. ITER will explore critical aspects of plasma confinement and stability, producing fusion power of up to 500 MW for short durations. Unlike DEMO, which aims to demonstrate the economic feasibility of fusion reactors, ITER will not generate electricity but will focus on validating operational regimes and testing key systems under fusion-relevant conditions, demonstrating fusion reactors technology feasibility.

Among the pivotal systems tested in ITER there are the Test Blanket Modules (TBM), which play a crucial role in advancing the technologies required for the DEMO *breeding blanket*. These modules are integrated into the ITER structure to evaluate the performance of various *breeding blanket* concepts. The *TBM* program will provide invaluable data on heat transfer, neutron flux resilience, and tritium recovery, directly informing the design and optimization of various concepts, including the DEMO WCLL *breeding blanket*. Thus, ITER acts as a bridge between experimental fusion research and the practical realization of fusion energy, laying the groundwork for the technological innovations required in DEMO.

Given the current understanding, continuous operation at constant power is not feasible in a fusion reactor based on tokamak technology. Reference studies for DEMO propose pulsed operation, with full-power cycles lasting 2 hours (referred to as *pulse*) followed by 10 minutes at nearly zero power (*dwell*). This mode of operation introduces new and significant challenges for the design, reliability, and safety of the *breeding blanket* and the DEMO BoP. In particular, the components most impacted by this operation are the first wall, the steam generator, and the turbine. For the first two, the design, analysis, and experimental demonstration of feasibility and reliability are ENEA responsibility and are, in part, the subject of this thesis.

To address the unique challenges posed by the pulsed operation of DEMO, the Once-Through Steam Generator (OTSG) was selected for the steam generator design due to its lower thermal inertia compared to conventional U-tube generators. This reduced thermal inertia, a result of the OTSG lower water mass, allows it to respond more effectively to the rapid power fluctuations. Furthermore, the OTSG benefits from extensive validation in Pressurized Water Reactor (PWR) applications, where thermodynamic conditions at full power are comparable, further enhancing its suitability for DEMO.

The main objective is the conceptual design of the DEMO steam generator test section and the experimental campaign aimed at demonstrating the stability of the main thermal-hydraulic parameter during the component operation, as well as its performance and the effectiveness of the adopted control strategy. The achievement

of this objective included fulfilling several other significant secondary milestones relevant to both research and professional growth, such as: 1) contributing to the design of the STEAM facility, acquiring expertise in steam system design and in using support codes; 2) studying measurement devices and their application; 3) providing support through numerical simulations in the design of control and acquisition systems for the test section; 4) contributing to the design of the Water Loop facility; 5) participating in the drafting of technical supply specifications for the Water Loop and STEAM facilities; 6) participating in a large international project, working at the Brasimone Research Centre with the ENEA Division of Experimental Engineering; 7) improving skills in thermal-hydraulics and in the use of the RELAP5 code, further enhanced through a three-month internship at the Idaho National Laboratory (INL).

The activity involved contributing to the design and analysis of the W-HYDRA experimental platform (Section 3), which includes the Water Loop facility for experimental tests on DEMO *breeding blanket* components and ITER TBM, as well as the STEAM facility for steam generator experimentation. Water Loop and STEAM facilities address complementary objectives in the study of fusion reactor components, but, after sensitivity analyses, their primary loops were integrated into a single W-HYDRA primary circuit, with the aim of optimizing the design while maintaining the distinct functionalities of the facilities, reducing redundancy and minimizing the costs.

Initially, the scaling and conceptual design of the steam generator test section (i.e., Once Through Steam Generator) were developed, followed by a study to assess its representativeness under the reference operating conditions (Section 4). The thermal-hydraulic analyses performed using the RELAP5 code validated the design and enabled comparisons with the DEMO reference configuration. The goal was achieved by proposing the experimental campaign to be conducted, the control strategy to be implemented, the conceptual design of the test section (including supply specification), and the necessary instrumentation for control and data acquisition.

Subsequently, the focus shifted to the design and analysis of the STEAM experimental facility (Section 5). The objective was to ensure that the facility had a power variation dynamic capable of adequately simulating the power variations expected in DEMO during the test section experiments. A critical issue in choosing the plant architecture was limiting the absorbed power to 4 MW. Additionally, numerical analyses were performed to assess critical components such as air coolers and the performance of the low-pressure section of the secondary loop under various operating scenarios. Finally, incident scenarios focused on pump failures (e.g., *Loss Of Flow Accident* and *Loss Of Heat Sink*) were studied to assess the facility dynamics.

Since the primary circuit of the STEAM facility is interconnected with that of the Water Loop, the performed studies and analyses covered both high-power operation (3.1 MW) and lower power operation (800 kW). In the former case, the power from the electric heaters is removed through the steam generator, while in the latter, it is removed through single-phase heat exchangers, whose design and regulation were also investigated. Sensitivity analyses were conducted to optimize the integration between Water Loop and STEAM to reduce facility costs by minimizing the number of components. The proposed configuration of the Water Loop can test various test sections, including plasma-facing components, over a wide range of power, flow rates, temperatures, and pressures. The RELAP5 analyses showed that it is also possible to perform pulse-dwell-pulse transitions and simulate incident transients.

Even though STEAM and the Water Loop share part of the primary loop, they are characterized by extremely different purposes. STEAM aims to provide a structure for a component-level investigation, focusing on the characterization of the steam generator mock-up under various operational and accidental scenarios. Within this framework, the performed analyses supported the design of the facility to ensure that it replicates the thermal-hydraulic responses of the DEMO plant in terms of boundary conditions across all considered scenarios, even though it is not representative of the DEMO plant itself. For this reason, proportional-integral control systems were implemented to ensure the accuracy and stability of the boundary conditions. Consequently, safety analyses performed for STEAM—such as transient simulations—are not aimed at supporting the safety of the DEMO reactor. Instead, they serve as pre-test analyses to guarantee the proper functioning of the facility itself. In this phase, in fact, STEAM primary purpose is to demonstrate the performance and reliability of the steam generator mock-up under pulsed operational conditions, with other analyses focused exclusively on supporting the facility operation.

In contrast, the Water Loop is designed to perform system-level analyses where the thermal-hydraulic response of the entire system is as critical as that of the test section. For this reason, the analyses conducted with the Water Loop aim to support the safety aspects of the ITER design by assessing the integrated behavior of the system under a variety of scenarios.

Thanks to the work undertaken and the results obtained, an experimental activity was designed to demonstrate the feasibility of operating a steam generator in pulsed mode. An experimental platform capable of testing test sections for components such as steam generators, plasma-facing components, and simulating transient accidents has been developed. Additionally, technical specifications for the supply of systems and components currently under construction or subject to tendering have been produced. Therefore, this PhD activity represents a significant and decisive contribution to defining and realizing a unique experimental infrastructure in the international landscape for qualifying components and technologies of ITER TBM, DEMO *breeding blanket*, and BoP.

TABLE OF CONTENTS

LIST OF FIGURES

LIST OF TABLES

LIST OF ABBREVIATIONS

AC	Air Cooler
BB	Breeding Blanket
BoL	Beginning Of Life
BoP	Balance of Plant
BDBA	Beyond Design Basis Accident
BZ	Breeding Zone
CAS	Cassette
CAD	Computer Aided Design
CHF	Critical Heat Flux
CL	Cold Leg
CNR	Consiglio Nazionale delle Ricerche
COB	Central OutBoard
CSM	Centro Sviluppo Materiali
CREATE	Consortium for Research and Education in Advanced Technologies
DBA	Design Basis Accident
DC	Downcomer
DCD	Direct Coupling Design
DEMO	DEMOnstration fusion power plant
DIAEE	Department of Astronautic, Electrical and Energetic Engineering
DIV	Divertor
EBG	Electron Beam Gun
ECO	Economizer
ECRH	Electron Cyclotron Resonance Heating
ENEA	Italian National Agency for New Technologies, Energy and Sustainable Economic Development
EoL	End Of Life
Eq. FW	Equatorial First Wall
ESS	Energy Storage System
EU	European Union
EUROFER	European Reduced Activation Ferritic/Martensitic Steel
EUROfusion	European Consortium for the Advancement of Fusion Energy
FF	Fouling Factor
FLiBe	Fluoride Lithium Beryllium
FW	First Wall
HCLL	Helium Cooled Lithium Lead
HCPB	Helium Cooled Pebble Bed
HL	Hot Leg
HP	High Pressure
HS	Heat Structure
HT	Heater
HTC	Heat Transfer Coefficient
HX	Heat Exchanger
ICD	Indirect Coupling Design
IHTS	Intermediate Heat Transfer System

INEL	Idaho National Engineering Laboratory
INL	Idaho National Laboratory
INFN	Istituto Nazionale di Fisica Nucleare
ITER	International Thermonuclear Experimental Reactor
LMTD	Logarithmic Mean Temperature Difference
LOFA	Loss Of Flow Accident
LOHS	Loss Of Heat Sink
LP	Low Pressure
LPS	Low-Pressure Section
LWR	Light Water Reactor
MCP	Main Coolant Pump
MeV	Mega Electron Volt
MFR	Mass Flow Rate
MJ	Multiple Junction
MU	Mock-Up
NBI	Neutral Beam Injection
NBR	Nucleate Boiling Region
Non-Eq. FE	Non Equatorial First Wall
NPP	Nuclear Power Plant
NRC	Nuclear Regulatory Commission
NUC-ING	Nuclear Engineering Division
OTSG	Once-Through Steam Generator
PCS	Power Conversion System
PE	Postulated Event
PFC	Plasma Facing Components
PFD	Process Flow Diagram
PFU	Plasma Facing Unit
PHTS	Primary Heat Transfer System
PI	Proportional-Integral
PIE	Postulated Initiating Event
PORV	Pressure Operating Relief Valve
PPPT	Power Plant Physics & Technology
PS	Primary Side
PU	Pump
P-S HX	Primary-Secondary Heat Exchanger
RAFM	Reduced Activation Ferritic-Martensitic
RELAP	Reactor Excursion and Leak Analysis Program
RF	Radiofrequency
RPM	Revolutions per Minute
R&D	Research and Development
SBO	Station Blackout
SG	Steam Generator
SE	Separator
SHR	Superheating Region
SJ	Single Junction
SRV	Safety Relief Valve
SS	Secondary Side

SYS-TH	System Thermal-Hydraulic
S-T HX	Secondary-Tertiary Heat Exchanger
TBM	Tritium Breeding Blanket Modules
TC	Thermocouple
TDJ	Time-Dependent Junction
TDV	Time-Dependent Volume
TES	Tritium Extraction System
TS	Test Section
T	Tertiary
TSP	Tube Support Plates
T/H	Thermal-Hydraulic
VCS	Volume Control System
VV	Vacuum Vessel
WCLL	Water-Cooled Lithium-Lead
WL	Water Loop
WPBB	Work Package Breeding Blanket
WPBoP	Work Package Balance of Plant
W-HYDRA	Water thermal-HYDRAulic

1 INTRODUCTION

The ever-increasing global demand for energy, coupled with the environmental challenges posed by the combustion of fossil fuels and the resultant rise in CO_2 emissions, has underscored the urgent need for sustainable energy solutions [1], [2]. The current trajectory of energy consumption, primarily fueled by finite fossil fuel resources, is untenable in the long term due to its detrimental impact on the environment and climate.

In response to these pressing challenges, nuclear energy has emerged as a promising alternative, offering a reliable and low-carbon source of electricity generation [3]. Unlike traditional fossil fuels, nuclear power plants produce negligible greenhouse gas emissions during operation, making them an attractive option for mitigating climate change. However, conventional nuclear fission reactors still present concerns regarding safety, nuclear waste disposal, and proliferation risks associated with fissile materials [4].

In this context, nuclear fusion has garnered significant attention as a potential game-changer in the quest for clean and abundant energy. Fusion, the process that powers the sun and stars, offers inherent safety features, minimal long-lived radioactive waste, and virtually unlimited fuel resources [5]. By harnessing the power of fusion reactions, humanity has the potential to meet its energy needs sustainably, without the adverse environmental consequences associated with fossil fuels or the drawbacks of conventional nuclear fission.

To realize the promise of fusion energy, international collaboration and concerted research efforts are essential. The "Roadmap to the Realization of Fusion Energy," developed in 2012 under the auspices of the European Fusion Development Agreement (EFDA), outlines the strategic steps and milestones necessary to achieve practical fusion power generation by 2050 [6]. This roadmap provides a comprehensive framework for addressing the key challenges in fusion research and development, breaking down the quest for fusion energy into eight distinct missions:

1. Demonstrate plasma regimes of operation (based on tokamak configuration);
2. Demonstrate a heat exhaust system capable of withstanding the high thermal loads expected in future fusion reactors;
3. Develop materials capable of withstanding the intense neutron fluxes (i.e., 14 MeV) generated in fusion reactions without compromising their structural integrity;
4. Ensure tritium self-sufficiency, emphasizing the development of technologies for tritium Breeding Blankets (BBs) to sustain fusion fuel production;
5. Implement intrinsic safety features incorporating the experience gained from ITER into the design of DEMO;
6. Integrate various fusion technologies into DEMO design, including heat transfer systems (i.e., Balance of Plant) and associated electrical generation systems;
7. Ensure economic viability, directing efforts towards reducing capital costs and developing long-term technologies;
8. Mature the stellarator line to achieve maturity in fusion research.

Each mission within the roadmap is accompanied by an assessment of the current research status, identification of open issues, proposed research and development plans, and resource estimates. Moreover, it underscores the importance of industrial involvement and collaboration beyond Europe to accelerate progress in fusion research.

In alignment with this global initiative, this doctoral research aims to address the thermal-hydraulic challenges associated with the pulsed operation of fusion reactors. To this end, the proposed construction of the STEAM experimental facility seeks to investigate the behavior of the steam generator during power oscillations typical of fusion reactor operation.

Therefore, this research primarily supports Mission 6 of the roadmap. Specifically, the design and analysis of the DEMO steam generator test section (TS), to be tested in the STEAM facility, directly address the challenges of pulsed operation, contributing to the optimization of the BoP. While the main emphasis is on Mission 6, the research also supports aspects of Mission 4 by contributing to the technological development of the Breeding Blanket (BB) systems. The Water Loop facility, designed as part of this research, will test key BB components under representative thermal-hydraulic conditions, enhancing their technological readiness and robustness in cooling and energy transfer systems. Additionally, insights gained from the STEAM experimental campaign and associated numerical analyses will further optimize the integration of the steam generator into the DEMO system.

1.1 National and international framework of the activity

The PhD research activity represents a collaboration between the Department of Astronautic, Electrical and Energetic Engineering (DIAEE) [7] at the University of Rome and the Nuclear Engineering Division (NUC-ING) of ENEA C.R. Brasimone, strategically aligned within the framework of the European Consortium for the Advancement of Fusion Energy (EUROfusion) [8].

EUROfusion consortium was established in 2014 and represents a collaborative effort among thirty leading research organizations and universities across Europe and Switzerland. Focused on fusion research, spanning from fundamental plasma physics to engineering challenges associated with future fusion power plants, EUROfusion aims to advance sustainable energy solutions through international cooperation.

Italian prominent role within EUROfusion is exemplified by the leadership and expertise of ENEA, that collaborates with many major universities, (e.g., Sapienza University of Rome, University of Pisa, and University of Torino), university consortia (e.g., CREATE), industrial partners (e.g., Ansaldo Nucleare, CSM) and research institution (e.g., INFN, CNR).

NUC-ING stands as a hub of nuclear expertise within ENEA, driving cutting-edge research and innovation in fusion technology. Research and activities are focused on advancing the Water-Cooled Lithium-Lead design within the framework of the Breeding Blanket (WPBB) and Balance of Plant (WPBoP) Projects. This work is integral to EUROfusion Power Plant Physics & Technology (PPPT) Programme, representing Italy dedication to driving fusion energy innovation.

1.2 Objective and innovation of the research activity

The main objective of this research is to address some of the technological challenges associated with the pulsed operation of the DEMO reactor, particularly under the framework of a WCLL concept. Pulsed operation introduces significant challenges due to the highly variable thermal and hydraulic conditions that must be managed effectively. Among these challenges, one of the most critical is the steam generator operation across an unprecedented power range, varying from as low as 1% to 100% of nominal load, conditions never before tested or implemented in the industry.

The innovation of this research lies in the development and analysis of the steam generator TS to be tested in the STEAM facility, specifically designed to replicate the operating conditions of the DEMO steam generator during pulsed operation. Traditional steam generators, typically used in steady state mode, have not been engineered for such variable regimes, introducing an innovative framework to simulate and evaluate the component performances under such demanding conditions. By accurately modeling this behavior, the study provides essential insights into the thermal-hydraulic dynamics and stability of steam generators, setting the stage for safer and more efficient designs for future fusion reactors.

The use of a power-to-volume scaling methodology, combined with advanced numerical simulations performed with RELAP5/Mod3.3, ensures representativeness of the mock-up with respect to the full-scale system. While the methodologies employed are standard in the nuclear engineering field, their application to the pulsed operation of a steam generator within the framework of fusion reactors represents a valuable contribution to the development of experimental and numerical approaches for addressing fusion-specific challenges. This approach directly supports the technological development of a Tokamak Fusion Reactor based on a WCLL BB concept, which is crucial for the EU-DEMO reactor. Moreover, the objective is to demonstrate the suitability and technological readiness of water-cooled systems for breeding blanket applications, advancing the overall feasibility of water-based technologies in fusion reactors.

A secondary objective of this research was to design a facility capable of housing and operating the STEAM TS under specified thermal-hydraulic conditions. This facility, integral to the research, ensures the proper operation of the TS and includes advanced control strategies and operational adjustments based on numerical simulations. These strategies aim to enhance the performance and safety of both the TS and the overall facility during normal, pulsed, and transient conditions. The insights gained contribute to refining design and operational protocols for future fusion reactors.

In addition, the research extended to the design and analysis of the Water Loop facility, a key component of the broader W-HYDRA infrastructure. W-HYDRA is an extensive experimental setup designed to investigate various fusion-related technologies. The Water Loop, closely interconnected with the STEAM facility, is designed to be highly versatile, allowing for the investigation of multiple components and test sections under different operational scenarios. It focuses on lower power operations and dynamic responses, complementing the high-power testing conducted in the STEAM facility.

The integration of the STEAM and Water Loop facilities within the W-HYDRA infrastructure provides a holistic approach to study the thermal-hydraulic behavior of fusion reactor components and the feasibility of a tokamak reactor based on a WCLL BB. The STEAM test section offers a detailed examination of pulsed operation conditions, while the Water Loop supports a range of testing scenarios and dynamic responses. This combined approach enhances the simulation and analysis capabilities for future fusion energy systems.

1.3 Overview of the research activity

The main objective of this thesis is to study the thermal-hydraulic behavior of proven nuclear equipment within the unique environment of fusion reactors, specifically characterized by pulsed operation. This complex operational regime necessitates a comprehensive approach that combines both experimental and numerical methodologies to fully understand and address the challenges presented.

As a correlated objective, the thesis aims at supporting the design of the W-HYDRA experimental infrastructure for the investigation of water and lithium-lead technologies applied to fusion reactors.

To achieve the primary objective, the research is structured around three foundational pillars: facility design, test section development, and the definition of a test matrix. These pillars are interconnected, providing a holistic framework that enhances the investigation of water and lithium-lead technologies applied to fusion reactors.

The first pillar, facility design, is intertwined with the correlative objective. Within the framework of investigating water and lithium-lead technologies, several key facilities have been developed, including the STEAM facility, the electron beam (EB) gun, the Water Loop, and the LIFUS5MOD4 facility. Each of these components plays a critical role in supporting various experimental scenarios and advancing the understanding of thermal-hydraulic behavior in fusion applications.

The second pillar is the test section development, which includes several significant mock-ups and experimental setups:

- The DEMO WCLL BB OTSG mock-up tested in the STEAM facility.
- The DEMO WCLL BB first wall, evaluated through both the Water Loop and EB gun.
- The WCLL BB manifold, also tested using the Water Loop.
- The In-Box LOCA tests, conducted in the LIFUS5MOD4 facility in a configuration connected with the Water Loop.

These test sections are essential for validating theoretical models and numerical predictions, allowing for a deeper understanding of the interactions and behaviors of materials and systems under fusion-relevant conditions.

The third pillar comprises the test matrix, which outlines the experimental test design required to explore various operational scenarios. This includes:
- Steady-state qualification.
- Low-power operation assessments.
- Operational transients, specifically pulse-dwell-pulse analysis.
- Investigation of accidental transients.

The integration of these three pillars leads to a comprehensive approach to facility and test section design, focusing on the following key aspects:
- Definition of operational states and conditions.
- Sizing and design of systems and components.
- Numerical pre-test activities.
- Development of technical specifications for components.
- Acquisition of systems and components.

Collectively, these efforts contributed to the fulfillment of the thesis objectives, achieving significant milestones in the research process:
- The conceptual design of the W-HYDRA platform has been successfully completed.
- Relevant technical specifications have been prepared for the procurement phase.
- The design of experiments has been thoroughly articulated.

In summary, the thesis aims to resolve the challenges associated with pulsed operation in fusion reactors through a robust experimental framework that is underpinned by advanced numerical simulations. The synergistic relationship between the W-HYDRA facilities, the various test sections, and the experimental test matrix creates a comprehensive research strategy aimed at enhancing the understanding and operational viability of fusion reactor technologies.

The overview of the research activity is schematically shown in Fig. 1.

1.4 Structure of the thesis

The present thesis is organized to reflect the logical progression towards achieving the primary, secondary, and related objectives, detailing the design and analyses conducted as illustrated in Fig. 1.

Sect. 2 provides the necessary context for understanding the significance of the research. It introduces the concept of nuclear fusion and the principles of magnetic confinement tokamaks, followed by an overview of pulsed operation in tokamak reactors. Detailed discussions on breeding blanket technologies follow, focusing on ITER and DEMO reactors, and the DEMO Breeding Blanket Steam Generator technology. A comprehensive overview of numerical tools, with an emphasis on the RELAP5 thermal-hydraulic code, is provided, emphasizing nodalization techniques and models for fluids and materials.

Sect. 3 describes the design and functionality of the different branches of the W-HYDRA infrastructure, focusing on the integration of its various components. It details the STEAM high-power branch and the Water Loop low-power branch, providing a thorough examination of their primary and secondary loops, as well as the three loops of the Water Loop and its associated test sections. The discussion highlights how the integration of these facilities within the W-HYDRA infrastructure offers a comprehensive approach to studying the thermal-hydraulic behavior of fusion reactor components. This holistic approach supports a range of testing scenarios, from high-power to low-power operations.

Sect. 4 is dedicated to the primary objective of the thesis: the design and analysis of the STEAM test section. This section details the scaling procedure from the 3.1 MW OTSG steam generator, including thermal-hydraulic analysis using the RELAP5/Mod3.3 model. The results of the simulations and comparisons between the BB and STEAM OTSGs are discussed, along with the analysis of scaling-induced distortions.

Sect. 5 delves into the comprehensive numerical simulations performed to optimize both the design and operational performance of the STEAM facility. This section is crucial as it aligns with the primary objective of the thesis, which focuses on the design and analysis of the STEAM test section, and also addresses a related objective: the optimization and refinement of the entire STEAM facility. This section is divided into sub-sections that cover the primary and secondary loop preliminary analyses, optimization for low-power operation, and characterization of operational and accidental scenarios. Detailed descriptions are provided for the developed RELAP5/Mod3.3 models and the control strategies implemented to manage pulse-dwell-pulse transitions and emergency conditions, such as LOFA and LOHS.

Sect. 6 focuses on the secondary objective of the thesis, which is the design and analysis of the Water Loop. It provides an overview of the preliminary analyses supporting the WL design, including initial configuration, design feasibility analysis, and final configuration. Strategies for regulation, RELAP5/Mod3.3 modeling, and steady-state characterization are discussed, as well as accidental scenarios. This chapter demonstrates how the Water Loop, integrated with the STEAM facility, contributes to evaluating low-power operations and dynamic responses.

Finally, Sect. 7 summarizes the achieved results, highlighting how the primary and secondary objectives have been met. It discusses the impact of the innovations introduced and the implications for future reactor design and development.

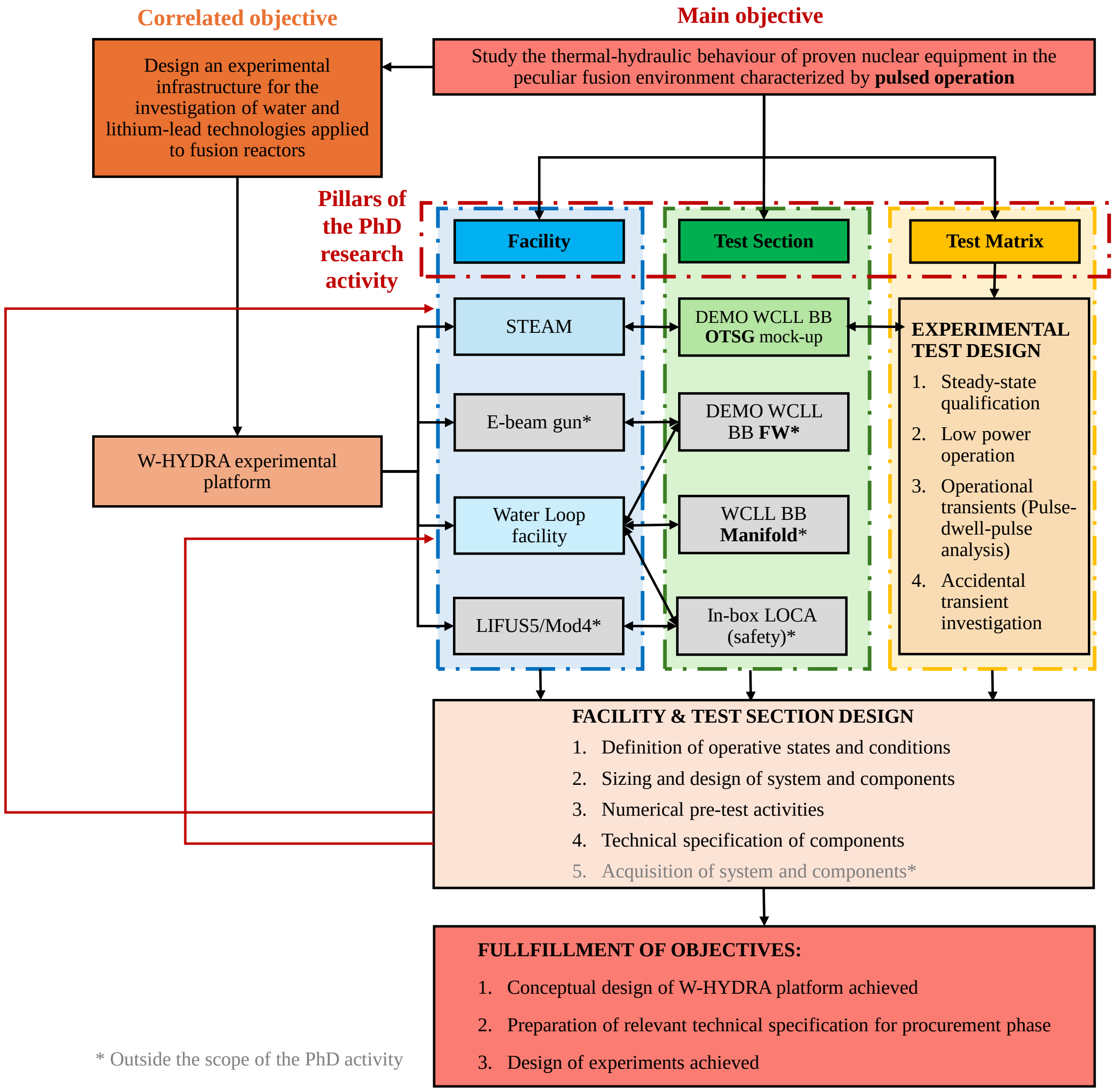

Fig. 1. Main objectives of the PhD research activity

2 BACKGROUND

2.1 Introduction to magnetic confinement fusion

Nuclear fusion [9] is a process in which two light atomic nuclei combine to form a heavier nucleus, releasing a large amount of energy in the process [10] [11]. This phenomenon, that powers and drives the production of energy in stars, is described by Einstein equation, $E=mc^2$, where E represents energy, m represents mass, and c is the speed of light. In the context of fusion, this equation illustrates how a small amount of mass is converted into a large amount of energy, as the combined mass of the fusion products is less than the mass of the original nuclei. The amount of released energy depends on the specific reaction and is primarily distributed between the fusion products inversely proportional with respect to the masses, with a smaller portion carried by neutrinos, photons, and kinetic energy of the remaining particles [12]:

D + T	→	^{4}He (3.5 MeV)	+	n (14.1 MeV)
D + D	→	T (1,01 MeV)	+	p (3,02 MeV)
D + D	→	^{3}He (0,82 MeV)	+	n (2,45 MeV)
T + T	→	^{4}He	+	2 n (11,3 MeV)
D + ^{3}He	→	^{4}He (3,6 MeV)	+	p (14,7 MeV)

Among the many possible fusion reactions, the most promising involves hydrogen isotopes, such as deuterium (D) and tritium (T) [14]. Deuterium, a stable isotope of hydrogen, is abundant in water, while tritium, a radioactive isotope that undergoes β-decay with a half-life of about 12.3 years, can be produced by neutron interactions with lithium in a fusion reactor [13]. Is indeed the availability of the two isotopes on a terrestrial scale, the amount of energy produced compared to the other nuclear reactions and the cross-section of this reaction which makes the D-T the most favorable reaction in terms of fusion efficiency [15].

To achieve controlled nuclear fusion reactions, it is imperative to overcome the electrostatic repulsion between positively charged nuclei, a phenomenon governed by the Coulomb force. This force becomes significant at close distances, requiring extremely high temperatures and pressures to bring nuclei within fusion range. Achieving these conditions demands plasma confinement, a critical aspect of fusion research. Plasma confinement serves the dual purpose of maintaining the extreme temperatures and pressures required for fusion reactions while preventing the plasma from escaping. Confinement methods can be broadly categorized as either inertial [16] or magnetic [17]. Inertial confinement involves rapidly compressing a fuel pellet to achieve fusion conditions, while magnetic confinement relies on powerful magnetic fields to contain and manipulate the plasma, thus enabling sustained fusion reactions.

Among the devices used for magnetic confinement [18], two of the most prominent are tokamaks and stellarators. Both devices aim to confine plasma using magnetic fields but differ in their design and operational principles.

Stellarators [19] are magnetic confinement devices that use only external magnets to generate the magnetic field necessary to confine plasma, avoiding the need for a plasma current. This design reduces the risk of certain instabilities, though it requires a complex magnetic field configuration. Despite the challenges in their design and construction, stellarators offer potential advantages in terms of continuous operation and stability, making them a valuable alternative in the pursuit of controlled fusion.

In contrast, tokamaks [10] are torus-shaped devices that generate a magnetic field using a combination of external magnets and a current induced within the plasma itself. This configuration creates a strong magnetic field that confines and stabilizes the plasma, making tokamaks one of the most researched designs in fusion technology. The term "tokamak" is derived from the Russian words "toroidalnaya kamera magnitnaya" (toroidal magnetic chamber). In tokamaks, plasma—a hot, ionized gas made up of ions and electrons—is confined within the toroidal vacuum vessel, facilitating the conditions necessary for thermonuclear fusion reactions.

The tokamak operates by creating a magnetic field that confines and stabilizes the plasma, preventing it from coming into contact with the vessel walls, minimizing energy loss due to particle-wall interactions and enabling sustained fusion reactions. The magnetic field, generated by a combination of toroidal and poloidal magnets, guides the plasma motion along a toroidal closed path within the vacuum vessel: charged particles are constrained to follow the field lines, preventing their free movement across the vessel. Such flow of electric current within the plasma induces the plasma current, that plays a crucial role in confining the plasma, generating additional magnetic fields.

The operation of a tokamak device is rather complex since it involves many systems and components:

- Magnets [20]:
  - poloidal coils generate a poloidal magnetic field along the toroidal axis, shaping and stabilizing the plasma;
  - toroidal field coils produce the primary toroidal magnetic field, confining the plasma within the vacuum vessel and maintaining its stable shape;
- Vacuum system [17]:
  - the vacuum vessel provides a sealed environment for plasma containment, maintaining low pressure conditions necessary for fusion reactors;
  - various pumping system evacuates gases and impurities, maintaining the required vacuum level within the vessel.
- Breeding Blanket [21]: it surrounds the plasma and serves multiple functions, including tritium breeding, heat removal, and neutron shielding. It breeds tritium from lithium isotopes, removes excess heat generated during fusion reactions, and provides shielding from high-energy neutrons.
- Plasma facing components (PFCs) [22]: positioned directly in contact with the plasma, they act as plasma/reactor boundary. Playing a vital role in managing plasma-wall interactions and maintaining plasma stability, PFCs include materials and structures designed to withstand high heat fluxes and particle bombardment while minimizing material erosion and impurity contamination. Typical PFC include the first wall (thermally and mechanically integrated with the BB), the divertor (dedicated to high duty exhaust management) and the limiter (auxiliary sacrificial component for divertor and machine protection during plasma transients). These components are subjected to extreme thermal and mechanical stresses, requiring advanced materials and cooling techniques to ensure their performance and longevity.
- Cryogenic system [23]: it maintains the magnets at cryogenic temperatures necessary to maintain their superconducting state and therefore achieving the required magnetic field strength.
- External shielding: between the vacuum vessel and the external shielding, vacuum is created to reduce heat exchange, eliminating convention and conduction, thus minimizing thermal losses towards the coils.
- Plasma confinement and heating systems [10].
  - Neutral Beam Injection (NBI): NBI systems inject high-energy neutral particles into the plasma, transferring energy and heating it to fusion-relevant temperatures.
  - Radiofrequency (RF) Heating: RF systems use radiofrequency waves to further heat the plasma and drive current within it, enhancing confinement.
  - Electron Cyclotron Resonance Heating (ECRH): ECRH systems employ high-frequency electromagnetic waves to selectively heat and control the electron population in the plasma.
- Plasma diagnostics: diagnostic systems are employed to monitor and characterize the properties of the plasma, including temperature and density.
- Plasma Control Systems: Sophisticated control systems regulate the plasma parameters to maintain stability and optimize fusion performance.

Additionally, the plasma reaches the required high temperatures through internal and external heating mechanisms. Magnetic fields themselves generate heat by Joule effect. Neutral beam injection introduces additional heat through neutral particles, with hydrogen isotopes in the chamber maintained in a plasma state, confined and stabilized by the magnetic field.

Despite their promise, tokamaks face significant challenges and limitations. Controlling plasma instabilities, managing high temperatures and pressures within the vacuum vessel, and identifying suitable materials for components exposed to high-energy plasma are among the key challenges researchers must address. However, recent advancements in plasma heating and confinement systems, as well as ongoing research into novel materials and reactor designs, offer hope for overcoming these obstacles.

It is worth noting that unlike fission reactors, where the risk of accidents may arise from uncontrolled power divergence, fusion reactors are inherently safe. The power output of a fusion reactor is limited and self-regulating, as it operates in pulsed mode, meaning that the fusion process naturally stops after each pulse, mitigating the risk of runaway reactions.

While fusion reactors are inherently safer than fission reactors, they still present unique safety challenges that must be addressed [24]. One major concern is the management of tritium, whose effective containment have to be ensured as well as leakage into the environment should be minimized for both operational safety and public acceptance. Another safety challenge lies in the containment of neutron radiation produced during the fusion process. These high-energy neutrons can activate surrounding materials, making them radioactive over time. Therefore, developing advanced shielding materials and strategies for managing activated components is essential for long-term safety. Additionally, the design of the vacuum vessel and associated components must account for potential mechanical failures or disruptions, such as plasma instabilities or loss of coolant scenarios, which could compromise the integrity of the reactor. Robust systems for monitoring, containment, and emergency shutdown are necessary to ensure that any unexpected event can be managed without significant risk to personnel or the environment.

2.2 Pulsed operation in tokamak reactors

In tokamak-based fusion reactors, plasma confinement relies on the principles of magnetic confinement, where a magnetic field confines charged particles, such as ions and electrons, within a defined region [10]. Tokamaks are equipped with a central solenoid that carries a variable electric current, which, according to Ampère's law, induces a time-varying magnetic flux, resulting in a magnetic field inside the tokamak vacuum vessel [4]. This magnetic field induces an electric field within the plasma, following Faraday law of electromagnetic induction. As a consequence, the plasma, being a conductor, experiences a time-varying induced electric field, which drives a plasma current. This induced current generates a poloidal magnetic field component that contributes to the confinement of the plasma within the torus [11].

While the induction of a plasma current is crucial for maintaining confinement, it is not feasible to sustain the central solenoid variable current indefinitely. Practical limitations, such as energy consumption and material constraints, dictate the duration for which the plasma current can be maintained. Consequently, pulsed operation involves alternating cycles of discharge, during which the plasma current is induced, and rest phases, where the current is allowed to decay.

Within each pulse cycle, the reactor Primary Heat Transfer Systems (PHTSs) must efficiently manage the removal of the reactor nominal thermal power [25]. During the dwell, instead, plasma is inactive, and the power retained within this structure approaches approximately 1 % of the nominal value. During the ramps, the power varies from 1% to 100% and vice versa.

Pulsed operation presents several technological implications and challenges that influence the design and operation of fusion reactor components. Some significant aspects include:

- Cyclic Stresses: Rapid temperature and pressure variations during discharge and rest phases can cause thermal and mechanical stress on reactor materials and components, requiring resilient materials and efficient cooling systems to ensure structural integrity and component longevity.

- Dynamic Cooling Requirements: Cooling systems must be designed to handle variable and transient heat fluxes in response to plasma power and temperature variations during pulsed operation. This necessitates dynamic cooling solutions and advanced control systems to maintain optimal operating temperatures.
- Fast Responses: Components must be able to respond quickly to load variations and changing operating conditions during pulsed operation, requiring high-speed actuators and control systems with short response times.
- Testing and Validation: Pulsed operation imposes challenges and performance requirements that necessitate specific testing and validation to ensure reliable and safe operation in the context of nuclear fusion.

Furthermore, the operation of a fusion reactor differs not only in terms of its pulsed nature but also in terms of thermal loads and neutron flux when compared to fission reactors. Despite some components used in the fission industry being considered for fusion reactors, their utilization is contingent upon demonstrating feasibility after being tested in fusion-like environments, through the use of experimental facilities.

The unconventional pulsed operation that characterizes fusion reactors poses unique challenges to the operation of systems and components, making it mandatory to test their behavior during rapid power variations. Experimental facilities are therefore necessary to characterize and demonstrate the suitability of components and technologies to fusion environment.

2.3 ITER and DEMO fusion reactors

Looking ahead, addressing challenges and harnessing the potential of tokamak technology holds the key to unlocking the promise of fusion energy as a clean, sustainable, and virtually limitless source of power. In particular, two key projects represent significant milestones in the development of fusion energy: ITER [26] and DEMO [21].

ITER (International Thermonuclear Experimental Reactor) is a multinational research project aimed at demonstrating the feasibility of nuclear fusion as a large-scale and carbon-free energy source. Located in Cadarache, France, ITER will be the world largest tokamak when completed and is designed to produce 500 MW of fusion power.

DEMO (DEMOnstration Power Plant) is envisaged as the next step beyond ITER, representing a prototype commercial fusion power plant that will demonstrate the viability of fusion energy for electricity generation. Unlike ITER, which is primarily an experimental reactor, DEMO will be optimized for steady-state operation and electricity production, with a steady-state pulse power of 2 GW_{th}.

One significant difference between ITER and DEMO is their respective approaches to tritium breeding and fuel production. Before addressing this aspect, it is important to underline the context of ITER as an experimental reactor. As an experimental facility, the probability that ITER experiences transient events and plasma disruptions, including potential plasma-wall interactions are non-zero. This necessitates the use of specialized materials (e.g., thick tungsten layer) for the first wall, capable of withstanding such incidents, often referred to as plasma displacement events.

Due to these safety considerations, the first wall in ITER may not be entirely covered by the breeding blanket. Despite this limitation, the breeding blanket remains a crucial component for future fusion reactors, including DEMO. ITER will therefore be equipped with Tritium Breeding Blanket Modules (TBMs), which aims to demonstrate tritium self-sufficiency through breeding tritium from lithium in the blanket material of different BB concepts, serving as a testing ground in an integrated fusion environment.

In contrast, DEMO will focus on optimizing tritium breeding and fuel production for steady-state operation and electricity generation. DEMO approach to tritium breeding and fuel production will be crucial for demonstrating the feasibility of fusion energy as a reliable and sustainable power source on a commercial scale.

Additionally, it is worth noting that the operational cycles of ITER and DEMO differs from one another. ITER operational cycle is characterized by a 200-second ramp-up phase, followed by a 450-second pulse phase, a 200-second ramp-down phase, and finally, a 90-second dwell phase [27]. Conversely, DEMO operational cycle consists of a 2-hour pulse phase, followed by a 150-second ramp-down phase, a 600-second dwell phase, and a 150-second ramp-up phase [25].

2.4 Breeding Blanket

Within the intricate design of a tokamak fusion reactor, the breeding blanket occupies a crucial position [28]. Surrounding the plasma within the vacuum vessel, it serves as a protective layer with multifaceted functionalities essential for the success of fusion reactions [29]:

- Recovery and conversion of fusion power: it captures the energy produced by fusion reactions occurring within the plasma. After D-T fusion, 80% of the energy is immediately discharged from the plasma as kinetic energy carried by 14-MeV neutrons. These neutrons serve as a volumetric heat source, depositing a portion of their kinetic energy into the blanket structure while undergoing scattering processes. The blanket must then convert this energy into heat, which can be extracted using a suitable cooling system and transformed into electric power via heat exchangers and turbines. Coolant fluids circulate throughout the blanket structure to facilitate this process. The remaining 20% of the fusion energy, along with all externally supplied energy used to heat the plasma, exits the plasma as energetic charged particles, atoms, or radiative energy. Regardless of the form, this energy constitutes a surface heat source that impacts the first material surface facing the plasma.

- Tritium production: tritium can be generated within the breeding blanket through neutrons interactions with lithium isotopes contained within the material. This self-sustaining process ensures a continuous supply of tritium fuel for the reactor [30]. The main reactions involved in tritium production are:

  $$^{6}\mathrm{Li}+n \rightarrow {}^{4}\mathrm{He} + \mathrm{T} + 4.78\ \mathrm{MeV}$$
  $$^{7}\mathrm{Li}+n \rightarrow {}^{4}\mathrm{He} + \mathrm{T} + n - 2.47\ \mathrm{MeV}$$

  The first reaction, involving lithium-6, exhibits a high cross-section for thermal neutrons, meaning it is more likely to occur with neutrons that have lost much of their kinetic energy due to scattering interactions. This reaction is exothermic, and both the kinetic energy and the reaction energy are removed by the coolant in the form of heat. Conversely, the second reaction is more probable with fast neutrons and is endothermic. In this case, a negligible portion of the kinetic energy is transformed into heat due to reduced interactions with the material. The activation energy threshold of 2.47 MeV implies that no energy is produced unless neutrons have sufficient kinetic energy. As the first reaction is better suited for energy production, natural lithium, which contains 92.44% lithium-7, is enriched up to 90% lithium-6 [28].

- Neutron Shielding: neutrons released during fusion reactions possess high energy levels, making them potentially damaging to reactor components. The breeding blanket acts as a shield, absorbing and dissipating neutrons, energetic charged particles and atoms, thereby protecting sensitive reactor elements from radiation damage.

To fulfill these functions, the breeding blanket is composed of various components, each serving a specific purpose:

- The structural material provides mechanical support and ensures the integrity of the blanket under the harsh conditions of a fusion environment. Various materials, such as martensitic steels, vanadium alloys, chromium alloys, and silicon carbide composites (SiCf/SiC), are being considered for this purpose. Additionally, reduced activation ferritic martensitic (RAFM) steels, such as EUROFER, are being extensively studied for their suitability in fusion reactor applications. These materials are selected based on their ability to withstand high temperatures, neutron irradiation, and mechanical stress while maintaining structural integrity over the lifetime of the reactor. RAFM, in particular, are designed to have reduced activation characteristics, minimizing the long-term radioactivity of reactor components and simplifying decommissioning and waste disposal processes.
- The coolant is responsible for extracting heat generated within the breeding blanket and transferring it to the power conversion system for electricity generation. Several coolant options are being explored, including water, helium, liquid metals such as Pb–17Li and lithium, and molten salts such as FLiBe. Each coolant has its advantages and challenges in terms of thermal conductivity, corrosion resistance, compatibility with structural materials, and ability to withstand high temperatures and neutron irradiation.
- The breeder material is essential for tritium production through neutron capture reactions. Typically, lithium-containing materials are used as breeder materials due to their high neutron capture cross-section and abundance of lithium isotopes. These materials absorb neutrons released during fusion reactions and produce tritium as a by-product. The choice of breeder material is critical for achieving tritium self-sufficiency and maximizing the efficiency of the fusion reactor.
- Neutron multipliers, such as beryllium and lead, are employed to enhance neutron multiplication within the breeding blanket. These materials efficiently absorb neutrons and release additional neutrons through (n, 2n) reactions, thereby increasing the neutron population available for tritium production. Neutron multipliers play a vital role in compensating for neutron losses and optimizing the breeding ratio within the blanket.
- The tritium carrier, or tritium transport medium, transfers the tritium produced from the breeding material to the Tritium Extraction System (TES) [29]. This component ensures that tritium is collected and utilized efficiently. There are various methods for managing tritium transport within the breeding blanket system, and the choice depends on the specifics of the blanket design and operational requirements. One method involves using a purge gas in conjunction with the coolant flow. The purge gas, typically helium containing a small percentage of hydrogen (0.1% w.t.H2), is circulated through the blanket, helping to prevent tritium buildup within the blanket and ensuring efficient tritium management. Additionally, tritium permeation barriers are employed to prevent the diffusion of tritium from the breeding material into other components.

Numerous breeding blanket concepts have undergone development worldwide for decades. Considering specific requirements and feasibility issues like material compatibility and behavior under irradiation, various concepts potentially meet minimal performance standards [31], each one presenting also critical challenges requiring further research and development. Recent attention has focused on promising candidate concepts categorized by the type of breeder utilized:

- Liquid metal breeders main option include Pb–17Li (17 at.% Li) with a melting temperature of 235°C and pure lithium with a melting temperature of 177°C. These choices offer advantages like mitigating irradiation-induced damage, facilitating tritium extraction, enabling online lithium replenishment, while being characterized by high power density. The main drawbacks are represented by magnetohydrodynamic (MHD) effects, determining extremely high pressure drops, corrosivity and the lithium strong interaction with water and air. For Pb–17Li-based concepts, self-cooled or water-cooled designs are feasible. While self-cooled options offer reduced reactivity with air and water, water-cooled variants minimize MHD-related challenges. Helium-cooled concept is not particularly promising due to the low tritium breeding.

- Molten Salt Breeders, such as FLiBe (Li_2BeF_4, melting temperature of 459°C), provide advantages like low operating pressure and electrical conductivity, mitigating MHD issues. Nonetheless, lower tritium breeding ratios and compatibility challenges with structural materials due to the high melting temperature pose concerns.

- Li ceramic options include Li_2O, Li_4SiO_4, Li2TiO$_3$, and Li_2ZrO_3. These concepts typically utilize ferritic–martensitic steel as structural material, high-pressure helium as coolant and beryllium as neutron multiplier. Both ceramics and beryllium are usually used in form of pebbles or, less commonly, pellets, as the pebble-bed help to reduce thermal stress and allow for greater flexibility in breeder material management, reducing the risk of damage due to swelling under neutron irradiation. Forms like plates and blocks can be adopted too, presenting large reliability issues though.

Additionally, for liquid breeders, there exist several concepts differing in their approach to coolant management and thermal regulation within the breeding blanket:

- In dual coolant concepts, two separate coolant systems are employed, one for cooling the breeder material and another for cooling the structural components.
- Separate coolant concepts utilize a single coolant system, but with separate channels for cooling the breeder material and structural components.
- Self-cooled concepts rely solely on the inherent thermal properties of the breeder material for cooling, without the need for a separate coolant system.

Each approach has its advantages and challenges, depending on factors such as heat transfer efficiency, thermal stress management, and overall system complexity.

Some of the most promising breeding blanket concepts therefore are [32][33]:

- Water-Cooled Lithium-Lead Blanket:
  - Coolant: water in PWR conditions (15.5 MPa, 295°C - 328°C);
  - Breeder, neutron multiplier and tritium carrier: PbLi;
  - Structural material: EUROFER 97

- Helium Cooled Lithium-Lead (HCLL):
  - Coolant: helium;
  - Breeder, neutron multiplier and tritium carrier: PbLi;
  - Structural material: EUROFER 97;

- Helium Cooled Pebble-Bed (HCPB):
  - Coolant: helium (8 MPa, 300°C - 500°C);
  - Breeder: lithium, contained in ceramic pebbles;
  - Neutron multiplier: beryllium, in the form of pebbles;
  - Tritium carrier: helium;
  - Structural material: SiC_f/SiC composite;

- Self Cooled Lithium-Lead Blanket (referred to as TAURO in [33]):
  - Coolant, breeder, neutron multiplier and tritium carrier: Pb-17Li;
  - Structural material: SiC_f/SiC composite;

WCLL and HCPB are considered the most viable short-term concepts. ENEA and its third parties (including Sapienza University) have recently focused their research and efforts on the WCLL BB concept.

2.5 EU-DEMO WCLL Breeding Blanket

The DEMO reactor design of the European DEMO is advancing towards its Conceptual phase, anticipated to conclude by the end of 2027 [25]. This phase will result in the selection of a reference concept for the Breeding Blanket. Within this context, ENEA is developing the WCLL BB concept. Achieving this goal depends on demonstrating the maturity of certain technological characteristics of this blanket concept.

The design of the DEMO WCLL BB is composed by 16 identical toroidal sectors (22.5°), each one consisting of five BB segments [34], as shown in Fig. 2 and Fig. 3. Sectors are furtherly divided into two Inboard Blanket (IB) segments (i.e., Left IB, LIB and Right IB, RIB) and three Outboard Blanket (OB) segments (i.e., Central OB, COB, Left OB, LOB and Right OB, ROB).

A typical segment of the WCLL BB is structured into various subregions, each serving specific functions within the fusion reactor system:

- The **First Wall/Side Wall** (FW/SW) complex is a barely U-shaped plate. The straight surface facing the plasma (i.e., the FW) is armored with 2mm of tungsten to withstand high thermal loads and minimize erosion from plasma interactions. Plasma heat flux gradually decreases on the bent FW regions down to zero in correspondence of the SW. The FW, experiencing the highest thermal loads, receives heat flux due to both plasma and charged particles and it is cooled by counter current square channels located at 3mm from the armor facilitate efficient heat dissipation. Fig. 4 shows the poloidal distribution of the Neutron Wall Loading estimated for inboard and outboard poloidal sectors, highlighting higher values are in the outboard and inboard equatorial zone (1.33 MW/m^2 and 1.1 MW/m^2 respectively), while the poloidal average is 0.93 MW/m^2. Due to this non-uniform heat distribution along the poloidal direction, the pitch of FW cooling channels varies accordingly. [35]

- The **Breeding Zone** (BZ), enclosed between the FW/SW and a Back-Plate (BP), serves primarily for tritium breeding and heat removal. Stiffening plates (SPs) enhance mechanical stability, with toroidal radial SPs (horizontal) dividing the segment into slices and poloidal radial SPs (vertical) further dividing each slice into sub-cells. A horizontal baffle plate within each slice guides PbLi flow, ensuring a radial-poloidal-radial path. A horizontal baffle plate within each slice guides PbLi flow, ensuring a radial-poloidal-radial path. Cooling is facilitated by bundles of Double Walled Tubes (DWTs) submerged in PbLi. DWTs consist of concentric tubes separated by a 0.1 mm of iron or copper layer to prevent tube rupture. This design choice significantly reduces the likelihood of tube rupture, crucial for preventing accidents such as Loss Of Coolant Accidents (LOCA) and the consequent pressurization of the BZ and PbLi/water interaction [36]. Various layouts, including helical DWTs (see Fig. 5), are considered to optimize cooling efficiency while minimizing the total number of tubes and welds, enhancing manufacturing reliability. A steel BP plate, 20 mm thick, separates the BZ from the manifold region and houses holes for PbLi inlet/outlet and DWT access. This configuration allows for efficient tritium breeding and heat management while ensuring structural integrity and mechanical stability of the BB segment.

- The **Manifold** region, enclosed between the BP and the BSS, houses water and PbLi manifolds. It is subdivided into three distinct sections, each dedicated to either distributing or recollecting a specific process fluid: cooling water for the First Wall/Side Wall (FW/SW) and Breeding Zone (BZ), as well as liquid Lead-Lithium (PbLi).
  The PbLi manifold, positioned after the BZ, consists of six parallel subchannels divided by vertical stiffening plates (SPs). These subchannels are fed in parallel via a collector in the lower segment, with

each divided into inlet and outlet sections by a 3 mm partition wall. At the top of the segment, PbLi is collected and directed to the outlet pipe.
Adjacent to the PbLi manifold, the water manifold region handles the distribution and recollection of cooling water for both FW/SW and BZ circuits. Water inlet pipes are positioned in the upper port, while PbLi inlet pipes are routed through the lower port. The system incorporates descending manifolds to route water distributed to FW/SW channels and BZ tubes to the segment bottom. Different paths are followed by FW/SW and BZ circuits, with recirculation manifolds ensuring optimal water distribution. This layout (see Fig. 6), tailored for IB and OB segments, undergoes continuous optimization for enhanced structural integrity and fluid management efficiency within the WCLL BB.

- The **Back Supporting Structure** (BSS) serves as the backbone of the blanket segment, providing structural support and facilitating connections between the BB and the VV. Its substantial thickness (100mm) contributes to load-bearing capacity and shields internal components.

- The **Bottom and Top Caps** (BC and TC) serve as upper and lower terminations of the BB segment. Designed to withstand pressure differentials, these caps feature enhanced thickness and incorporate cooling channels to manage thermal loads effectively.

- A network of **Feeding Pipes** facilitates the routing and recollection of water and PbLi between the BB and the VV. Segmented into upper (Fig. 3) and lower ports, these pipes ensure the controlled flow of operational fluids within the fusion reactor system.

2.6 EU-DEMO WCLL Balance of Plant

In fusion reactors like DEMO, aimed at energy production, the Balance of Plant plays a pivotal role in ensuring efficient operation, by guaranteeing the heat exchange from the primary system, represented by the PHTS, and the secondary system, embodied by the Power Conversion System (PCS).

The coupling of the PHTS and PCS can be realized through two distinct schemes: direct and indirect. The Direct Coupling Design (DCD) involves the direct connection of the PHTS to the PCS via the Steam Generator (SG). Conversely, Indirect Coupling Design (ICD) employs an Intermediate Heat Transfer System (IHTS), leveraging technologies like molten salt Energy Storage System (ESS) to deliver to the turbines 100% of the nominal power during the dwell phase, ensuring continuous operation. ESS in Fig. 7 is composed of the Molten Salt (MS) Tanks that feed the Helicoidal Coil Steam Generators (HCSG).

The reference variant of the DEMO WCLL is the Direct Coupling Design (WCLL DCD BoP) with a small ESS, capable of providing the turbine the sufficient steam flow to drive the turbine and keep the main PCS component hot.

The selection of this coupling configuration was made to limit BB PHTS complexity, while enhancing overall safety of the system. By avoiding the additional components and subsystems required in an ICD, such as the IHTS and molten salt ESS, the DCD reduces the number of potential failure points, which inherently lowers the likelihood of malfunctions or leaks. Furthermore, the simplicity of the DCD facilitates more straightforward operation, maintenance, and monitoring of the PHTS. This reduction in system complexity not only minimizes human error but also allows for faster response times in the event of anomalies. In addition, the reduced number of intermediate heat transfer steps limits the potential for energy losses or unanticipated thermal stresses, ensuring stable and predictable operation, even during transient conditions like the dwell phase.

Considering the WCLL DCD, the BoP (see Fig. 7 and Fig. 8) is mainly composed of:

- **Primary Heat Transfer Systems**, responsible for managing the heat produced during the nuclear fusion process and channeling it towards other systems within the reactor for useful purposes, such as electricity generation or maintaining optimal operational conditions. To effectively manage the diverse heat sources and ensure efficient reactor operation, the PHTS is subdivided into several specialized subunits:
    - BB PHTS, tasked with removing power from the BB components and to deliver it to the Power Conversion System by means of four identical steam generators. The system is divided into two independent primary systems: the BZ PHTS and the FW PHTS. Each PHTS is articulated in two cooling loops, each consisting of: In-VV cooling system, a SG, two Main Coolant Pumps (MCPs) and the connecting piping between these components. The two BZ PHTS share a pressurizer, as well as the two FW PHTS. The water operates at 15.5 MPa, 295-328°C.
    - Vacuum Vessel (VV) PHTS [38], responsible of the heat transfer within the vacuum chamber. It utilizes two independent loops, delivering a total power of about 86 MW to the PCS, using pressurized water at 3.1 MPa with inlet/outlet temperatures of 190°C and 200°C, respectively.
    - Divertor Plasma Facing Unit (DIV-PFU) PHTS [38], serves as both a containment boundary for the primary coolant and a means of removing thermal power from the DIV PFCs and transferring it to the PCS. The DIV PFC PHTS operates with water at 5 MPa (DIV PFCs inlet pressure) and temperatures of 130°C to 136°C,
    - Divertor Cassette (DIV-CAS) PHTS [39], responsible for managing the heat generated within the divertor cassettes and transferring it to the PCS. This system is articulated into two independent circuits, each fed by water at pressures of 35 bar and inlet temperatures of 180 °C, with an outlet temperature of approximately 210 °C.

- **Power Conversion System**, composed by a single loop, thermally coupled to the PHTS through the steam generator. It is also connected with VV, DIV-PFU and DIV-CAS PHTSs, to use their power as feedwater preheaters. The PCS operates following a Rankine cycle that employes water/steam at 6.41 MPa with temperature ranging from 238°C to >300°C. The steam produced during the pulse phase is directed towards the turbine.

- A small **Energy Storage System** (small ESS) **PCS** is also connected to the steam line reaching the turbine, feeding it with about 10% of the nominal steam flow rate during the dwell phase and maintaining the connection with the electrical grid. It is composed of a pump, a tank (containing approximately 2700 tons of molten salt inventory in 1500m^3), electrical heaters, a steam generator, and the piping between these components. The total thermal energy stored is about 200 GJ.

2.7 EU-DEMO WCLL Breeding Blanket Steam Generator

The DEMO WCLL BB PHTS [40] will much likely adopt the Once Through Steam Generator technology for the realization of the main heat sinks, tasked with efficiently dissipating the heat generated within power systems while concurrently producing superheated steam at constant pressure for turbine inlet utilization. In particular, the current BB PHTS configuration envisages four identical steam generators with reference power of 477MW each [41]. The design of the BB PHTS OTSG is inspired to the Babcock & Wilcox (B&W) [42] layout and adapted considering the thermo-dynamic constraints for PHTS and PCS water [43].

Within the OTSG, whose concept is shown by Fig. 9, primary coolant collected in the hemispherical upper plenum enters the tube-side through the upper tube-sheet. It flows downwards, exchanging power with the secondary fluid, and exits through the lower tube-sheet towards the lower plenum.

Structurally, the tube bundle region is enclosed by the shroud, forming the riser while the space between the outer shell and the shroud constitutes the downcomer, segmented into upper and lower downcomers. Riser and downcomer are connected through the water ports, located in correspondence of the lower tube-sheet, and through the steam ports, placed in correspondence of the upper tube-sheet. Approximately three-quarters up the height, the shroud features a recirculation window (or aspirator port), situated just above the feedwater inlet.

Secondary fluid (i.e., feedwater), is collected within semi-circular headers and it is sprayed down into the lower downcomer. Subcooled water mixes with dry steam from the riser through the recirculation window, heating up as steam condenses, aspirating more steam. Reaching saturation before inverting its direction in correspondence of the lower tube sheet, feedwater enters the riser through the water ports, initiating boiling as it flows upwards.

The heat transfer process within the riser involves three distinct regions, each with its own characteristics. The first one is the nucleate boiling region (NBR), where bubbles form on the surface of the tubes, enhancing turbulence while the tube surfaces remain wetted by the high-density fluid. The second region is the film boiling region (FBR), where a saturated steam blanket forms on the surface of the tubes, leading to a sharp reduction in the heat transfer coefficient (HTC). Finally, the superheating region (SHR) is characterized by the presence of low-density superheated steam, which has a significantly lower HTC. Since the NBR is associated with a higher HTC, its extent is approximately proportional to the power exchanged by the component, which can therefore be correlated with the riser collapsed level.

Superheated steam reaching the riser top is diverted towards the steam downcomer by the upper tube-sheet and it exits the component through two outlet nozzles. The lower region of the steam downcomer (below the steam outlet nozzles) is referred to as “dead zone”, stagnant steam is present.

2.8 Numerical tool: RELAP5 System Thermal-Hydraulic code

RELAP5 [44][45][46] is a sophisticated thermal-hydraulic code designed for the analysis of nuclear systems, developed and continuously refined by international institutions. Originating at the Idaho National Laboratory (INL), RELAP5 has undergone extensive qualification projects and sensitivity analyses worldwide [47]. Although initially developed for light water reactor (LWR) systems, RELAP5 has also found applications in fusion research. It is used to model and analyze the thermal-hydraulic behavior of fusion reactors, where it simulates coolant system transients and the coupled behavior of reactor systems under both normal and off-normal conditions.

RELAP5, written in Fortran 77, addresses one-dimensional fluid dynamics and heat exchange problems with a generic modeling approach. It can simulate a broad range of thermal-hydraulic systems, including turbines, condensers, and secondary feed-water systems. The code includes detailed models for pumps, valves, pipes, heat-releasing or absorbing structures, and reactor kinetics. It also features special process models for phenomena such as form loss, flow at abrupt area changes, branching, choked flow, boron tracking, and non-condensable gas transport. This versatility allows RELAP5 to handle diverse hydraulic and thermal transients, not only in nuclear systems but also in non-nuclear systems and fusion reactors involving mixtures of steam, water, and solutes.

RELAP5/Mod3 operates based on a one-dimensional, transient, non-homogeneous, and non-equilibrium hydrodynamic model for steam and liquid phases. It employs a set of six partial derivative balance equations and accounts for non-condensable components in the steam phase, assuming they move with the same velocity and temperature as the vapor phase [44]. The code uses a semi-implicit numerical scheme to solve these equations within control volumes connected by junctions. Fluid scalar quantities such as pressure, energy, density, and void fraction are averaged over control volumes, while vector quantities like velocities are computed at junctions, representing mass and energy flows. Heat transfer is modeled in one dimension using a staggered mesh for temperature and heat flux calculations. This approach facilitates accurate simulations of pipe walls, heater elements, nuclear fuel pins, and heat exchanger surfaces. Additionally, RELAP5 provides flexibility in selecting convection boundary types to account for various flow field and hydraulic geometry conditions that impact heat transfer coefficients [48].

2.8.1 Nodalization feature

The following general criteria are applied in developing the nodalization:

- The “node to node ratio”, defined as the ratio between two adjacent control volumes, has been maintained below the reference value of 1.25, resulting in a more homogeneous nodalization with reduced possibility of numerical error occurrence;
- The “Slice modelling approach”, which requires same mesh lengths for volumes belonging to different control systems and for heat structures if connected and positioned at the same axial level, has been adopted. This technique has been adopted in particular for the Once Through Steam Generator nodalization: in particular, a vertical segmentation has been performed on the basis of reference selected quotes, chosen to keep the actual design elevations. The axial mesh related to all the OTSG components (tube bundle for the primary side and lower downcomer, lower/upper riser and steam downcomer for the secondary one) has been obtained respecting these reference fixed heights. As a result, the same mesh length (or submultiple) was used for the vertical control volumes belonging to different nodalization regions positioned at the same axial level. This technique improves the capability of the code to reproduce natural circulation. When adopted, fluid properties are evaluated at the same axial elevations for all the nodalization regions, resulting in a proper evaluation of the natural circulation driving force and avoiding an error source on the simulation outcomes.
- Total loop lengths and volumes have been maintained, with some exceptions linked to the low degree of details of some components (i.e, pumps, filters).

2.8.2 Fluids and materials

RELAP5 code requires the user to specify for each system the fluid type, whose properties are stored in an external data file, named tpf + fluid name [49][44]. In case of water, the external data file provided to the code is labeled “tpfh2onew”.

As regards materials involved in heat transfer problems, RELAP5 code requires the user to enter the thermal properties. The required input data consists of two tables collecting the thermal conductivity and heat capacity trends against temperature [49]. The provided properties are used to solve the Fourier’ Law for heat conduction in solid layers [50].

The selected material for both primary and secondary piping and for pressurizer, heaters and condensate tank vessels is AISI 316 [51], since it is applicable at the primary side design temperature (360 °C) and it is also highly wieldable and corrosion resistive [52]. All the components in direct contact with the external environment are equipped with ISOVER insulation in order to reduce heat losses. The insulation thickness is preliminary adopted equal to 10 cm for all the components. The material selected for the OTSG tube bundle is the INCONEL 690 [51], characterized by improved corrosion and erosion resistance. Heating structures have been realized with concentric layers of constantan (internal), ceramic (annular) and alloy 800 (external). The material properties were derived from ASME code [53].

2.8.3 Control systems

The RELAP5 nodalizations can be equipped with control systems that monitor main parameters in order to regulate their evolution with time and facilitate the steady-state operations. Proportional-Integral (P-I) controllers are mostly employed, defined on the following steps:

- Continuous measurement of the "measured variable", which is the parameter to be monitored by the dedicated sensor;
- Definition of the "set-point" as the desired value for the measured variable;
- Calculation of the "error" as the difference between the controlled variable and the set point or vice-versa;
- Definition of the "regulated variable" as the parameter to be regulated as a result of the control system actuation.

The value of the error determines the entity of the system actuation, which depends on the kind of controller adopted. In particular, PI controller operates as:

$$Y = S\left[A_1V_1 + A_2\int_0^t V_1 dt\right]$$

Where:

- Y is the value assumed by the regulated variable in time;
- S is the scaling factor;
- V_1 is the error between the set point and the measured variable;
- A_1 is the proportional parameter;
- A_2 is the integral parameter.

The value of the proportional coefficient depends on the variables involved (i.e., the variable to be measured and the variable to be regulated). Its initial evaluation is approximately performed by considering the ratio between the variation of the regulated variable over the variation of measured variable that determined it. For example, when regulating temperature by varying the mass flow rate, an initial estimate is obtained as the ratio between the maximum variation in flow rate and the corresponding expected maximum variation in temperature. The integral parameter, instead, is in first approximation evaluated according to the Ziegler-Nichols (Z-N) Oscillation Method [54][55]. Both the parameters are then fine-tuned based on the results of simulations.

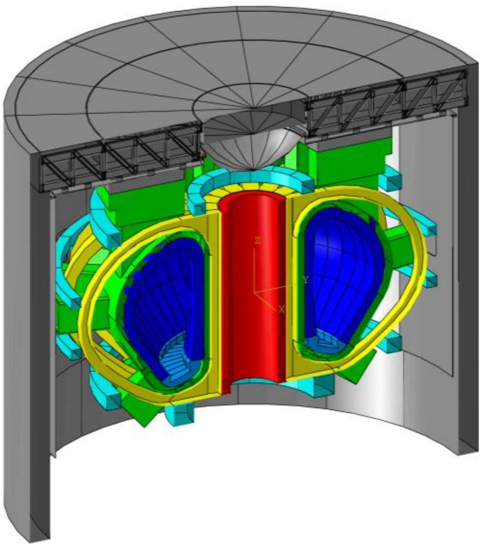

Fig. 2. DEMO reactor [36]

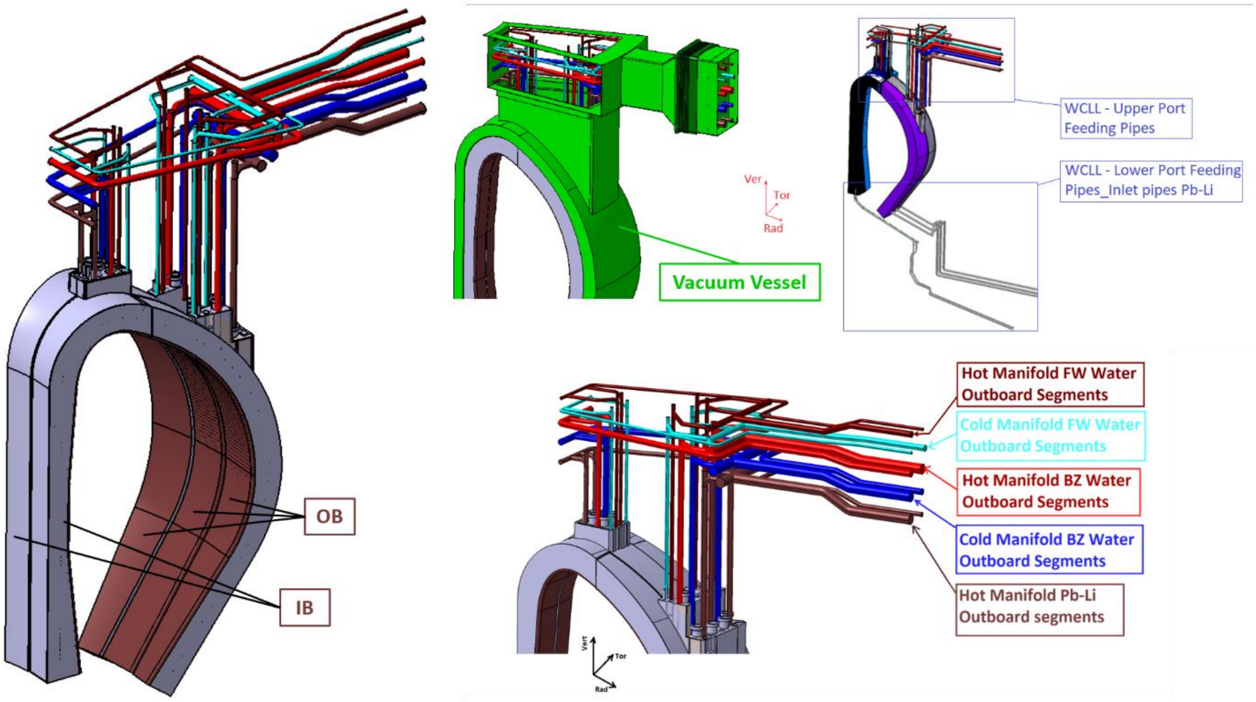

Fig. 3. Architecture of a WCLL BB sector

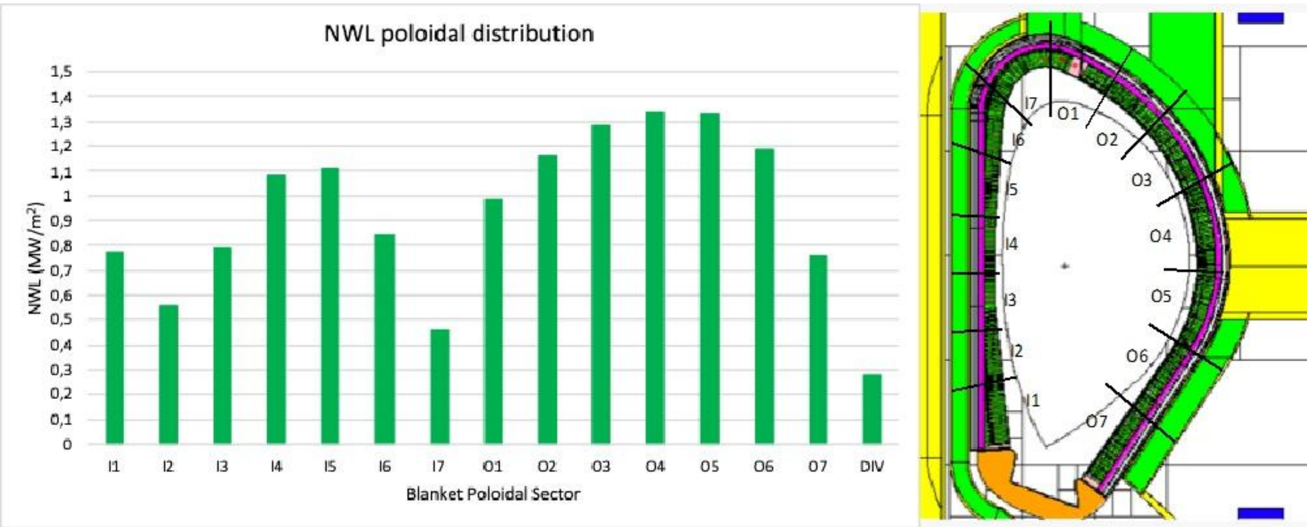

Fig. 4. Neutron Wall Loading normalized poloidal distribution [35]

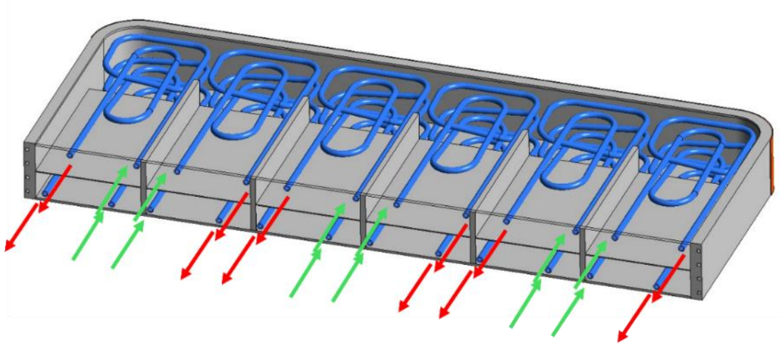

Fig. 5. Helical DWTs for COB slice

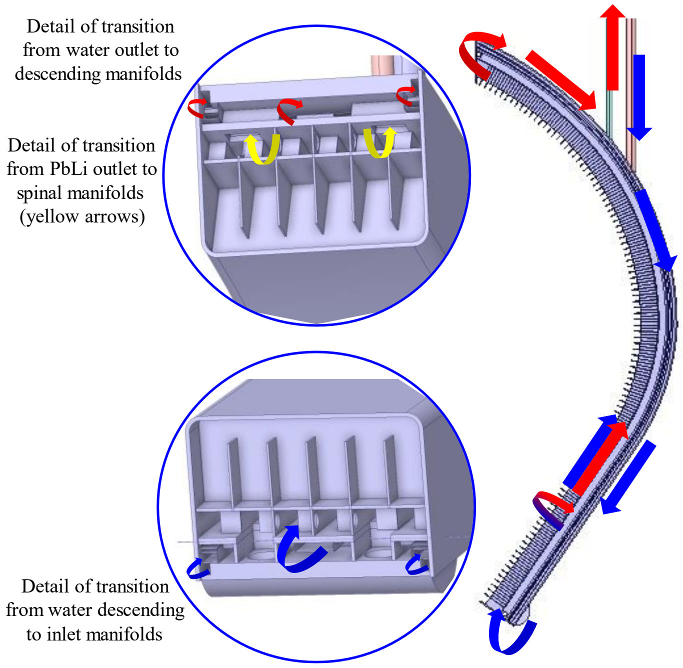

Fig. 6. Detail of fluid paths within the manifolds.

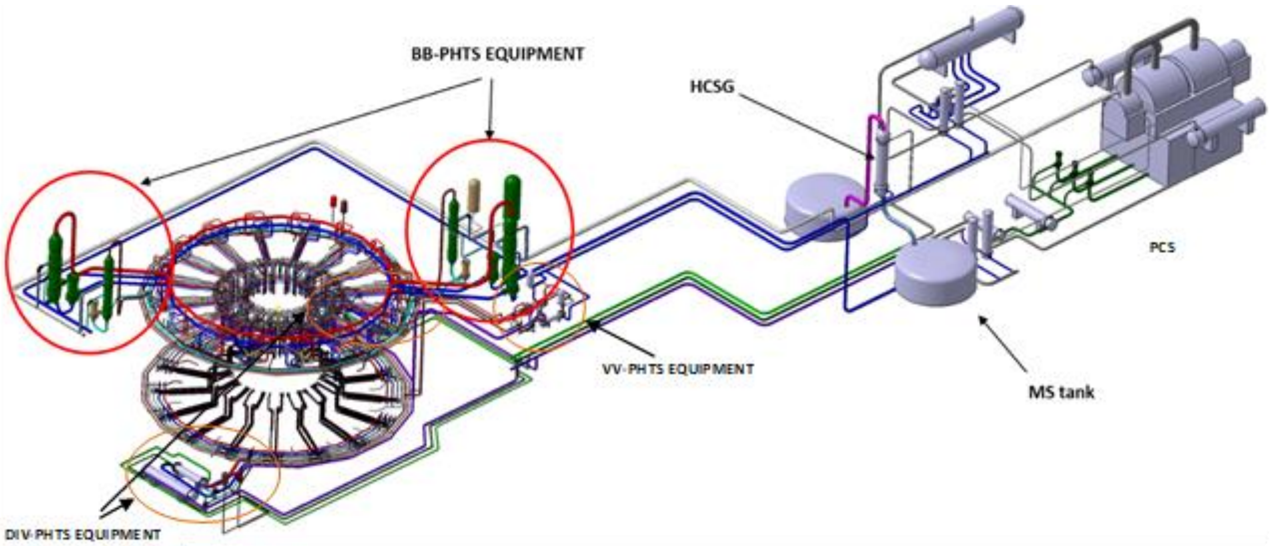

Fig. 7. WCLL BoP reference configuration: direct coupling design with small energy storage system, 3D CAD model.

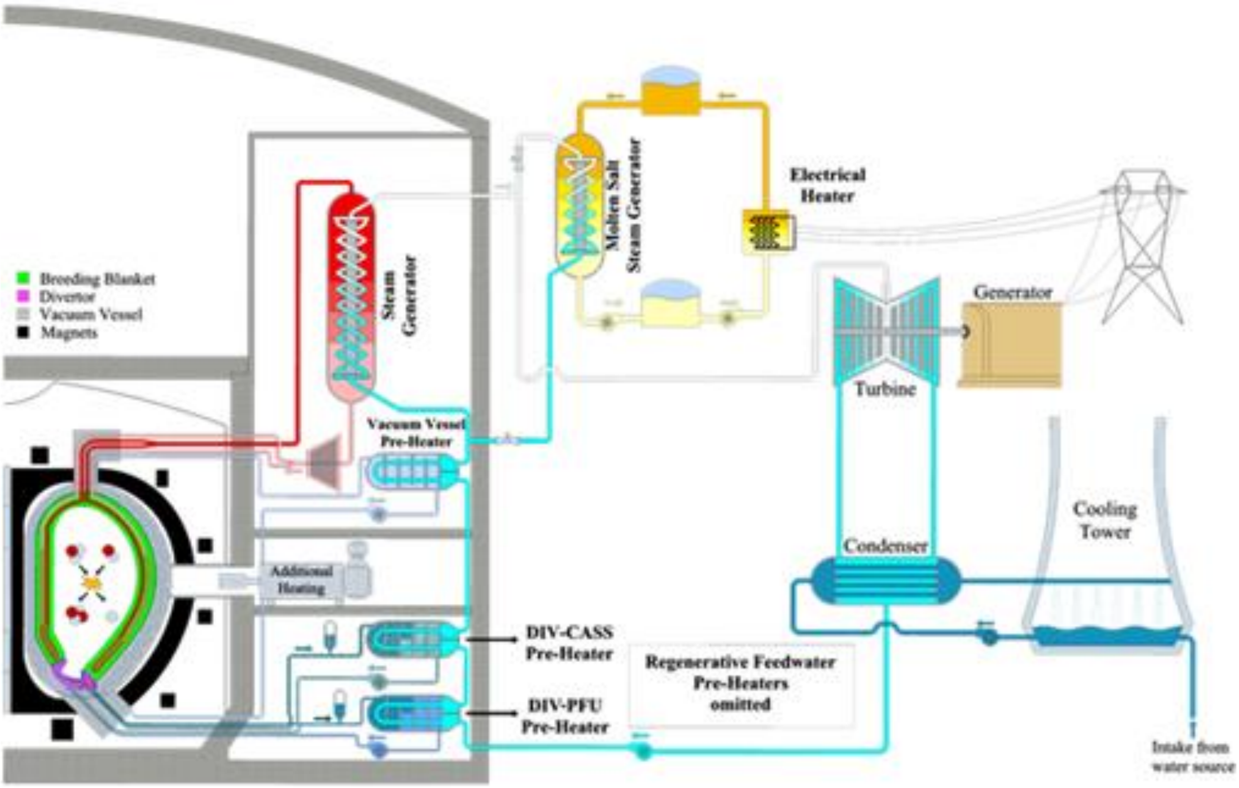

Fig. 8. WCLL DCD BoP simplified layout [37]

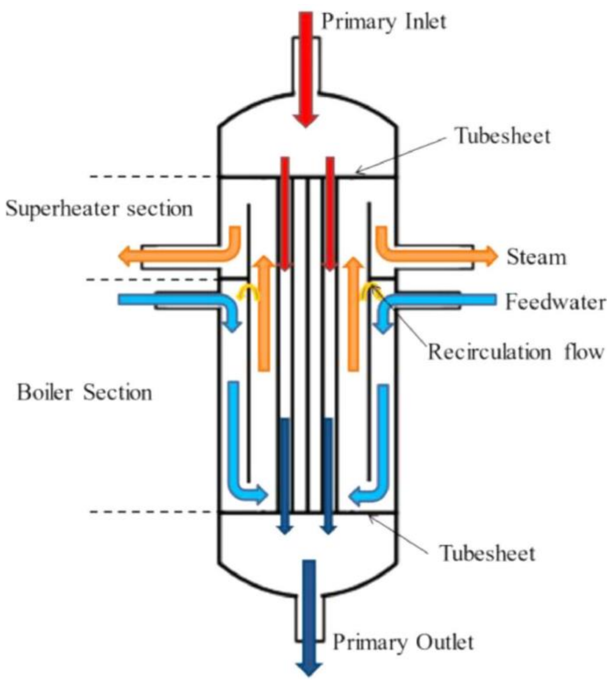

Fig. 9. DEMO WCLL B Once Through Steam Generator concept [43]

3 W-HYDRA: AN EXPERIMENTAL INFRASTRUCTURE FOR TESTING THE WCLL BREEDING BLANKET SYSTEM AND COMPONENTS

The design and development of the European DEMO fusion reactor, particularly the BB and BoP components, require thorough testing and validation to ensure their reliability and performance under operational conditions. This is where the experimental platform W-HYDRA plays a crucial role for the following reasons:

- Design Assessment: Fusion reactors operate in extremely harsh environments, with high temperatures, intense radiation, and cyclic stresses. Testing components, such as the First Wall, under some of these conditions ensures operational safety, minimizing the risk of failure.
- Operational Feasibility and Reliability: The pulsed nature (see Sect. 2.2) of fusion reactors subjects components to dynamic conditions. Traditional designs and operational paradigms, which rely on steady-state conditions, are insufficient to predict the performance and lifespan of components under these dynamic conditions. Experimental validation ensures components can reliably perform under these unique conditions.
- Proven Technology Adoption: Utilizing thoroughly tested technologies (such as valves) ensures components can withstand expected operational conditions, confirming new technologies effectiveness and safety before deployment.
- Comprehensive Testing: Experimental facilities enable detailed testing and characterization of BB and BoP components, including material behavior, durability, and instrumentation performance.
- Safety Assessment: Reproduction postulated accidents provides unavoidable support for the safety evaluation and the licensing process.
- Data for Simulation Models: Experimental data is crucial for validating simulation models predicting component performance under various scenarios, ensuring accuracy and reliability.

To address these challenges, experimental facilities provide a controlled environment where components can be tested under realistic operational scenarios. This includes subjecting materials and systems to simulate fusion reactor conditions to gather data on their behavior, performance limits, and failure mechanisms. The insights gained from these experiments are essential for refining the design, improving the robustness, and ensuring the safety of the breeding blanket and associated systems. Moreover, the validation of simulation codes and models through experimental data is another crucial aspect facilitated by these platforms. Accurate models are necessary to predict the behavior of the WCLL breeding blanket under various operational conditions, and experimental validation ensures these models are reliable and reflective of real-world performance.

W-HYDRA [56] is a multipurpose experimental platform designed to support the research and development activities for the WCLL BB and BoP concepts, with the primary aim of characterizing and validating both the components and the instruments to be adopted. Its construction is envisaged at the ENEA R.C. of Brasimone and it comprises three distinct experimental facilities (Fig. 10), each targeting specific aspects of the DEMO BB, the ITER TBM, and the DEMO BoP of the WCLL BB concept. These facilities are:

- **STEAM**, W-HYDRA high-power branch: A facility aimed at testing steam generator components and systems, critical for the BoP operations in the fusion reactor. In particular, the objective of the water-water SG campaign is to demonstrate the capability of the SG to perform as intended during the DEMO period, currently characterized by the alternation of pulses, dwell periods and corresponding transitions. These phases are exactly the conditions addressed by the planned experimental campaign to achieve the stated general objective.

- **Water Loop** (**WL**), W-HYDRA low-power branch: Designed to investigate the thermal-hydraulic performance and material behavior under water cooling conditions typical of the WCLL BB. Specifically, it serves as a versatile bed for studying various phenomena and components, including the manifold and the First Wall, testing multiple test sections or mock-ups. Additionally, the WL provides a full-scale platform for the test of the WCS of the ITER WCLL TBM. This includes evaluating the overall circuit performances under nominal and accidental conditions, testing specific components and procedures, collecting significant data for the validation of numerical codes and safety analysis models and training operators. The WL also enables the assessment of the thermal-hydraulic and thermo-mechanical performance of components exposed to high heat fluxes, such as plasma facing components.
- **LIFUS5/Mod4**: This PbLi facility investigates the interaction between PbLi and water, a critical safety concern for the WCLL BB/TBM. It simulates in-box Loss Of Coolant Accidents (LOCA) by reproducing scenarios involving the rupture of a cooling tube in PbLi.

These integrated facilities provide a comprehensive testing environment to simulate realistic operational scenarios of fusion reactors, gather critical data on component behavior, performance limits, and failure mechanisms. This data is essential for refining designs, improving robustness, and ensuring the safety and reliability of the breeding blanket and associated systems. Moreover, the experimental results will support the validation of simulation models, ensuring they accurately reflect real-world performance and predict the behavior of the WCLL breeding blanket under various operational conditions.

W-HYDRA comprises several key circuits and test sections, each contributing to its robust experimental capabilities:

- **Loops** (or, equivalently referred to as **sides**):
    - **W-HYDRA primary loop**, that can be operated either as STEAM primary loop or WL primary loop, is a closed water loop that replicates the thermodynamic conditions of PHTS in ITER and DEMO (i.e., 295-328°C at 15.5 MPa). This circuit is equipped with isolation valves allowing for the non-simultaneous operation of the loop under either STEAM primary or Water Loop primary conditions. In the WL configuration, non-simultaneously operated test sections are placed within a vacuum chamber, where the presence of an electron beam gun (EBG) reproduces the heat flux generated by the plasma to simulate its effect on WCLL BB components mock-ups. This EB gun can deliver a nominal power of 0.5 MW/m^2 on an area of 0.8 m^2 and up to 5 MW/m^2 on around 10% of the mock-up surface in short transient.
    - **STEAM secondary loop** is thermally coupled with the W-HYDRA primary loop when the Test Section 1 is operated. It is a closed loop working with two phase fluid (water/steam) that reproduces the DEMO PCS thermal hydraulic conditions (i.e., 238-300°C, 6.4 MPa) at the test section. It is equipped with air coolers operating at 2.5 MPa acting as the steam generator mock-up heat sink.
    - **Water Loop secondary loop** is thermally coupled with the W-HYDRA primary loop and with the Water Loop tertiary loop by means of two dedicated heat exchangers. It uses single-phase liquid water at 7.0 MPa with temperature ranging from 132.4 to 240 °C.
    - **Water Loop tertiary loop** is thermally coupled with the WL secondary loop, and being equipped with a cooling tower, it is the WL facility heat sink (i.e., 50-80°C at 0.6 MPa).

- **Vacuum Chamber loop** (**VC loop**) is the cooling system devoted to the vacuum chamber internal walls. In fact, when a target (i.e., a test section) is irradiated within the chamber, part of the heat flux produced by the electron beam gun is reflected towards the walls, that therefore require a dedicated cooling system.

- **Electron Beam Gun loop** (**EBG loop**) is the cooling loop devoted to the EBG vacuum pumps, EBG control cabinets and EBG power exhaust. It is constituted by two parallel loops: EBG 1 is in charge of the cooling of the low-mass flow utilities such as the vacuum pumps and the EBG cabinets, while EBG 2 cools the high-mass flow utilities like the transformer and the EBG itself.

- **LIFUS5/Mod4 loop** adopts PbLi eutectic alloy as interacting medium with the water from the W-HYDRA primary loop. This facility is operated with the TS4.

- **Auxiliary loop**: fill&drain, Demineralized water system (Demi water or Volume Control system, VCS) and compressed air system are installed in the infrastructure.

- **Test sections:**

  - **Test Section 1** (**TS1**) is the DEMO WCLL BB PHTS steam generator mock-up (see Sect. 4). When operated, this component thermally couples the W-HYDRA primary loop (flowing tube-side) and the STEAM secondary loop (flowing shell-side).

  - **Test Section 2** (**TS2**) is the experimental mock-up of the manifold system installed in the Central OutBoard (COB) segment devoted to the WCLL BZ. It is installed on the W-HYDRA primary loop, and it exploits the steam generator as heat exchanger with the STEAM secondary loop acting as heat sink.

  - **Test Section 3** (**TS3**) is the mock-up of the WCLL FW, placed within the vacuum chamber to simulate the effect of the plasma irradiation. It is hydraulically connected to the W-HYDRA primary loop. Being the plasma heat flux non-uniform along the poloidal coordinate, both the mock-up of the Equatorial FW (TS3) and the mock-up of the Non-Equatorial FW (TS3 bis) will be investigated.

  - **Test Section 4** (**TS4**) is a mock-up of one or more Breeding Units (BUs) of the WCLL BB or of the TBM, where the tube rupture simulating the in-box LOCA occurs. It is installed on the W-HYDRA primary loop in the WL configuration and, when operated, TS4 is also linked to LIFUS5/Mod4 facility.

  - **Test Section 5** (**TS5**) is the mock-up of the WCLL BB TBM to be installed in the ITER reactor. It can be installed within the W-HYDRA primary loop and placed inside the vacuum chamber.

  - From **Test Section 6** to **Test Section 15** are eligible mock-ups characterized by different thermodynamic operative conditions, preliminary investigated to define the design parameters of the loops (Tab. 7).

The main cooling system design conditions are listed in Tab. 1.

Tab. 3 collects the nominal operative conditions expected from the systems involved on the operation of TS1 to TS5, while thermodynamic conditions of both envisaged (TS1 to TS5) and eligible (TS 7 to TS 15) are listed in Tab. 7

3.1 W-HYDRA primary loop

The W-HYDRA primary loop is a medium-scale facility designed with several essential objectives. It plays a critical role in supporting and enhancing the design study of the Steam Generator of the DEMO BB PHTS through targeted R&D. Additionally, it serves as a testing ground for specific components and their associated operating procedures, ensuring that these elements perform as expected under operational conditions. The facility also provides a versatile platform for testing the WCLL BB, allowing for the examination of various phenomena and components such as manifolds and the First Wall through multiple test sections and mock-ups. Furthermore, the W-HYDRA primary loop is instrumental in acquiring significant data to validate numerical codes and models used in system safety analysis. In addition, it facilitates the testing of the thermal-hydraulic and thermo-mechanical performance of other components exposed to high heat fluxes, including plasma-facing components.

Moreover, the W-HYDRA primary loop, in conjunction with the LIFUS5/Mod4 facilities, will serve as the first separate effect test facility for studying the water/PbLi reaction in a WCLL-representative geometry. Experimental tests in LIFUS5/Mod4 will help extend the validation of numerical models using different codes (Simmer III and IV, RELAP5) to geometries relevant to WCLL.

As previously highlighted, STEAM and WL share the same primary loop, namely the W-HYDRA primary loop. Manual valves enable the W-HYDRA primary loop to operate in two distinct configurations, though not simultaneously. In the STEAM mode, also known as high-power mode, the loop is configured to test the Steam Generator (TS1) or any test section, such as the manifold, requiring high power (i.e. larger than 800kW) or high flow (i.e. larger than 5 kg/s). Then, the WL mode, or low-power mode, can be used for other experimental needs, such as the First Wall test section (TS3) or the PbLi-water interaction tests (TS4). In this configuration the facility is operated using only single-phase systems, which are simpler and safer to be operated at low-power condition. This architecture will allow the installation of different test sections, for a more efficient execution of the experiments.

W-HYDRA primary loop PFD is shown in Fig. 11. Fluid paths are explained in Sect. 3.2.1 (STEAM configuration) and in Sect. 3.3.1 (WL configuration).

The main components of the primary loop are:

- Test Section 1 (TS1): heat exchanger mock-up integrated inside the primary loop. It is placed between W-HYDRA primary loop and STEAM secondary loop. More details are reported in Sect. 7
- Heat exchanger (HX-WHP-001): counter-current heat exchanger to transfer heat to the WL secondary loop.
- Filter (FI-WCP-150): installed on the cold leg upstream the main circulation pumps.
- High-mass flow circulation pump (PU-SCP-001): a centrifugal pump installed on the cold leg of the circuit capable of guaranteeing a maximum flow rate of 20 kg/s.
- Low-mass flow circulation pump (PU-WCP-001): a centrifugal pump installed on the cold leg of the circuit capable of guaranteeing a maximum flow rate of 5 kg/s.
- Electrical heaters (HT-WHP-101 & HT-SHP-101): tube and shell heater assembly made up of various electric rods with a nominal heat power to the fluid of 3100 kW. HT-WHP-101 is also referred to as “WL heater”, while HT-SHP-101 is also labeled as “STEAM heater”. STEAM heater is always intercepted in WL configuration, while both WL and STEAM heaters are usually on operation in STEAM configuration.

- Pressurizer (SE-WPP-001): pressurized tank located in the highest part of the hot leg of the loop. The component contains water inside at saturated condition and is half filled with liquid water to act as an elastic member of the circuit to maintain the correct nominal pressure of 15.5 MPa.
- Relief tank (SE-WRT-004): adopted for the depressurization of the pressurizer SE-WPP-001 thanks to a PORV line (PP-WRT-002).

It is worth clarifying that, even if STEAM and WL share the same primary loop, hot leg and cold leg do not completely coincide. This is because the primary power source is not the same for all test sections. Specifically, in the configuration where the steam generator is tested, the power source consists of the two electric heaters. In the manifold configuration, a single electric heater provides the necessary power to compensate for thermal losses. When other test sections located inside the vacuum chamber are tested, the thermal source is the electron beam gun, while the heater is either turned off or used only to achieve the steady state test conditions or compensate heat losses.

In the first two cases, the hot leg begins downstream of the electric heaters. However, in the case of other test sections, the hot leg starts downstream of the vacuum chamber. For this reason, the distinction between hot leg and cold leg is not adopted for the primary loop of W-HYDRA.

3.2 STEAM facility: the W-HYDRA high-power branch

STEAM is a 3.1 MW water facility conceived to investigate the impact of the rapid load variations typical of fusion tokamaks on the steam generator design envisioned for DEMO [57] [58]. The experimental setup will host two loops thermally coupled by the DEMO SG mock-up (furtherly detailed and investigated in Sect. 4). They will reproduce the thermal hydraulic conditions of pressure and temperatures characterizing the DEMO BB PHTS and PCS. The facility main characteristics are listed in Tab. 4.

The strategic objective of the STEAM facility is to establish an experimental infrastructure capable of investigating the WCLL DEMO BoP, from an experimental standpoint. The general goal is to support and complement the design study of critical BoP components, specifically the Steam Generators of the DEMO BB PHTS through focused R&D. Despite the WCLL BB PHTS incorporating components of well-proven technology used in Nuclear (Fission) Power Plants, including the water-water SG, the unconventional operation of the system—due to the pulsating nature of the plasma-generated thermal power—poses unique challenges to the functional feasibility of this component in the reference BoP configuration considered (i.e., the WCLL BB BOP with direct coupling [37]). Therefore, it is deemed critical and requires thorough design and validation.

The objective of the STEAM water-water test campaign is to demonstrate the SG capability to perform as intended during the DEMO period, which, according to the current conceptual design, involves a 2-hour pulse at full power followed by a 10-minute dwell at decay power [59]. This scenario outlines three operational phases of the SG: the full power phase during the pulse period, the low (decay) power phase during the dwell period, and the transient phase during the transition from pulse to dwell operation. These phases are the central focus of the planned experimental campaign aimed at achieving the overall objective.

During the High-Power Phase, tests will simulate the component operation under full power conditions. Although no operational issues are anticipated for the SG in this mode, it is crucial to demonstrate the adequacy of the design and the reliability of numerical simulations.

In the Low-Power Phase, the campaign will involve tests simulating the steam generator operation during dwell conditions. The main emphasis will be on assessing the thermal-hydraulic stability of the component operation, its overall performance, and the effectiveness of the adopted regulation strategy. Testing potential alternatives is also anticipated during this phase, which is pivotal in demonstrating the BoP reference concept since the SG power duty is significantly lower than the minimum values recommended by standard practice.

Lastly, the Pulsed-Dwell Phase aims to evaluate the SG operation during the transition from pulse to dwell, focusing on the component performance and the appropriateness of the control strategy. Additionally, this phase will include tests to identify the operational thermal-hydraulic parameters necessary for ensuring safe, stable, and efficient SG performance. Completing this phase will substantiate the functional feasibility of the SG within the WCLL BB BoP architecture in the DEMO pulsating scenario.

The STEAM facility is designed to meet a set of functional requirements that ensure its relevance and effectiveness in addressing the challenges of pulsed operation in the DEMO steam generator. These requirements focus on achieving accurate thermal-hydraulic characterization at the component level:

- Thermal-Hydraulic Representativeness: Given that the primary objective of the STEAM facility is to characterize the DEMO steam generator at the component level, it is essential to ensure that the boundary conditions provided to the steam generator mock-up accurately represent the thermal-hydraulic conditions of the full-scale DEMO component.
- Component Representativeness: The mock-up of the DEMO steam generator tested within STEAM must preserve the key characteristics of the full-scale component, avoiding the introduction of thermal-hydraulic distortions that could compromise the validity of the experimental results. This includes maintaining geometric similarity, material properties, and operational parameters to ensure that the test results can be reliably scaled to the DEMO application.
- Safety and Control Systems: The facility must be equipped with safety and control systems analogous to those used in the full-scale DEMO steam generator. This ensures that operational behavior under both nominal and off-normal conditions is accurately reproduced, allowing for the evaluation of control strategies and safety protocols in a controlled environment.
- Instrumentation for Data Collection: STEAM must include advanced instrumentation capable of acquiring high-fidelity data for validating thermal-hydraulic and safety codes, encompassing both system-level simulations and detailed CFD models. The instrumentation should capture critical parameters such as temperature, pressure, mass flow rates, and heat flux to support comprehensive analysis and model validation.
- Future Upgrades: The facility design must anticipate future upgrades to accommodate evolving research needs while preserving the thermal-hydraulic representativeness of the boundary conditions provided to the steam generator mock-up. This adaptability ensures that the STEAM facility remains a relevant and cutting-edge tool for fusion research as requirements and objectives evolve.

3.2.1 STEAM primary loop

W-HYDRA primary loop operated in STEAM configuration constitutes the STEAM primary loop. It is a closed loop designed to mirror the thermodynamic conditions of the DEMO WCLL BB PHTS. It maintains a nominal pressure of 15.5 MPa, with the SG ensuring inlet and outlet temperatures of 328°C and 295°C respectively, while facilitating the exchange of a nominal thermal power of 3.1 MW. To effectively manage this thermal load under standard conditions, a water mass flow rate of 16.05 kg/s is necessitated. The loop nominal parameters are collected in Tab. 5.

With reference to Fig. 11, fluid is propelled by the high mass flow circulation pump (PU-SCP-001), being small mass flow circulation pump intercepted. In the cold leg, fluid flows through the filter (FI-WCP-150), ensuring the removal of the impurities. The flow is then symmetrically distributed between the two electric heaters, each with a power of 1.55 MW (HT-WHP-101 and HT-SHP-101), where it is heated from 295°C to 328°C. Fluid is then routed towards the STEAM hot leg (Vacuum Chamber line is intercepted by means of VM-WHP-160 and VM-WHP-170 valves). It finally reaches the Steam Generator (TS-TS1), where thermal power is transferred to the secondary loop through the tube bundle, determining the temperature to drop from 328 to 295 °C, before being routed back to the pump. The pressurizer (SE-WPP-001), located along the uppermost leg of the loop (hot leg), maintains the water circuit pressure at the rated value of 15.5 MPa. It contains a mixture of liquid water and steam at saturation conditions and regulates pressure via a spray line injecting cold water from the cold leg and an electrical heater (HT-SHT-102).

W-HYDRA primary loop P&ID is shown in Fig. 12.

3.2.2 STEAM secondary loop

STEAM secondary loop consists of a closed, demineralized, two-phase flow loop serving as final heat sink for the removal of 3100 kW of maximum power. Being an experimental facility not connected to the electrical grid, the steam produced within the SG does not expand in a turbine but is instead condensed through Air Coolers (ACs), which employ forced air convection to cool the working fluid. The cooling process is divided into two separate components: the de-superheating and condensation air cooler (divided into four parallel modules), referred to as A.C.1, and the sub-cooling module, labeled as A.C.2.

The STEAM facility is designed to investigate the operation of the OTSG at various power levels and mass flow rates. To ensure accurate performance across all power phases, the de-superheating air cooler is divided into four modules, each receiving one-fourth of the total mass flow through four 2” lines originating from a 5” steam line. Each module is equipped with two valves to regulate mass flow and allow module interception.

Referring to Fig. 13, subcooled fluid at 210°C is routed by the pump (PU-SCS-001) towards the electric heater (HT-SCS-002) that heats it up to 238°C. It enters the SG (TS-TS1), the heat source for this loop, where it absorbs 3.1 MW from the primary side, raising its temperature from 238°C to over 300°C. A lamination valve (VP-SHS-R01) on the STEAM line regulates the OTSG outlet pressure by performing an isenthalpic transformation, reducing the pressure from 6.4 MPa to 2.5 MPa. This decouples the SG from the rest of the loop, preventing instability propagation towards the test section. Under nominal conditions, the temperature across the component drops from 300°C to 245.4°C.

The four parallel modules of A.C.1 (HX-SHS-001 to HX-SHS-004) handle the de-superheating and condensation of the steam produced within the SG, reducing the temperature from 245.4°C to 224°C. The liquid in saturation conditions collected at the A.C.1 outlet is stored inside the condensate tank (SE-SCS-001) which maintains loop pressure through pressure regulation systems (electric heaters, relief valve) and a water level control connected to a fill and bleed system. Fluid is then routed to A.C.2 (HX-SCS-001), tasked with the purpose of cooling it from 224 to 210°C, guaranteeing that no cavitation occurs at the pump suction. After purification by a filter (FI-SCS-001), the fluid returns to the pump. The loop nominal parameters are collected in Tab. 6.

The STEAM secondary loop can be divided into two parts based on the operative thermal-hydraulic conditions: a high-pressure section (HP section) and a low-pressure section (LP section). The HP section, operating at a nominal pressure of 6.4 MPa, is dedicated to ensuring the correct operation of TS1. An electric heater is used to restore the temperature required at the mock-up inlet, which ranges between 210°C and 238°C. Within this section, the steam generator fluid thermodynamic conditions are aligned with those of the DEMO PCS, where the fluid experiences a temperature rise from 238°C to over 300°C at 6.4 MPa, due to the heat exchange with the primary loop through the tube bundle structure.

On the other hand, the LP section, operating at 2.5 MPa, is responsible for dissipating the heat removed from the primary loop within TS1. To achieve this, air coolers are installed to cool down the fluid from 245.4°C to 210°C within this section. A lamination valve performs the necessary pressure reduction at the test section outlet, while a pump restores the pressure upstream of the electrical heater.

STEAM secondary loop main instrumentation is shown in the P&ID in Fig. 14.

3.3 Water Loop: the W-HYDRA low-power branch

Water Loop, the "low power branch" of the W-HYDRA platform, serves as a versatile and comprehensive Integral Test Facility specifically designed for the Water Cooling System (WCS) of the ITER WCLL TBM. It replicates the functions, layout, and components of the WCS to enable full-scale thermal-hydraulic and structural testing of WCLL TBM mock-ups and their ancillary systems.

To ensure its effectiveness and relevance, the Water Loop is designed to meet the following functional requirements:

- Thermal-Hydraulic Representativeness: The facility must replicate the WCS thermal-hydraulic conditions, including operating pressure, temperature, and mass flow rates.
- Behavioral Representativeness: It must maintain similar distances between components, elevations, and pressure drops to accurately represent the WCS thermal-hydraulic behavior.
- Safety and Control Systems: The WL must be equipped with the same type of safety and control systems as the WCS to reproduce its operational behavior.
- Instrumentation for Data Collection: It must include advanced instrumentation capable of collecting data for the validation of thermal-hydraulic and safety codes, including both system codes and CFD models.
- Future Upgrades: The design must anticipate future upgrades to adapt to evolving research needs.
- Compatibility with Test Sections: The WL should allow for connections with various test sections, such as LIFUS5/Mod4, the Vacuum Chamber, and WCLL BB test sections, ensuring versatility in experimental setups.

The primary objective of Water Loop is to characterize specific components, assess overall circuit performance, evaluate operational procedures, and gather essential data for validating models and numerical codes crucial for fusion energy research. Its flexibility allows for thermal-hydraulic and thermo-mechanical testing of various BB sub-components using specially designed mock-ups such as the First Wall (FW), Breeding Zone (BZ), and manifolds.

This facility plays a critical role in advancing fusion energy research by simulating also the operational conditions comparable to those expected in ITER and future DEMO reactors. It is configured as a three-loop facility capable of delivering water at Pressurized Water Reactor (PWR) conditions to test sections placed within a vacuum chamber. Operating at 15.5 MPa and 295°C, it meets the thermal-hydraulic requirements of WCLL BB and TBM. The facility capability extends to coupling with the LIFUS5/Mod4 facility to investigate water/PbLi reactions.

A simplified scheme of the facility is shown in Fig. 19. PFDs of the three loops are illustrated in Fig. 11, Fig. 15 and Fig. 17.

To replicate the heat flux experienced by both the TBM and blanket FW, the WL features an electron beam (EB) gun installed in the dedicated vacuum chamber. This EB gun can de-liver a nominal power of 0.5 MW/m² on an area of 0.8 m² and up to 5 MW/m² on around 10% of the mock-up surface in short transient. This infrastructure will be used to reproduce the heat flux due to plasma radiation during the flat-top operation. Moreover, the presence of an EB gun facilitates the investigation of various effects, such as thermal cycling fatigue, as well as localized overheating of FW regions, assessing the response of coolant, structural materials, and armor materials.

The power provided by the EBG depends on the test section being investigated. The facility is designed to operate in three distinct configurations to meet the specific requirements of each test section. These configurations manage the flow of primary, secondary, and tertiary fluids differently to achieve the desired thermal conditions.

In the **standard configuration**, the primary fluid, shown in red in Fig. 19, is pumped towards an electrical heater. This heater compensates for heat losses and ensures the required temperature at the test section inlet. The heat from the EBG is then transferred within the HS-WHP-001 (P-S HX) from the primary fluid to the secondary fluid. The secondary fluid, depicted in blue in Fig. 19, absorbs heat from the primary side in the P-S HX and then flows on the shell side of the HX-WHS-001 (ECO) HX, where it preheats the tube-side fluid. Subsequently, it is further cooled by the tertiary fluid within the HX-WCS-001 (S-T HX). The cooled secondary fluid is then pumped back towards the tube side of the ECO for preheating. The tertiary fluid, represented in green in Fig. 19, acts as the ultimate heat sink for the facility. It is circulated towards the S-T HX, where it absorbs heat by cooling the secondary fluid, and is then cooled by a cooling tower.

In the **full bypass of the Economizer configuration**, the secondary fluid bypasses the ECO completely. Instead of preheating the tube-side fluid in the ECO, the hot secondary fluid moves directly to the S-T HX, where it is cooled by the tertiary fluid. This configuration facilitates a more rapid transfer of heat to the tertiary loop, which is then dissipated through the cooling tower, making it more suitable for test sections with lower temperatures.

The **direct primary-tertiary heat exchange mode** involves completely closing off the secondary loop. In this mode, the primary fluid exchanges heat directly with the tertiary fluid. The tertiary fluid flows on the shell side of the HS-WHP-001 (P-S HX) and absorbs heat directly from the primary fluid, while the HX-WCS-001 (S-T HX) remains closed. The absorbed heat in the tertiary fluid is then dissipated through the cooling tower, allowing for a more straightforward heat dissipation process, particularly useful for test sections operated at very low temperatures.

These versatile configurations enable the Water Loop facility to adapt to different test conditions and thermal management requirements, ensuring optimal performance across a range of scenarios. Details regarding the design phase of the facility loop and heat exchangers are collected in Sect. 6.

3.3.1 Water Loop primary side

W-HYDRA primary loop operated in Water Loop configuration constitutes the Water Loop primary loop. It is a closed loop designed to replicate the thermodynamic conditions required for the DEMO WCLL TBM and for the rest of the test sections envisaged (see Sect. 3.3.4).

In the TBM and FW configuration, the Electron Beam Gun within the chamber provides the necessary heat flux to elevate the test section outlet temperatures to 328°C, heating the fluid from 295°C. Meanwhile, a heat exchanger efficiently regulates the primary coolant temperature, cooling it from 328°C to 295°C to ensure the thermal cycle integrity and operational stability.

Power, temperatures and correspondent mass flow rates differ for each test sections and are listed in Tab. 7

With reference to Fig. 11, fluid is routed by the small mass flow circulation pump (PU-WCP-001), being the high mass flow circulation pump intercepted. It is then directed to the HT-WHP-101 electrical heater. In this configuration, the HT-SHP-101 heater is off and intercepted by valves, meaning the fluid flows through only one of the two heaters, allowing a maximum power of 1.55 MW to be provided. This heater can either pre-heat the fluid directed to the test section or compensate for heat losses to maintain the required temperature at the TS inlet.

Fluid is then directed to the Test Section, that can be placed within the vacuum chamber, where it is irradiated by the EBG. Vacuum chamber bypass line is intercepted, keeping the VM-SHP-160 closed. Fluid reaches the P-S HX where it is cooled down by the secondary loop and is finally purified by the filter (FI-WCP-150). P-S HX is equipped with a bypass line for the temperature regulation.

The pressurizer (SE-WPP-001) is connected to the hot leg and can work either in the STEAM or in the Water Loop configuration.

W-HYDRA primary loop P&ID is shown in Fig. 12.

3.3.2 Water Loop secondary side

The secondary fluid plays a crucial role in the thermal management process within the Water Loop system. Initially, it removes heat from the primary side within the P-S HX, significantly increasing its temperature.

After being heated in the P-S HX, the secondary fluid flows on the shell side of the economizer, where it preheats the tube-side fluid. This preheating process improves the system efficiency, as it ensures that the residual heat from the secondary fluid is effectively utilized before further cooling.

Fluid then moves toward the S-T HX, where it transfers its absorbed heat to the tertiary fluid, resulting in a significant temperature drop. The now-cooled secondary fluid is then pumped back toward the tube side of the ECO to re-start the cycle, where it is pre-heated by the shell-side fluid.

Additionally, the secondary side (SS) is equipped with a pressurizer, connected to the loop in the section downstream the P-S HX, which is the hottest and highest part of the circuit. This pressurizer is crucial for maintaining the system pressure within optimal levels, ensuring safe and efficient operation.

The Economizer component features two bypass lines, the first one for mass flow regulation during normal operation, the second allowing for the complete bypass of the ECO, diverting the entire flow of the secondary fluid around it. These bypass lines provide additional flexibility and control over the thermal management process, enabling adjustments to be made based on operational requirements.

3.3.3 Water Loop tertiary side

The tertiary loop operates as an open circuit designed to discharge the heat generated within the W-HYDRA primary loop to the final heat sink, represented by the cooling tower (HX-WHT-001). The WL tertiary loop can interface with the WL secondary loop via the HX-WHS-001 heat exchanger or directly with the W-HYDRA primary loop via the HX-WHP-001, depending on the required operating conditions. The maximum power capacity of the WL tertiary loop is 800 kW.

The WL tertiary circuit is segmented into two subsystems operating under different thermal-hydraulic conditions: a high-pressure system (HP-system) and a low-pressure system (LP-system), with nominal pressures of 0.6 MPa and 0.1 MPa, respectively. The nominal temperature range for these systems is 20-80°C.

The HP-System main task is to remove heat from the heat exchangers. It draws water from a low-temperature vessel (SE-WCT-001), sends it towards the heat exchangers and then transfers it to a high-temperature vessel (SE-WHT-001). In the high-pressure system fluid encounters a filter (FI-WCT-001), a circulation pump (PU-WCT-001), and a heat exchanger, which can either be the shell-side of the HX-WHP-001 or the shell-side of HX-WHS-001, depending on the configuration, before reaching the high-temperature vessel. The system uses ball valves to switch between heat exchangers as needed, and the pump flow rate is adjusted according to the specific system requirements.

The LP-System dissipates the heat removed by the HP-System in the cooling tower. It draws water from the high-temperature vessel and conducts it to the low-temperature vessel. This system includes a circulation pump (PI-WCT-001), a three-way regulation valve (VP-WHT-R01), and the cooling tower (HX-WHT-001). The circulation pump operates at a constant volumetric flow rate of 85 m³/h. The three-way valve regulates the flow rate into the cooling tower, thus managing the amount of power dissipated to maintain the correct temperature in the low-temperature vessel that feeds the heat exchangers.

The WL tertiary loop operates in two main configurations: interfacing the secondary loop in the S-T HX or interfacing the primary loop in the P-S HX. Either way, tertiary fluid flows shells-side.

3.3.4 Water Loop Test Sections

The WL facility is designed to accommodate a range of thermal and hydraulic (T/H) conditions and power levels. This adaptability allows for the testing of various components, such as the manifold, equatorial First Wall, non-equatorial First Wall, TBM. To facilitate future refurbishments, other eligible test sections characterized by different powers and T/H conditions were investigated. The manifold is engineered to operate under isothermal conditions, while the other components are placed within the vacuum chamber and subjected to heating by an electron beam gun. The main thermal hydraulic parameter of

Manifold (TS 2)

The manifold functions as a scaled-down test section, replicating an Outboard Segment manifold of the WCLL BB for the European DEMO. Its primary goal is to study the fluid hydraulic behavior under different operational conditions. It specifically aims to verify the flow distribution across various breeding units within the full-scale manifold and to validate the computational tools used for design and analysis.

The manifold is designed to operate under isothermal conditions at the primary loop maximum temperature (i.e., 328 °C). The nominal primary side (PS) mass flow rate is 16.05 kg/s, consequently, the flow will be directed to the STEAM Steam Generator since the WL P-S HX tubes are designed for lower mass flow rates. Fluid in the SG undergoes the temperature difference of 328-295 °C thanks to the thermal exchange with the secondary side that works in the STEAM nominal conditions. Thermal power is restored thanks to the electrical heater.

Equatorial and Non-Equatorial FW (TS 3 and TS 3 bis)

Recognizing the complexity of the actual First Wall design, a simplified structure was selected to balance manufacturing feasibility and cost-effectiveness. A flat design was chosen for the Mock-Up (MU) to simulate a full-scale section of the plasma-facing FW. The MU serves as a platform for experimental investigations into the thermal, hydraulic, and structural behaviors of the current FW design under significant heat loads expected during operational conditions.

To replicate the thermal loads experienced in the DEMO, the MU is heated using both an Electron Beam (EB) gun, simulating the heat flux from the plasma, and heating cables, mimicking the thermal flux provided by the BB lithium lead to the fluid. This approach is consistent for both the equatorial and non-equatorial FW configurations.

Test Blanket Module, TBM (TS 5)

Test Blanket Modules (TBMs) are crucial components of the ITER experimental setup. They are specifically designed to test and validate the performance of various materials and components, particularly those used in the Breeding Blanket, under the conditions expected in future fusion power plants. TBMs are experimental platforms that allow researchers to study the behavior of materials subjected to the extreme conditions inside a fusion reactor, such as the high-energy neutron flux, which can significantly impact the structural materials.

Given ENEA recent emphasis on the WCLL BB solution, there has been a concerted effort to plan a corresponding TBM mock-up. This mock-up aims to gather preliminary experimental data on component performance in a simulated fusion environment. The simulation involves placing the TBM mock-up inside a vacuum chamber, where it is subjected to the direct flux of an electron beam gun, replicating the thermal and radiation conditions of a fusion reactor.

Other eligible Test Sections

Additional test sections with varying power values and thermal-hydraulic conditions have been analyzed to explore the potential for future refurbishments. Specifically, **TS 6** and **TS 6** bis are designed to operate at 7.5 MPa, experiencing a temperature difference of 130-149°C. They have power values of 400 kW and 500 kW, respectively. On the other hand, test sections **TS 7** through **TS 15** operates at 4 MPa with a temperature difference ranging from 60 to 80°C. The power values for these sections vary between 130 kW and 430 kW.

Tab. 1. Design conditions of the W-HYDRA main cooling systems

Parameter	**Unit**	**W-HYDRA primary loop**	**STEAM secondary**		**WL secondary**	**WL tertiary**		**VC loop**	**EBG loop**	
			HP	**LP**		**HP**	**LP**	**Primary side**	EBG 1	EBG 2
Fluid		Water	Water/ Steam	Water/ Steam	Water	Water	Water	Water	Monitored Water	Monitored Water
p_{des}	MPa	18.5	8.5	4.0	8.4	1	0.2	0.2	0.5	0.5
T_{des}	°C	360	330	280	300	90	90	100	50	50
Tsat @p_{des}	°C	359.3	299.3	250	298.4	179.8	133.5	120	151.8	151.8
MFR_{des}	kg/s	20	2	2	8	25	28	12	2	3

Tab. 2. Systems involved in the different mock-up experiments.

Mock-up / **System**	**TS1**	**TS2**	**TS3 TS3bis**	**TS4**	**TS5**	**TS6 to TS15**
W-HYDRA primary loop	Y	Y	Y	Y	Y	Y
STEAM secondary loop	Y	Y				
WL secondary loop			Y	Y	Y	Y
WL tertiary loop			Y	Y	Y	Y
VC loop			Y		Y	Y
EBG loop			Y		Y	Y
LIFUS5/Mod4				Y		
Demi	Y	Y	Y	Y	Y	Y
VCS	Y	Y	Y	Y	Y	Y

Tab. 3. Nominal operating conditions of the W-HYDRA cooling systems listed for Test Sections

Test Section	**Parameter**	**W-HYDRA primary**	**STEAM secondary loop**		**WL secondary loop**	**WL tertiary loop**		**VC loop**	**EBG loop**	
			HP	**LP**		**HP**	**LP**	**1ry**	**EBG 1**	**EBG 2**
TS1 (OTSG)	**P_{nom} [MPa]**	15.5	6.4	2.5						
	MFR_{nom} [kg/s]	16.05	1.63							
	T_{min} - T_{max} [°C]	295-328	210-300							
	W_{nom} [kW]	3100	3100							
TS2 (MANIFOLD)	**P_{nom} [MPa]**	15.5	6.4	2.5						
	MFR_{nom} [kg/s]	16	1.63							
	T_{min} - T_{max} [°C]	328	210-300							
	W_{nom} [kW]	-	3100							
TS3 (FW eq)	**P_{nom} [MPa]**	15.5			7	0.6	0.1	0.15	0.4	0.4
	MFR_{nom} [kg/s]	1.26			1.33	1.94	23.6 (1.94)	10.656	0.17	3.15
	T_{min} - T_{max} [°C]	295-328			132.4-240	50-80	50-80	30-40	25-35	25-31
	W_{nom} [kW]	244.16			244.16	244.16		400*	7	71.5
TS3 bis (FW non eq)	**P_{nom} [MPa]**	15.5			7	0.6	0.1	0.15	0.4	0.4
	MFR_{nom} [kg/s]	1.05			1.11	1.61	23.6 (1.61)	10.656	0.17	3.15
	T_{min} - T_{max} [°C]	295-328			132.4-240	50-80	50-80	30-40	25-35	25-31
	W_{nom} [kW]	202.4			202.4	202.4		400	7	71.5
TS4 (L5M4)	**P_{nom} [MPa]**	15.5			7	0.6	0.1			
	MFR_{nom} [kg/s]	3.74			3.95	5.75	23.6 (5.75)			
	T_{min} - T_{max} [°C]	295-328			132.4-240	50-80	50-80			
	W_{nom} [MW]	722.34			722.34	722.34				
TS 5 (TBM)	**P_{nom} [MPa]**	15.5				7				
	MFR_{nom} [kg/s]	3.74				3.95				
	T_{min} - T_{max} [°C]	295-328				132.4-240				
	W_{nom} [MW]	722.34				722.34				

**Power to be handled by the VC depends on the reflection coefficient of the material of the test section under investigation*

Tab. 4. STEAM main characteristics

General characteristics	
Facility type	Forced circulation, non-isothermal water loop
Operating fluid	Demineralized water
Heat source and nominal power	Electrical heater, 3.1 MW (main heater)
Primary loop key components	Electrical heater, Once Through Steam Generator mock-up (primary side), circulation pump, pressurizer, valves and instrumentation.
Secondary loop key components	Electrical heater, Once Through Steam Generator mock-up (secondary side), pumping system, condensate tank, air coolers, valves and instrumentation.
Other characteristics	Plug and play layout for all the test sections
Primary side characteristics	
Fluid	Pressurized water (liquid)
Nominal temperature range	295-328°C
Nominal pressure	15.5 MPa
Nominal mass flow rate	16.05 kg/s
Key instrumentation	Temperature, flow rate, absolute pressure, differential pressure, levels
Secondary side characteristics	
Fluid	Pressurized Water (liquid/steam)
Nominal Temperature Range	238-300°C (inlet-outlet OTSG)
Nominal pressure	6.4 MPa/2.5 MPa (upstream/downstream lamination valve)
Nominal mass flow rate	1.68 kg/s
Key instrumentation	Temperature, flow rate, absolute pressure, differential pressure, levels

Tab. 5. STEAM primary system nominal data

Primary system nominal conditions			
Parameter	**Unit**	**Value**	**Description**
P_{nom}	MW	3.1	Nominal power delivered by the TS primary side to the secondary side
p	MPa	15.5	Nominal loop nominal pressure
T_{HL}	°C	328.0	Nominal Hot Leg temperature (from e-heater outlet to SG inlet)
T_{CL}	°C	295.0	Nominal Cold Leg temperature (from SG outlet to e-heaters inlet)
$\Delta T_{H2O,1}$	°C	33.0	Nominal temperature difference within the SG and the e-heaters
$\Gamma_{H2O,1}$	kg/s	16.05	Nominal mass flow rate

Tab. 6. STEAM secondary system nominal data

High pressure sector nominal conditions			
Parameter	**Unit**	**Value**	**Description**
P_{nom}	MW	3.1	Nominal power removed from the TS primary side by the secondary side
$p_{upstream\ lam.}$	MPa	6.4	Nominal pressure in the secondary side upstream the lamination
$T_{H2O,in,2}$	°C	238.0	Nominal temperature at the TS inlet
$T_{H2O,out,2}$	°C	>300.0	Nominal temperature at the TS outlet
$\Gamma_{H2O,2}$	kg/s	1.69	Nominal mass flow rate
Low-pressure sector nominal conditions			
$p_{downstream\ lam.}$	MPa	2.5	Nominal pressure in the secondary side downstream the lamination
$T_{downstream\ lam.}$	°C	245.4	Nominal temperature dowmstream the lamination valve
$T_{condensate\ tank}$	°C	224.0	Nominal temperature inside the condensate tank (i.e., saturation conditions)
$T_{upstream\ pump}$	°C	210.0	Nominal temperature upstream pumping system

Tab. 7. WL envisaged and eligible configurations

Ref. name	**Power [kW]**	**P/Pn [%]**	**PS thermal cycle**			**Regulation strategy**	**Ref. Sect.**
			T_{min} [°C]	**T_{max} [°C]**	**p [MPa]**		
100%-1% Regulation with reference Thermal Cycle	800	100	295	328	15.5	HXs tube-side bypass (Sect.6.2.1)	Sect. 0
	720	90					
	640	80					
	560	70					
	480	60					
	400	50					
	320	40					
	240	30					
	160	20					
	80	10					
	40	5					
	8	1					
TBM	722	90.3	295	328	15.5	HXs tube-side bypass (Sect.6.2.1)	Sect. 0
Equatorial FW	244	30.5	295	328	15.5		Sect. 0
Non-equatorial FW	25.3	202	295	328	15.5		Sect. 0
Manifold	0	-	295	328	15.5	Regulation strategy in the Manifold configuration (Sect.6.2.4)	Results similar to those of STEAM configuration (Sect.5.3.1)
TS 6	500	62.5	149.9	130	7.5	Total bypass of the Economizer (Sect. 6.2.2)	Sect. 0
TS 6 bis	400	50	149.9	130	7.5		
TS 7	132.2	16.5	60	80	4	Total bypass of the secondary loop (Sect. 6.2.3)	Sect. 0
TS 8	182.35	22.8	60	80	4		
TS 9	196.8	24.6	60	80	4		
TS 10	139.75	17.5	60	80	4		
TS 11	212.5	26.6	60	80	4		
TS 12	220.65	27.6	60	80	4		
TS 13	259.7	32.5	60	80	4		
TS 14	268.8	33.6	60	80	4		
TS 14 bis	279.36	34.9	60	80	4		
TS 15	432.95	54.1	60	80	4		

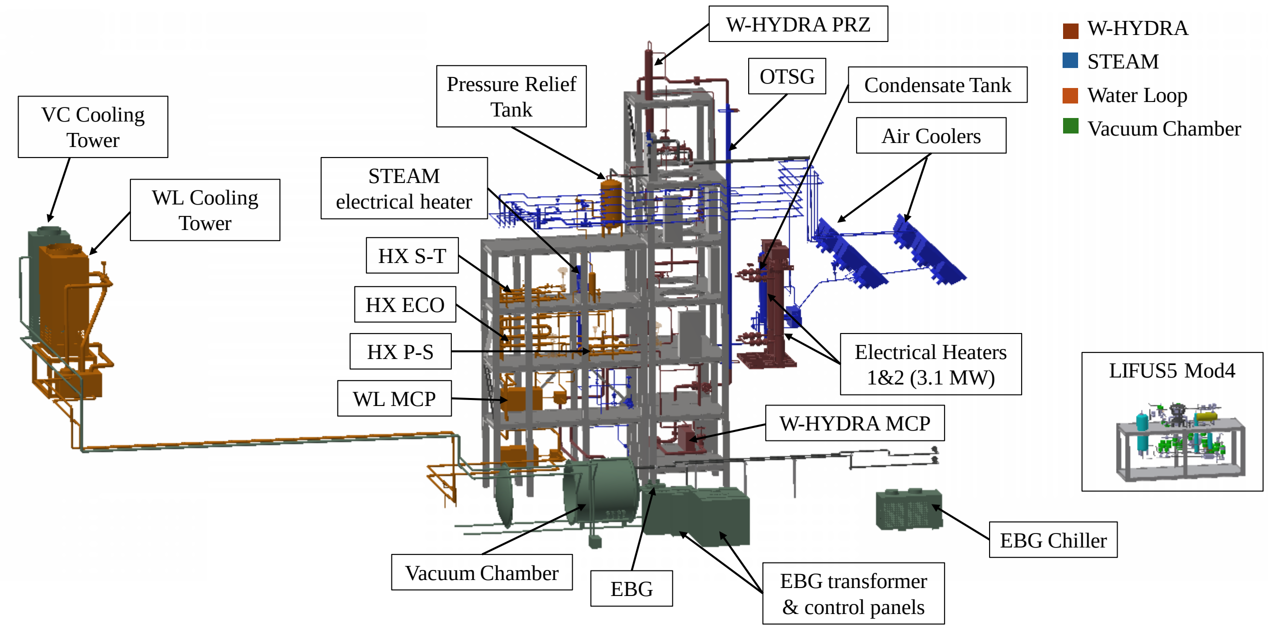

Fig. 10. W-HYDRA platform with detail of the different components (top right figure: WL in blue, STEAM in green, and LIFUS5/Mod5 in red).

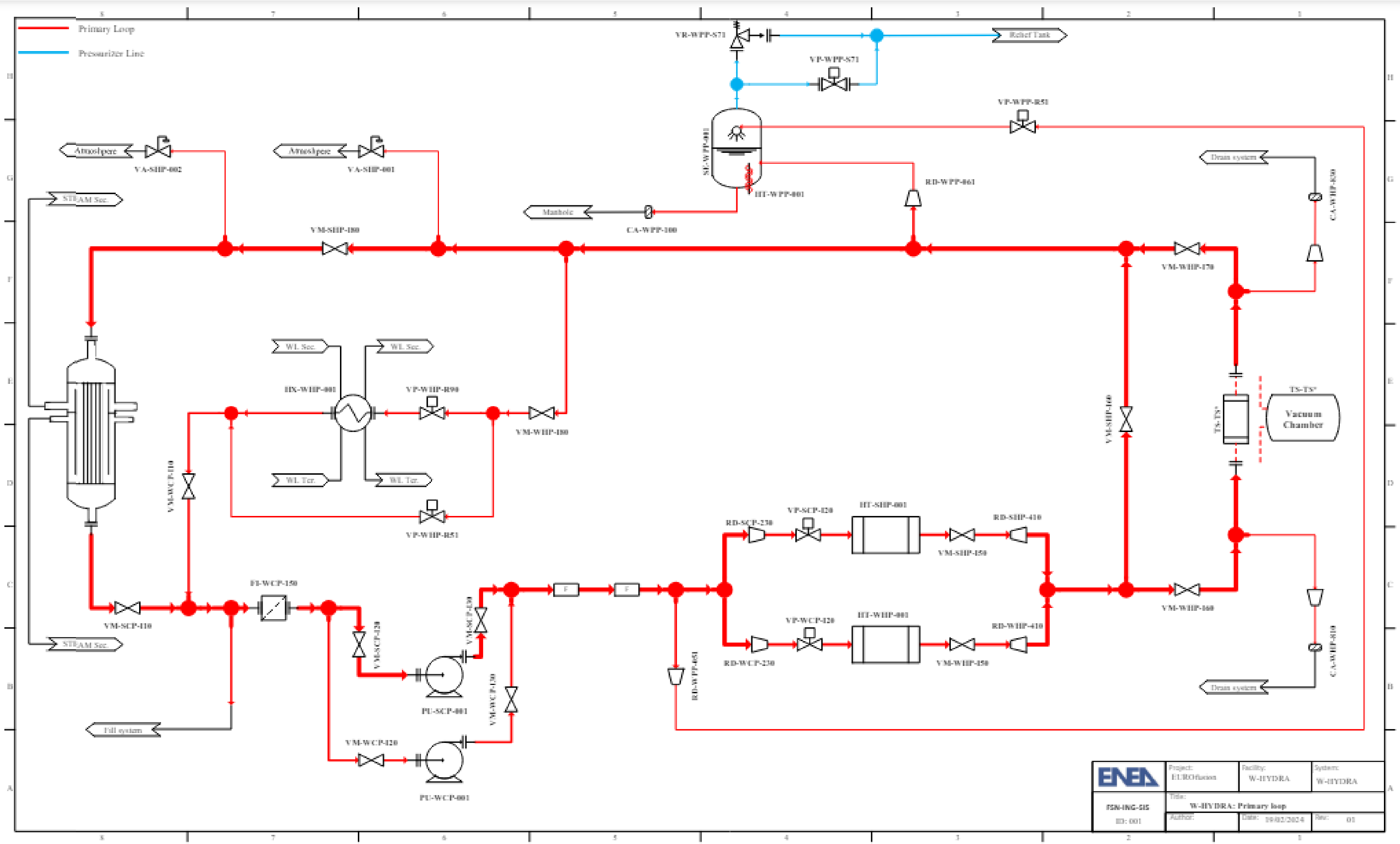

Fig. 11. W-HYDRA primary loop PFD

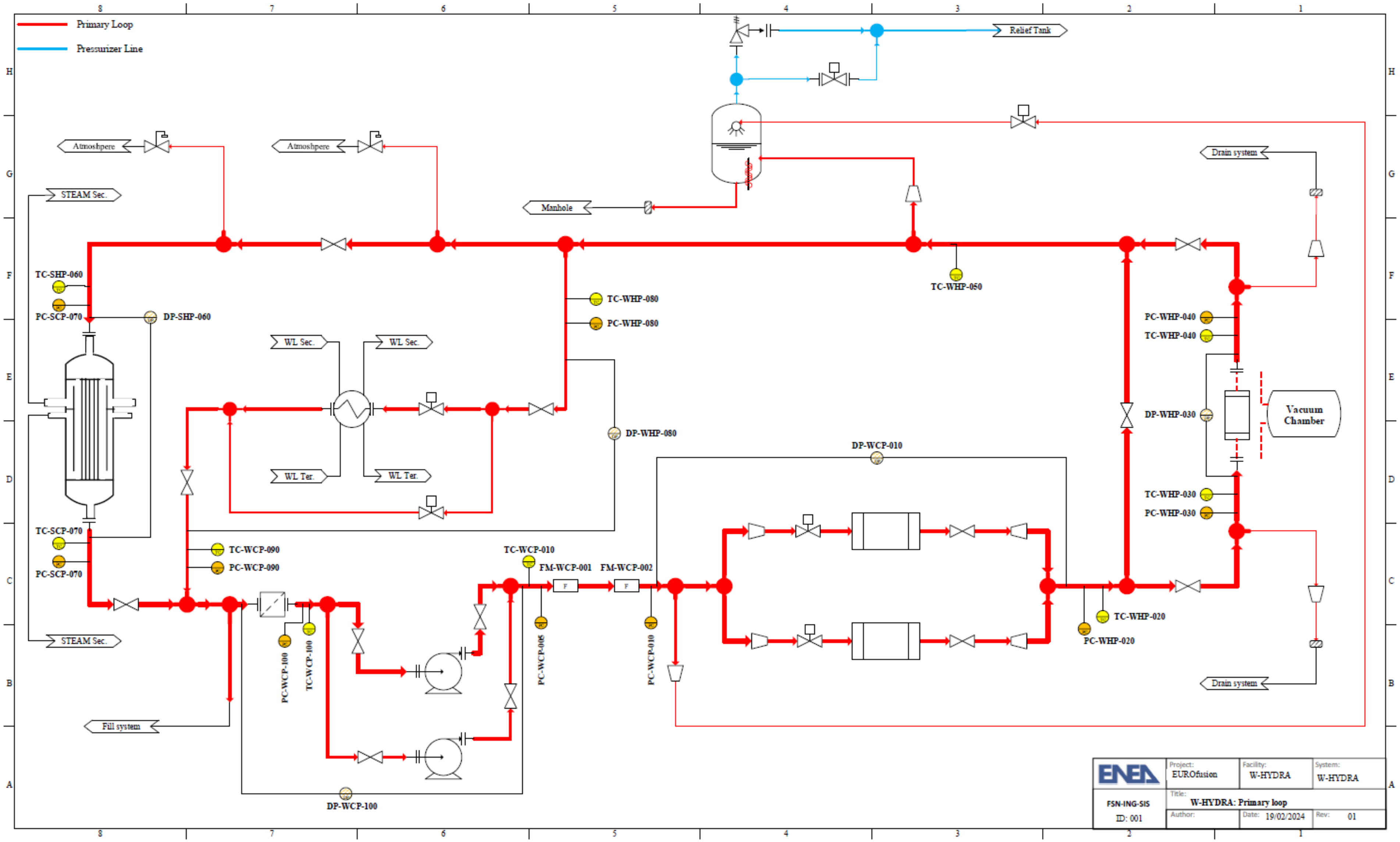

Fig. 12. W-HYDRA primary loop P&ID

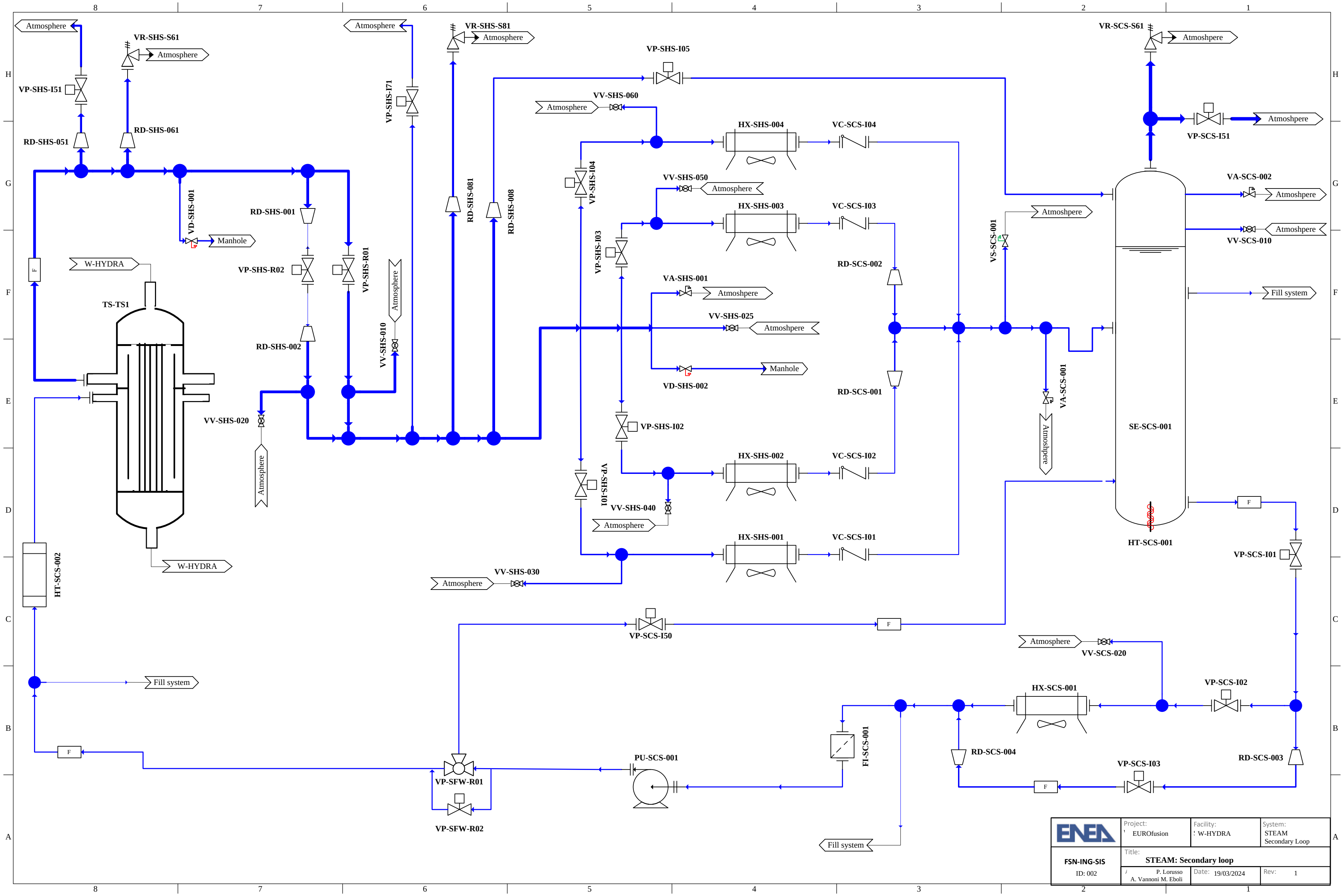

Fig. 13. STEAM secondary loop PFD

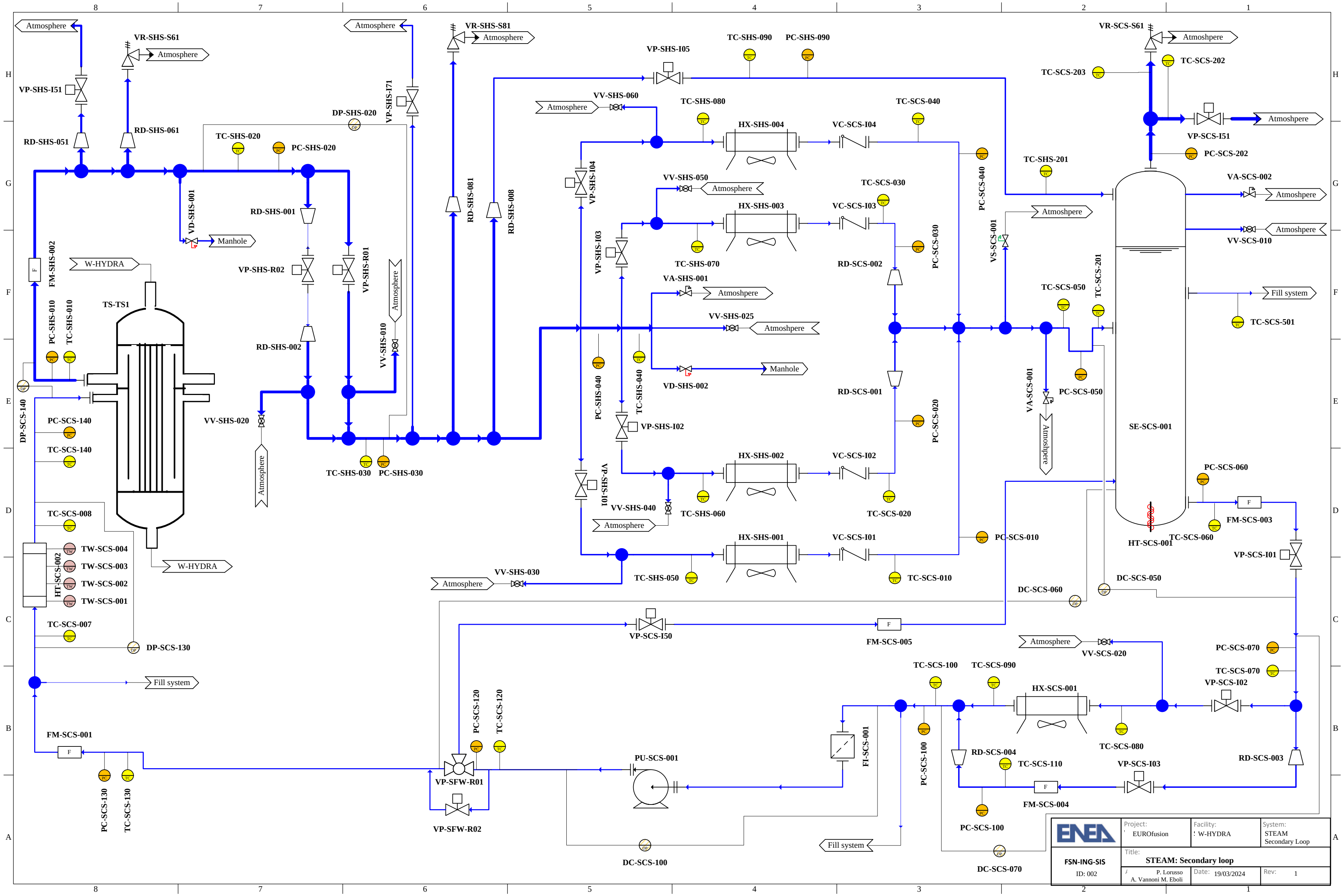

Fig. 14. STEAM secondary loop P&ID

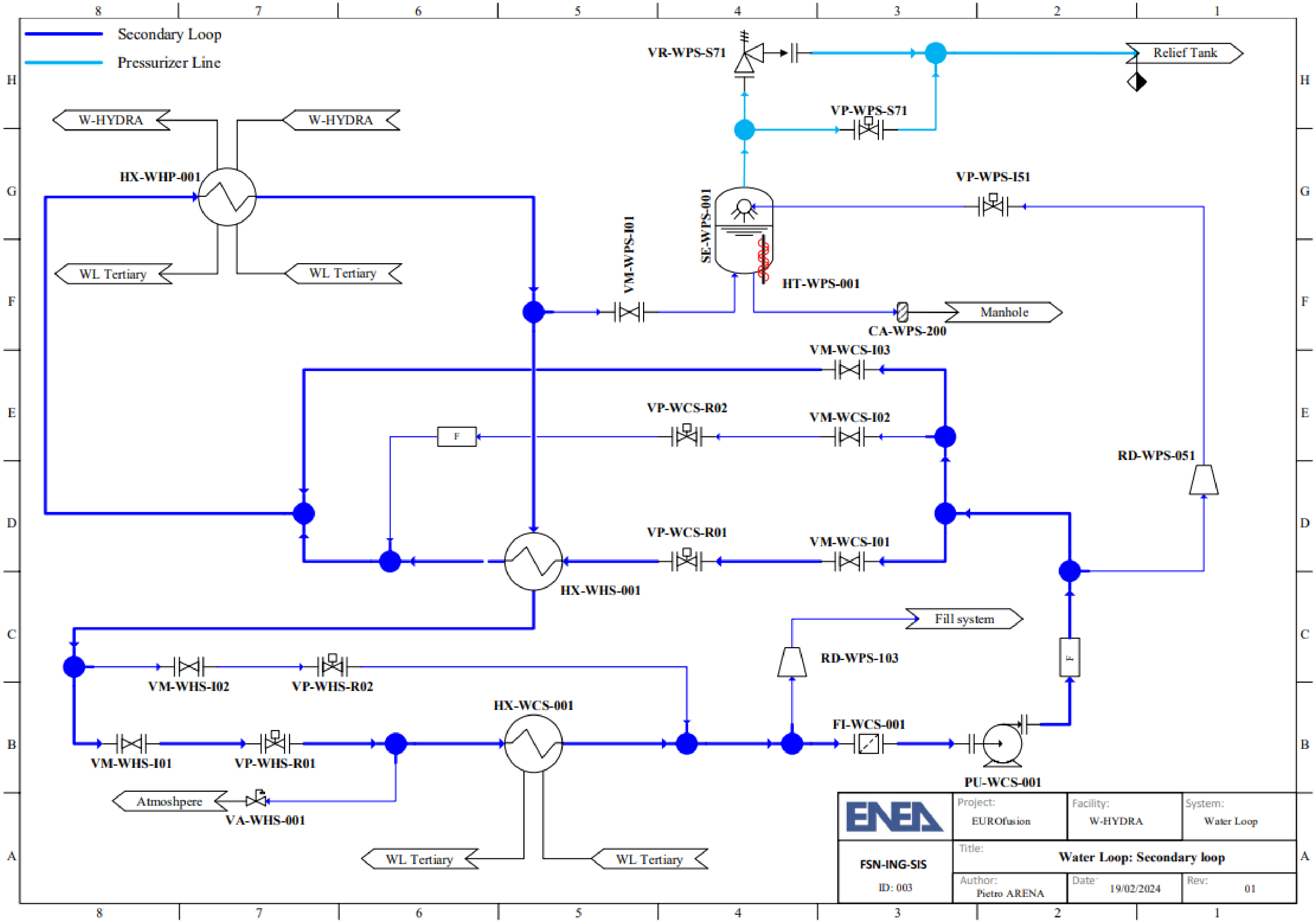

Fig. 15. Water Loop secondary side PFD

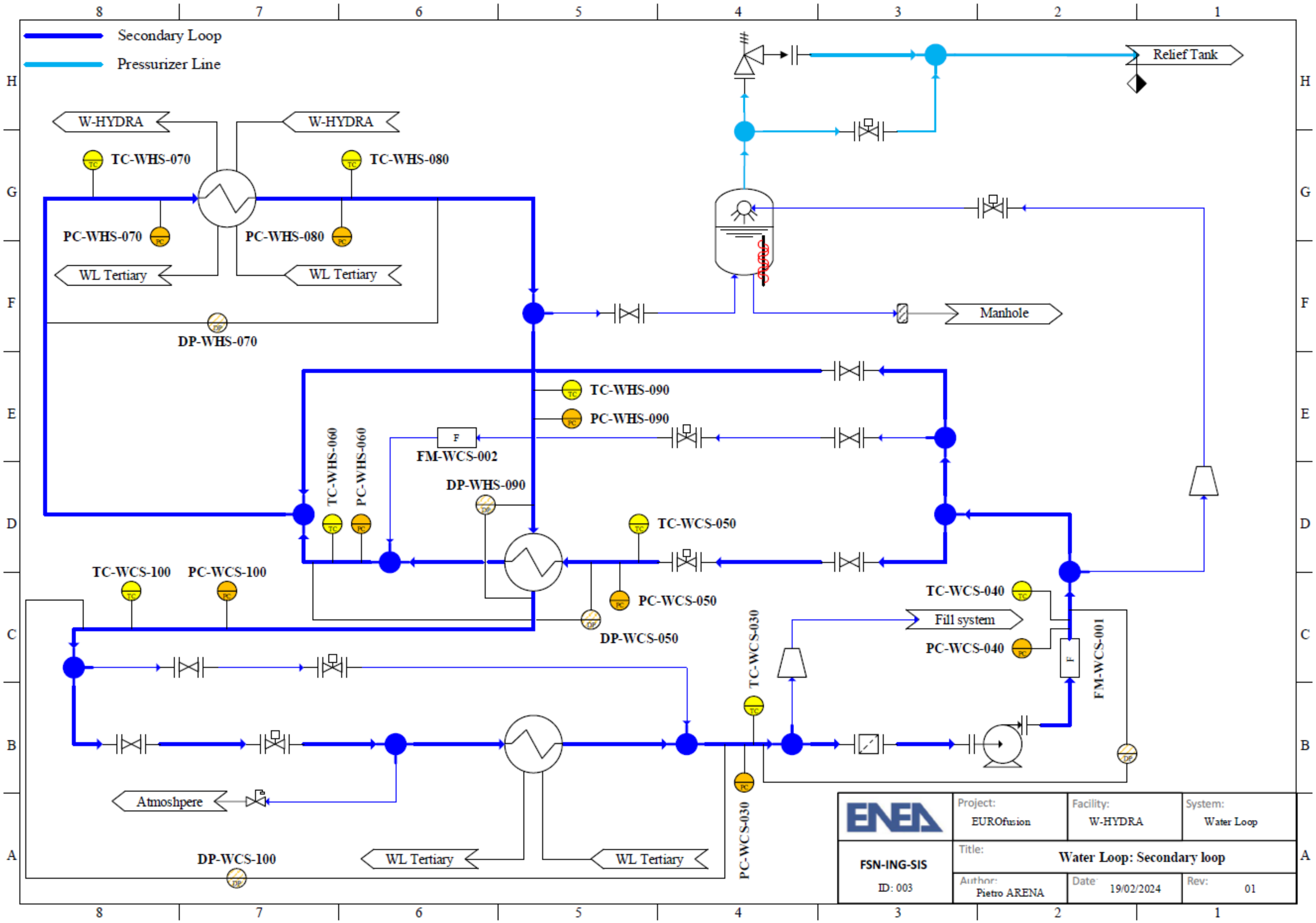

Fig. 16. Water Loop secondary circuit P&ID

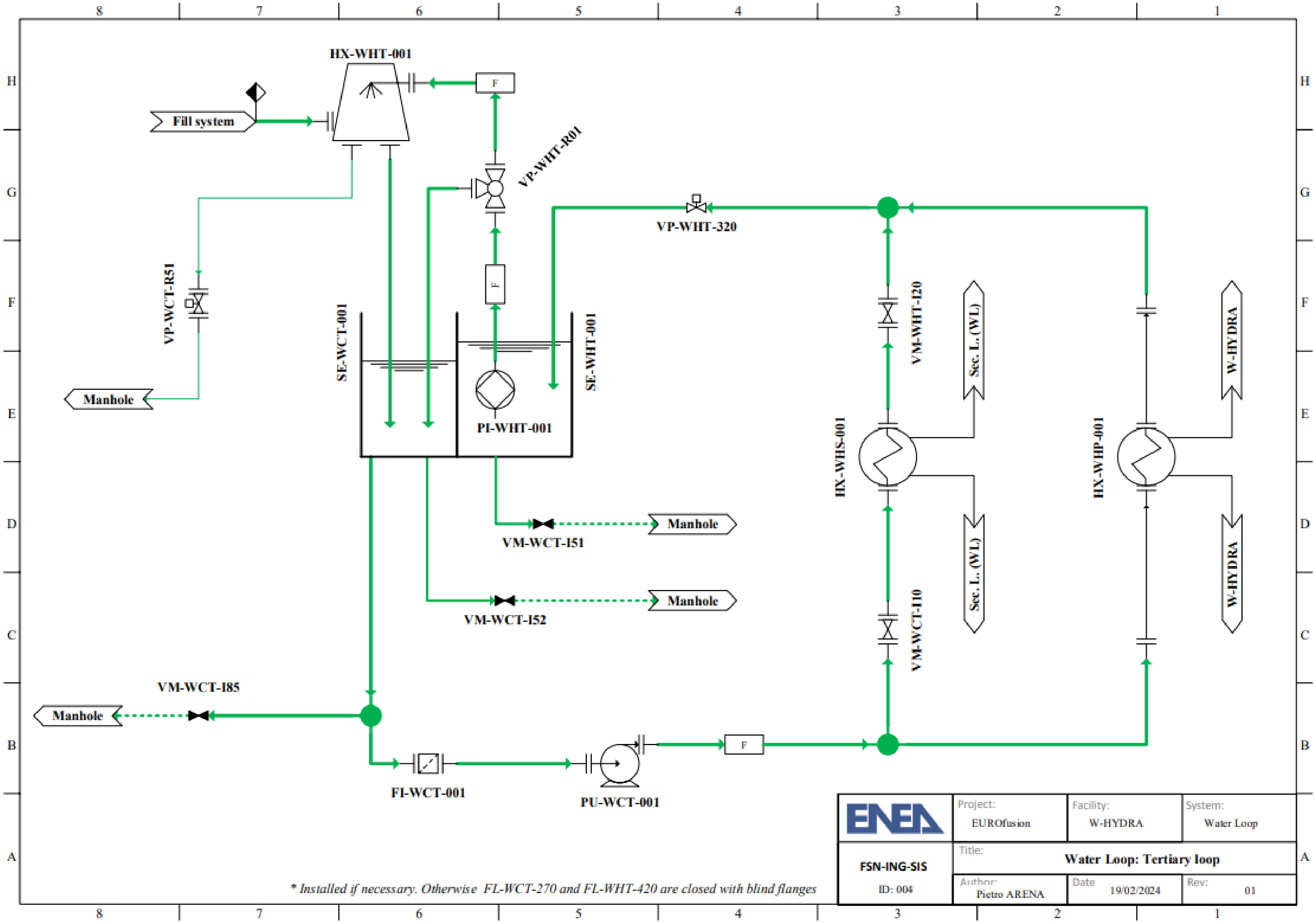

Fig. 17. Water Loop tertiary side PFD

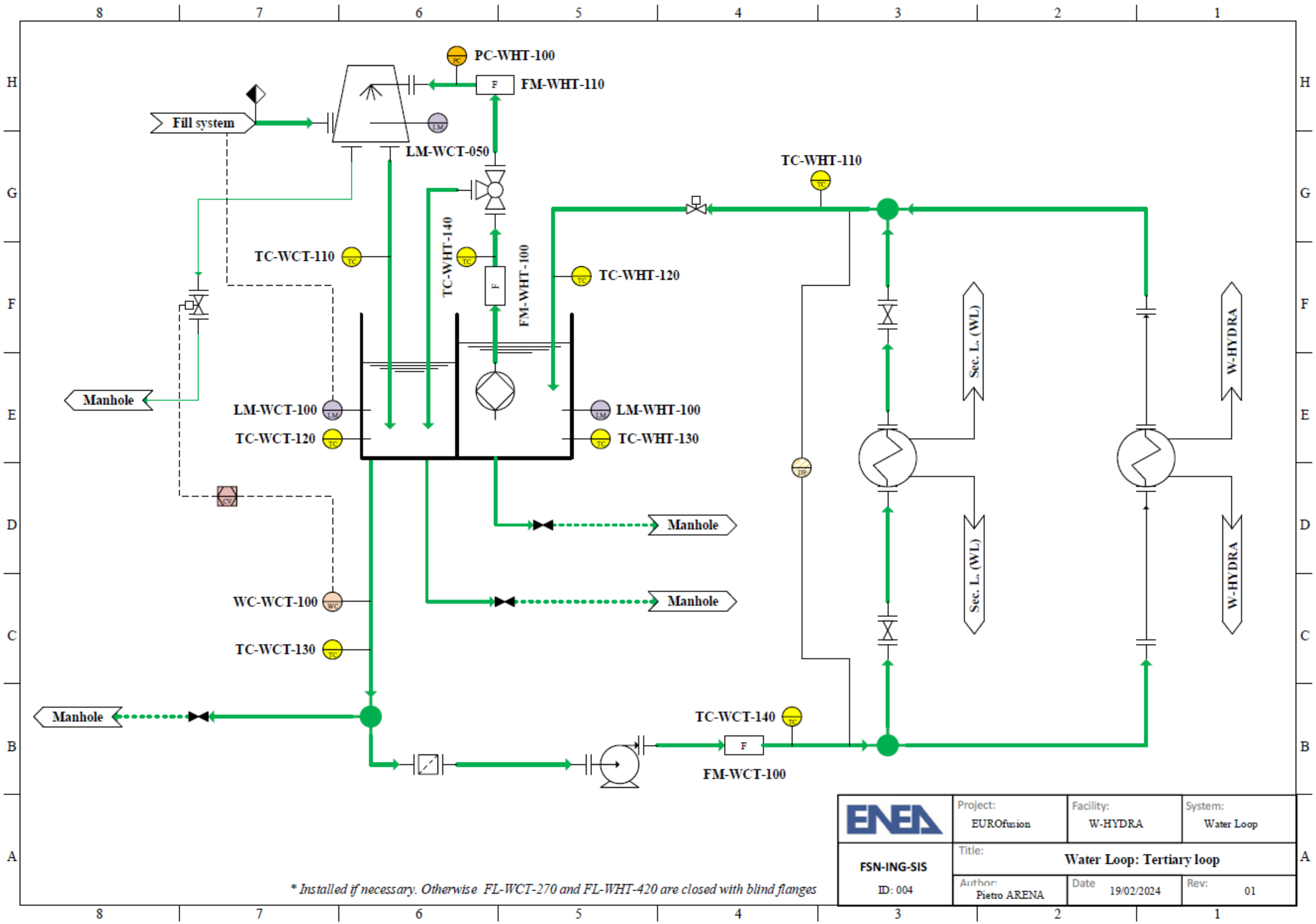

Fig. 18. Water Loop tertiary circuit P&ID

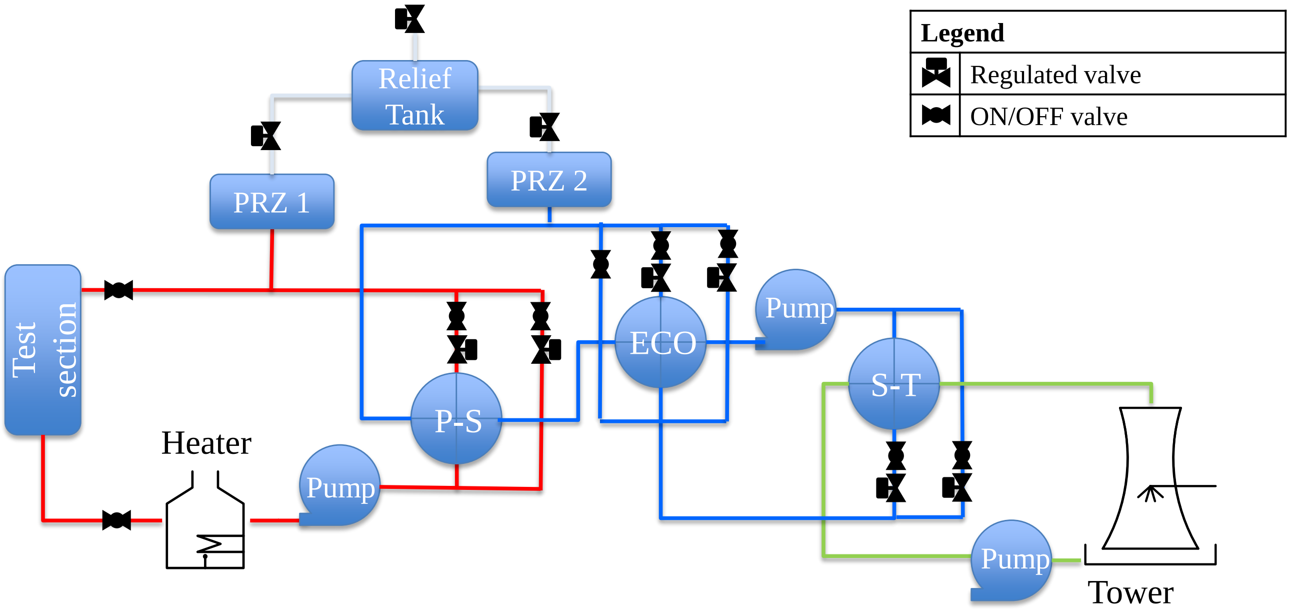

Fig. 19. Simplified schematization of the Water Loop layout with primary (red), secondary (blue) and tertiary (green) loops

4 STEAM TEST SECTION DESIGN

In addressing the thermal hydraulic challenges inherent to fusion reactor operations, the Once Through Steam Generator (OTSG) has emerged as favorable option for the realization of the primary heat sink. This choice is based on two key factors: its extensive utilization and testing in fission reactors and its compatibility with fusion reactor requirements. Unlike fission reactors, which typically operate at nearly constant power close to nominal values, fusion reactors experience rapid power fluctuations and dwell periods where power levels significantly deviate from nominal values. The OTSG lower thermal inertia, resulting from its reduced water mass compared to conventional U-tube generators, makes it well-suited to accommodate these dynamic operating conditions. Furthermore, the OTSG applicability is enhanced by the fact that the thermodynamic conditions of water are comparable to those in Pressurized Water Reactors (PWRs), where the OTSG has been extensively tested.

Given the imperative nature of characterizing and validating the OTSG in fusion-like extreme dynamic conditions, the STEAM experimental facility will host the mock-up of the DEMO WCLL BB OTSG (also referred to as Test Section 1, TS1). This comprehensive testing initiative will encompass all fusion reactor power states, investigating the robustness and reliability of the OTSG under varying operational scenarios.

In this section, the STEAM facility OTSG will be designed following a scaling procedure [60] that keeps unaltered the BB OTSG main features (see Sect. 2.7). The comparison of the geometrical parameters and the thermal-hydraulic results will be presented too.

4.1 Scaling procedure

The scaling procedure for the DEMO WCLL BB PHTS OTSG mock-up used Beginning of Life (BoL) conditions as a reference point. This choice ensures that the facility can meet its power requirements even under less-than-optimal conditions, such as End of Life (EoL) scenarios characterized by performance degradation due to tube fouling and plugging. Although the STEAM facility operates for a significantly low number of hours as an experimental setup, it is unlikely to experience the fouling and plugging conditions expected at EoL. Consequently, the test section, designed for BoL conditions, will be oversized, capable of producing superheated steam at higher temperatures.

The DEMO WCLL BB PHTS OTSG mock-up to be tested in STEAM facility was developed using a scaling procedure based on the "power to volume" approach, while maintaining the full-length scale of the Breeding Zone (BZ) OTSG [61]. By assuming that the “power/tube” ratio remains constant, a scaled 1:1 in length mock-up for the STEAM OTSG was devised. This involved the selection of a tube bundle comprising 37 tubes, utilizing identical geometry and pitch as the BB OTSG original design. This tube number selection aimed to ensure the creation of a hexagonal tube bundle with four complete ranks, thereby minimizing distortions resulting from tube asymmetries or excessively high bypasses. The decision to adopt four ranks was a compromise between the attempt to enhance the test section representativeness, which diminishes with reducing the number of tubes, and economic considerations related to electrical power usage, as the power exchanged by the test section is supplied to the primary fluid by electric heating cables.

As a consequence of adopting full-length tubes, the scaling factor – that should be calculated as the ratio of the powers or the volumes – coincides with the tubes ratio:

$$f_{scaling} = \frac{n_{tubes_{STEAM}}}{n_{tubes_{BZ}}} = \frac{37}{5696} = 0.0065$$

STEAM test section main parameters, such as power and flow areas, were accordingly scaled with the same scaling factor:

$$P_{STEAM} = P_{BB} \times f_{scaling} = 477 \times 0.0065 = 3.1\ MW$$

STEAM nominal mass flow rates were determined by applying the same scaling factors, while T/H conditions (pressures and temperatures) are assumed to be equal to the ones of DEMO WCLL BB PHTS OTSGs. The summary of the component nominal conditions and the comparison with the BB OTSG reference is reported in Tab. 9 [62].

The adopted proportionality factor applied is 1:154. The adoption of such a low scaling factor (which, as discussed, is constrained by factors related to the electrical power to be supplied to the facility) results in a very low value of the downcomer area. This has significant implications for the STEAM configuration obtained from the scaling procedure. Specifically, maintaining the geometric and main characteristics of the OTSG model of the DEMO WCLL BB, the direct consequence is the creation of a DC annular gap that is 2 cm thick, a feature that poses challenges in practical realization due to manufacturing tolerances of coaxial pipes. Furthermore, this configuration would complicate the installation of instrumentation in the riser and DC. To address these issues, riser and downcomer were thermally decoupled and an external DC pipe was implemented instead of the originally planned annular region surrounding the riser.

The area of the riser was hexagonally shaped (as shown in Fig. 20) to reduce the side effects, that becomes more significant as the power reduces. The picture shows also one of the thirteen tube support plates (TSP) planned for installation, spaced approximately one meter apart, to mitigate mechanical issues and tube vibrations.

The OTSG for the Breeding Blanket and the final layout of the STEAM mock-up are illustrated in Fig. 21, while the comparison of the main geometrical parameters is reported in Tab. 8. Several design adjustments were made in the STEAM OTSG mock-up, resulting in specific distortions.

First, instead of being scaled, the OTSG inlet and outlet nozzles were matched to the sizes of the standard commercial pipelines used in the STEAM facility system. These sizes include 6” Sch. 160 for primary side inlet and outlet nozzles, and 1 ½” Sch. STD and 3 ½” Sch. STD for secondary side feedwater inlet and steam outlet nozzles, respectively. This decision may influence localized pressure drops.

Additionally, the radial extension of the OTSG was reduced due to the removal of the annular downcomer and the reduction in areas induced by scaling. As a result, the plena became cylindrical rather than spherical, with height and diameter equal to the shroud internal diameter. The thickness of the tube sheet was also reduced from 53.34 cm to 10 cm, and two BZ primary side outlet nozzles were replaced with a single outlet nozzle.

The downcomer hydraulic diameter was adjusted. The free flow area was proportionally scaled, but the wetted perimeter now only considers the pipe's internal perimeter. The water ports connecting the downcomer and riser were replaced with two commercial pipes of 2 ½” Sch. 80, chosen because their combined size closely approximates the flow area of the downcomer. The same approach was applied to the steam ports.

Given the physical separation of the riser and downcomer in the STEAM OTSG, the recirculation window that cuts through the shroud in the BZ OTSG to connect these two regions was replaced by an external pipe. The riser hydraulic diameter was also adjusted, influenced by both the tubes and the hexagonal shell perimeters. When scaling down from the BB, the weight of the hexagonal shell, which was not scaled, increased, leading to distortion. To withstand different external pressures, the shroud thickness was increased.

Moreover, the adjustable orifice plate, which was calibrated to determine and maintain a static head in the downcomer to allow recirculation and stabilize the flow, was eliminated. However, the corresponding concentrated loss coefficient and flow area reduction were retained. The semi-circular headers for the feedwater inlet in the BB OTSG were removed, and the spray system was envisioned to be placed within the external downcomer component. Finally, the downcomer dead zone was disregarded since the steam downcomer feeds directly into the steam line. This modification has a minimal impact on the overall results.

4.2 Comparison of the thermal-hydraulic behavior of the BB PHTS OTSG and the STEAM test section

The design process was supported by thermal-hydraulic analyses using the SYS-TH code RELAP5/Mod3.3. Initial validation of the code was conducted based on data from the B&W OTSG of Three Mile Island (TMI), demonstrating its suitability for the design activities [63]. The mono-dimensional nodalization of both BB and STEAM OTSG components were performed, using pipes, branches, single junctions (SJs), multiple junctions (MJs), time-dependent-volumes (TDVs) and time-dependent-junctions (TDJs). Heat structures (HSs) were adopted to simulate thermal coupling between components (active HS) and heat losses towards the environment (passive HS). The comparison of the RELAP5 nodalization is shown in **Errore. L'origine r iferimento non è stata trovata.** (with Fig. 23 detailing the heat structures characteristics. The list of the components is reported in Tab. 10.

The boundary conditions were established using time-dependent volumes and junctions to define key parameters. The inlet time-dependent volume controlled the fluid inlet temperature, the inlet time-dependent junction imposed the mass flow rate, and the outlet time-dependent volume set the outlet pressure, as detailed in Tab. 11.

To efficiently manage heat removal from the PHTS and maintain the primary system at its designated temperature, the feedwater mass flow rate was regulated by a Proportional-Integral (P-I) control system. For this reason, feedwater mass flow rate is not considered a boundary condition.

The primary objective of the PCS (secondary side) is to efficiently remove heat from the PHTS (primary side) and restore the primary system to its designated temperature. To achieve this, the feedwater flow rate is controlled by a system capable of adjusting its value to meet a specific temperature set point. This control system is essential due to the sizing of the OTSG, which is designed to exchange nominal power even at End of Life conditions. This means that the heat exchange surface area is oversized to handle 3.1 MW at the Beginning of Life stage. Consequently, to prevent the primary system from cooling excessively due to the exchange of power higher than the nominal value, the flow rate of the secondary system is reduced. With the inlet temperature and flow rate of the primary system fixed by the TDV and TDJ, and the exit temperature controlled by the secondary system, a consistent exchange of 3.1 MW occurs. However, by decreasing the feedwater mass flow rate while maintaining its inlet temperature and the exchanged power constant, the exit steam temperature will exceed the nominal temperature.

To manage this, a Proportional-Integral (P-I) controller is employed. In this system, the primary side outlet temperature serves as the "measured variable," while the "set-point" is the desired primary side OTSG outlet temperature, set at 295°C. The "error" is calculated as the difference between the set point and the measured variable, and the "regulated variable" is the feedwater mass flow rate. If the measured temperature is lower than the set point, it indicates excessive power exchange, prompting the control system to decrease the flow rate. Conversely, if the measured temperature exceeds the set point, it suggests insufficient power exchange, leading the control system to increase the flow rate to adjust accordingly. The logic scheme of the pump velocity control system is illustrated in Fig. 24

Comparative RELAP5 results for the BB 477 MW and STEAM 3.1 MW models, compiled in Tab. 12 and depicted in Fig. 25 to Fig. 31 [63], reveal that the velocity and heat transfer coefficients (HTC) on both the primary and secondary sides of the two models are nearly identical. The void fraction and static quality along the thermal length also exhibit similar patterns. However, notable differences emerge in the axial profile of the downcomer void fraction: compared to the BB model, the STEAM downcomer level is higher, primarily due to two reasons. In the STEAM model, no heat transfer occurs between the downcomer and the riser, resulting in only heat losses. Additionally, the substitution of the lower ports with smaller feedwater pipes leads to higher pressure drops in the recirculating loop.

Tab. 12 highlights that neither heat losses nor mass inventory are appropriately scaled. In the STEAM system, the heat losses are higher compared to the scaled value because the scaling procedure does not preserve the external surface-to-volume ratio, which instead increases, amplifying the significance of heat losses in percentage terms. Moreover, the use of an external downcomer instead of an annular one contributes to this effect by exposing both the downcomer and the riser to thermal losses with the surroundings.

Further analysis of mass inventory, detailed in Tab. 13 reveals that concerning the primary loop, while the tube bundle mass inventory is correctly scaled, the inventories of the plena and tube-sheet are reduced relative to the scaled value. This reduction is attributed to the altered (i.e., reduced) length of these components during scaling. On the secondary side, distortions in the feedwater downcomer arise from the higher liquid collapsed level and the presence of smaller feedwater pipes connecting the downcomer and the riser. Distortions in the steam downcomer result from an increase in mass inventory in the BB model corresponding to the dead zone, which is absent in the STEAM mock-up, while in the STEAM model, it is increased by the inclusion of smaller steam tubes that are not present in the BB OTSG. After accounting for these contributions, the mass inventory of the steam downcomer aligns with correct scaling.

4.3 Analysis of the scaling-induced distortions

The RELAP5 results for both the BB 477 MW and STEAM 3.1 MW models are compiled in Tab. 12 and depicted in Fig. 25 to Fig. 31. The comparison indicates that both compared models exhibit similar velocity and heat transfer coefficients (HTC) on both primary and secondary sides. Moreover, the void fraction and static quality along the thermal length are nearly identical. However, differences arise in the collapsed level of the downcomer (see Tab. 12) and in the axial profile of void fraction (Fig. 31).

The STEAM system shows a higher downcomer liquid collapsed level, which is primarily due to the absence of heat transfer between the downcomer and the riser, resulting in only heat losses. Additionally, increased pressure drops in the recirculating loop are caused by the replacement of lower ports with smaller feedwater pipes.

Regarding the axial profile of the downcomer void fraction, STEAM exhibits a slightly lower void fraction in the first 3 meters compared to the BB OTSG, followed by a sudden reduction associated with the condensation of recirculated vapor, occurring roughly one meter downstream.

A series of simulations were conducted to identify the parameters most influencing the downcomer behavior. The primary factors considered were the absence of heat exchange between the riser and downcomer in the STEAM configuration, the increased heat losses from the downcomer due to its exposure as an external component, and the variation in hydraulic diameters of both the riser and downcomer.

To investigate these factors, two distinct types of analyses were performed. First, to examine the influence of heat exchange and heat losses, an electric wire was installed around the downcomer to simulate the intended power from the riser and the additional heat lost due to its external placement. The results indicated minimal differences, suggesting that this solution is not economically viable.

Second, to evaluate the impact of hydraulic diameter variations, several simulations were conducted. These included adjusting the hydraulic diameter of the STEAM riser to match that of the BB model (STEAM_ris), adjusting the hydraulic diameter of the STEAM downcomer to match the BB model (STEAM_dc), and adjusting both the STEAM riser and downcomer hydraulic diameters to those of the BB model (STEAM_ris_dc). Results from Fig. 32 demonstrate that using the BB riser hydraulic diameter (STEAM_ris in blue) brings results closer to the BB model (in black) compared to the reference STEAM configuration (in red). The influence of the BB downcomer hydraulic diameter is more significant than that of the riser and combining both effects produces a profile that closely resembles the BB model.

Tab. 8. Comparison between BB and STEAM scaled-down OTSG geometrical features

Parameter	**Unit**	**BB**	**STEAM**	**Rel. Factor**
Active Length	m	12.98	12.98	1:1
Tube O.D.	mm	15.875	15.875	1:1
Tube Thickness	mm	0.8636	0.8636	1:1
p/D	-	1.4	1.4	1:1
Lattice	-	Triangular	Triangular	/
Tube number	-	5696	37	1:154
PS inlet nozzle	m^2	0.4112	0.00943	1:43.6
PS plena height	m	0.9352	0.1615	-
PS plena area	m^2	2.6907 (sphere)	0.02049 (cylinder)	1:131
PS tube-side Flow Area	m^2	0.8954	0.0058	1:154
PS Tube-sheets thickness	m	0.5334	0.1	-
PS Tube-sheets area	m^2	1.6205	0.0095	1:171
PS Hyd./Heat. Diam.	mm	14.147	14.147	1:1
SS inlet nozzle	m^2	0.134	0.00132	1:102
SS Downcomer Flow Area	m^2	0.87	0.0056	1:154
SS Downcomer Hydr. Diam	mm	274.73	84.65	1:3.25
SS Water ports Area	m^2	0.8458	2 × 0.002734	1:755
SS Steam ports Area	m^2	0.8665	2 × 0.002734	1:773
SS Rec. window area	m^2	0.0463	0.00030	1:154
SS Rec. window elevation (from lower tube sheet)	m	8.72	8.72	1:1
SS Orifice plate Area	m^2	0.1248	0.00081	1:154
SS Shell I.D./Hexagonal flat to flat	m	1.82	0.1397	1:13
SS Riser total Area	m^2	2.6030	0.01691	1:154
SS Riser Flow Area	m^2	1.4756	0.0096	1:154
SS Riser Hyd. Diam.	mm	20.37	16.46	1:1.24
SS Riser Heat. Diam.	mm	20.78	20.78	1:1
SS Riser TSP Area	m^2	0.6669	0.00433	1:154
SS outlet nozzle	m^2	2 × 0.4758	0.0064	1:149

Tab. 9. Comparison of the BB and STEAM OTSGs nominal T/H data

Parameter	**Unit**	**BB**	**STEAM**
Power	MW	477	3.1
Primary Side			
Inlet Temperature	°C	328	328
Outlet Temperature	°C	295	295
Reference pressure	MPa	15.5	15.5
Mass flow rate	kg/s	2469.5	16.05
Secondary Side			
Inlet Temperature	°C	238	238
Outlet Temperature	°C	312.5	312.5
Steam line pressure	MPa	64.1	64.1
Mass flow rate	kg/s	252.9	1.64

Tab. 10. RELAP5/Mod3.3 components of BB and STEAM OTSG nodalizations

Component	**BB**	**STEAM**
Primary loop		
Inlet time-dependent-volume*	TDV 109	TDV 101
Inlet time-dependent-junction*	TDJ 110	TDJ 102
Inlet nozzle	Branch 111	Branch 103
Upper plenum, upper tube-sheet, tube bundle, lower tube-sheet, lower plenum (as specified in Errore. L'origine r iferimento non è stata trovata.and Fig. 23)	Pipe 113	Pipe 104
Outlet nozzle	Branch 114	Branch 105
Outlet time-dependent-volume*	TDV 115	TDV 106
Secondary loop		
Inlet time-dependent-volume*	TDV 201	TDV 201
Inlet time-dependent-junction*	TDJ 202	TDJ 202
Feedwater inlet nozzle	Branch 203	Branch 203
Feedwater downcomer	Pipe 204, Pipe 205	Pipe 204, Branch 205
Connection between DC and riser	MJ 220	Pipe 206, Pipe 207
Lower Riser	Pipe 206, SJ 221, Pipe 207	Branch 208, Pipe 209, Branch 210
Aspirator port (for recirculation)	SJ 223	Branch 211
Upper Riser	Pipe 208, SJ 224, Pipe 209	Pipe 212, Branch 213
Connection between riser and DC (water ports and external pipe, respectively)	MJ 210	Pipe 214, Pipe 215
Steam DC	Pipe 211, SJ 212, Pipe 213	Branch 216, Pipe 217
Dead Zone	SJ 225, Pipe 214	-
Steam outlet nozzle	Branch 215	Branch 218
Outlet time-dependent-volume*	TDV 216	TDV 219
** TDVs and TDJs set boundary conditions.*		

Tab. 11. BB and OTSG boundary conditions

Parameter	**Unit**	**BB**	**STEAM**
Primary Side			
Inlet Temperature	°C	328	328
Outlet Pressure	MPa	15.5	15.5
Mass flow rate	kg/s	2469.5	16.05
Secondary Side			
Inlet Temperature	°C	238	238
Outlet Pressure	MPa	6.41	6.41
Mass flow rate*	kg/s	252.9	1.64
** SS mfr is not properly a B.C. (it is regulated by a control system)*			

Tab. 12. RELAP5 results for the BB OTSG and the STEAM mock-up

Parameter	Unit	BB	STEAM	Rel. Factor
Exchanged Power	MW	477	3.1	1:154
Heat Losses	kW	17.4	7.2	1:2
Prim. Side Temp. Outlet	°C	295.0	295.0	/
Sec. Side Temp. Outlet	°C	312.3	314.3	/
Feedwater Mass Flow	kg/s	252.9	1.63	1:154
Sec. Side Rec. Mass Flow	kg/s	31.5	0.227	1:139
Riser Level	m	1.91	1.9	/
Downcomer Level	m	3.42	4.8	/
Prim. Side Δp	kPa	127.3	94.9	/
Sec. Side Δp	kPa	162.2	208.3	/
Prim. Side Water Mass	kg	11073	57.51	1:193
Sec. Side Water Mass	kg	5342	41.3	1:129

Tab. 13. Mass Inventories comparison between BB OTSG and STEAM mock-up

Parameter	Unit	BB	STEAM	Rel. Factor
Primary side				
Upper & Lower Head	kg	2388.7	4.6	1:519
Tube Bundle (without tubesheet)	kg	8018.6	52.9	1:152
Tubesheet	kg	665.47	0.81	1:822
Total	kg	11073	57.5	1:192
Secondary side				
Lower Downcomer	kg	2784.5	24.1	1:116
Lower Riser	kg	2435.9	15.8	1:154
Upper Riser	kg	197.1	1.3	1:154
Steam Downcomer*	kg	231.0	0.7	1:330
Steam Downcomer (without Dead Zone and little steam tubes)	kg	95.9	0.6	1:160
Total	kg	5648.5	41.9	1:135

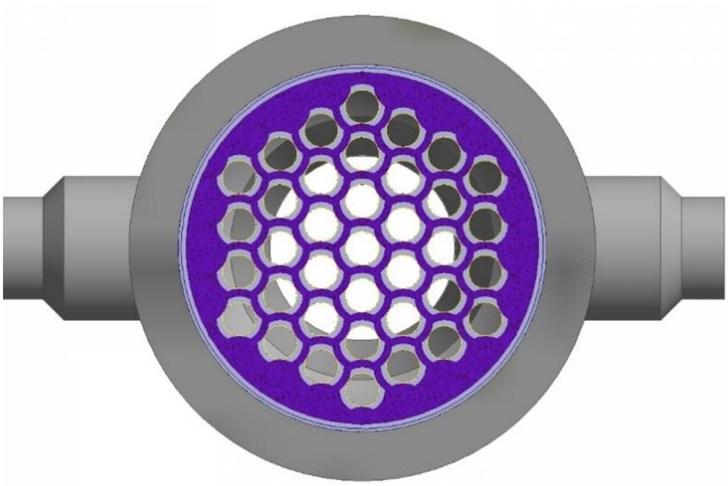

Fig. 20. Hexagonally shaped riser with a detail of the tube support plate (TSP).

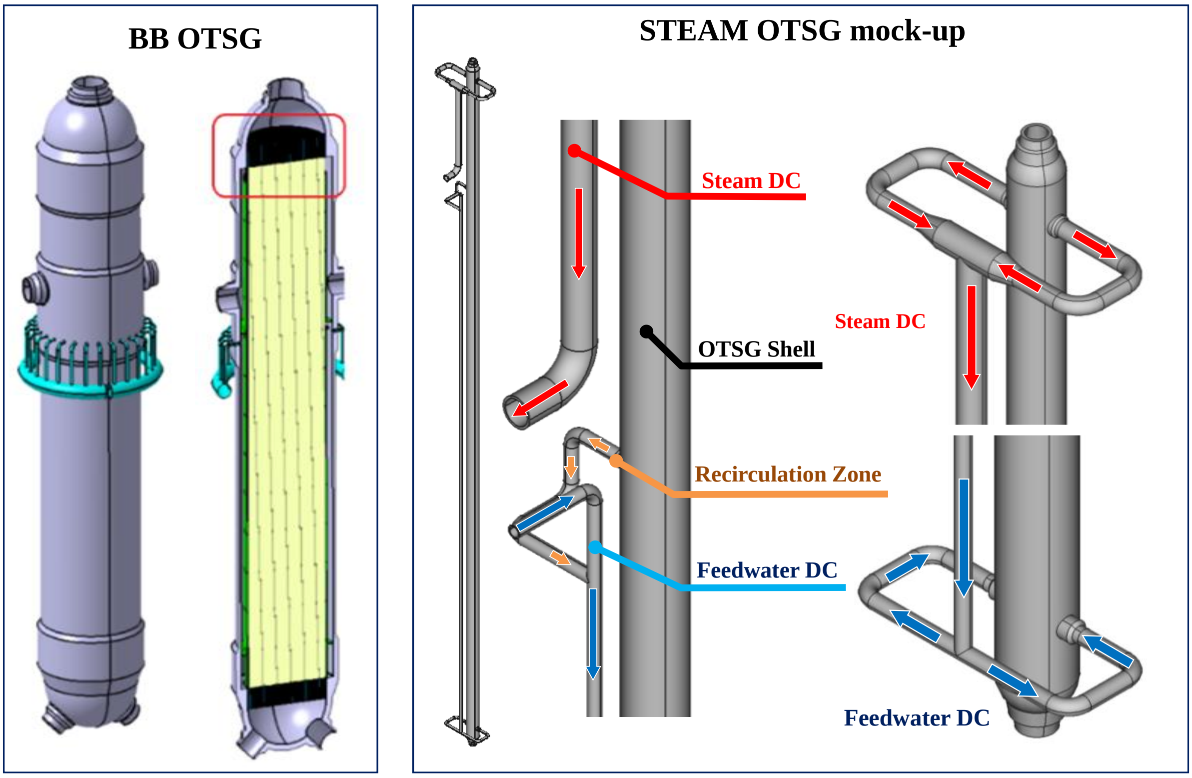

Fig. 21. BB OTSG (left) and STEAM OTSG mock-up (right)

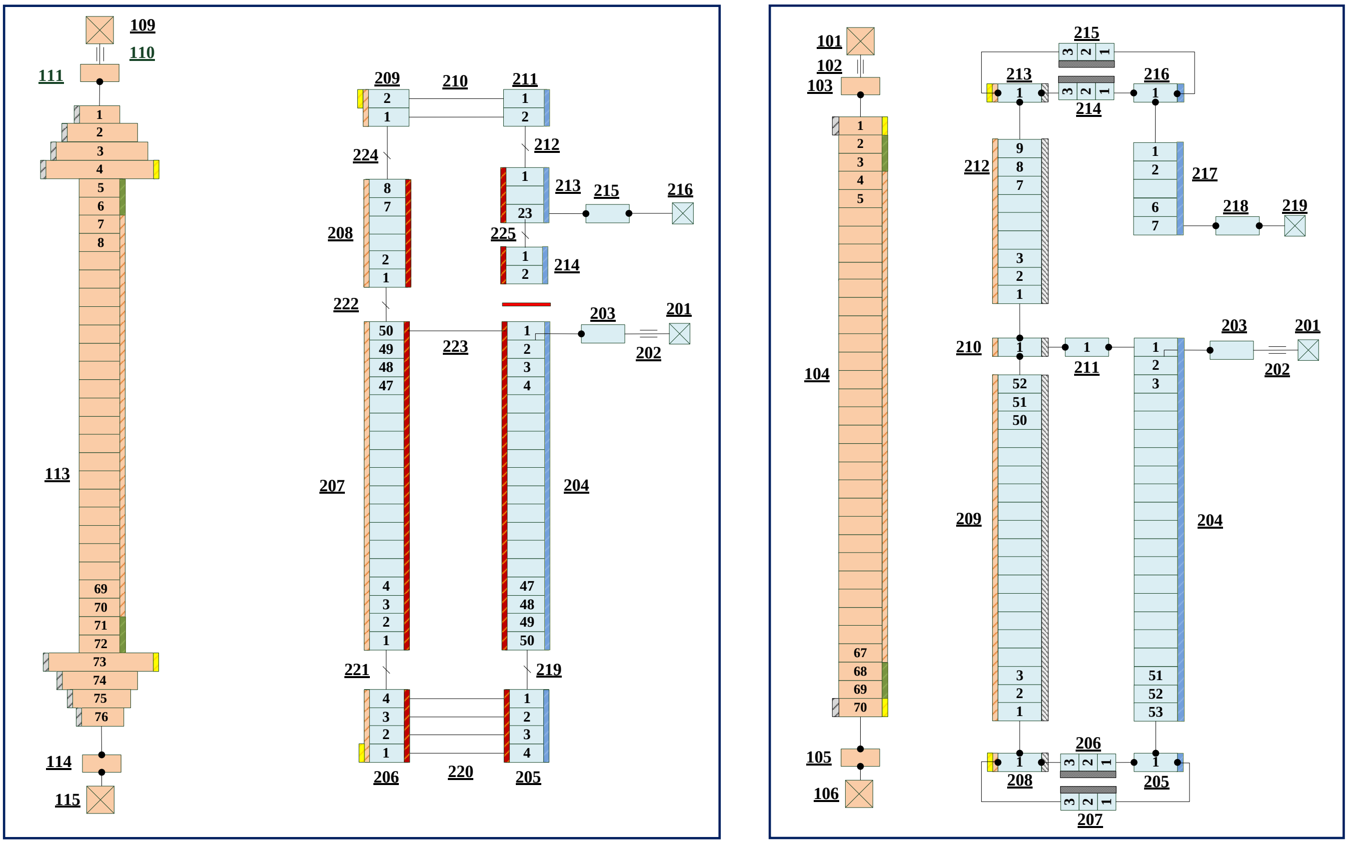

Fig. 22. BB OTSG (left) and STEAM OTSG mock-up (right) RELAP5/Mod3.3 nodalization

Symbol	Breeding Blanket OTSG					STEAM OTSG				
	HS	**L.B.***	**R.B.***	**Size**	**Description**	**HS**	**L.B.**	**R.B.**	**Size**	**Description**
	113-1	113	209, 208, 207, 206	5696 x ID=7.074m s=0.864mm	OTSG tube bundle (active HS)	104-1	104	213, 212, 210, 209, 208	37 x ID=7.074m s=0.864mm	OTSG tube bundle (active HS)
	113-2	113	-	h_{tsheet}=533.4mm	OTSG tube bundle inside tube-sheet	104-2	104	-	h_{tsheet}=100mm	OTSG tube bundle inside tube-sheet
	113-3	113	209, 206	A_{tsheet}=2.0440m^2	OTSG tubes-heets	104-3	104	213, 208	A_{tsheet}=0.00958m^2	OTSG tube-sheets
	113-4	113	-	IR=1.182m OR=1.288m	OTSG lower and upper emi-spherical heads	104-4	104	-	h=r=161.5mm	OTSG lower and upper cylindrical heads
	310-1	208 207	213-214 204	Shroud thickness=38.1m m	Shroud (thermal coupling between riser and DC)	-	-	-	-	No thermal coupling between riser and DC
	-	-	-	-	Riser is not insulated	210-1 210-2	210, 209, 208 213, 212	-	D=0.1397m (hexagonal flat to flat)	Riser shell (=shroud) insulation
	312-1	211, 213, 214 204, 205	-	IR=1.182m OR=1.288m	Steam downcomer ins. Water downcomer ins.	212-0 212-1	204, 205 216, 217	-	IR=0.0423m OR=0.0508m	Steam downcomer ins. Water downcomer ins.
	-	-	-	-	Riser and DC are connected by water and steam ports	212-2 212-3	214, 215 206, 207	-	2 ½’’ Sch. STD	Little steam and feedwater lines connecting riser and dc

* L.B. Left Boundary (fluid region exchanging heat with the inner surface of the solid structure), R.B. Right Boundary (fluid region exchanging heat with the outern surface of the solid structure. When not specified, R.B. is the environment and the structureis insulated).
1xx refers to STEAM-WL primary loop, 2xx refers to STEAM secondary loop, 3xx refers to WL tertiary loop and 4xx refers to WL secondary loop

Fig. 23 RELAP5/Mod3.3 modelling of BB and STEAM OTSGs heat structures referring to *Errore. L'origine riferimento non è stata trovata.*

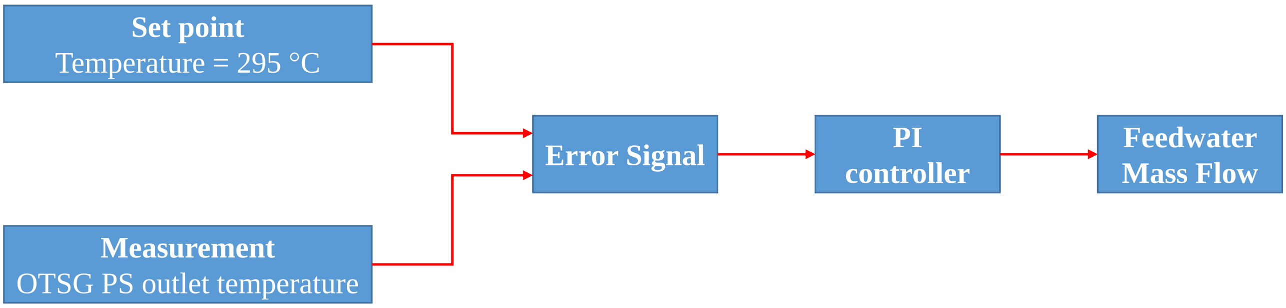

Fig. 24. Feedwater mass flow P-I control system logic

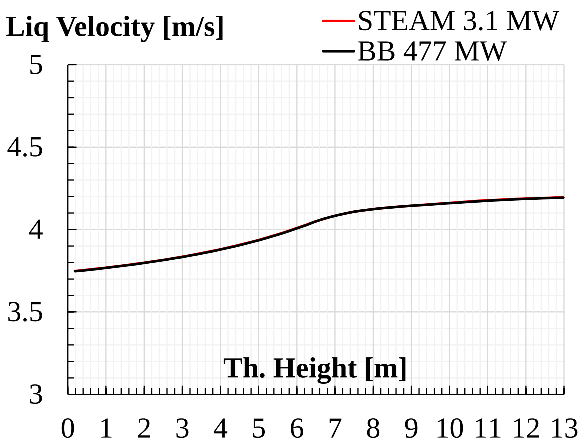

Fig. 25. Comparison between BB 477 MW and STEAM 3.1 MW: PS liquid velocity profile

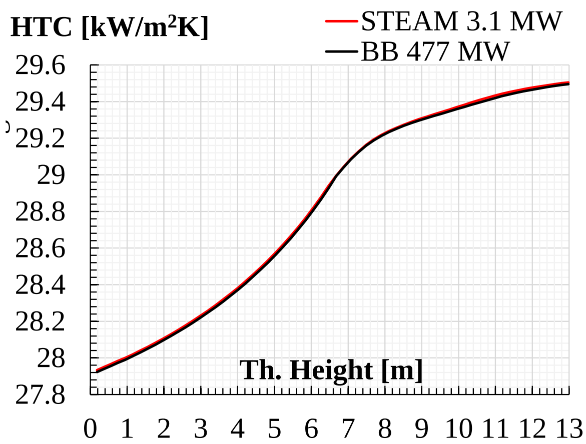

Fig. 26. Comparison between BB 477 MW and STEAM3.1 MW: PS HTC profile

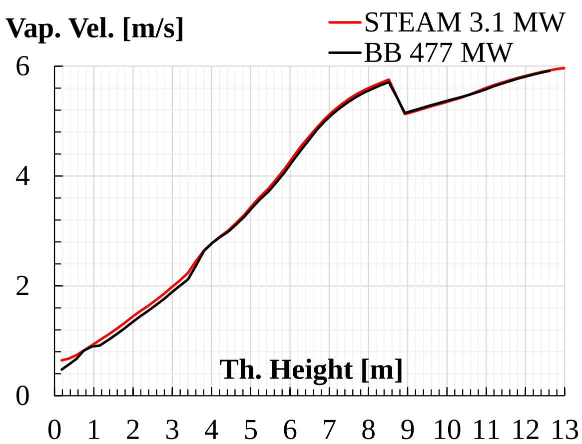

Fig. 27. Comparison between BB 477 MW and STEAM 3.1 MW: SS steam velocity profile

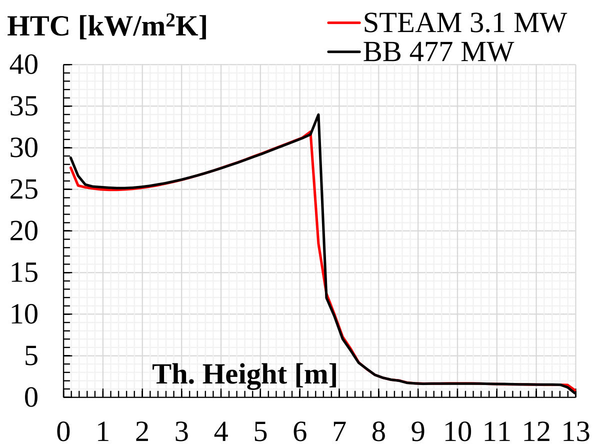

Fig. 28. Comparison between BB 477 MW and STEAM 3.1 MW: SS HTC profile

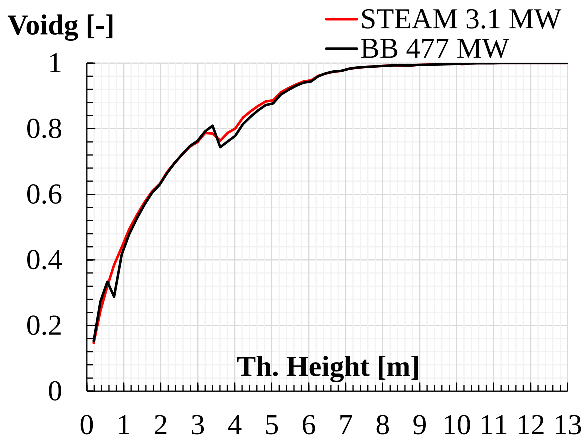

Fig. 29. Comparison between BB 477 MW and STEAM 3.1 MW: SS void fraction profile

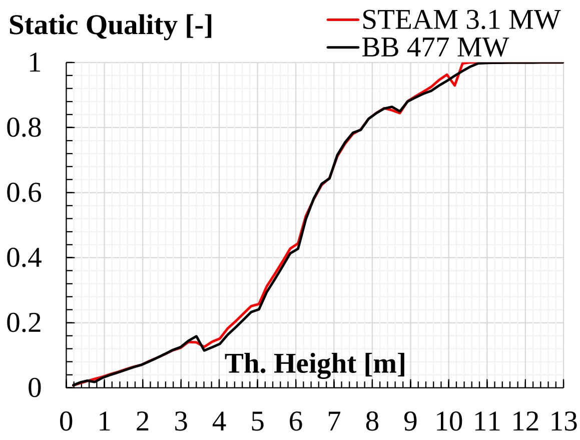

Fig. 30. Comparison between BB 477 MW and STEAM 3.1 MW: SS static quality profile

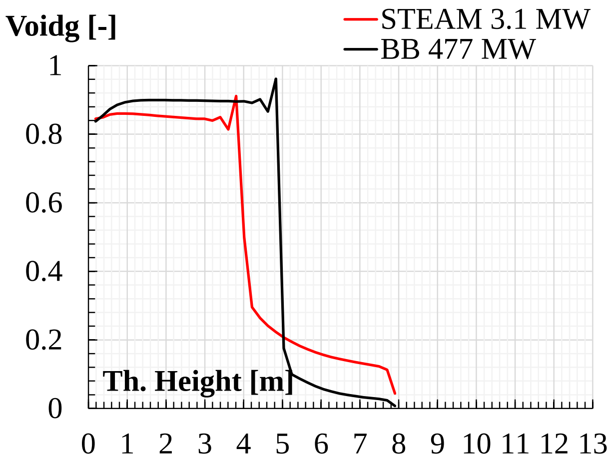

Fig. 31. Comparison between BB 477 MW and STEAM 3.1 MW: DC void fraction profile

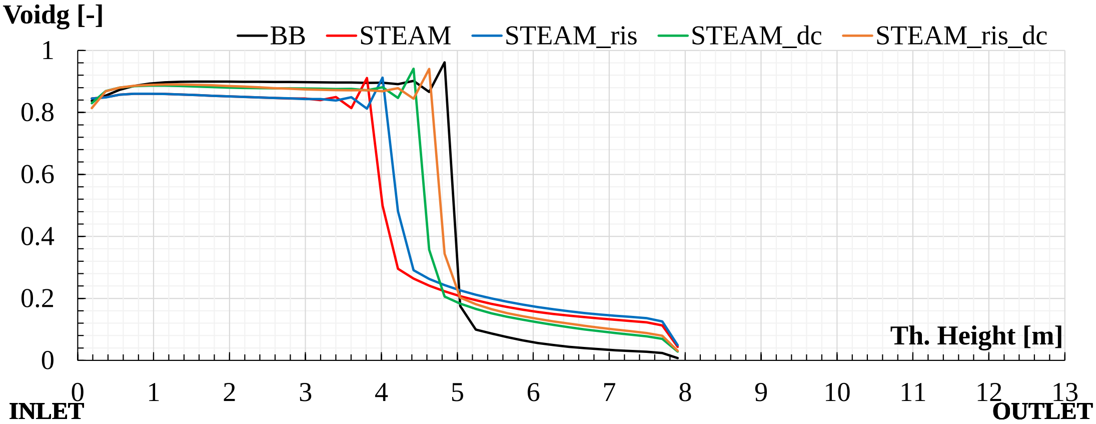

Fig. 32. Comparison between BB and STEAM different configurations: DC void fraction profile

5 NUMERICAL ANALYSIS IN SUPPORT OF THE STEAM FACILITY DESIGN

The STEAM design was objective of several analyses to investigate the performance while characterizing systems and components operation in fusion reactors. RELAP5/Mod3.3 code was used to assess specific criticality with focus on the secondary loop. The nodalization and the performed analyses are reported in this Section.

STEAM pre-test analysis was assessed too, being it a crucial phase in the experimental campaign (see Sect. 3.2) designed to assess the performance and stability of the system under various operating conditions. The methodologies and results obtained from a series of tests conducted at different power levels and during specific transition phases were analyzed: the gained insights provide essential feedback on system performance, allowing for fine-tuning and optimization before full-scale operation. By identifying potential issues and verifying the system capability to handle various scenarios, these analyses form the foundation for subsequent experimental investigations and ensure that the system is prepared for efficient and safe operation.

5.1 RELAP5 nodalization

RELAP5 mono-dimensional nodalization of both the primary and secondary loop was performed, allowing for the thermal-hydraulic analysis of the facility. Sensitivity analysis on the time step was performed, varying the maximum time step from $5 \cdot 10^{-4}$ and $5 \cdot 10^{-2}$. Since no variations were detected in the results, the maximum time step was adopted.

5.1.1 Primary loop

STEAM and Water Loop facility share the same primary loop (i.e., W-HYDRA primary loop, Sect. 3.1), that can be operated in the two different configuration thanks to the presence of manual valve. With reference to the nodalization of Fig. 33, the fluid path in the STEAM configuration is described in Sect. 3.1, while the Water Loop one is explained in Sect. 6.3.1. As reminded in Sect. 3.1, WL and STEAM hot and cold legs do not coincide.

Hydraulic components

The RELAP5/Mod3.3 nodalization of the W-HYDRA primary loop is shown in Fig. 33. The list of hydrodynamic components is presented below. Gray-marked components refer to part of the loops that are not operated in the STEAM configuration.

- OTSG
  - Branch 103 simulates the inlet nozzle.
  - Pipe 104 simulates the upper plenum, the tube bundle and the lower plenum.
  - Branch 105 reproduces the outlet nozzle.

- STEAM cold leg:
  - Pipes 106 and 108 reproduce the part of the loop from the OTSG outlet nozzle to point where the WL and the STEAM cold leg rejoin. Component 107 is one of the manual valves that allow the interception of either STEAM or WL. It is closed in WL operation and opened in STEAM configuration.
  - Components from 109 to 126 are not involved in the STEAM operation. Specifically, valves 110, 114, 121 and 125 are closed.
  - Branch 127 is the point where the WL and the STEAM cold leg rejoin.
  - Pipe 128, branch 129 and pipe 130 reproduce the part of the cold leg upstream the filter, common to both loops.

- Branch 131 stands for the filter.
- Pipe 132 simulate the part of the cold leg downstream the filter and upstream the pumps bifurcation branch, common to both the configurations.
- Branch 133 is the bifurcation branch, where the cold leg splits into two parallel pipes reaching the two pumps.
- Components 134 to 140 reproduce the high-mass flow pump line. Component 137 simulate the high-mass flow rate pump. Valves 135 and 139 represent the manual valve for the interception of this loop: they are closed for mass flow rates lower than 5 kg/s and opened for mass flow rates within 5 and 20 kg/s. They are both open in STEAM operation.
- Components from 141 to 147 are not involved in STEAM operation. Specifically, valves 142 and 146 are closed.
- In branch 148, the reconnection of the pump lines occurs.
- Pipe 149, branch 150 and pipe 151 stand for the part of the cold leg downstream the pump lines connection and the heater lines bifurcation.
- Branch 152 simulates the bifurcation point for the two parallel small cold lines.
- Components from 153 to 157 simulate the STEAM heater small cold line. Valve 155 is the manual valve for heater interception. It is opened in STEAM operation and closed in WL configuration.
- Components from 164 to 168 represent the WL heater small cold line. Valve 166 is the manual valve for heater interception. It is open in both STEAM and WL operation.

➢ STEAM power source
  - Pipe 158 reproduces the STEAM heater (HT-SHP-001).
  - Pipe 169 simulates the WL heater (HT-WHP-001).

➢ STEAM hot leg
  - Components from 159 to 163 stand for the STEAM heater small hot line. Valve 161 is the manual valve for the heater interception. It is opened in STEAM operation and closed in WL configuration
  - Components from 170 to 174 represent the WL heater small hot line. Valve 172 is the manual valve for heater interception. It is open in both STEAM and WL operation.
  - In branch 175, the reconnection of the heater lines is realized.
  - Pipe 176 constitute the section of the loop that connects the heater lines with the branch where the bifurcation between the WL test section line and its bypass line (that would be part of the STEAM hot leg) are placed.
  - Branch 177 realize the bifurcation between the WL test section and its bypass line.
  - Components from 178 to 180 simulate the WL test section bypass line (i.e., part of the STEAM hot leg). Specifically, component 179 is the manual valve that is opened in STEAM configuration and closed when WL is operated.
  - Components from 181 to 193 are not involved in STEAM operation. Valves 182 and 192 are closed.
  - In branch 194, the WL test section line and its bypass line reconnect.
  - Pipe 195, branch 196 and pipe 197 reproduce the section of the loop that can be considered hot leg for both STEAM and WL.
  - In branch 198 the bifurcation between the steam generator line and the WL heat exchanger is placed.
  - Components from 100 to 102 realize the part of the STEAM hot leg that reaches the steam generator. Valve 101 is the hot leg manual valve that allows the interception of the steam generator. It is open during STEAM operation, and it is closed in WL configuration.

➢ Surge line
  - Branch 601, pipe 602 and branch 603 simulate the surge line;

- Spray line
  - Components from 6015 to 619 represent the part of the spray line connected to the cold leg;
  - Component 620 is the spray valve;
  - Pipe 621 and branch 622 simulate the part of the steam line from the spray valve to the upper part of the pressurizer;

- Pressurizer
  - Pipe 605 and pipe 607, connected by multiple junction 606 realize the pressurizer.

- Pressurizer safety valves
  - Component 610 is the PORV (Pressure Operating Relief Valve);
  - Component 612 is the SRV (Safety Relief Valve);
  - Time-dependent volumes 613 and 611 simulate the draining tank where the steam is discharged in case of PORV and SRV opening.

Heat structures
Thermal interactions within the modeled systems and with the surrounding environment are represented through heat structures (HS). These heat structures are classified into three distinct types, as referenced in Fig. 34:

Active heat structure are the components where power is produced. They are simulated as rods composed of concentric layers of constantan (inner), ceramic (middle annular), and alloy 800 (outer). Primary loop power sources are the electric heaters (158-1 and 169-1) and the pressurizer heating elements (HS 607-5).

Coupling heat structures facilitate power exchange between different systems or between various parts of the same system. For instance, the primary and secondary sides are coupled via HS 104-1, which models the INCONEL tubes that separate the primary fluid (flowing downwards on the tube-side) from the secondary fluid (flowing upwards on the shell-side) inside the Test Section, specifically the Steam Generator.

Insulated heat structures encompass all other HSs and simulate power exchange with the external environment. Heat losses through these structures are calculated with an external air temperature assumed to be 10°C and a fixed dissipative heat transfer coefficient of 8 W/m²K.

Control systems
The RELAP5 model was equipped with a series of control systems, whose operation is based on the monitoring of a set of parameters. The acquisition of this parameters is realized by sensors whose nomenclature refer to Fig. 12. Specifically, the PI controllers adopted operate following the scheme reported in Fig. 35.

Pump Velocity Control Systems
The primary side mass flow is directly influenced by the pump velocity, which is regulated by a PI controller to maintain the nominal mass flow rate. The measured variable is the pump mass flow rate, monitored by the flow meter MF-WCP-001 (Fig. 12). The set point for this control system is a nominal mass flow rate of 16.05 kg/s. The error is the difference between the set point and the measured variable, while the regulated variable is the pump velocity (rpm). If the measured mass flow rate exceeds the set point (resulting in a negative error), the pump velocity is reduced to decrease the mass flow.

Heater Power Control System
The heater power control system regulates the primary side heater power to achieve a fixed OTSG inlet temperature, which depends on the exchanged power affected by both primary and secondary mass flows. The control system ensures that the OTSG inlet temperature remains at its nominal value despite variations in parameters. The measured variable here is the OTSG inlet temperature, measured by thermocouple TC-SHP-

060 (see Fig. 12), with a set point of 328°C. The error is the difference between this set point and the measured temperature, and the regulated variable is the heater power supplied to HSs 158-1 and 169-1 (Fig. 34). If the measured temperature exceeds the set point (indicating a negative error), the heater power is reduced to lower the temperature.

Pressurizer Heater Power Control System

For the pressurizer heater power control system, the pressurizer manages the system pressure and is equipped with safety and relief valves to prevent overpressure. It also includes an electrical heater to avoid depressurization. The measured variable for this control system is the pressure at the top of the pressurizer. The set point is a nominal pressure value of 15.5 MPa, with the error being the difference between the measured pressure and the set point. The regulated variable is the pressurizer heater power, provided to HS 607-5 (Fig. 34). This control system uses a general table to relate pressure differences to power values, where a smaller error results in higher power supplied to the electrical heater. It is important to note that even with a null error, some power is required to compensate for heat losses.

5.1.2 Secondary loop

Hydraulic components

The RELAP5/Mod3.3 nodalization of the STEAM secondary loop is shown in Fig. 36 and it is composed by the following components:

- OTSG
  - Branch 203 stands for the inlet nozzle, that is connected to the second volume of the DC (pipe 204), since the feedwater is sprayed below the aspirator junction, simulated in the first volume;
  - Pipes 204 and branch 205 simulate the external downcomer;
  - Pipes 206 and 207 reproduce the external piping that connects downcomer to riser to downcomer;
  - Branch 208, pipe 209 and branch 210 represent the lower part of the riser up to the recirculation zone;
  - Branch 211 is the riser recirculation pipe;
  - Pipe 212 and branch 213 stand for the upper riser (above the recirculation zone);
  - Pipes 245 and 216 reproduce the external piping that connects riser to downcomer;
  - Branch 216 and pipe 217 simulate the steam external downcomer;
  - Branch 218 is the OTSG outlet nozzle;

- Steam line
  - Pipe 216 represents the 5” main steam line;
  - Component 220 and 299 are the 5” and the 1 ½” lamination valves;
  - Pipe 221 and branches 222, 223, 224 and 225 simulate the 1 ½” steam line;

- Air Cooler 1 (de-superheating and condensation)

The RELAP5 nodalization of the four modules of which the A.C.1 is made up is symmetric, even if the tubes lengths are different. It has been realized using numbers from 300 to 385, in the following referred to using X, Y and Z, where X=0,2,4,6, Y=1,3,5,7 and Z=0,1,2,3,4,5:

  - Components 3X0 is the small steam line upstream the air cooler regulation and interception valve;
  - Pipe 3X1 is the regulation and interception valve;
  - Component 3X2 represents the part of small steam line that connects the valve with the air cooler;
  - Branches 3X3, 3X4, 3X5, 3X6 and 3X7 realize the inlet header (1 ¼” Sch. STD);
  - Pipes 3X8, 3X9, 3Y0, 3Y1, 3Y2 are the air cooler active tubes: each tube collapses the flow area of 11 tubes for a total of 55 tubes for module;
  - Branches 3Y3, 3Y4, 3Y5, 3Y6 and 3Y7 realize the outlet headers (1 ¼” Sch. STD), allowing the reaching of a uniform temperature;

- Components 3Y8 and 38Z represent the small condensation line (1 ¼” Sch. STD);
- Valve 3Y9 is the interception line installed on the small condensation line (1 ¼” Sch. STD);
- Couples of one pipe and one branch then connect the small condensation lines to the main condensation line: 380 and 381 for the first module, 382 and 383 for the second, 384 and 385 for the third, while the fourth is directly connected to the line;

In particular:

  - X=0,Y=1 and Z=0,1 define the first A.C. module;
  - X=2, Y=3 and Z=2,3 define the second A.C. module;
  - X=4, Y=5 and Z=4,5 define the third A.C. module;
  - X=6 and Y=7 define the fourth A.C. module.
- Components from 1 to 20 represent the four Air Cooler air side:
  - Components 1, 6, 11 and 16 are the time-dependent volumes that impose the air inlet conditions;
  - Time-dependent junctions 2, 7, 12 and 17 fix the inlet air mass flow;
  - Pipes 3, 8, 13 and 18 stand for the Air Cooler shells, where the first one is the active volume;
  - Single junctions 4, 9, 14 and 19 allow the connection to the time-dependent volumes;
  - Time-dependent volumes 5, 10, 15 and 20 impose the air outlet pressure.

➢ Feedwater line
- Pipe 228 is the part of the feedwater line connecting the A.C.1 to the condensate tank;

➢ Condensate tank and pressure regulation system
- Branch 230 stands for the tank inlet nozzle;
- Pipe 231 reproduces the condensate tank;
- Component 260 is the safety valve;
- Time-dependent volume 261 simulates the fluid discharge tank;
- Branch 232 represents the tank outlet nozzle.

➢ Feedwater line
- Pipe 233, valve 234, pipe 235, valve 236 and pipe 237 reproduce the part of the feedwater line that goes from the tank outlet nozzle to the A.C.2;

➢ Air Cooler 2 (Sub-cooling)
- Branches 238 and 239 reproduce the air cooler inlet header;
- Pipes 240 and 241 realize the air cooler active tubes: each pipe collapses the flow area of 9 tubes for a total of 18 tubes;
- Pipes 242 and 243 simulate the air cooler outlet header;

➢ Feedwater line
- Pipe 244 stands for the part of the feedwater line connecting the A.C.2 to the filter;
- Branch 245 is the filter inlet nozzle;
- Pipe 246 simulates the filter, whose dimensions are assumed to be equal to the piping. The height difference between filter inlet and outlet pipes has been simulated by giving the component the misalignment as vertical elevation;
- Branch 247 realizes the filter outlet branch;
- Pipe 248 goes from the filter outlet nozzle to the pump;
- Component 249 is the pump;

- Pipe 250 reproduces the part of the feedwater line from the pump to three-ways valve;
- Component 251 simulates part of the three-ways valve (simulated with two valves);
- Pipe 252 represents the part of the feedwater loop from the three-ways-valve to the heater;

➢ Electrical Heater
- Branch 253 stands for the heater inlet nozzle;
- Pipe 254 simulates the heater;
- Branch 255 is the heater outlet nozzle;

➢ Feedwater line
- Pipe 254 reproduces the part of the feedwater line from the heater to the OSG inlet nozzle;

➢ A.C.1 bypass line
- Branch 270 and pipe 271 realizes part of the A.C.1 bypass line;
- Component 272 is the A.C.1 bypass valve;
- Pipe 273 and branch 273 simulate the rest of the A.C.1 bypass line;

➢ Feedwater bypass line
- Component 500 simulates part of the three-ways valve;
- Pipe 501 reproduces the feedwater bypass line;
- Component 502 is the valve in charge of the pressure reduction of the liquid from 64 to 25 bar;
- Branch 503 realizes the connection of the feedwater bypass line to the feedwater line upstream the A.C.2.

Heat structures
Heat exchanges within the simulated systems, as well as between the systems and their surrounding environment, are modeled through heat structures (HS), which are detailed in Fig. 37 These heat structures fall into three distinct categories.

Active heat structure, simulated as rods composed of concentric layers of constantan (inner layer), ceramic (middle annular layer), and alloy 800 (outer layer). These structures are the sites where power is generated. Specifically, there is the main electric heater (254-1) and the condensate tank heater (231-2).

Coupling heat structures facilitate the transfer of power between different systems or between various parts of the same system. For example, the primary and secondary sides are interconnected through HS 104-1, which represents the INCONEL tubes separating the primary fluid (flowing downwards on the tube-side) from the secondary fluid (flowing upwards on the shell-side) within the Test Section, specifically the Steam Generator. Additionally, the four modules of the A.C.1 system are connected to ventilated external air through multiple heat structures, including HS 308-1, 311-1, 328-1, 331-2, 348-1, 351-2, and 368-1, 371-2. The subcooling air cooler is similarly connected to external ventilated air via HS 240-1.

Insulated heat structures encompass all other HSs directly interacting with the external environment. Heat losses through these structures are calculated assuming an external air temperature of 10°C and using a fixed dissipative heat transfer coefficient of 8 W/m²K.

Control systems
The operation of control systems is guided by the scheme depicted in Fig. 35. The acquisition of measured variable values is managed by sensors, as referenced in Fig. 14.

Pump Velocity Control Systems

The pump velocity control system directly influences the secondary side mass flow. To maintain the nominal mass flow rate, a PI controller is employed. Specifically, the pump mass flow rate is measured by the flow meter FM-SCS-001 (see Fig. 14). The set point for this system is a mass flow rate of 1.64 kg/s, which ensures the primary side OTSG inlet temperature is at its nominal value. The error represents the difference between this set point and the measured variable, while the regulated variable is the pump velocity (rpm). When the measured mass flow rate exceeds the set point (resulting in a negative error), the system reduces the pump velocity to decrease the mass flow rate.

Heater power Control Systems

In the heater power control system, the power supplied to the secondary side heater is regulated to achieve a fixed OTSG inlet temperature for the feedwater. This temperature is influenced by both primary and secondary mass flows. The PI controller ensures the OTSG inlet temperature remains at its nominal value despite parameter variations. The temperature is measured by thermocouples TC-SCS-140 (refer to Fig. 14) , with a nominal set point of 238°C. The error is the difference between this set point and the measured temperature, and the regulated variable is the heater power provided to the heat structure HS 254-1 (Fig. 37). If the measured temperature exceeds the set point (indicating a negative error), the heater power is reduced, which lowers the temperature.

Sub-cooling A.C. control system

The sub-cooling air cooler (A.C.2) controls the cooling of the fluid from saturated to subcooled conditions. Its cooling power is regulated by an integral control system to achieve a nominal temperature of 210°C at the A.C.2 outlet. The outlet temperature is measured by thermocouple TC-SCS-090 (see Fig. 14), , with the set point being 210°C. The error represents the difference between this set point and the measured temperature, and the regulated variable is the air mass flow to the A.C.2 secondary side. A negative error (measured temperature lower than the set point) results in a reduction of the air mass flow, decreasing the cooling power and increasing the A.C.2 outlet temperature.

Condensate Tank heaters power Control Systems

For the condensate tank heaters, which maintain the Low-Pressure Section of the STEAM secondary loop at 2.5 MPa, a control system manages the heater power. The pressure at the top of the condensate tank is measured, and the set point is 2.5 MPa. The error is the difference between this measured pressure and the set point, and the regulated variable is the power supplied to the heater within heat structure HS 231-2 (see Fig. 37). The control system uses a general table to correlate pressure differences with power values. Smaller errors result in higher power to the heater, though some power is still required to compensate for heat losses even when the error is zero.

Additional source power Control Systems

Results of Sect. 5.3.1 will show that secondary side vapor outlet temperature exceeds the nominal value. A higher OTSG outlet temperature determines higher enthalpy at the lamination valve suction, meaning that the expansion through the valve should occur at higher enthalpy. However, in the volume downstream the valve where chocked flow occurs, enthalpy is not correctly conserved in the RELAP5 model. An additional power source, regulated by an integral control system, is used to replicate the expected enthalpy conditions upstream of the valve. The enthalpy downstream of the lamination valve is the measured variable, while the set point is the enthalpy upstream of the valve, which can vary. The error is the difference between these values, and the regulated variable is the additional source heater power provided through HS-221-2 (see Fig. 37). Since no enthalpy sensors are present in the loop, this additional source serves to accurately simulate the isenthalpic expansion through the RELAP5 lamination valve component. A negative error (higher downstream enthalpy than upstream) leads to a reduction in the additional source power, which decreases the downstream enthalpy.

5.2 RELAP5 preliminary analyses

5.2.1 De-superheating and condensation air cooler assessment

The A.C.1, responsible for the de-superheating and condensation of the steam produced within the SG, is a delicate component, whose operation needs thorough investigation. Thermal-hydraulic requirements of the components are listed in Tab. 14. Its preliminary design was provided by “La casa del radiatore” manufacturer (see Fig. 38) and was therefore thermal-hydraulically investigated by means of the RELAP5/Mod3.3 code. The main geometrical data of the components are reported in Tab. 15.

The first numerical activity involved a preliminary analysis aimed at validating the geometry provided by the manufacturer. To do so, a simplified RELAP5/Mod3.3 model was developed, collapsing the four modules into one and adopting time-dependent volumes and time-dependent junctions to fix inlet temperature, outlet pressure and mass flow rate of both steam and air sides. The system was analyzed keeping the steam flow constant but varying the air mass flow values (Γ) from 0% to 342% of the nominal value, since the air-side constitutes the limiting resistance to the heat exchange.

Results of Fig. 39 show that with zero air mass flow, superheated steam is present at the air cooler outlet and the void fraction is one. Increasing the air mass flow reduces the void fraction, cooling the steam from superheated to saturation conditions and leading to condensation. Further increases in air mass flow cause phase separation, where part of the fluid cools below saturation while saturated vapor remains.

The comparison with a horizontal bundle was also performed, aiming at investigating the effect of the bundle inclination on the component performance. Results confirmed the adoption of a vertical bundle was preferred because, with respect to the horizontal bundle, they generally offer superior thermal-hydraulic performance compared to horizontal tube condensers [68].

Once characterized the performance of the single-module system, the modulation of the component in four sub-systems was investigated. As specified in Sect. 3.2.2, this partialization facilitates the facility operation at different power levels. To assess the condensation power of the four modules, RELAP5/Mod3.3 analyses were performed adopting the nodalization section related to the only air cooler (with reference to Fig. 36, components from 221 to 228 for the steam/water side and from 1 to 20 for the air side), omitting the rest of the loop by utilizing time-dependent volumes and junctions to impose nominal inlet temperature, outlet pressure and mass flow rate.

Each module is equipped with a valve that operates based on specific set points, aiming at modulating the mass flow entering each module to maintain optimal system performance. Specifically, as the vapor mass flow decreases and reaches these set points, the corresponding valve closes, diverting the flow to the remaining open modules. The first valve closes when the mass flow rate drops to 3/4 of the nominal value. The second valve closes at 2/4, and the third valve at 1/4. The fourth module remains open to ensure continuous operation until 1% of the mass flow rate, when steam is expelled in the environment through a dedicated valve. Each module is also equipped with check valves installed on the outlet line to avoid reverse flow.

To test the system behavior under the specified control logics, analyses were performed varying the inlet vapor mass flow from the 120% to the 10%, with variations of 10 %, and from 5% to 1% with variations of 1%. Results of Fig. 40 shows that the total mass flow does not equally distribute among the four modules, progressively decreasing from the first to the last, due to the different chain of pressure drops due to small geometrical asymmetries in the pipes realization. As the vapor mass flow decreases, valves progressively close the corresponding air coolers, redistributing the remaining mass flow among the active modules. This results in oscillations in the system mass flow, particularly as modules are intercepted.

Consistently with observations from the single module nodalization, phase separation and horizontal stratification at the air cooler outlet were observed, indicating that no mixing ensures equilibrium conditions. Superheated vapor cools to saturation, and as part of the vapor condenses, its higher heat transfer coefficient causes sub-cooling while saturated vapor remains.

The modulated component was then tested in nominal steady state conditions, to characterize its behavior in the expected working conditions. RELAP5/Mod3.3 simulations show that no standard control logic can regulate the air mass flow: operating in saturation, the outlet temperature is not an indicator of the fluid outlet thermo-dynamic conditions. As already noted, inside the air cooler, phase separation occurs because the condensed liquid has a higher heat transfer coefficient compared to the saturated vapor. This results in significant sub-cooling of the liquid phase while not all the steam has condensed yet. Therefore, secondary air velocity has been selected to obtain fluid outlet conditions that fit nominal ones as closely as possible, without causing excessive sub-cooling.

RELAP5 results are collected in Tab. 16. Mass flow uneven distribution between the four modules of the first air cooler (Fig. 41) results from the different chains of pressure drops characterizing the lines reaching each module due to geometrical asymmetries in the pipe paths. Higher module mass flow should result in higher fluid outlet enthalpy, but the different operating pressures of the modules, listed in Tab. 16, influence the condensation power of the modules (Fig. 42). Further investigations show that mass flow does not equally distribute in the tubes of each module either, decreasing progressively from the first to the last pipe (Fig. 43). Exchanged power, consequently, follows the same trend (Fig. 44). Fig. 45 reports the axial value of the thermodynamic quality (quale) for the first and the last tubes of the four modules. Being an indicator of the fluid thermo-dynamic conditions, it assumes values between 0 and 1 for saturation conditions, values >1 for superheated conditions, and <0 for sub-cooling conditions.

5.2.2 RELAP5 assessment of the STEAM secondary loop Low-Pressure Section

The Low-Pressure Section (LPS) is the part of the STEAM secondary loop that is actually in charge of the heat removal. It includes the A.C.1, the condensate tank and the A.C.2, whose operation, therefore, requires comprehensive assessment.

To ensure optimal performance and reliability of these components, detailed analyses were conducted using RELAP5/Mod3.3 nodalization, focusing on specific elements such as the A.C.1 modules, the condensate tank, and A.C.2 (with reference to Fig. 36, components from 221 to 244 for the steam/water side and from 1 to 25 for the air side), using time-dependent volumes and time-dependent junctions to fix the inlet temperature, outlet pressure and mass flow rate.

To understand the impact of various factors on the LPS, several non-nominal scenarios were thoroughly examined.

The impact of air velocity changes on the A.C.1 was a key focus. This scenario investigated how fluctuations in air mass flow affect the A.C.1 and, in turn, the performance of the entire LPS. The analysis aimed to understand the system's behavior under different airflow rates and its implications for overall performance.

Another critical examined scenario involved variations in fluid conditions upstream of the lamination valve, with the assumption that the valve maintains an isenthalpic process at a pressure of 25 bar. This scenario included assessing changes in OTSG outlet thermal-hydraulic conditions and fluctuations in the vapor mass flow at the air cooler outlet.

Given that A.C.1 operates under saturation conditions, outlet temperature is not a reliable performance indicator. Instead, sensitivity analyses determined acceptable air velocities, with each A.C.1 module equipped with an inverter for eventual independent velocity modulation in response to changes in vapor mass flow from the OTSG.

A.C.1 air velocity sensitivity

The influence of the A.C.1 air mass flow variation not only affects the operation of the heat exchanger itself but also impacts on the condensate tank and the A.C.2. For this reason, after characterizing the A.C.1 operation in nominal conditions, RELAP5/Mod3.3 simulations were performed to assess the system response while varying the A.C.1 modules air mass flow rates.

As the air velocity increases, the power of A.C.1 also increases (Fig. 46), leading to enhanced heat exchange. This results in a decrease in the fluid temperature at the tank inlet (Fig. 47), which subsequently lowers the void fraction at the tank inlet (Fig. 48). The tank liquid collapsed level rises due to this increased condensation (Fig. 49). Conversely, A.C.2 velocity and power decrease (Fig. 50 and Fig. 51), as the control system regulates the A.C.2 mass flow to maintain a fixed outlet temperature necessary for the pump correct operation, thus preventing cavitation. This balance ensures that the system operates efficiently without risking damage to the pump.

Results indicate that with the selected A.C.1 geometry, an air velocity of at least 7.2 m/s is necessary for correct system operation. Specifically, with a lower air mass flow, the lower exchanged power would not be enough to guarantee the condensation of a significant amount of vapor, leading to too high void fraction at the tank inlet that provokes the liquid collapsed level of this component to drop below the minimum value required for safety reasons. In order to allow the system to operate in this condition, too high condensation power and therefore air velocity would be required by the A.C.2. With a higher mass flow, instead, the higher exchanged power would determine excessive sub-cooling of the operating fluid. The overcooled fluid entering the tank determines the temperature to drop, leading to the condensation of the present vapor and the formation of a level higher than the safety margin. The tank becomes solid (i.e., full of water) and loses its capability to regulate pressure. Furthermore, as the fluid temperature decreases, the A.C.2 velocity and power reduce and go to zero for inlet temperatures lower than the outlet required one (210°C). An excessive overcooling of the fluid could affect the operation of the steam generator if the electrical power provided by the heater is not sufficient to heat it up to the temperature required at the SG inlet.

As the main result of this section, it is possible to state that to unalter the SG operation, the A.C.1 air velocity must remain within a range where the lower limit is imposed by the maximum power that the A.C.2 can provide, while the upper limit is determined by the maximum electrical power that the heater can provide.

Variation of the OTSG Outlet Thermal-Hydraulic Conditions

The OTSG outlet temperature was varied between 285°C and 320°C to determine the A.C.1 air velocity required to achieve the necessary saturated liquid conditions at the outlet. The simulations test matrix is reported in Tab. 17, together with the temperature difference associated to the isenthalpic transformation occurring in the lamination valve. For temperatures below 285°C, A.C.1 should be bypassed.

As expected, results indicates that higher OTSG temperatures requires increased air velocities (Fig. 52) and mass flow (Fig. 53) in the four modules, and a proportional increase of the A.C.1 power exchange (Fig. 54).

The enthalpies at the air cooler outlet for the modules should theoretically be constant, reflecting the saturated liquid condition needed at the A.C.1 outlet. However, results of Fig. 55 and Tab. 18 show that the outlet enthalpies are not identical across the four modules, indicating variations in performance based on the fluid thermal-hydraulic conditions. The first module displays a higher variability in outlet enthalpy (±10% from the required value), whereas the second and third modules have negligible or very low errors. The fourth module consistently shows a negative error, likely due to receiving less vapor for condensation as it is located at the end of the steam line. Despite these variations, the average enthalpy across all modules varies by less than ±3%, suggesting that overall system performance is acceptable.

Fig. 56 shows that the tank inlet liquid temperature fluctuates within a ±3% error margin from the nominal value of 224°C. However, the requirement of having a tank inlet liquid fraction equal to one is respected (Fig. 57) and a stable liquid level is maintained within the tank (Fig. 58). The A.C.2 outlet temperature was regulated to ensure 210°C at the pump suction (Fig. 59), preventing cavitation.

Variation of the Vapor Mass Flow at the Air Cooler Outlet

The condensation capability of the four modules was investigated across different values of the vapor mass flow to be condensed. This investigation aims to develop an operative map that shows the required module velocities to achieve saturated liquid conditions at the system outlet for each vapor mass flow value. Specifically, vapor mass flow rates ranging from the nominal value of 1.64 kg/s down to 0.3 kg/s have been

explored. The necessary amount of air mass flow was manually determined in each scenario, ensuring that all parameters remained within their operative ranges.
Fig. 60 and Fig. 61 illustrate the variation in A.C.1 air velocity and mass flow corresponding to changes in the vapor mass flow. As the vapor mass flow decreases from the nominal value, the velocity of the four air coolers decreases uniformly in line with the reduced condensation power requirement. Upon reaching the first set point, the corresponding module is intercepted by closing the interception valves, which causes the air fans of that module to switch off, dropping the air velocity to zero. When a module closes, the vapor mass flow redistributes among the remaining modules, increasing their air requirements. This regulation necessitates an inverter on each module to accommodate the adjustments.

The exchanged power is directly proportional to the mass flow, as depicted in Fig. 62, which follows the same trend. As the vapor mass flow decreases, the power decreases, and at a mass flow rate of 0.3 kg/s, the total power aligns with the fourth module alone.

This analysis highlights the system capability to manage varying amounts of vapor while maintaining consistent outlet conditions. At high vapor mass flows, as shown in Fig. 63, the modules' outlet enthalpies remain relatively constant, though the first module exhibits higher variability. When modules are bypassed, their outlet enthalpies rise to the upstream module value as the air velocity drops to zero instantaneously. The variations in the modules outlet enthalpies, as discussed in previous sections, point to operational asymmetries caused by disparities in pipe construction. Tab. 19 lists the modules air cooler outlet enthalpies and corresponding relative errors, marked as "-" when a module is bypassed.

The first module consistently shows the highest relative error, which is always positive or null. The second and third modules exhibit very low relative errors, indicating operation close to the nominal point. In contrast, the fourth module consistently has a negative error, resulting in vapor sub-cooling due to its position farthest from the vapor source. Despite these discrepancies, the average relative error for the modules' outlet enthalpies remains within ±3%.

Key parameters to monitor during this activity include ensuring proper tank operation. As shown in Fig. 64, the fluid entering the tank maintains a liquid fraction close to one, as required, and the liquid temperature demonstrates minimal variability, with a relative error below ±3%. This error is consistently negative, indicating sub-cooling conditions, which helps maintain a nearly constant liquid level inside the tank, as illustrated in Fig. 65. Finally, the fluid reaches A.C.2, where the air mass flow is adjusted to keep the outlet temperature stable, as depicted in Fig. 66.

5.2.3 Design optimization for low-power operation

As discussed in Sect. 3.2, a low-power experimental campaign will be conducted on the STEAM facility to simulate the SG operation at power levels significantly lower than the nominal values.

The low-power testing of the steam generator involves a substantial reduction in the power exchanged between the primary and secondary loops within the SG. This reduction is achieved by decreasing the feedwater mass flow directed to the SG while maintaining constant mass flows on both the primary and secondary sides, with pumps operating at a constant speed. Valves that regulate flow area based on the mass flow rate control this operation.

A 1 ½" Sch. STD three-way valve (VP-SFW-R01 in Fig. 14, modeled as component 251 in Fig. 36) is installed on the feedwater line downstream the pump, allowing the total mass flow to be divided between the feedwater line and the feedwater bypass. Preliminary analysis indicates precise regulation from 100% to just below 10% of the nominal mass flow. For finer control below 10%, an additional ½" Sch. STD valve (VP-SFW-R02 in Fig. 14, simulated with component 298 in Fig. 36) has been added to regulate mass flow down to 1%. The valve operation is illustrated in Fig. 67.

A 5" Sch. STD valve (VP-SHS-R01 in Fig. 14, modeled as component 220 in Fig. 36) is planned for installation on the steam line downstream of the SG. Its flow area is regulated based on upstream pressure to perform steam lamination from 64.1 to 25 bar. Preliminary analyses show that the valve area regulation ensures the correct isenthalpic process for mass flow rates from 100% to 10%. An additional 1 ¼" Sch. STD valve (VP-SHS-R02 in Fig. 14, modeled as component 299 in Fig. 36) was included in the RELAP5 model to provide further regulation down to 1%. Both valves operate under the condition that upstream pressure is ≥ 64.1 bar. The valve operation schemes are illustrated in Fig. 68.

The mass flow paths under the analyzed conditions are highlighted in Fig. 69 and Fig. 70. At 10% and 5% of nominal power, the produced vapor is condensed by one module of A.C.1. At 1% power, the vapor bypasses the A.C.1 modules and, remaining as superheated vapor, is sent directly to the condensate tank.

Among the control systems implemented in the RELAP5 code, the one regulating the primary side heater power operates with a different set-point during low-power tests. This adjustment is necessary because the primary side temperature difference directly correlates with the exchanged power (P=mcpΔT), meaning reduced power results in a reduced ΔT. To maintain a constant average temperature in the primary loop, the set-point (i.e., the hot leg temperature equal to the SG inlet) is calculated as follows:

$$Set\ Point = T_{av} + \frac{\left(\frac{\Delta T}{2}\right)}{100} P_{\%}$$

Where:

- T_{av} is the primary loop average temperature;
- ΔT is the primary loop temperature difference ($T_{HL} - T_{CL}$)
- P% is power percentage at which the analysis is performed (i.e., 10%, 5% and 1%).

To enhance the precision of the controller, the specific heat (cp) is averaged over the entire component length, including inlet and outlet nozzles. The operational scheme for the primary heater power control system is illustrated in Fig. 4.10.

5.3 Operative scenarios

5.3.1 Full power characterization

The full power characterization [64] [65] involves assessing the system under nominal conditions to understand its behavior and gather performance data. RELAP5/Mod3.3 nodalization of the primary (Fig. 33) and secondary loop (Fig. 36), coupled by means of the steam generator tube-bundle heat structure, was adopted to perform a steady-state "null transient" calculation over a period of 40000s to ensure that the main parameter trends are stable and compliant with design values. With reference to each of the quantities in Tab. 20, the solution is stable with an inherent drift < 1% / 100 s.

Full power steady-state results showed that the secondary side vapor outlet temperature exceeded the nominal value. This discrepancy arises from the scaling of the STEAM Once-Through Steam Generator (OTSG) based on DEMO BB PHTS OTSG at BoL conditions (see Sect. 4.1). This scaling ensured the facility could meet its power requirements even under EoL conditions, which are marked by performance degradation due to tube fouling and plugging. Consequently, at BoL, the absence of fouling and plugging results in enhanced heat transfer capability and an increased vapor outlet temperature.

This elevated temperature at the OTSG outlet leads to higher enthalpy at the lamination valve suction, causing expansion through the valve to occur at higher enthalpy. However, the RELAP5 code cannot accurately reproduce the isenthalpic process downstream of the valve. To address this, a source term was introduced at the valve outlet to provide the secondary water with the needed power to restore the enthalpy content from the steam generator outlet section. This adjustment, labeled as 'SS additional source' in Tab. 20, aligns the temperature mismatch observed at the SG outlet and valve outlet.

The analysis also highlighted discrepancies in the performance of the Air Cooler (A.C.1). the distribution of mass flow among the four modules of A.C.1 results directly from the distinct chain of pressure drops characterizing the lines leading to each module. Small deviations are due to geometrical asymmetries in the pipe routing (see Sect. 5.2.1). The fluid outlet enthalpy is linked to the mass flow in the modules, with higher mass flow corresponding to higher enthalpy (Fig. 74). However, the different operating pressures of the modules significantly impact the condensation power of each module (Fig. 75). The air side outlet temperature is also connected to the fluid mass flow within the tubes, as it is characterized by the same trend (Fig. 76)

Further investigations reveal an uneven distribution of mass flow within the tubes of each module (Fig. 77). Specifically, it decreases in approaching the further tubes. The exchanged power is a direct outcome of the mass flow and exhibits a similar trend (Fig. 78). The fluid outlet thermodynamic conditions are measured by the thermodynamic quality (Fig. 79), with values ranging from 0 to 1 for saturation conditions, values >1 for superheated conditions, and <0 for subcooled conditions. The air mass flow is constant and uniform for all the modules, whereas the vapor mass flow varies in each tube of every module. A decrease in vapor mass flow aligns with a reduction in tube outlet enthalpy, leading to increased subcooling and a greater liquid collapsed level within the tube (higher subcooling of the tube in Fig. 79 in the furthest tubes).

Fluid from the four modules of A.C.1 is collected in the condensate tank, which operates under saturation conditions. The tank operational point can vary widely in pressure and liquid collapsed level, influenced by the thermodynamic conditions of the fluid from A.C.1 and the initial water quantity in the system.

The power supplied by A.C.2 and the air velocity within it depend on the fluid conditions at the A.C.1 outlet. A control system manages the A.C.2 air mass flow to achieve 210°C, a temperature sufficiently below the saturation. The A.C.2 power is lower than the reference data because the fluid undergoes some subcooling in A.C.1. Thanks to the A.C.2 regulation system, the section of the secondary loop from A.C.2 to the OTSG inlet remains unaffected by variations in steam line conditions.

The pump processes the subcooled fluid from A.C.2 and is expected to deliver a minimum of 40 kW to the fluid, equivalent to nearly a 5°C temperature increase. However, the current RELAP5 model of the pump, based on preliminary homologous curves and design data, provides lower power. An update for the pump model is planned as soon as the datasheet of the actual component becomes available during the final design phase. To address this discrepancy, additional power is supplied by the electric heater, regulated by a control system to achieve 238°C at the OTSG inlet.

Fig. 72 and Fig. 73 trace the primary and secondary loop pressure profiles along the main components respectively. Static contributions of the descendent columns become significant in the primary loop that, being mono-phase liquid is characterized by higher density. As a result, pressure increases inside the downward-oriented OTSG tube bundle and in the part of the loop from the OTSG outlet to the filter. Both primary and secondary system heat losses are pictured in Fig. 80 and Fig. 81.

5.3.2 Low-power characterization

The low-power characterization of the STEAM facility [66] focuses on assessing its performance under reduced power conditions, crucial for understanding operational stability and efficiency. This analysis includes detailed evaluations of thermal behavior, fluid dynamics, and control system responses at lower power levels. These insights are instrumental in optimizing the system for diverse operational scenarios and ensuring reliability. Given the absence of established practices from fission reactors, which primarily operate at nominal power, this study assumes particular significance in characterizing and validating all components involved in fusion reactor construction.

RELAP5/Mod3.3 analyses were conducted to characterize the thermal hydraulic behavior of the facility at different low-power states (i.e., 10%, 5% and 1%). Such power reductions are achieved by significantly reducing the power exchanged between the primary and secondary loops across the steam generator. This is obtained by lowering the feedwater mass flow rate to the steam generator while maintaining constant the total mass flows on both the primary and secondary sides (i.e., pumps operating at constant speed). As discussed in Sect. 5.2.3, the feedwater reduction (i.e., the reduction of the mass flow directed to the steam generator) is allowed by the three-ways valve, which allows the partial recirculation of the secondary loop mass flow towards the tank. While primary fluid path is unaltered during the low-power operation, secondary fluid paths are highlighted in Fig. 69 and Fig. 70.

The test matrix for characterizing low-power conditions of the facility is detailed in Tab. 23. A RELAP5 steady state null transient of 40000s was performed for all the listed power levels.

Regarding the primary loop, the SG exchanged power variations of Tab. 23 are obtained keeping a constant mass flow (i.e., 16.05 kg/s), thereby ensuring a constant average temperature. This approach leads to a reduced total ΔT, which tends to align with the average temperature, as shown in Fig. 82: both the OTSG inlet and outlet temperatures tend to converge towards the average temperature because of the control system regulating the primary side heater power (see Fig. 71).

Fig. 83 illustrates the result of the three-ways valve operation: decrease in feedwater flow to the OTSG as corresponds to power levels decrease. This reduction prompts an increase in complementary bypass flow to maintain operational balance, affecting fluid velocity and subsequently reducing heat transfer coefficients, as shown in Fig. 84. Specifically, starting from the riser inlet (i.e., lower tube-sheet), the nucleate boiling region is characterized by a high HTC due to the turbulence resulting from bubble formation. At 100% power, the maximum HTC value, located at approximately 6.5 m, indicates the dry-out point where film boiling begins. Film boiling, which has a lower heat transfer coefficient, persists until 100% steam quality is achieved. After the two-phase region ends, the superheating region starts, characterized by a low heat transfer coefficient due to the low vapor density. As power decreases, the axial extension of the nucleate boiling region diminishes, causing an earlier onset of dry-out and the consequent peak, while extending the superheating region with its low heat transfer coefficient. Additionally, the Reynolds number, calculated for a saturated liquid, shows a decrease with power levels: approximately 30,000 at 100% power, 3,000 at 10%, 1,500 at 5%, and 300 at 1%. This indicates that the fluid is in the transition regime at 10% and 5% power, while it becomes laminar at 1% power.

Steam generator axial temperature profiles are shown in Fig. 85, Fig. 86, Fig. 87 and Fig. 88 for 100%, 10%, 5% and 1% respectively. They highlight the trend towards flattened primary fluid temperatures approaching the average (i.e., 311.5°C) with reducing power. Additionally, with decreasing power levels, the steepness of the secondary side temperature increment along the downcomer increases. This is because the pre-heating of the riser-spilled vapor (i.e., recirculating mass flow) in the downcomer is more effective at lower mass flow rates, resulting in a lower downcomer liquid collapsed level (see Fig. 89). Moreover, as power decreases, the secondary mass flows reach saturation at a lower height in the riser, leading to an earlier onset of dryout. Consequently, the superheating region starts earlier, which further reduces the riser collapsed level (see Fig. 89). The secondary side temperature increment is ultimately limited by the primary side temperature, impacting levels in both the downcomer and riser.

The operation of the tank within the STEAM facility secondary loop is highly dependent on the facility power. At 10% and 5% of nominal power, the superheated steam produced in the SG mock-up is cooled by the fourth module of A.C.1, while the other three modules are turned off. At 1% of nominal power, the steam bypasses all four modules via the A.C.1 bypass line and is directed straight to the condensate tank. Consequently, the tank behavior is closely connected to the A.C.1 condition (see Sect. 5.2.2).

At 10% and 5% of nominal power, the tank collects two types of flows. First, it receives the condensed stream at saturation temperature from one module of A.C.1, which is in equilibrium with the tank's thermodynamic conditions. Second, it receives the recirculating subcooled flow that bypasses the SG test section (approximately 210°C), which reduces the energy stored in the tank.

The tank is equipped with electrical heaters of 20 kW maximum power to prevent depressurization. However, this power is insufficient to compensate for the energy reduction caused by the subcooled mass flow recirculated from the feedwater bypass. According to the enthalpy balance, the power required to bring the bypassed mass flow to saturation condition is 59.9 kW at 10% power and 63.2 kW at 5% power (see Tab. 24). Without additional power input, the tank pressure would decrease. Sensitivity analyses on the air cooler were performed to address this issue. By slightly reducing the air mass flow, the condensed vapor exits the heat exchanger with slightly higher enthalpy than nominal, balancing the energy loss associated with the subcooled stream. As a result, the tank level (Fig. 91) is maintained near its nominal value of 2 meters.

At 1% of nominal power, the situation changes. The fluids reaching the condensate tank consist of superheated steam that bypasses the A.C.1 module, increasing the energy stored in the tank, and the recirculating subcooled flow that bypasses the SG, which decreases the energy stored in the tank.

As listed in Tab. 24, the power required to bring the bypassed feedwater mass flow to saturation at 1% power is 65.9 kW. This requirement must be lowered by the term needed to condense the SG mass flow (which depends on the SG outlet temperature) and the 20 kW from the tank heaters. However, these contributions are insufficient to offset the negative term introduced by the recirculating feedwater flow. Consequently, Fig. 91 indicates that the tank level decreases to a very low operative value under this condition.

The pressure profile along the primary loop, as shown in Fig. 92 , reveals that low-power conditions result in higher pressure levels compared to nominal operation. Notably, these low-power pressure values exceed the spray intervention setpoint of 15.7 MPa. This phenomenon occurs because the efficiency of the spray system in reducing pressure diminishes when the temperature difference (ΔT) between the hot and cold legs is reduced. Consequently, at a 1% power level, the primary loop operates with the spray system continuously opened, though with limited effectiveness in lowering the system pressure.

The pressure profile along the secondary loop is divided into Fig. 93 and Fig. 94, as the two loop sections operate at different pressures (refer to Sect. 3.2.2 for details). Fig. 93 demonstrates that low-power operation, achieved by reducing the feedwater mass flow, necessitates a significant pressure drop managed by the ½” valve located parallel to the three-way valve (see Fig. 67). The pressure drop becomes more pronounced with decreasing feedwater mass flow. Additionally, the pressure drops associated with the steam generator are negligible at low mass flow rates. The pressure in the section of the loop at 2.5 MPa (Fig. 94) is primarily influenced by tank operation, as previously discussed, and is contingent on the fluid conditions at the air cooler outlet.

5.3.3 Pulse-dwell-pulse transition

The full power – low power – full power transition [67] represents a significant operational scenario, necessitating thorough numerical analyses and experimental campaigns. In fusion power plants, the pulse-dwell-pulse transition is particularly relevant due to the pulsed plasma-generated power (see Sect. 2.2). The primary concern in this context is the thermo-mechanical stress induced on materials by abrupt power fluctuations, leading to temperature variations within the system. These fluctuations must be managed to prevent sudden temperature spikes that could compromise structural integrity.

To address this, the STEAM facility simulates the postulated normal operation of DEMO, focusing on the thermal-hydraulic behavior of its components. The objective is to demonstrate that the steam generator can be effectively controlled and can withstand sudden power variations. Achieving this requires the design of adequate control systems and ensuring the facility dynamic performance is sufficient.

The RELAP5 numerical simulation replicates the transient behavior in STEAM by modulating the facility power source, specifically the electrical heater, to match the plasma power profile. Starting from the steady-state conditions described in Sect. 5.3.1, the Start Of the Transient (SoT) occurs after 4000 seconds of steady-state conditions. The power profile for the electrical heater during this transition, shown in Fig. 95, includes several phases: 150 seconds of constant power at 100%, 150 seconds of a linear ramp down from 100% to 1% of the constant value [69], 600 seconds of constant power at 1%, and 150 seconds of a linear ramp up from 1% to 100%, peaking at 115% [70].

The capability of the STEAM facility to simulate such behavior is challenging and requires the design of an adequate control system to ensure acceptable dynamic performances. For this reason, the thermal-hydraulic response of the facility to this transient is simulated using the RELAP5/Mod3.3 code, aiming at providing operational feedback and validating the facility capability to manage the pulse-dwell-pulse transitions, ensuring the SG operational stability and integrity under varying power conditions.

The transient evolution was investigated using two different Proportional-Integral (PI) controllers, both regulating the feedwater mass flow while maintaining a constant primary side mass flow. The regulation of the feedwater mass flow aims at maintaining either the primary side average temperature (control system 1, referred to as "T average"), which is the average of the hot leg (OTSG PS inlet) and cold leg (OTSG PS outlet) coolant temperatures, or the primary side minimum temperature (control system 2, referred to as "T minimum"), which is the cold leg temperature.

The PI control system implemented in the RELAP5/Mod3.3 code operates as:

$$Y = S\left[A_1 V_1 + A_2 \int_0^t V_1 dt\right]$$

Where:

- S is the scaling factor, modifying the entity of the controller regulation;
- A1 is the proportional parameter;
- A2 is the integral parameter;
- V1 is the error (i.e., the difference between the “measured variable” and the set point).

The scaling factor was kept equal to 1, and the proportional and integral parameters were tuned after a scoping calculation, as shown in Tab. 25. The set point and the measured variable depend on the type of controller adopted. In the "T average" control system, the measured variable is the PS average temperature, calculated as the average of the hot leg (OTSG inlet) and cold leg (OTSG outlet) temperatures. These values are monitored by thermocouples TC-SHP-060 and TC-SCP-070, as shown in the P&ID in Fig. 12. The set point is the OTSG inlet and outlet design average temperature (311.5 °C). In the "T minimum" control system, the measured variable is the PS OTSG outlet temperature, monitored by thermocouple TC-SCP-070. The set point is the PS OTSG inlet design temperature. This controller uses a single temperature rather than a combination of two temperatures, making it simpler.

The control schemes for "T average" and "T minimum" are shown in Fig. 96 and Fig. 97. Both the controllers base their operation on minimizing the error calculated as (measured value – set point). The operation principle is common to both control systems. If a negative error occurs (measured value lower than the set point), it indicates an excess of exchange power. To reduce it, the feedwater mass flow has to be lowered.

The main difference between the two control systems lies in the thermal cycling amplitude experienced by the primary side components. The “T average” control system foresees an even thermal cycling amplitude for both hot and cold legs (ΔT=16.5 ◦C). On the other hand, the “T minimum” controller is characterized by a thermal cycling amplitude of 33 ◦C (i.e., the total nominal pulse phase ΔT) for the hot leg components, while the cold leg experiences no thermal cycling since its temperature is kept constant.

To enhance the responsiveness of the control logic described, an improvement can be made by resetting the accumulated error to zero at the end of the dwell phase. This enhancement can be integrated into the RELAP5 model by adjusting the error calculation in the controller as follows:

$$V_1 = [(Measured\ value - Set\ Point) \times T_1] + [(Measured\ value - Set\ Point) \times T_2]$$

Where:

- V1 is the error provided to the controller;

- Measured value and set point as specified above;
- T_1 is a trip that becomes true when the dwell phase ends;
- T_2 is a trip that becomes false when the dwell phase ends;

In this formulation, the error is computed as the sum of two terms, each calculated as the difference between the measured value and the set point, multiplied by a corresponding trip condition. When a term is multiplied by a false trip condition, its contribution to the error is zero. During the dwell phase, T_1 is true (allowing the error to accumulate over time), while T_2 is false (holding its contribution to zero). At the end of the dwell phase, T1 becomes false (resetting to zero), while T2 becomes true (starting from zero), thereby preventing any further error accumulation.

To achieve a comprehensive understanding of the pulse-dwell-pulse transient evolution in the facility, sensitivity analyses were performed to tune the proportional and integral parameters and determine their impact on the system performances. Parameters, main characteristics and key results are listed in Tab. 25. Reference values for both Proportional and Integral parameters were selected after a tuning procedure (described in Sect. 2.8.2) and are indicated in bold in Tab. 25.

Initial analyses (#1 and #2 in Tab. 25) were conducted using the "T average" control system for regulating feedwater during operational transients. Sensitivity studies with preliminary proportional and integral parameters highlighted issues with error accumulation during the dwell phase. This led to significant delays in system response following power increments typical of ramp-up scenarios. To mitigate these delays, an "Error resetting" technique was implemented, resetting error calculations post-dwell.

Further refinements in proportional (P) and integral (I) parameters (cases #3 to #8 in Tab. 25), led to the selection of a reference configuration (case #6 in Tab. 25) , minimizing transient distortions. Despite effective operation, the system does not achieve set-point temperatures in hot and cold legs during dwell phases, remaining approximately 1°C below (Fig. 98). This shortfall is influenced by the feedwater mass flow steepness (Fig. 99), constrained by proportional parameter adjustments limited by oscillations. Higher P parameters, in fact, reduce the delay in the FW regulation but their increment is limited by the insurgence of oscillations (see key points of Tab. 25). The HL over-temperature of approximately 2 ◦C following the ramp up is a direct consequence of the higher temperature imposed by the controller during the dwell phase. However, this temperature spike is quite reduced and considered acceptable.

During low-power phases, feedwater regulation ceases upon mass flow reaching zero, allowing temperatures to only rise until the next pulse (Fig. 98). Consequently, the primary side average temperature experiences a gradual positive drift that persists until the following pulse without causing any significant concern. Pressurizer level trend (Fig. 100) mirrors the PS hot leg temperature on which it is installed, fluctuating with primary loop density variations.

Conversely, the "T minimum" control system, simpler due to single-parameter monitoring, did not require error resetting post-dwell, effectively managing lower magnitude errors. Parameter tuning (cases #9 to #14 in Tab. 25) optimized proportional and integral settings, selecting a reference configuration (case #14) based on transient performance.

During ramp-up, a 5°C cold leg temperature peak above nominal values (Fig. 98) resulted from the fact that the error was not reset during dwell phases. Indeed, the error accumulated during the dwell causes a 30-second delay in feedwater response to power pulses (Fig. 99). Pressurizer level variations (Fig. 100) reflected density changes in the primary loop, showing significant level shrinking during the dwell. Furthermore, the delay in restoring the nominal level is exacerbated by temperature peaks.

From the comparison of the two controllers, it is evident that the "T minimum" control, managing single-point temperature regulation without error resetting, effectively avoids hot leg temperature peaks during ramp-ups. In contrast, the "T average" control required error resets post-dwell to accelerate system responses, safeguarding circuit integrity during operations while ensuring lower pressurizer level swelling.

Neither approach leads to hazardous conditions for the facility, therefore both control strategies will be further tested within the STEAM facility during the upcoming experimental campaign. These tests aim to provide valuable insights and assessments regarding control strategies for the DEMO reactor, ensuring the safe and efficient operation of the Steam Generator mock-up in both steady-state and pulsed operation scenarios.

5.4 Accidental scenarios

Fusion reactors, like all nuclear facilities, must be designed to handle a range of operational and emergency conditions. The study of accidental scenarios is crucial because they help understanding how the steam generator will behave under extreme conditions and identifying the necessary safety measures to mitigate risks.

The accidental scenarios analyzed in this study are primarily based on the failure of one or both primary and secondary pumps, often linked to the malfunctioning of electrical power. Analyzing these accidents involves understanding the thermal-hydraulic behavior of the cooling systems during such failures, with particular attention to managing temperature and maintaining the stability of the cooling system.

These scenarios are studied mainly through numerical simulations using the RELAP5 code, a powerful tool for simulating the thermal-hydraulic behavior of reactor systems under emergency conditions. RELAP5 allows for detailed investigation of potential failure modes and system responses, testing various failure hypotheses regarding the cooling systems and the reactor response.

The performed analyses are conducted under pulse conditions, when the reactor operates at maximum power. During this phase, the demand for power removal from the system is higher, making it a more conservative scenario for evaluating system robustness and safety. For the purpose of these analyses, it is also assumed that the reactor power output (i.e., the electrical heater power) remains constant over time, providing a worst-case scenario for assessing the system response to potential failures.

The main accidental scenarios studied include Loss of Flow Accident (LOFA), Loss of Heat Sink (LOHS), and a combined LOFA+LOHS scenario. These incidents are crucial to study because they simulate key failure modes that could lead to significant system instabilities. A LOFA event occurs when there is a loss or reduction of primary coolant flow, which can lead to overheating of the reactor components, including the plasma-facing materials, potentially resulting in damage or even failure of critical components. A LOHS event refers to the loss or reduction of secondary fluid flow and involves the loss of the ability to transfer heat from the primary loop, which can cause the system to overheat, as the thermal energy cannot be dissipated effectively from the reactor. When both conditions occur simultaneously in a LOFA+LOHS scenario, the risks are compounded, as the reactor is unable to both remove heat and maintain adequate cooling, significantly raising the likelihood of thermal damage and system failure. In fusion reactors, the absence of sufficient coolant flow can result in elevated temperatures in these components, potentially leading to damage or degradation of materials.

In the context of the STEAM facility, these studies are not only crucial for understanding the behavior of fusion reactors but also for ensuring the safety and reliability of the facility itself. Should STEAM encounter any of these scenarios, it is useful to have a comprehensive understanding of the expected system responses and necessary safety measures.

Tab. 26 is the test matrix of the investigated accidental scenarios, showing the PIEs and the main results obtained using RELAP5/Mod3.3 code.

5.4.1 LOFA

LOFA is a Design Basis Accident (DBA) commonly investigated in nuclear power plants. This type of transient occurs when a circulating pump fails for some reason, causing a significant reduction or complete cessation of coolant flow. The main consequence of this event is a diminished cooling capacity of the fluid, leading to system overheating. This overheating can jeopardize the structural integrity of key components, including the plasma facing component, the blanket, and the divertor, which could reach thermal limits critical for maintaining safe reactor conditions.

To address these risks, extensive analyses have been conducted using the experimental facility STEAM to test the behavior of components during this transient and ensure that conditions threatening the integrity of the plant do not occur.

A RELAP5 transient of transient 0f 9000s was performed to reproduce the LOFA accident and investigate the system thermal-hydraulic behavior following the event. The Postulated Initiating Event (PIE) is the failure of the MCP, occurring after 50s of steady state conditions at full power. The feedwater mass flow rate and temperature are assumed to be constant, as well as the power of the two electric heaters.

The MCP failure determines an instantaneous reduction of the primary coolant flow (Fig. 104). This leads to a power imbalance due to the SG reduced heat transfer capabilities, resulting in an increase in primary system pressure (Fig. 105), that is kept below 17 MPa by the spray and PORV multiple interventions.

Being the feedwater mass flow and inlet temperature constant, the SG power reduction induced by a lower PS mass flow rate (Fig. 106) determines the SG riser and downcomer collapsed level to rise (Fig. 107), reducing the SG superheated region. This leads to the feedwater outlet temperature dropping from superheated to saturation temperature (Fig. 108).

With the primary flow reduced and the constant power output from the electric heaters, the system average temperature rises (Fig. 109), resulting in a reduction of the fluid average density and a consequent increment of the pressurizer liquid collapsed level (Fig. 110). Additionally, the temperature difference between hot and cold leg (i.e., SG inlet and outlet) increases as well, facilitating natural circulation.

As the primary flow continues to decrease and the temperature increases, the fluid in the primary loop reaches saturation at the heater outlet and begins to vaporize. (Fig. 111). The SG effectively condenses all the produced steam (null outlet void fraction), ensuring several degrees of subcooling at the outlet, which helps maintain system stability and prevents further complications.

The instauration of the natural circulation allows the restoration of the SG nominal power exchange as well as the riser, downcomer and pressurizer level decrement (at values higher than the ones before the PIE due to density variation).

The sequence of main events and the corresponding timing is reported in Tab. 27.

RELAP5 results show that the system is capable of managing a LOFA without the power shutdown for a period longer than 9000s without jeopardizing the system integrity. The simulation confirms that the facility can maintain its structural integrity and safety despite the significant thermal-hydraulic challenges posed by a LOFA scenario.

5.4.2 LOHS

LOHS is another Design Basis Accident (DBA) frequently analyzed in nuclear power plants. This transient occurs when the secondary side heat removal capability is significantly reduced or completely lost. This can result from failures in the secondary cooling system, such as the loss of feedwater supply, malfunction of the condenser, or issues with the cooling towers.

The primary consequence of a LOHS event is the inability to effectively remove heat from the primary loop, leading to an increase in primary system temperature and pressure.

To predict the system behavior during an unprotected LOHS, the RELAP5 code was adopted. A transient of 9000s was performed starting from full power nominal conditions. The PIE, occurring at 50s, is the failure of the feedwater pump. In analyzing the worst-case scenario, the nominal heaters power was assumed to remain constant. This very severe scenario can be used to evaluate the system grace time. The modeled system includes a safety feature that shuts down the MCP if the fluid temperature rises to within 5°C of saturation to avoid cavitation.

Two different evolutions of the LOHS transient were reproduced, analyzed and compared. Both calculations were intentionally stopped when the temperature at the electric heater outlet insulating heat structure reached a predetermined threshold, as shown in Tab. 29. This approach allows for the assessment of 'grace time' before critical conditions are reached. The first scenario involves a complete loss of feedwater flow, where the feedwater pump shuts down at 50 seconds, causing the feedwater flow rate to drop to zero over the next 10 seconds. This scenario represents a complete loss of heat sink capability. In the second scenario, there is a partial reduction of feedwater flow, where the feedwater flow rate is reduced to 80% of its nominal value within 10 seconds, also starting at 50 seconds, representing a partial loss of heat sink capability. Comparison of the main thermal-hydraulic parameters are shown in Fig. 112 to Fig. 123.

In the first scenario, referred to as Case 0%, the rapid reduction in feedwater (Fig. 112) leads to an almost instantaneous decrease in the riser and downcomer levels in the steam generator (Fig. 114). Consequently, the power transferred in the SG diminishes significantly, while the power from the electric heaters remains nearly constant (Fig. 116). This causes the temperature of the heaters heating rods to increase (Fig. 118), leading to a rapid rise in the primary system temperature (Fig. 120) and pressure (Fig. 121).

The quick increase in primary temperature triggers the shutdown setpoint for the Main Coolant Pump, causing the primary flow rate to drop quite rapidly (Fig. 122). As a result, the entire primary loop transitions to saturation due to the inability to remove heat effectively, leading to a system-wide temperature increase that eventually causes the simulation to fail. The rapid temperature increase causes the primary system density to decrease, resulting in a faster increase in the pressurizer level (Fig. 123).

Additionally, due to the reduced primary flow rate, the fluid reaches saturation and starts to vaporize (Fig. 124). This is evidenced by the increase in void fraction at both the inlet and outlet of the steam generator. In Case 0%, the vapor generated is not effectively condensed by the secondary side, exacerbating the heat removal issue.

In the second scenario, referred to as Case 80%, the feedwater flow rate reduction is contained (Fig. 113). In this case, riser and downcomer levels drop much more slowly compared to Case 0%, reaching higher minimum values (Fig. 115). According to Fig. 117, the decrease in power transferred in the SG is less severe (exchanged power reduction is limited to the 80%, accordingly with the mfr), resulting in a slower increase in both the heating bars (Fig. 119) and the primary system (Fig. 120) temperatures.

Fig. 122 shows that, as the primary temperature rises more gradually, the MCP operates for a significantly longer period before the shutdown setpoint is reached. The reduced feedwater flow rate still leads to a gradual increase in primary temperature, causing the fluid density to decrease. As the MCP continues to run at a constant speed, it processes an increasingly lower flow rate until the pump shutoff temperature setpoint is reached, at which point the pump shuts down to prevent cavitation.

Following the MCP shutdown, the system loses forced circulation, with the primary loop operates at a higher average temperature. Despite the reduction in primary flow rate, the SG continues to transfer approximately 80% of the nominal power. This results in an increased temperature difference (ΔT) across the primary loop, facilitating the establishment of natural circulation due to the higher average operating temperature.

Moreover, in Case 80%, the void fraction increases at the SG inlet and outlet due to the reduced flow rate, but the secondary side manages to condense a significant portion of the vapor (Fig. 124). This helps to maintain a better heat removal capability compared to Case 0%.

The timing characteristics of the two different LOHS are compared in Tab. 28. In Case 0%, the temperature rise, and pressure increase occur much more rapidly compared to Case 80%. In Case 0%, the rapid temperature rise leads to a quick and significant increase in primary pressure, necessitating frequent spray system and

PORV interventions. In Case 80%, the slower temperature rise results in a more gradual increase in primary pressure, with fewer and safety system interventions required to maintain pressure within safe limits.

5.4.3 LOFA+LOHS

The simultaneous failure of both the MCP and the feedwater pump, referred to as "LOFA+LOHS," was also analyzed. This scenario, which simulates the loss of electric power in reactors, is extremely severe and approximates the conditions of a Station Blackout (SBO). Unlike Design Basis Accidents (DBAs), an SBO is considered a Beyond Design Basis Accident (BDBA).

A 9000s transient was performed with the PIE (failure of MCP and feedwater pump) occurring at 50s. Due to the severity of the imposed boundary conditions, the calculations crashes (see Tab. 29). Nevertheless, it is useful to evaluate the system grace time in the event of a station blackout with the plasma operating at maximum power.

In this scenario, both the primary and secondary cooling capabilities of the Steam Generator (SG) are compromised. Compared to previously analyzed transients, this scenario is more severe. The LOHS proved to be particularly critical, making this transient resemble a more aggravated version of LOHS. Initially, the primary coolant flow rate mirrors that of the early stages of a LOFA (see Fig. 104), while the secondary coolant flow rate mimics the early stages of the LOHS case 0 (Fig. 122), leading to a worsened overall scenario. The void fraction at the inlet and outlet of the SG follows a pattern similar to that observed in LOHS case 0 (Fig. 124). Due to the rapid reduction in primary flow rate, the fluid reaches saturation and begins to vaporize. This vaporization increases the void fraction, indicating the presence of steam in the primary loop. In LOFA+LOHS, the secondary side of the SG fails to effectively condense this steam, similar to what occurs in LOHS case 0. This failure further exacerbates the inability to remove heat from the primary loop, leading to increased temperatures and pressures.

This is evident as the temperature of the heater rods rises more significantly (Fig. 125) due to the simultaneous loss of both the heat sink and the primary coolant. Consequently, the heat exchanged between the two loops drops to zero, eliminating the temperature difference in the primary loop that could have ensured natural circulation (Fig. 126). Another notable difference between this case and LOHS case 0 is the temperature behavior at the heater inlet. In LOFA+LOHS, the heater inlet temperature rises more slowly because the primary flow rate is almost instantaneously reduced, causing the fluid to move much slower. Therefore, the heated fluid from the heater outlet takes longer to return to the heater inlet after circulating through the entire loop.

The sequence of main events and the corresponding timing is listed in Tab. 29.

Tab. 14. A.C.1 thermal-hydraulic parameters

Parameter	**Unit**	**Design**
p	MPa	2.5
$T_{upstream\ A.C.1}$	°C	245.4
$T_{downstream\ A.C.1}$	°C	224.0
$h_{upstream\ A.C.1}$	kJ/kg	2868.0
$h_{downstream\ A.C.1}$	kJ/kg	962.0
$VF_{upstream\ A.C.1}$	-	1.00
$VF_{downstream\ A.C.1}$	-	0.00
mfr	kg/s	1.64
Power	MW	3.125

Tab. 15. A.C.1 main geometrical features

Parameter	Unit	Value
Bundle	-	Vertical
Tubes O.D.	mm	21.3
Tubes Thickness	mm	1.5
Tubes I.D.	mm	18.3
Tubes Length	m	2.5
#Tubes/Bundle	-	55
Tubes row	-	1
Tubes/row	-	55
Passes	-	1
#Modules	-	4
#Tubes Total	-	220
Vertical Pitch	mm	48
p/d	-	2.25
Total Length	m	2.5
Bare tubes area	m^2	36.8
Finned tubes area	m^2	386.18
Surface corrective f	-	10.49
Surface effectiveness	-	0.78
Fouling Factor	-	8.18
Fin I.D.	mm	21.3
Fin Height	mm	12.0
Fin O.D.	mm	45.3
Fin Thickness	mm	0.4
Fins/m	-	255
# Fins Total	-	137500
Fins total surface	m^2	353.06
Fins total volume	m^3	0.069
Equivalent Fin O.D.		0.025
Heated diameter	m	0.0068

Tab. 16. RELAP5 results of the de-superheating and condensation air cooler operating in nominal conditions

Parameter	**Unit**	**Module #**				**R5 Total/ Avg**	**Des.**	**Er.***
		Module 1	**Module 2**	**Module 3**	**Module 4**			
$p_{upstream\ A.C.1}$	MPa	2.589	2.592	2.591	2.589	2.590	2.5	+3.6%
$P_{downstream\ A.C.1}$	MPa	2.589	2.592	2.591	2.589	2.590	2.5	+3.6%
$T_{upstream\ A.C.1}$	° C	243.7	244.1	243.8	243.5	243.8	245.4	-0.65°C
$T_{downstream\ A.C.1}$	° C	225.8	225.9	225.9	213.5	220.8	224.0	-3.2°C
$VF_{upstream\ A.C.1}$	-	1.00	1.00	1.00	1.00	1.00	1.00	-
$VF_{downstream\ A.C.1}$	-	0.81	0.27	0.06	0.00	0.28	0.00	+0.28
$h_{downstream\ A.C.1}$	kJ/kg	1083.94	981.31	972.48	914.01	987.93	962.0**	+0.5%
Power	MW	0.77	0.77	0.77	0.77	3.1	3.108	+2.7%
$T_{upstream\ C.T.}$	° C	223.1				223.1	224	-0.9°C
$Vf_{upstream\ C.T.}$	-	0.02				0.02	0.0	+0.02

**Error [%] = (R5–Ref)/Ref*
*** Enthalpy of the saturated liquid at 2.5 MPa.*

Tab. 17. OTSG T/H outlet conditions for different SG outlet thermal-hydraulic conditions

#	Upstream Lamination Valve				Downstream Lamination Valve			
	p [bar]	T [K]	T [°C]	h [kJ/kg]	p [bar]	T [K]	T [°C]	h [kJ/kg]
1	64	558.15	285	2805	25	497.97	224.82	2805
2		563.15	290	2827		504.86	231.71	2827
3		568.15	295	2848		511.75	238.60	2848
4		573.15	300	2868		518.58	245.43	2868
5		578.15	305	2887		525.33	252.18	2887
6		583.15	310	2905		532.01	258.86	2905
7		588.75	315.6	2925		538.80	265.65	2923
8		593.15	320	2940		545.13	271.98	2940

Tab. 18. A.C.1 four modules outlet enthalpies and relative error for different SG outlet thermal-hydraulic conditions

#	1st module		2nd module		3rd module		4th module		Average	
	Value kJ/kg	Error %	Value kJ/kg	Error %	Value kJ/kg	Error %	Value kJ/kg	Error %	Value kJ/kg	Error %
1	910	-5%	950	-1%	970	+1%	965	0%	949	-1%
2	861	-10%	963	0%	967	+1%	942	-2%	933	-3%
3	883	-8%	973	+1%	967	+1%	941	-2%	941	-2%
4	1054	+10%	971	+1%	967	0%	954	-1%	987	3%
5	995	+3%	970	+1%	966	0%	947	-2%	970	1%
6	1059	+10%	965	0%	965	0%	921	-4%	978	2%
7	965	0%	969	+1%	964	0%	886	-8%	946	-2%
8	1038	+8%	970	+1%	968	+1%	921	-4%	974	1%

Tab. 19. A.C.1 four modules outlet enthalpies and relative error at different vapor mass flows

#	Total mass flow rate kg/s	1st module		2nd module		3rd module		4th module		Average	
		Value kJ/kg	Error %	Value kJ/kg	Error %	Value kJ/kg	Error %	Value kJ/kg	Error %	Value kJ/kg	Error %
1	1.64	965	0%	969	+1%	964	0%	886	-8%	946	-2%
2	1.5	1058	+10%	970	+1%	967	0%	924	-4%	980	+2%
3	1.4	1072	+11%	966	0%	962	0%	926	-4%	981	+2%
4	1.3	1095	+14%	978	+2%	962	0%	898	-7%	983	+2%
5	1.2	961	0%	980	+2%	961	0%	895	-7%	949	-1%
6	1.1	2795	-	973	+1%	962	0%	908	-6%	948	-1%
7	1.0	2794	-	972	+1%	961	0%	919	-4%	951	-1%
8	0.9	2794	-	972	+1%	961	0%	932	-3%	955	-1%
9	0.8	2793	-	983	+2%	968	+1%	928	-4%	960	0%
10	0.7	2778	-	2664	-	961	0%	930	-3%	946	-2%
11	0.6	2793	-	2725	-	962	0%	923	-4%	942	-2%
12	0.5	2778	-	2673	-	974	+1%	927	-4%	951	-1%
13	0.4	2710	-	2544	-	982	2%	912	-5%	947	-2%
14	0.3	2710	-	2552	-	2228	-	938	-3%	938	-3%

Tab. 20. Steady-state characterization of RELAP5/Mod3.3 STEAM nodalization

Parameter	**Unit**	**Ref. Data**	**R5**	**±ε[a]**
Power				
PS e-heater	MW	3.1	3.1	0.0%
TS	MW	3.1	3.1	0.0%
PS pressurizer heaters	kW	12[b]	3.27	-
SS A.C.1	MW	3.108	3.25	+4.6%
SS A.C.2	kW	104.0	67.1	-55%
SS heater	kW	173.0	193.8	+12%
SS tank heaters	kW	25[b]	13.2	-
SS additional source	kW	-	226.17	-
Mass Flow				
PS	kg/s	16.05	16.05	0.0%
SS	kg/s	1.69	1.64	-3.0%
Temperature				
PS OTSG inlet/PS e-heater outlet	°C	328.0	328.0	0 °C
PS OTSG outlet/PS e-heater inlet	°C	295.0	295.0	0 °C
SS OTSG inlet/SS e-heater outlet	°C	238.0	237.8	-0.2°C
SS OTSG outlet	°C	300.0	314.7	+14.7°C
SS upstream A.C.1 (average of the four modules)	°C	245.4	264.6[c]	+19.2°C
SS tank	°C	224.0	219.0	-5.0 °C
SS A.C.2 outlet	°C	210.0	210.0	0 °C

[a] *Error [%] = (R5–Ref)/Ref*
[b] *Nominal installed power*
[c] *Temperature that corresponds to the computed SG outlet enthalpy at 25 bar*

Tab. 21. De-superheating and condensation air cooler RELAP5 results in full-power operation

Parameter	**Unit**	**Module #**				**R5 Total / Avg**	**Des.**	**Er.**
		Module 1	**Module 2**	**Module 3**	**Module 4**			
$p_{A.C.1}$	MPa	2.458	2.461	2.460	2.458	2.459	2.5	-1.6%
$T_{downstream\ A.C.1}$	°C	220.1	223.1	223.1	202.5	217.2	224.0	-6.8°C
$VF^{a}_{upstream\ A.C.1}$	-	1.00	1.00	1.00	1.00	1.00	1.00	0.0%
$VF^{a}_{downstream\ A.C.1}$	-	0.00	0.04	0.03	0.00	0.02	0.00	+2%
$h_{downstream\ A.C.1}$	kJ/kg	944.0	959.0	958.7	863.7	931.4	962.0	-3.2%
Power	MW	0.81	0.81	0.81	0.81	3.25	3.108	+4.6%
$T_{upstream\ C.T.}$	°C	220.8				217.3	224	-6.67°C

[a] VF stands for void fraction

Tab. 22. A.C.1 liquid collapsed level of the first and the last tube of each module.

Parameter	**Unit**	**Value**
Module 1 tube 1	m	0.026
Module 1 tube 5	m	0.372
Module 2 tube 1	m	0.027
Module 2 tube 5	m	0.366
Module 3 tube 1	m	0.027
Module 3 tube 5	m	0.366
Module 4 tube 1	m	0.026
Module 4 tube 5	m	0.384

Tab. 23. STEAM low-power test matrix

#	Power		Feedwater MF	
	kW	**%**	**kg/s**	**%**
1	310.0	10	0.168	10
2	155.0	5	0.084	5
3	31.0	1	0.017	1

Tab. 24. Condensate tank power required to bring to saturation the feedwater bypass mass flow at 10%, 5% and 1%

#	Power		Feedwater bypass MF		C.T. heater required power
	kW	**%**	**kg/s**	**%**	**kW**
1	310.0	10	1.512	90	59.9
2	155.0	5	1.596	95	63.2
3	31.0	1	1.663	99	65.9

Tab. 25. Scoping calculation test matrix

#	Type	P	I	Error reset	Description	Main results
1	Av.	1	0.01	✗	First guess parameters	Low system responsivity, high temperature peaks. Higher P parameters reduce the delay in the FW regulation.
2	Av.	5	0.01	✗		
3	Av.	1	0.01	✓	Sensitivity on the P parameter	• Resetting the error at the dwell phase end enhances the system responsivity. • Higher P parameter reduces the delay in the FW regulation. • Too high P parameter leads to the insurgence of oscillations.
4	Av.	5	0.01	✓		
5	Av.	10	0.01	✓		
6	**Av.**	**5**	**0.1**	✓	Sensitivity on the I parameter	• I parameter has smaller influence on the results with respect to the P one. • For I parameters lower than 0.1 temperature set-point is not reached during the dwell (low responsivity).
7	Av.	5	0.01	✓		
8	Av.	5	10^{-10}	✓		
9	Min.	1	0.01	✗	Sensitivity on the P parameter	• Sufficient responsivity also without resetting the error at the dwell phase. • P coefficient variability is limited by insurgence of big oscillations. • CL temperature peak of 5°C do not jeopardize the system. No peaks detected for the HL temperature.
10	Min.	0.1	0.01	✗		
11	Min.	0.05	0.01	✗		
12	Min.	0.1	10^{-10}	✗	Sensitivity on the I parameter	• The I parameter can be wider varied (below 0.01) without oscillations. • Higher I parameter determines higher system responsivity and a better control of the set-point temperature.
13	Min.	0.1	10^{-4}	✗		
14	**Min.**	**0.1**	**0.01**	✗		

Tab. 26. Test matrix of the accidental analyzed scenarios in STEAM configuration.

<table>
<tr><th colspan="2">Accident</th><th>MCP</th><th>Feedwater pump</th><th>Simul. time</th><th>Comments</th></tr>
<tr><td colspan="2">LOFA</td><td>OFF @ 50s (PIE)</td><td>ON</td><td>9000s</td><td>- Transition from forced to natural circulation.
- Higher temperature difference between hot and cold leg temperatures.
- PORV is triggered multiple times in the first part of the transient.
- Steam production at the e-heater outlet.
- Effective condensation in the SG.</td></tr>
<tr><td rowspan="2">LOHS</td><td>Case 0</td><td>ON (until T_{pump}< T_{sat}-5°C)</td><td>OFF @ 50s: feedwater goes to 0 in 10s (PIE)</td><td>645.2s</td><td rowspan="2">- Significant increase in heater rod temperatures due to the loss of heat sink.
- Natural circulation develops but is less effective compared to LOFA.
- Feedwater reduction to 80% allows for much higher grace time.
- Steam production in the Test Section.
- Effective condensation in the P-S HX only in case 80.</td></tr>
<tr><td>Case 80</td><td>ON (until T_{pump}< T_{sat}-5°C)</td><td>OFF @ 50s: feedwater goes to 0 in 10s (PIE)</td><td>1831.2s</td></tr>
<tr><td colspan="2">LOFA+LOHS</td><td>OFF @ 50s (PIE)</td><td>OFF @ 50s (PIE</td><td>705.2s</td><td>- Heater rod temperatures rise significantly higher compared to LOFA and.
- Natural circulation is almost ineffective, resulting in minimal heat transfer.
- The system experiences severe temperatures and pressure rise.
- Steam production in the Test Section.
- Ineffective condensation in the P-S HX.</td></tr>
</table>

Tab. 27. Sequence of main event after a LOFA occurring in STEAM operation.

#	Event	Timing
1	PIE: MCP failure	50s
2	PS MF < 80%	76s
3	Spray first intervention @16MPa	98s
4	PS MF < 50%	149s
5	Saturation conditions at the heater outlet	195s
6	PORV first intervention	232s
7	PRZ maximum level	8.98m @363s
8	Riser maximum level	6.54m @ 471s
9	PS MF < 20%	600 s
10	DC maximum level	7.77m @ 692s
11	FW < 50%	Not occurring
12	FW < 20%	Not occurring

Tab. 28. Sequence of main event after unprotected LOHS with feedwater reduction to 0 or to the 80% occurring in STEAM operation

#	Event	LOHS_0	LOHS_80
1	PIE: FW pump failure	50s	50s
2	FW < 80%	51s	60s
3	FW < 50%	55s	Not occurring
4	FW < 20%	58s	Not occurring
5	Spray first intervention @16MPa	74s	121s
6	PORV first intervention	93 s	602s
7	Saturation conditions at the heater outlet	157s	808s
8	MCP pump OFF (Tpump > Tsat – 5°C)	162s	960s
9	PS MF < 80%	166s	964
10	PS MF < 50%	215s	1030s
11	PS MF < 20%	260s	1176s
12	PRZ maximum level	8.99m @ 186s	9m @792s
13	Riser maximum level	1.88m before PIE	2.70m @ EOT
14	DC maximum level	4.82m before PIE	4.82m before PIE

Tab. 29. Sequence of main event after LOFA+LOHS occurring in STEAM operation

#	Event	Timing
1	PIE: FW pump failure	50s
2	PIE: MCP failure	50s
3	FW < 80%	52s
4	FW < 50%	55s
5	FW < 20%	58s
6	Spray first intervention @16MPa	73s
7	PS MF < 80%	75s
8	PS MF < 50%	135s
9	Saturation conditions at the heater outlet	143s
10	PORV first intervention	165s
11	PRZ maximum level	8.98m @ 169s
12	PS MF < 20%	236s
13	Riser maximum level	1.88m before PIE
14	DC maximum level	4.82m before PIE

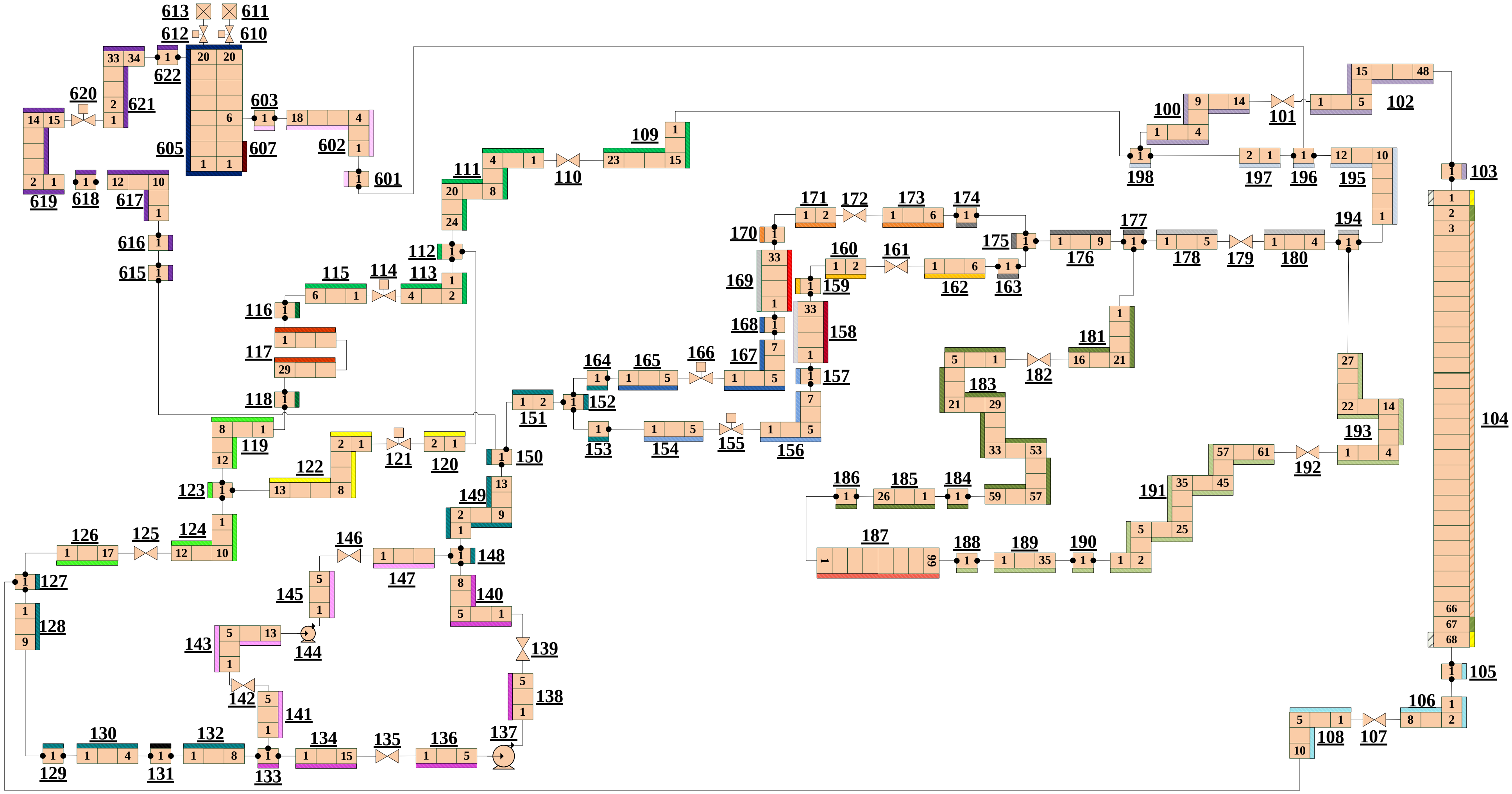

Fig. 33. W-HYDRA primary loop nodalization

#	HS	Components*	Symbol	Size	Description
1	100-0	100, 102, 103		6" Sch. 160	STEAM Hot Leg insulation
2	104-1	(104) – (213, 212, 210, 209, 208)		37 x ID=7.074mm s=0.864mm	STEAM OTSG tube bundle (active HS)
3	104-2	104		h_{tsheet}=100mm	STEAM OTSG tube bundle inside tube-sheet
4	104-3	(104) – (213, 208)		A_{tsheet}=0.00958m^2	STEAM OTSG tube-sheet
5	104-4	104		h=r=161.5mm	STEAM OTSG lower and upper heads
6	105-0	105, 106, 108		6" Sch. 160	STEAM Cold Leg insulation
10	109-0	109, 111, 112, 113, 115		3" Sch. 160	WL P-S HX Hot Leg insulation
11	116-0, 118-0	116 118		5" Sch. 80	WL P-S HX inlet and outlet plena (of the same size of the HX shell)
12	117-0	(117) – (404)		19 x 5/8" 18BWG	WL P-S HX tube bundle (active HS)
13	119-0	119, 123, 124, 126		3" Sch. 160	WL P-S HX Cold Leg insulation
14	120-0	120, 122		2" Sch. 160	WL P-S HX by-pass line
15	127-0 148-0	127, 128, 129, 131, 132, 133 148, 149, 150, 151, 152, 153, 164		6" Sch. 160	Cold Leg insulation (common to both STEAM and WL)
16	131-0	131		6" Sch. 160	Filter insulation
17	133-0	133, 134, 136, 138, 140		6" Sch. 160	STEAM pump line insulation
18	141-0	141, 143, 145, 147		3" Sch. 160	WL pump line insulation
19	154-0	154, 156, 157		4" Sch. 160	STEAM e-heater cold leg insulation
20	158-0	158		20" Sch. 160	STEAM e-heater insulation
21	158-1	158		196 x OD=16mm	STEAM e-heater active elements
22	159-0	159, 160, 162		4" Sch. 160	STEAM e-heater cold leg insulation
23	165-0	165, 167, 168		4" Sch. 160	WL e-heater cold leg insulation
24	169-0	169		20" Sch. 160	WL e-heater insulation
25	169-1	169		196 x OD=16mm	WL e-heater active elements
26	170-0	170, 171, 173		4" Sch. 160	WL e-heater cold leg insulation
27	175-0	163, 174, 175, 176, 177		6" Sch. 160	Part of STEAM HL / WL CL insulation
28	178-0	178, 180		6" Sch. 160	Part of STEAM HL (TS by-pass) insulation
29	181-0 185-0	181, 183, 184 185, 186		6" Sch. 160	TS CL insulation
30	187-1	187		2" Sch. 160	Test Section bundle (active HS)
31	188-0 190-0	188, 189 190, 191, 193		6" Sch. 160	TS hot leg insulation
32	194-0	194, 195, 196, 197, 198		6" Sch. 160	HL insulation (common to both STEAM and WL)
33	601-0 602-0	601 602, 603		3" Sch. 160 2" Sch. 160	Surge line insulation
34	607-0 607-1 607-2	607		16" Sch. 160	Body pressurizer insulation Bottom head pressurizer insulation Upper head pressurizer insulation
35	607-5	607		12 x OD=16mm	Heater active elements
36	615-0 616-0 617-0	615 616 617, 618, 619, 621, 622		6" Sch. 160 3" Sch. 160 1 1/2" Sch. 160	Spray line insulation

* Indicated as 'ccc' or 'ccc, CCC, …' if passive HS (insulation).
Indicated as '(ccc, xxx) – (CCC, XXX)' if active HS (ccc and xxx left boundary, CCC and XXX right boundary)
In the components, 1xx refers to STEAM-WL primary loop, 2xx refers to STEAM secondary loop, 3xx refers to WL tertiary loop and 4xx refers to WL secondary loop

Fig. 34. W-HYDRA primary loop heat structures

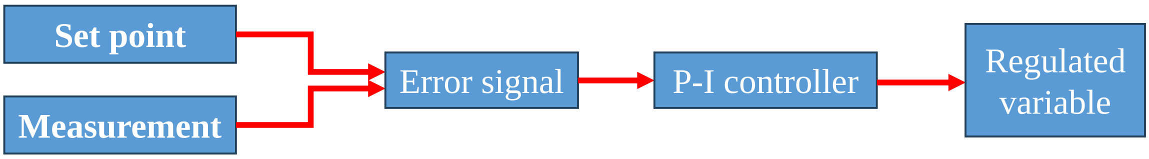

Fig. 35. RELAP5 implemented scheme for the control systems

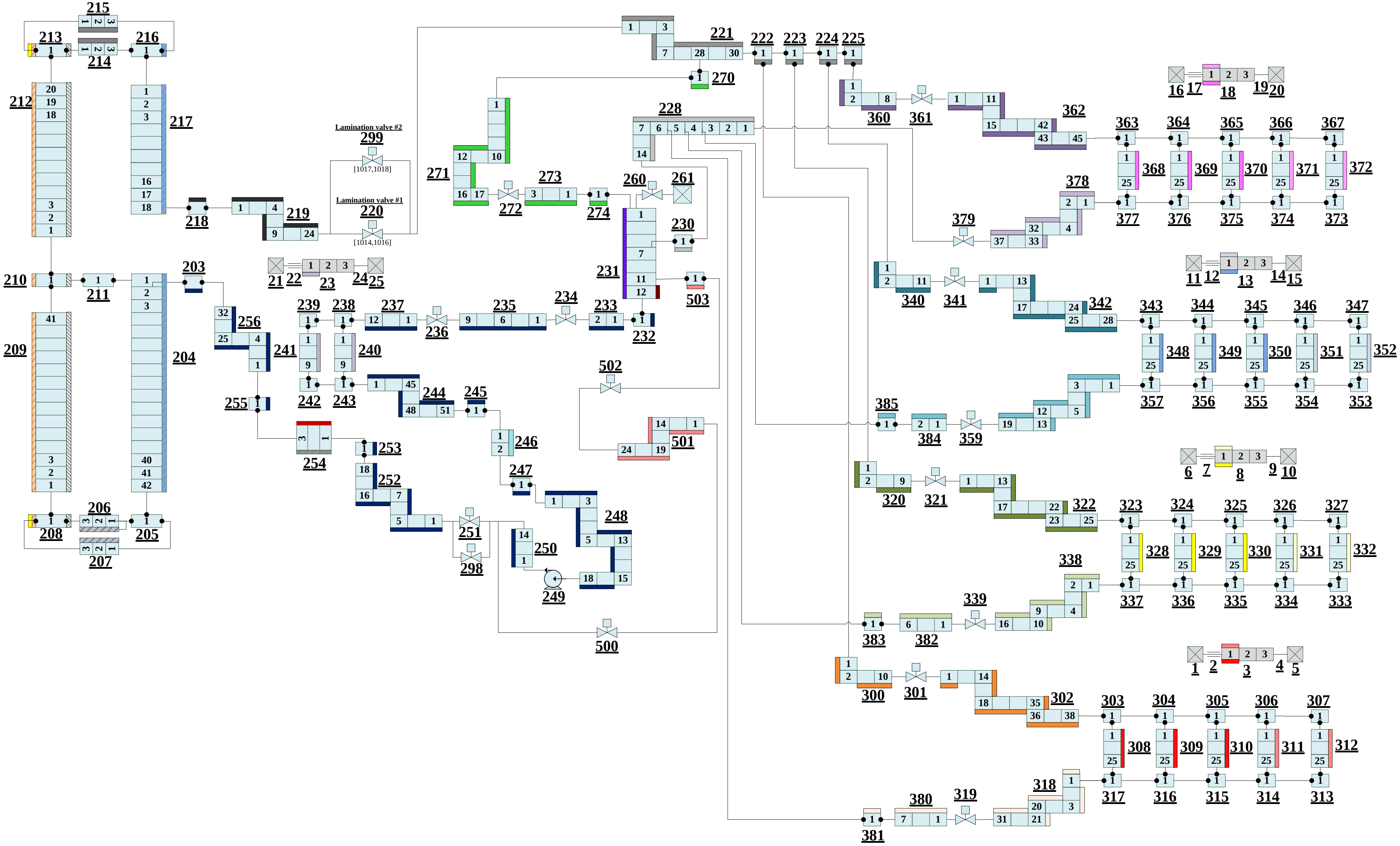

Fig. 36. STEAM secondary loop RELAP5/Mod3.3 nodalization

#	HS	Components*	Symbol	Size	Description
1	104-1	(104) – (213, 212, 210, 209, 208)		37 x ID=7.074mm s=0.864mm	STEAM OTSG tube bundle (active HS)
2	104-3	(104) – (213, 208)		A_{tsheet}=0.00958m^2	STEAM OTSG tube-sheet
3	210-1 210-2	210, 209, 208 213, 212		Scaled dimension	Lower riser insulation Upper riser insulation
4	212-0 212-1	204, 205 216, 217		Thickness of the 3 ½ Sch. STD	Feedwater downcomer Steam downcomer
5	212-2 212-3	214, 215 206, 207		2 ½” Sch. STD	Little external steam line insulation Little external feedwater line insulation
10	218-1	218, 219		4” Sch. STD	Steam line upstream lamination valve ins.
11	221-1	221, 222, 223, 224, 225		5” Sch. STD	Steam line downstream lamination valve ins.
12	300-1	300, 301, 302		2” Sch. STD	A.C.1 module 1 steam line
13	308-1 311-1	(308, 309, 310) – (3) (311, 312) – (3)		55xO.D.=21.3mm Thick.=1.5mm L=2.5m	A.C.1 module 1
14	318-1	318, 380, 381		1 ¼” Sch. STD	A.C.1 module 1 condensation line
15	320-1	320, 321, 322		2” Sch. STD	A.C.1 module 2 steam line
16	328-1 331-1	(328, 329, 330) – (8) (331, 332) – (8)		55xO.D.=21.3mm Thick.=1.5mm L=2.5m	A.C.1 module 2
17	338-1	338, 382, 383		1 ¼” Sch. STD	A.C.1 module 2 condensation line
18	340-1	340, 341, 342		2” Sch. STD	A.C.1 module 3 steam line
19	348-1 351-1	(348, 349, 350) – (13) (351, 352) – (13)		55xO.D.=21.3mm Thick.=1.5mm, L=2.5m	A.C.1 module 3
20	358-1	358, 384, 385		1 ¼” Sch. STD	A.C.1 module 3 condensation line
21	360-1	360, 361, 362		2” Sch. STD	A.C.1 module 4 steam line
22	368-1 371-1	(368, 369, 370) – (18) (371, 372) – (18)		55xO.D.=21.3mm Thick.=1.5mm L=2.5m	A.C.1 module 4
23	378-1	378		1 ¼” Sch. STD	A.C.1 module 4 condensation line
24	228-1	228, 230		1 ½” Sch. STD	Main condensation line
25	231-1	231		A=0.1507m^2	Condensate tank insulation
26	231-2	231		16 x OD=16mm	Condensate tank electric heater
27	232-1 244-1 247-1 255-1	232, 233, 235, 237 244, 245 247, 248, 250, 252, 253 255, 256, 203		1 ½” Sch. STD	Feedwater line upstream A.C.2 Feedwater line upstream filter Feedwater line upstream e-heater Feedwater line upstream SG
28	240-1	(240, 241) – (23)		36xO.D.=25.4mm Thick.=1.65mm, L=0.9m	A.C.2
29	246-1	246		TBD (for calc: 1 ½” Sch. STD)	Filter
30	254-1	254		9x U-bended O.D.=16mm	E-heater heating bars
31	254-2	254		A=0.04572m^2	E-heater insulation
32	271-1	271, 272, 273		2” Sch. STD	A.C.1 modules by-pass line
33	501-1	501, 503		1 ½” Sch. STD	Three-ways valve recirculation line

* Indicated as ‘ccc’ or ‘ccc, CCC, …’ if passive HS (insulation).
Indicated as ‘(ccc, xxx) – (CCC, XXX)’ if active HS (ccc and xxx left boundary, CCC and XXX right boundary)
In the components, 2xx refers to STEAM secondary loop, 3xx refers to the A.C.1 system, x and xx refers to A.C.s air side

Fig. 37. STEAM secondary loop heat structures

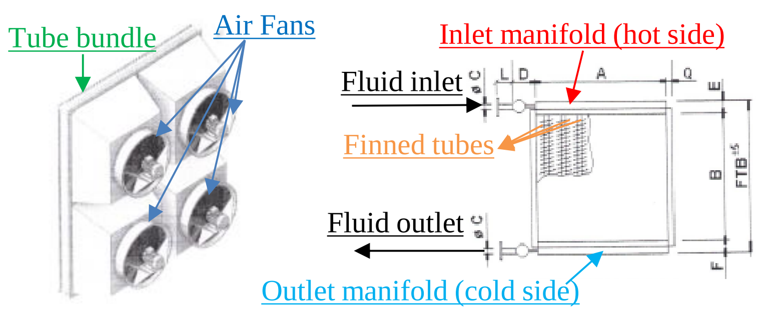

Fig. 38. De-superheating and condensation air cooler module: 3D view (left) and cutaway view of the cooling bundle (right)

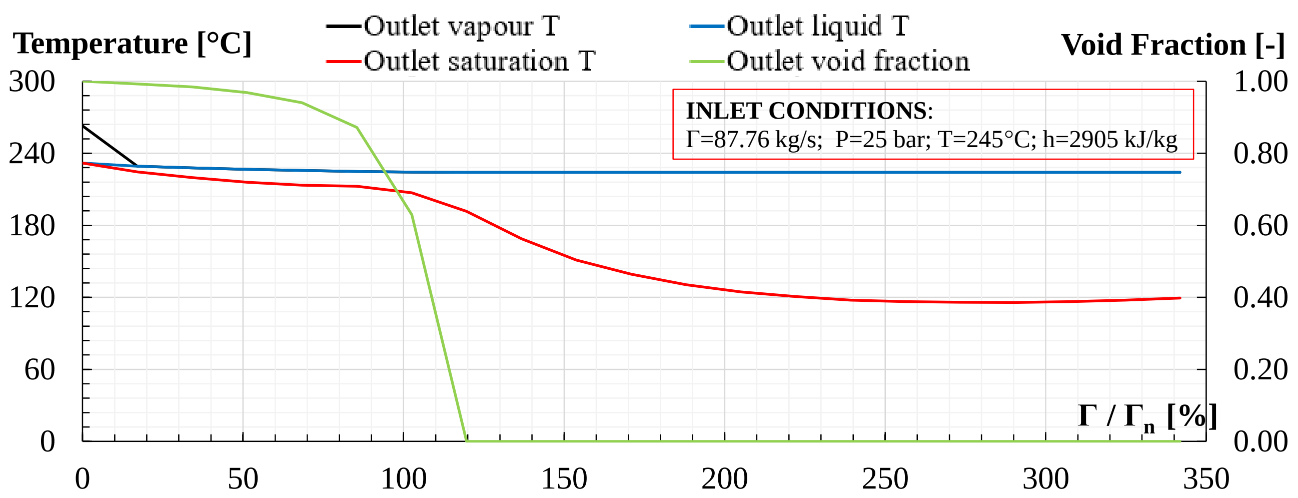

Fig. 39. Tube-bundle fluid outlet conditions with variable air mass flow rates

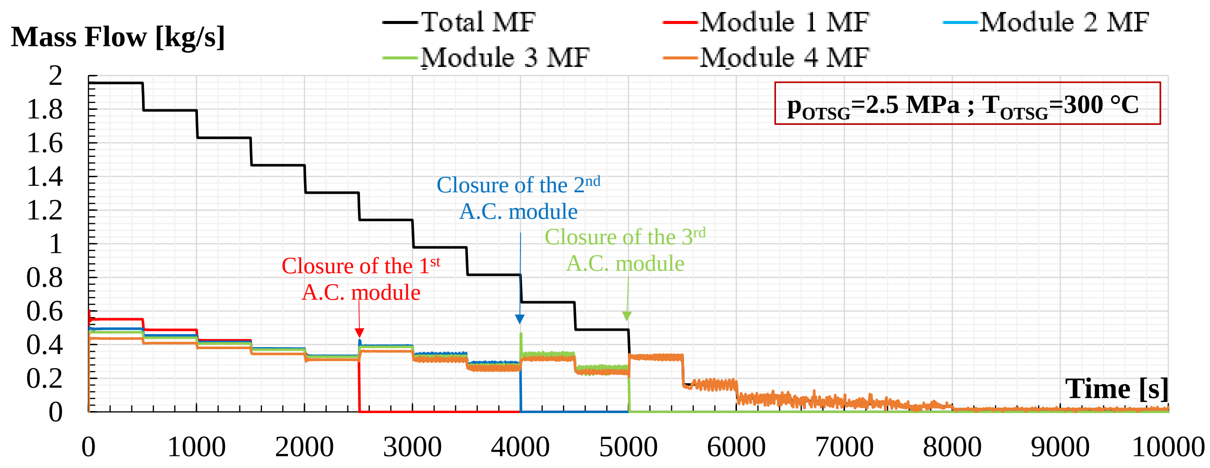

Fig. 40. Modulation of decreasing vapor mass flow at air coolers inlet

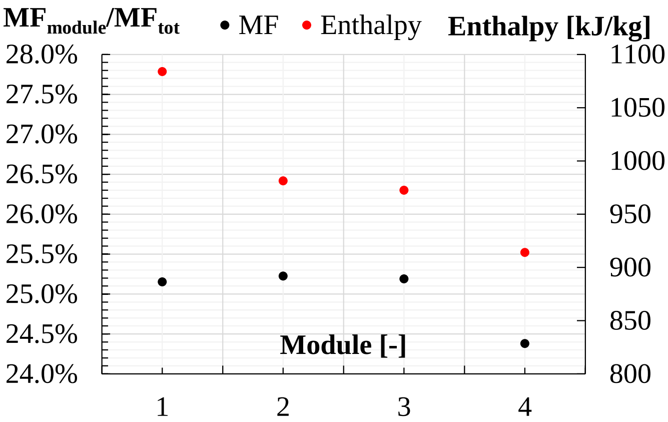

Fig. 41. De-superheating and condensation air cooler mass flow distribution among the modules and fluid outlet enthalpy in nominal conditions

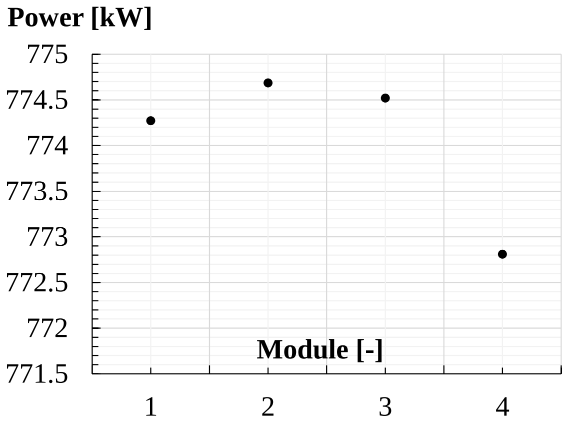

Fig. 42. A.C.1 modules exchanged power with steam at nominal conditions

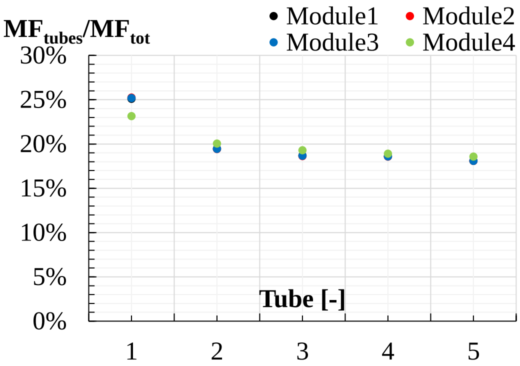

Fig. 43. A.C.1 mass flow distribution with steam at nominal conditions

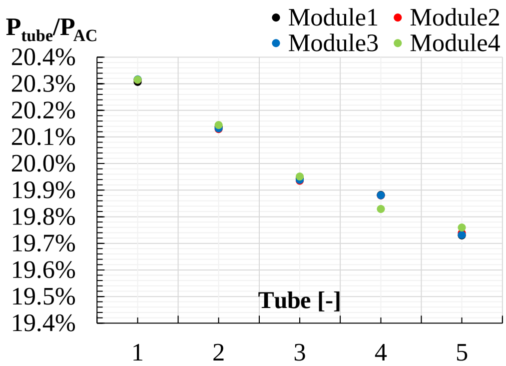

Fig. 44. A.C.1 power distribution with steam at nominal conditions

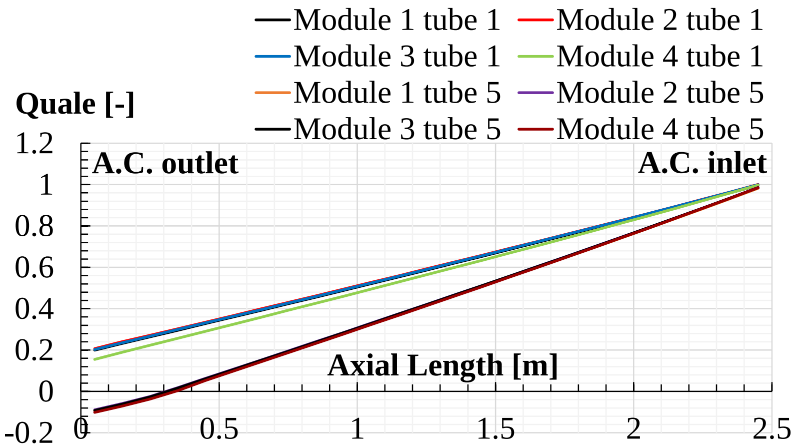

Fig. 45. A.C.1 equilibrium quality axial profile along the first and the last tube of each module with steam at nominal conditions

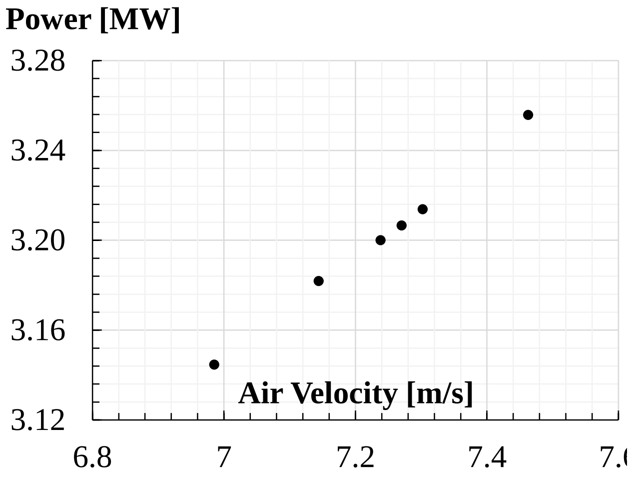

Fig. 46. A.C.1 power variation with A.C.1 air velocity

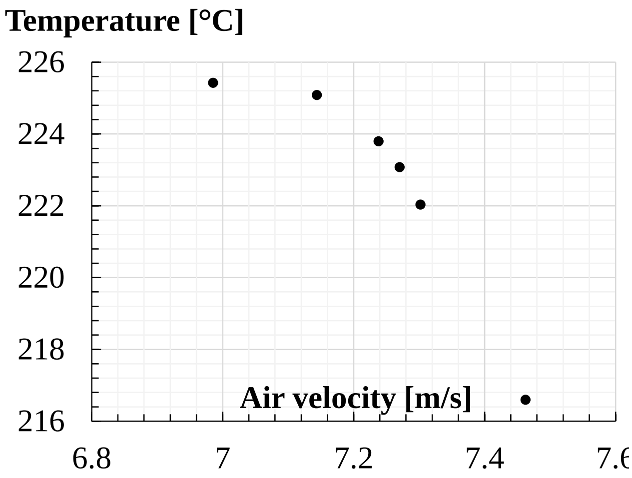

Fig. 47. Inlet tank temperature variation with A.C.1 air velocity

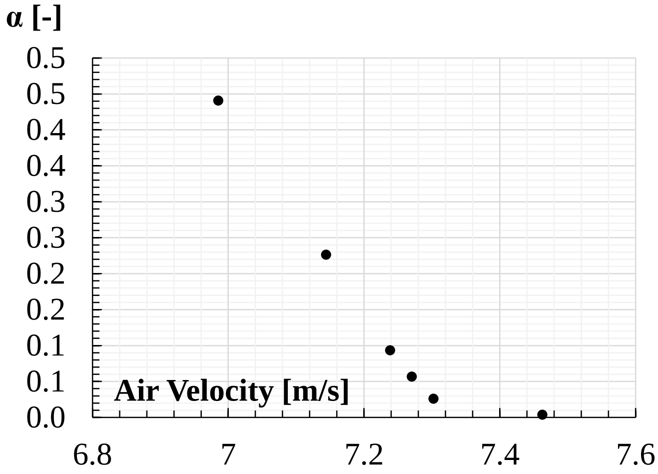

Fig. 48. Inlet tank void fraction variation with A.C.1 air velocity

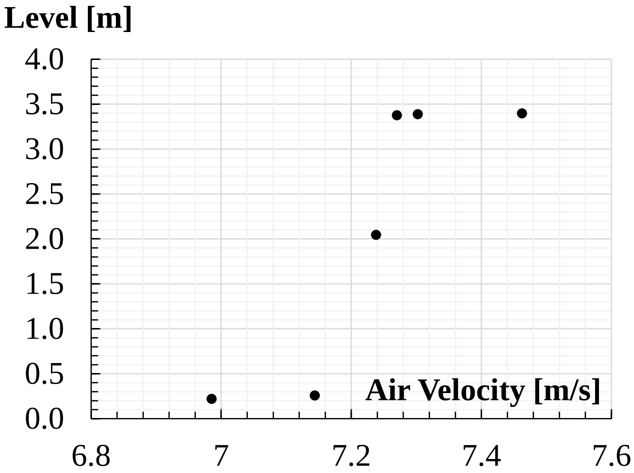

Fig. 49. Condensate tank level variation with A.C.1 air velocity

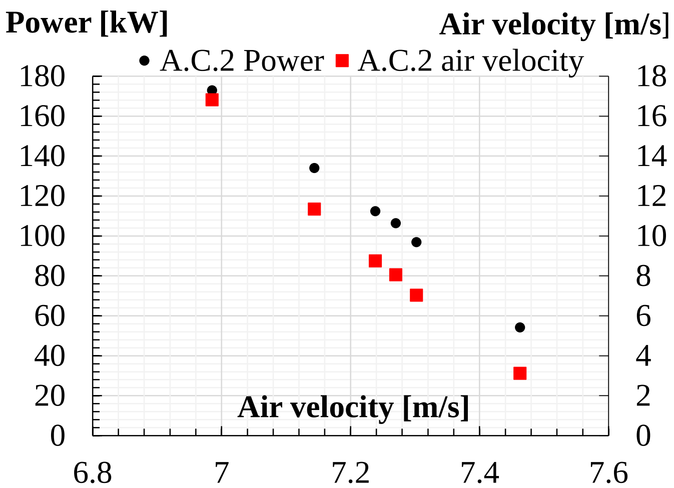

Fig. 50. A.C.2 power and air velocity variation with A.C.1 air velocity

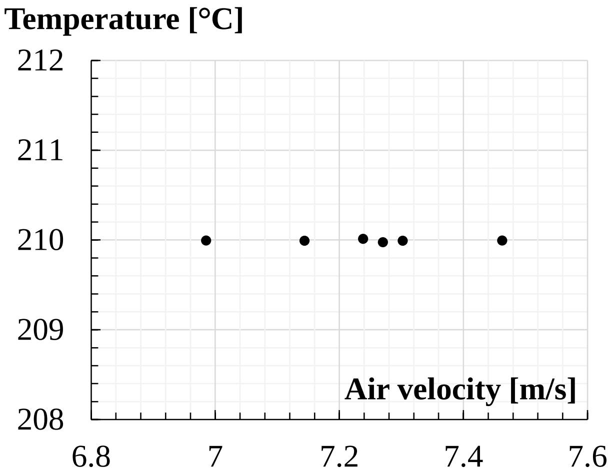

Fig. 51. A.C.2 outlet temperature variation with A.C.1 air velocity

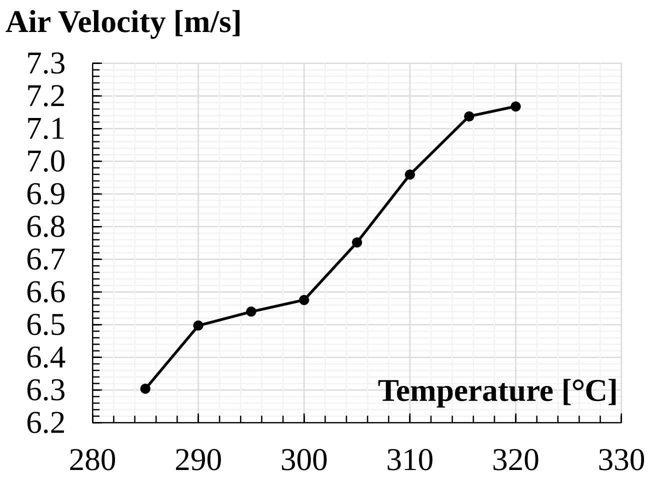

Fig. 52. A.C.1 modules air velocity variation with the OTSG outlet temperature

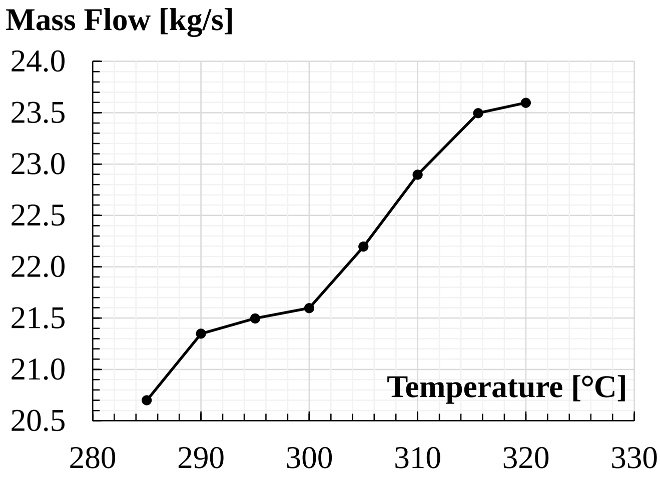

Fig. 53. A.C.1 modules mass flow variation with the OTSG outlet temperature

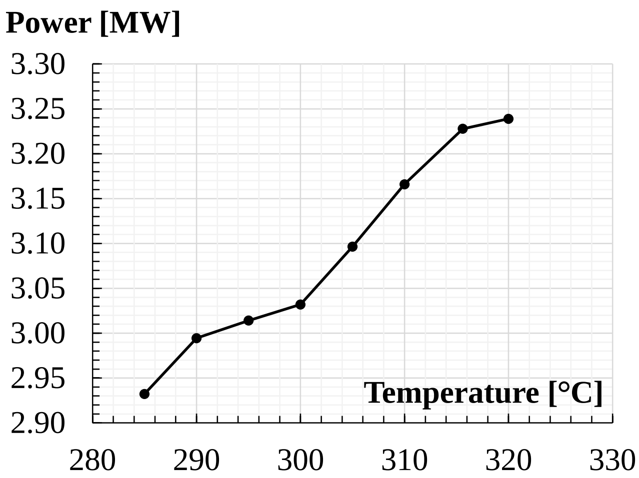

Fig. 54. A.C.1 power variation with the OTSG outlet temperature

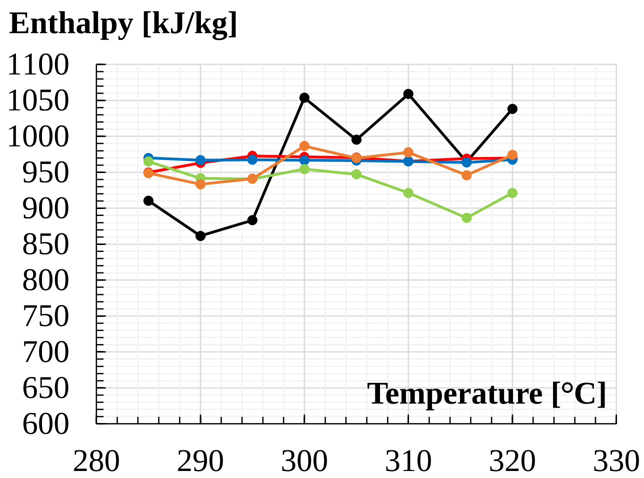

Fig. 55. A.C.1 modules outlet enthalpy variation with the OTSG outlet temperature

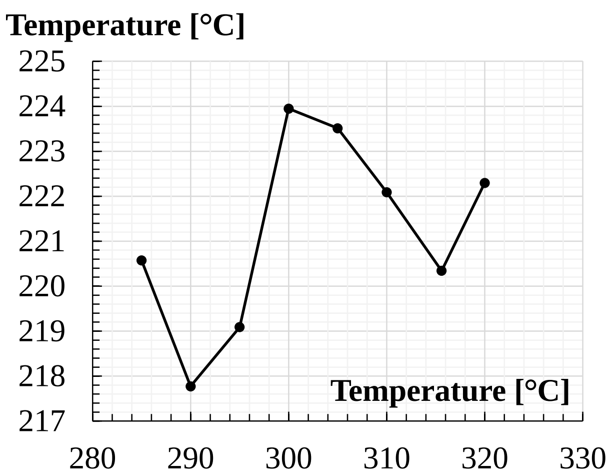

Fig. 56. Tank inlet liquid temperature variation with the OTSG outlet temperature

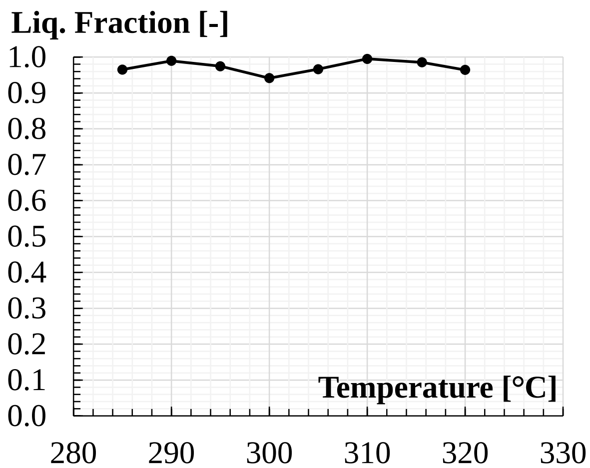

Fig. 57. Tank inlet liquid fraction variation with the OTSG outlet temperature

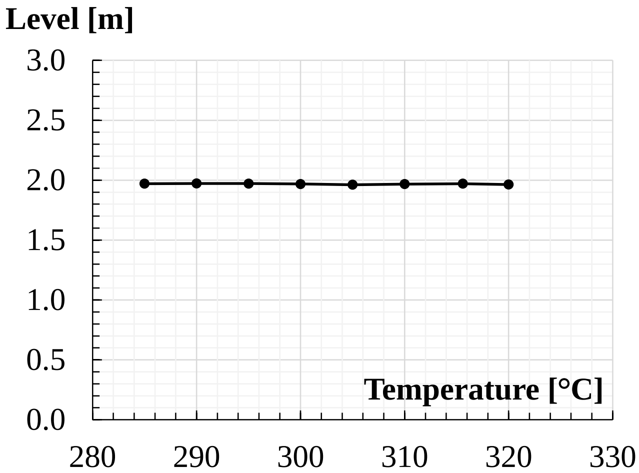

Fig. 58. Tank liquid collapsed level variation with the OTSG outlet temperature

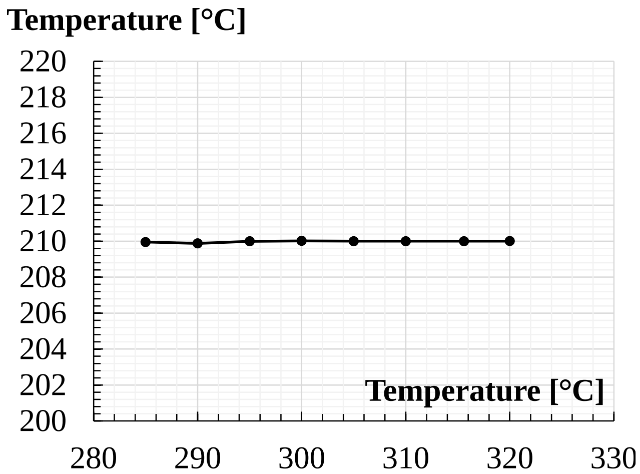

Fig. 59. A.C.2 outlet temperature variation with the OTSG outlet temperature

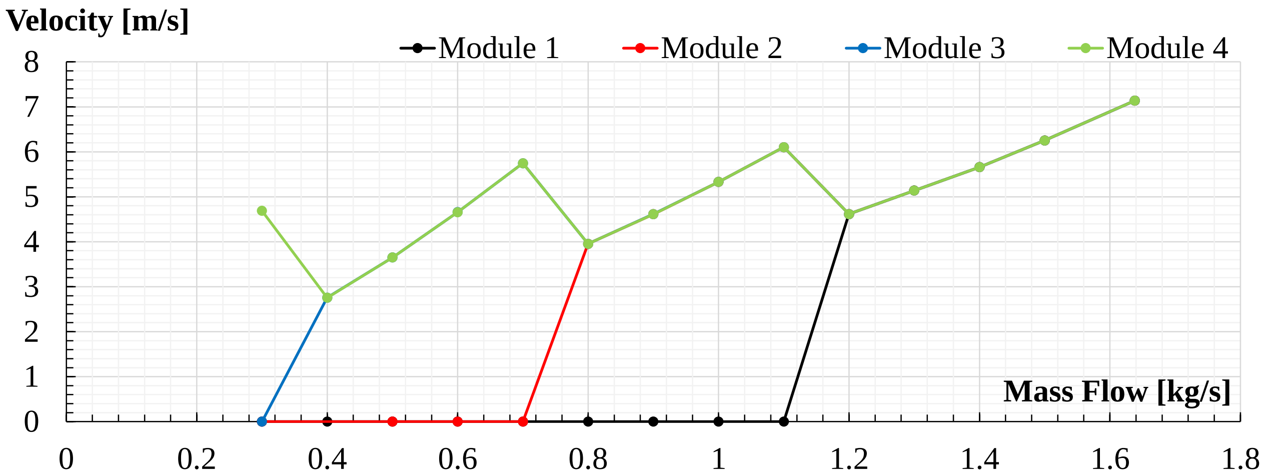

Fig. 60. A.C.1 four modules air velocity variation with vapor mass flow

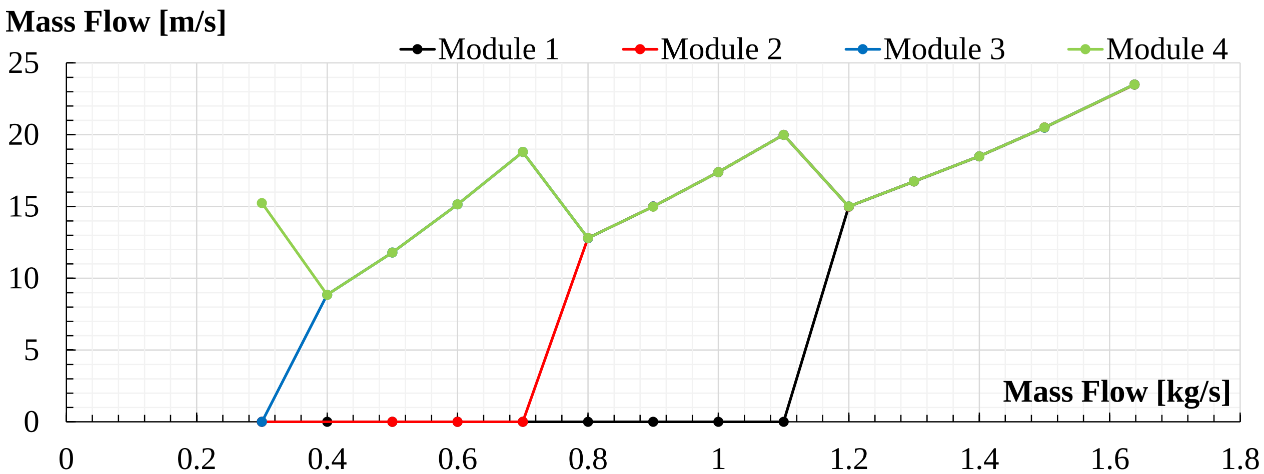

Fig. 61. A.C.1 four modules air mass flow variation with vapor mass flow

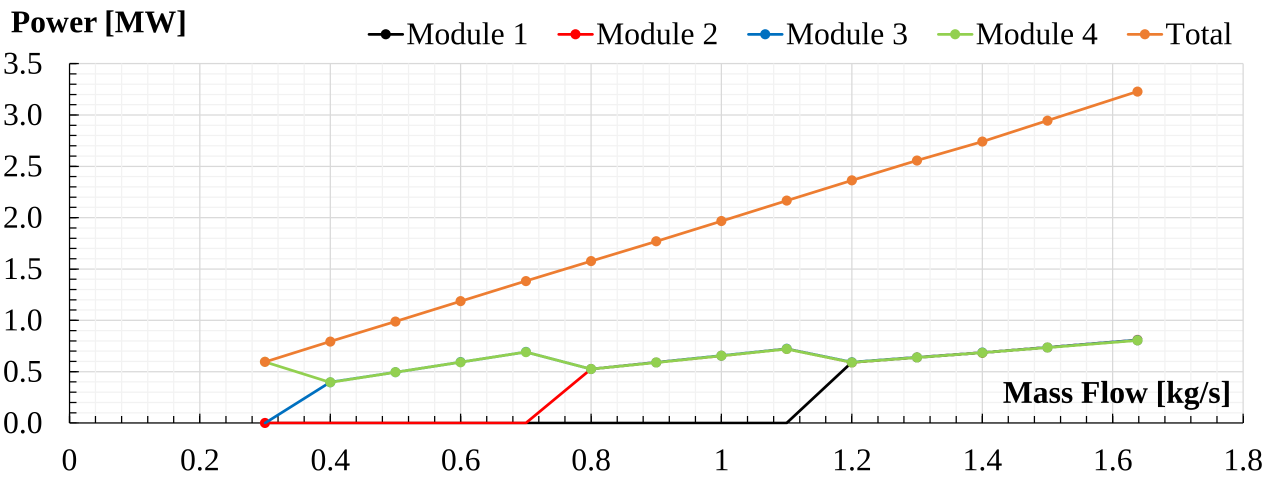

Fig. 62. A.C.1 four modules power variation with vapor mass flow

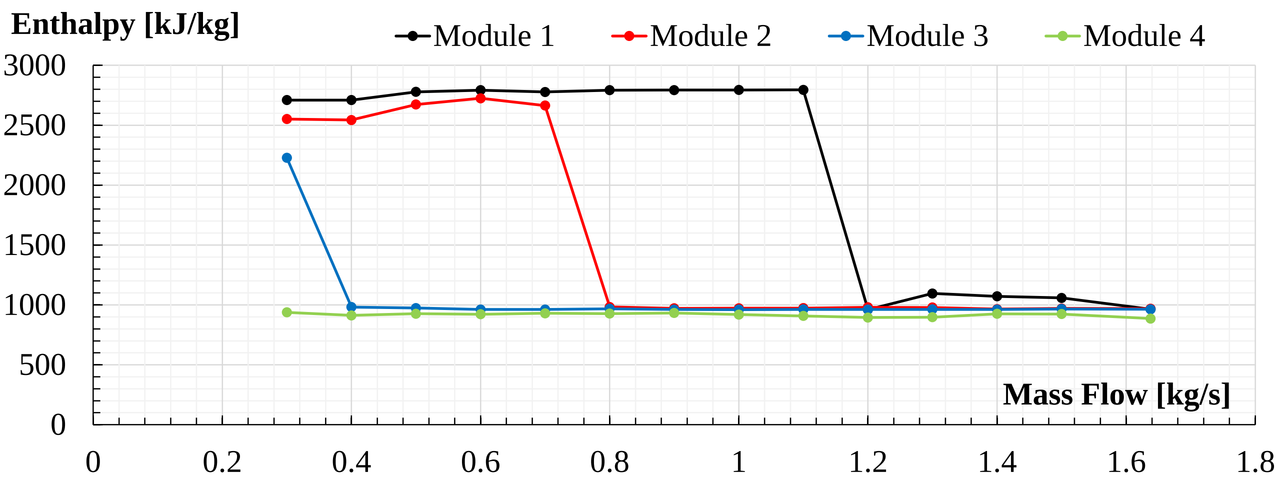

Fig. 63. A.C.1 four modules outlet enthalpy variation with vapor mass flow

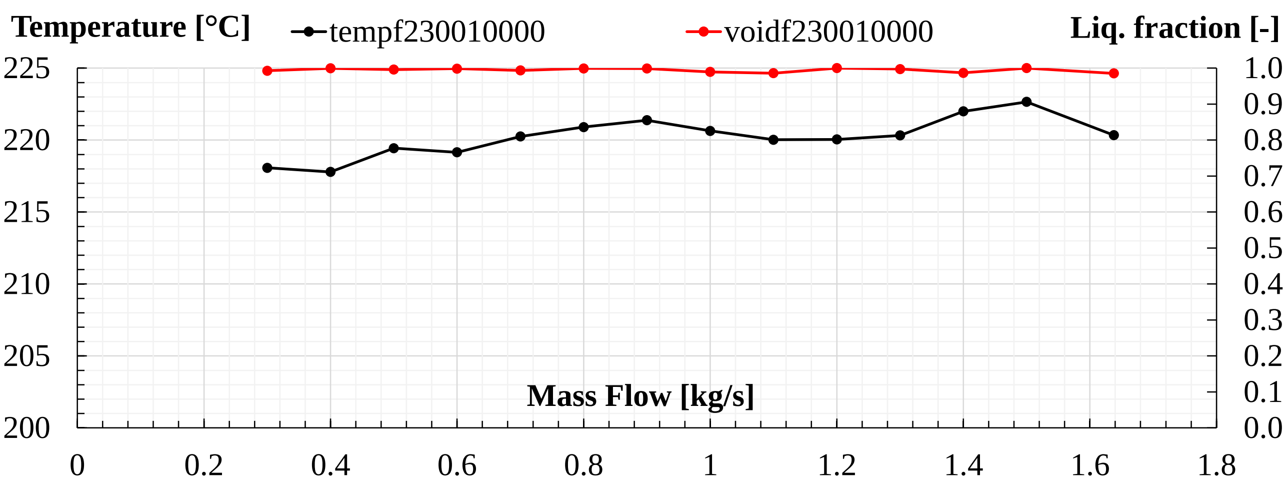

Fig. 64. Inlet tank temperature and liquid fraction variation with vapor mass flow

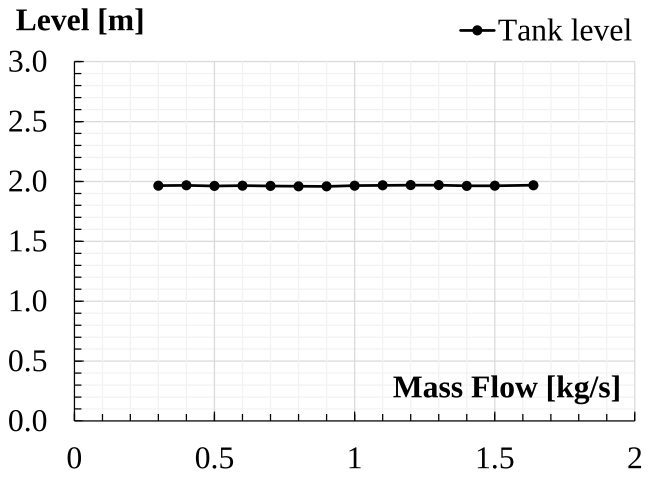

Fig. 65. Condensate tank level variation with vapor mass flow

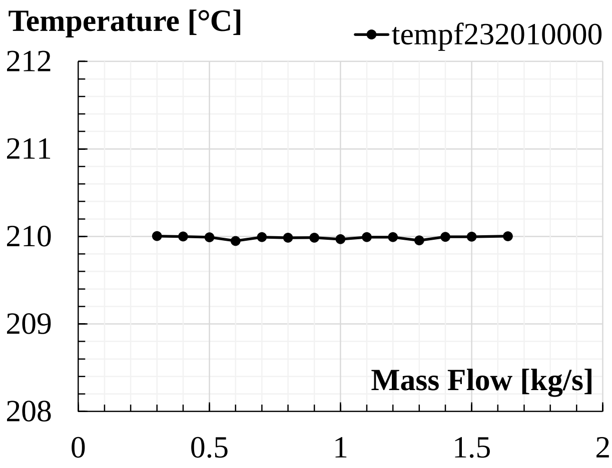

Fig. 66. A.C.2outlet temperature variation with vapor mass flow

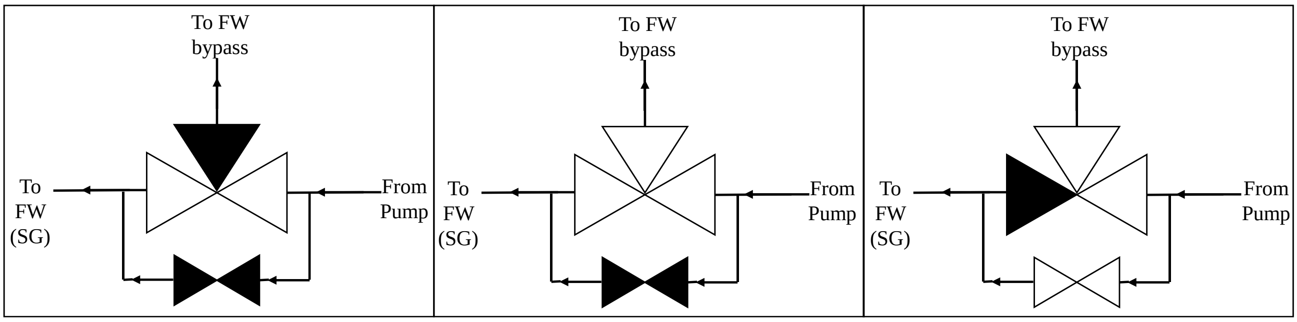

(a) ***(b)*** ***(c)***

Fig. 67. Three-ways valve and additional valve operation at nominal power (a), in regulation condition between 100% and 10% (b) and between 10% and 1% (c)

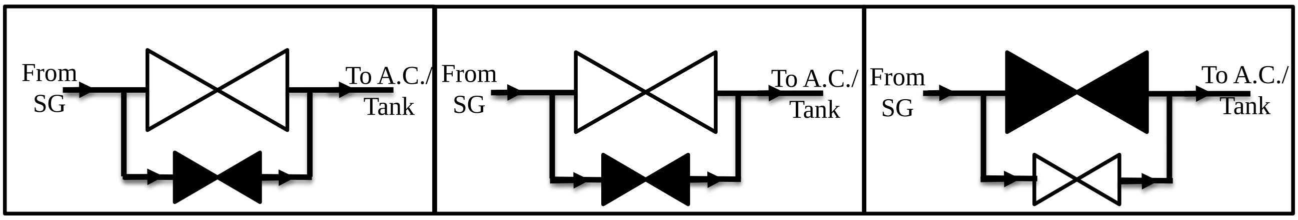

(a) ***(b)*** ***(c)***

Fig. 68. Lamination valves operation at nominal power (a), in regulation condition between 100% and 10% (b) and between 10% and 1% (c)

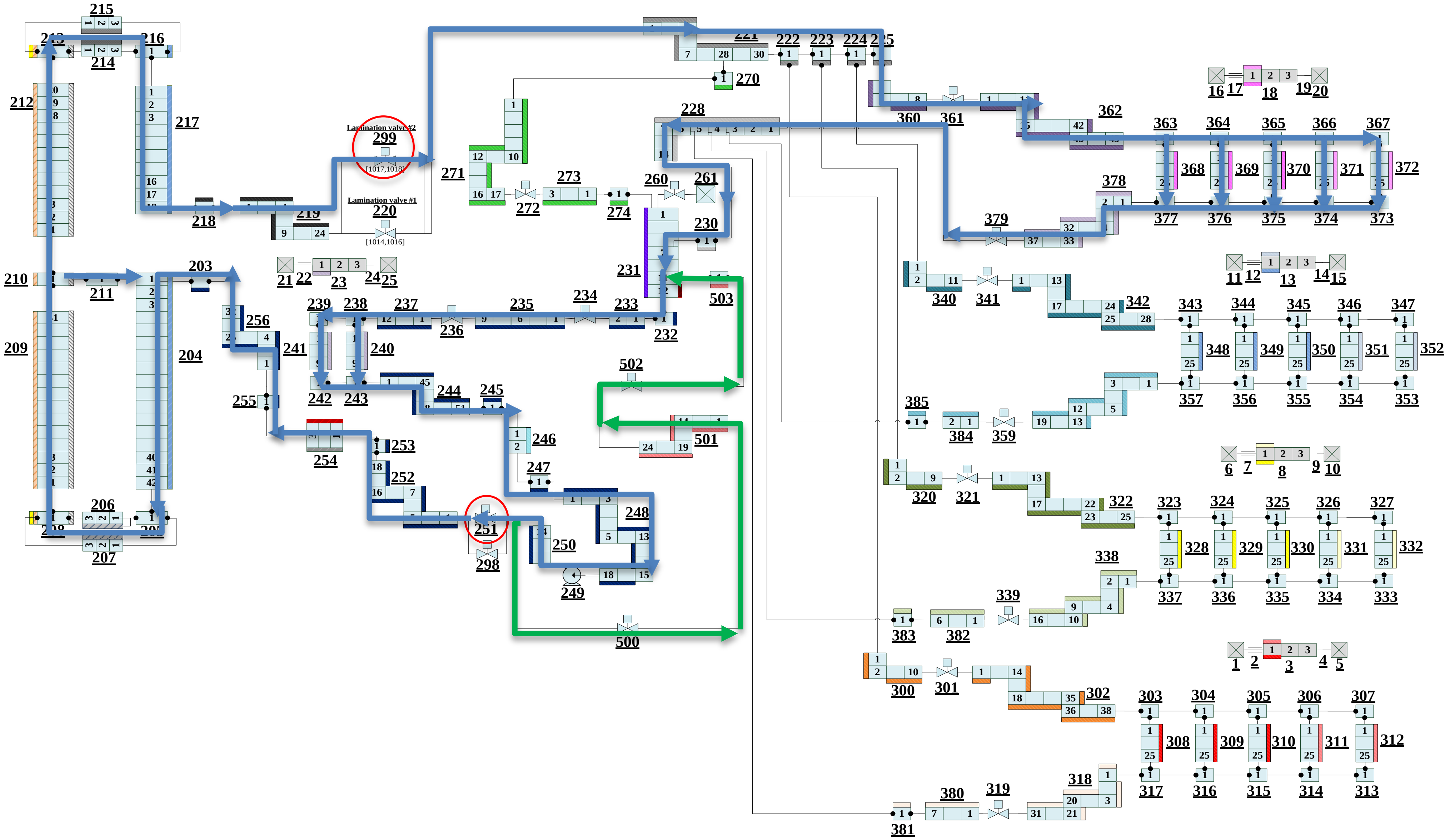

Fig. 69. Main stream (blue) and feedwater bypass (green) flow path at 10% and 5% of the nominal power

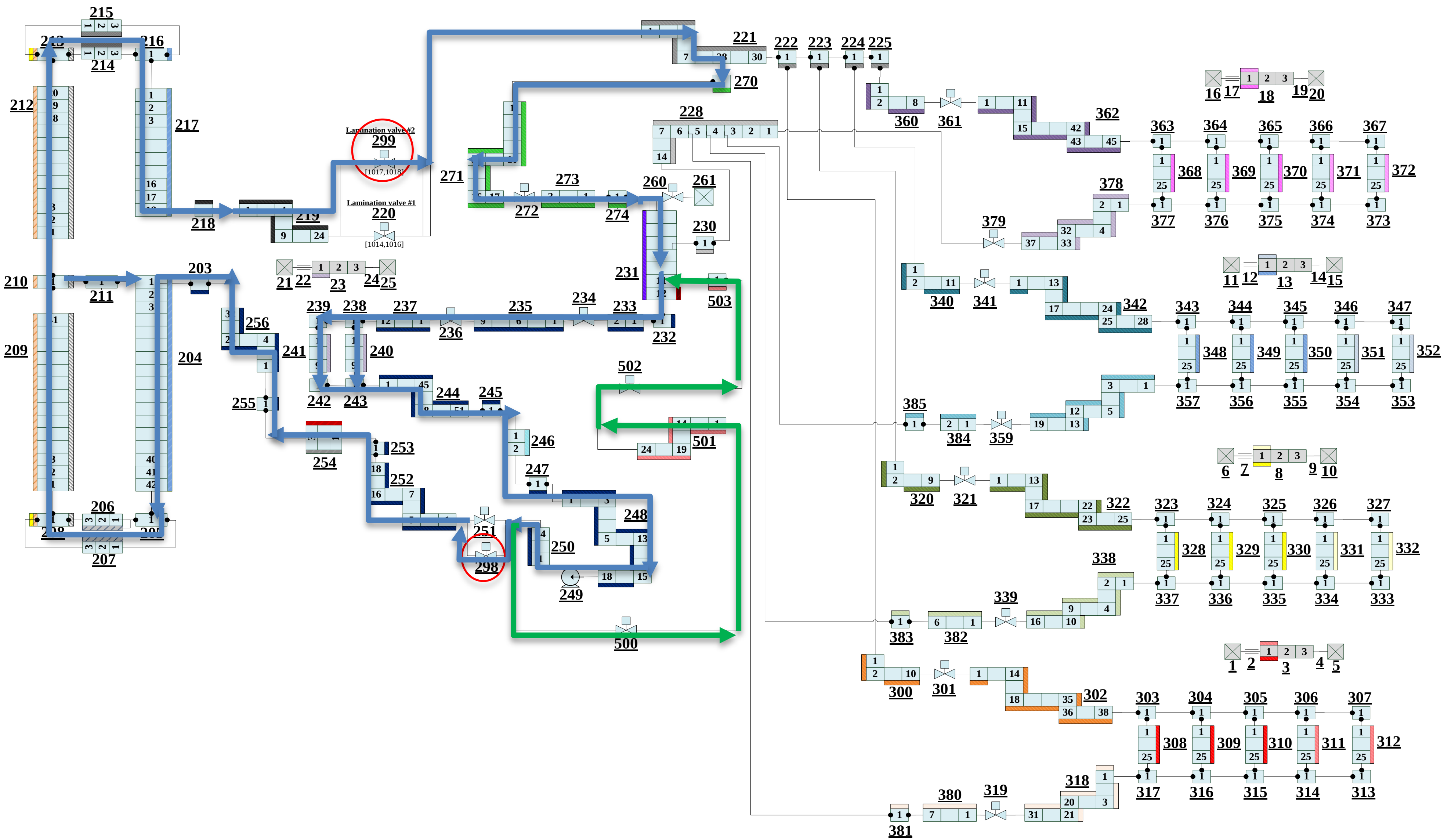

Fig. 70. Main stream (blue) and feedwater bypass (green) flow path at 1% of the nominal power

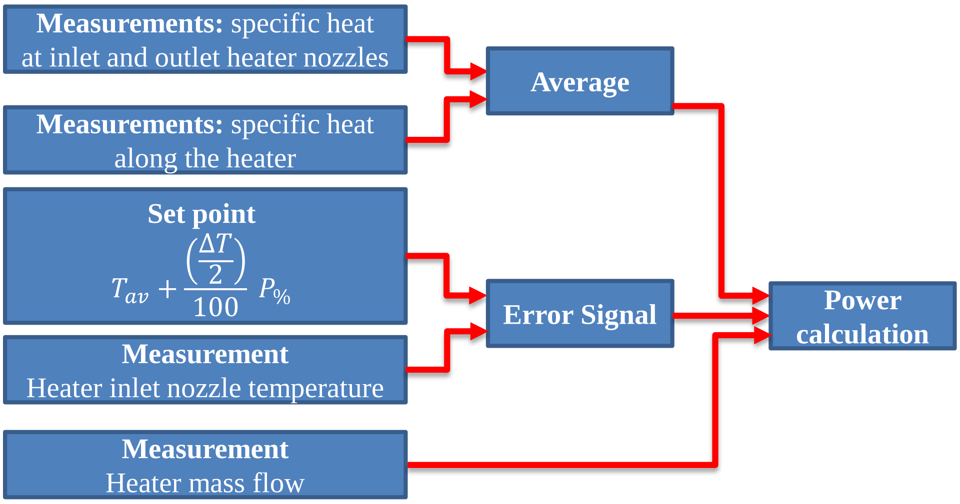

Fig. 71. RELAP5 implemented control logic for the primary side heater during low power operations

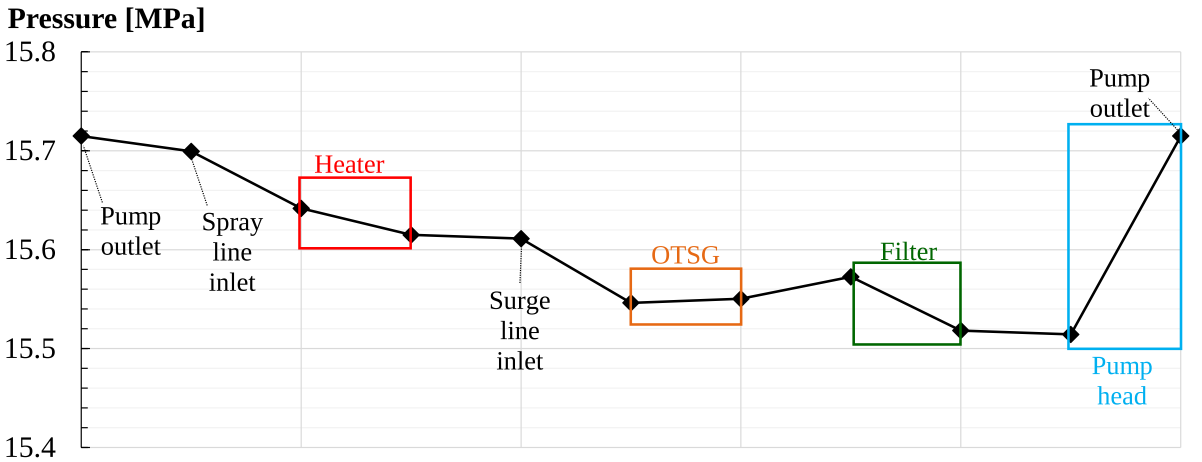

Fig. 72. Pressure profile along the Primary Loop main components

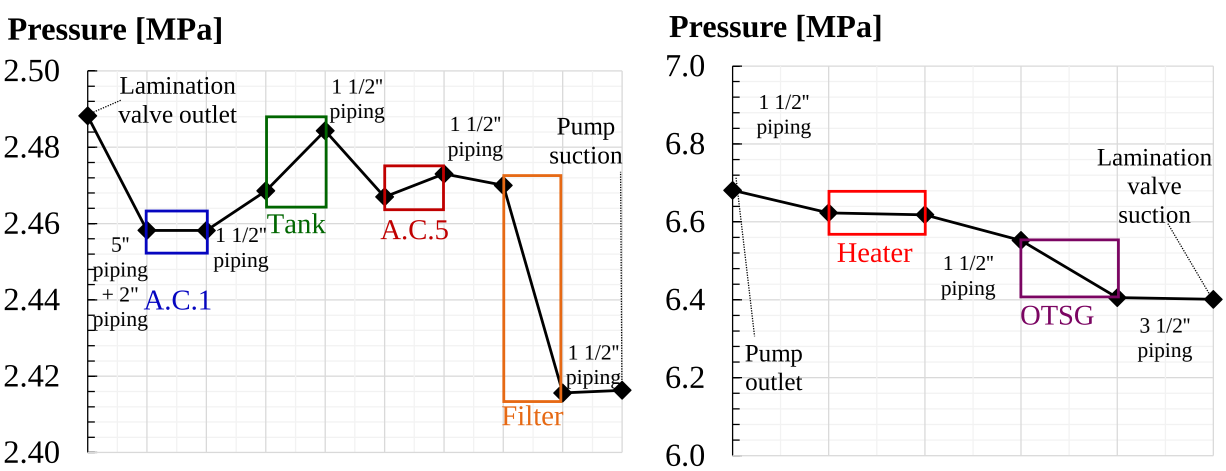

Fig. 73. Pressure profile along the Secondary Loop Low-Pressure Section (left) and High-Pressure section (right)

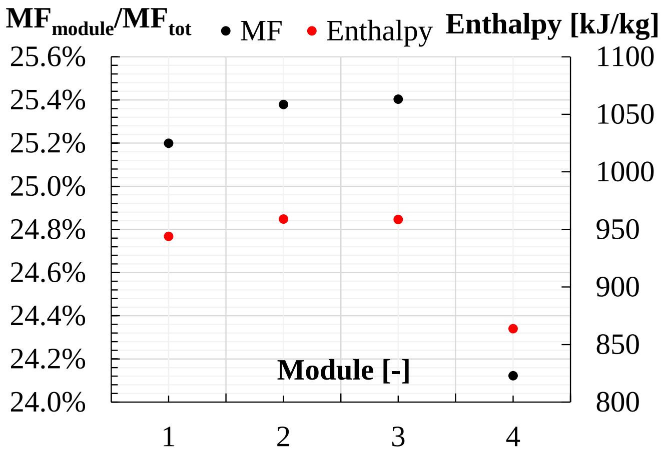

Fig. 74. A.C.1 mass flow distribution among the modules and fluid outlet enthalpy.

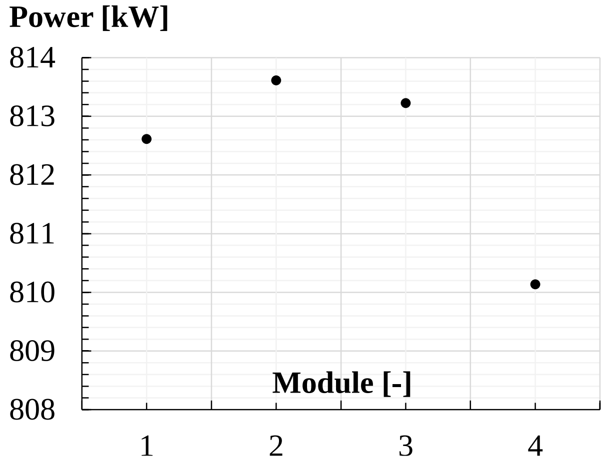

Fig. 75. A.C.1 modules exchanged power.

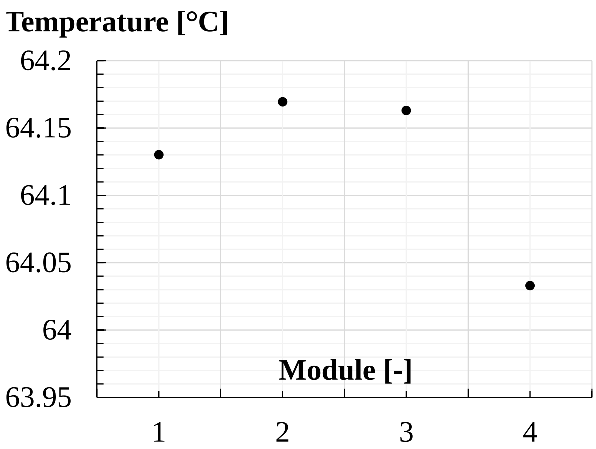

Fig. 76. A.C.1 modules air outlet temperature.

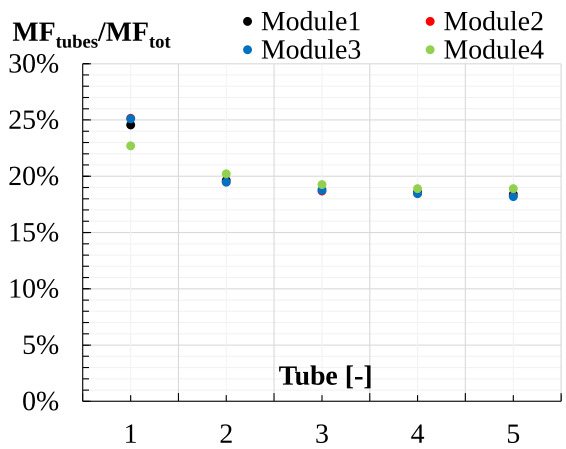

Fig. 77. A.C.1 mass flow distribution.

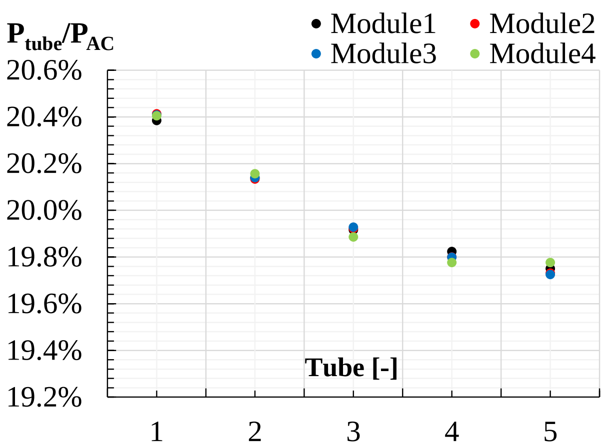

Fig. 78. A.C.1 power distribution.

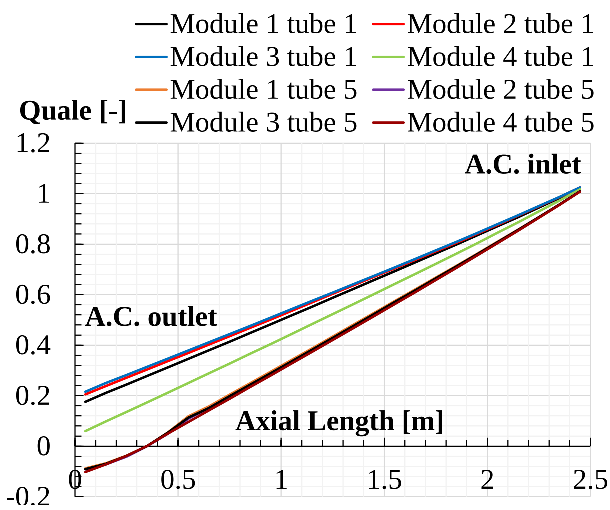

Fig. 79. A.C.1 equilibrium quality (Quale) axial profile along the first and the last tube of each module.

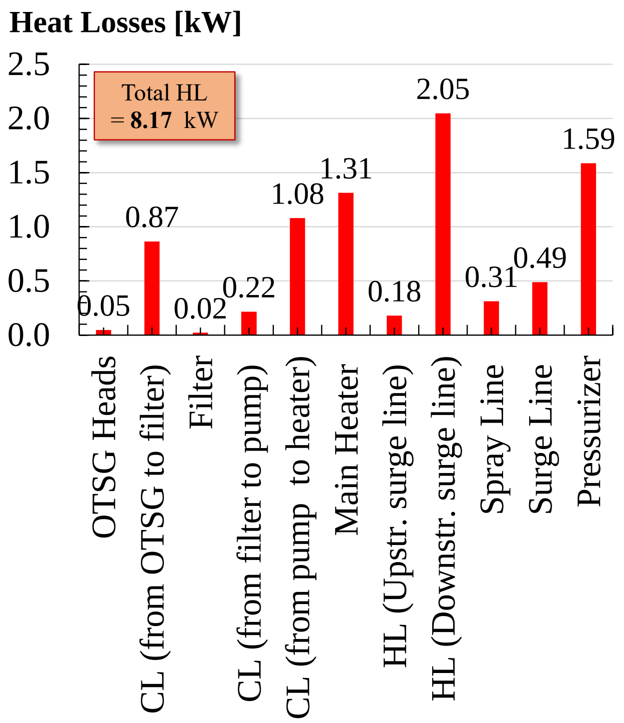

Fig. 80. Primary loop heat losses distribution.

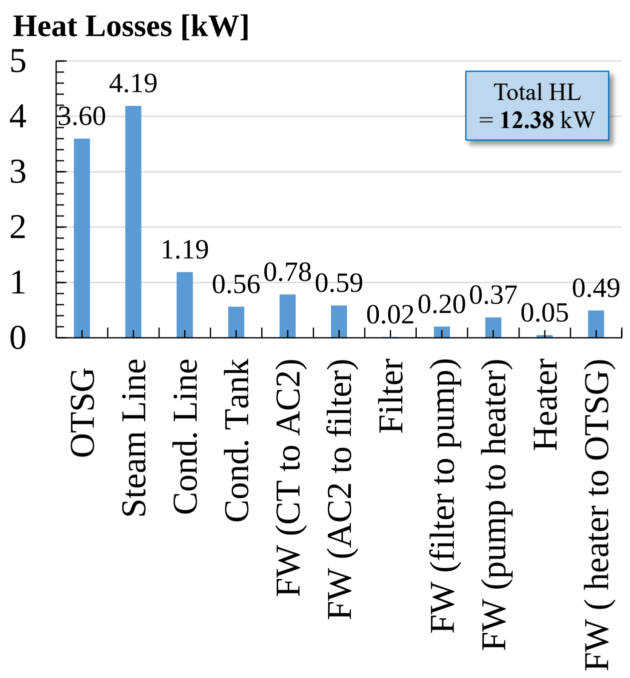

Fig. 81. Secondary loop heat losses distribution.

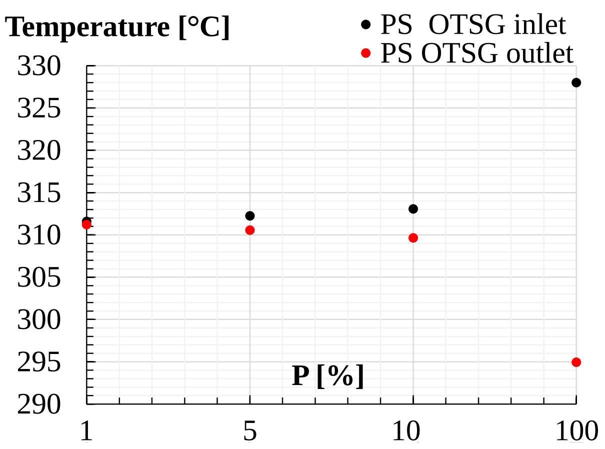

Fig. 82. Primary side OTSG inlet and outlet temperatures at the investigated power states

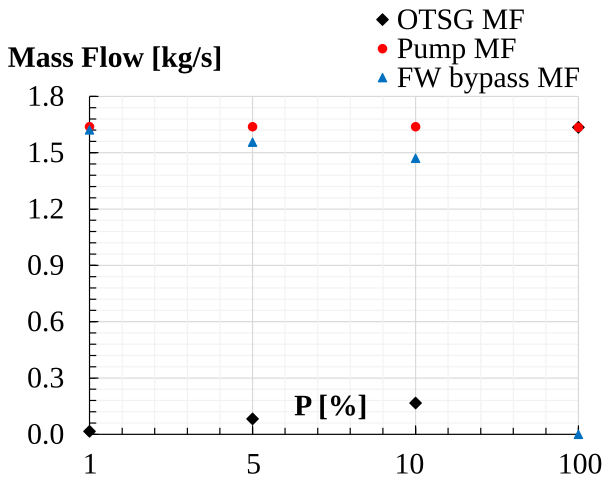

Fig. 83. Secondary loop flow repartition among the feedwater and the bypass at different power states

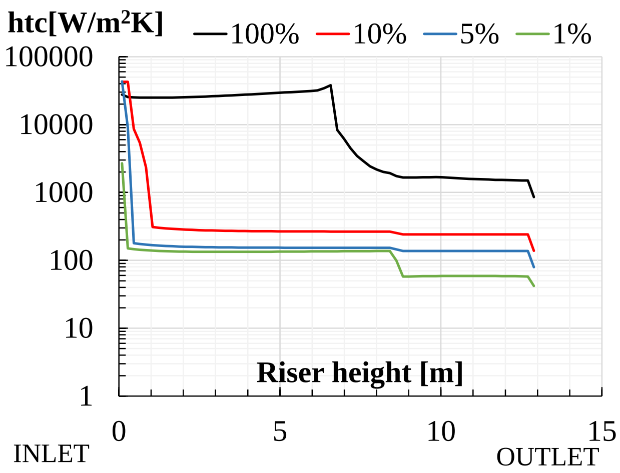

Fig. 84. SG secondary side heat transfer coefficient along the height

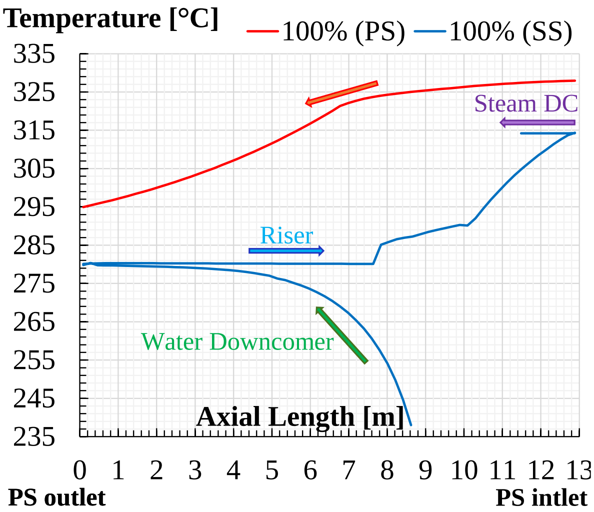

Fig. 85. SG axial temperature profiles of primary and secondary fluids at 100% of the nominal power.

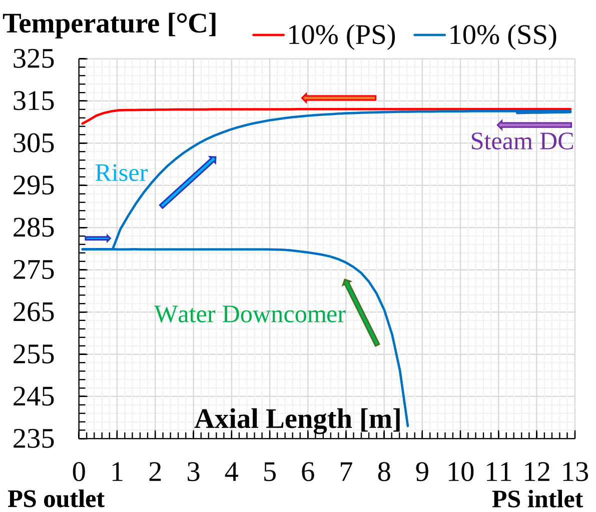

Fig. 86. SG axial temperature profiles of primary and secondary fluids at 10% of the nominal power.

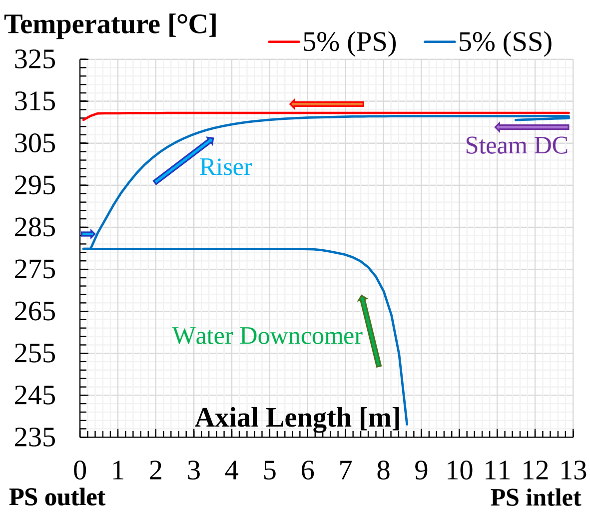

Fig. 87. SG axial temperature profiles of primary and secondary fluids at 5% of the nominal power.

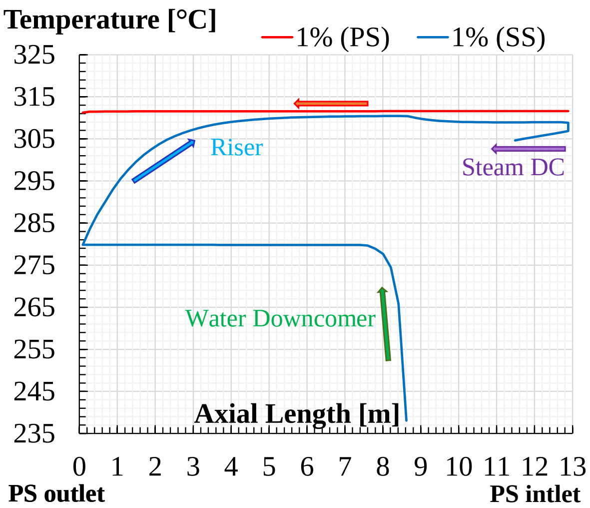

Fig. 88. SG axial temperature profiles of primary and secondary fluids at 1% of the nominal power.

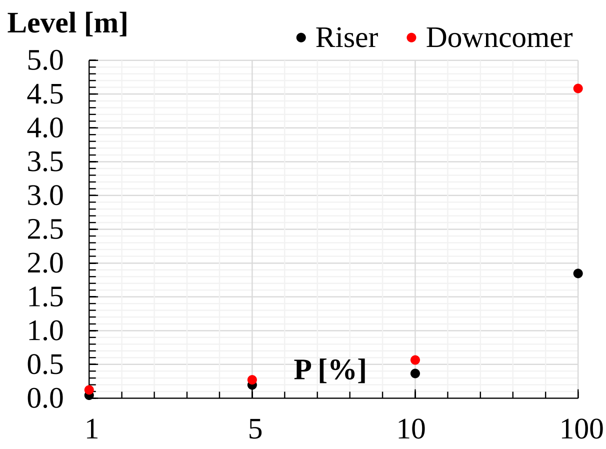

Fig. 89. Riser and downcomer levels at the investigated power states.

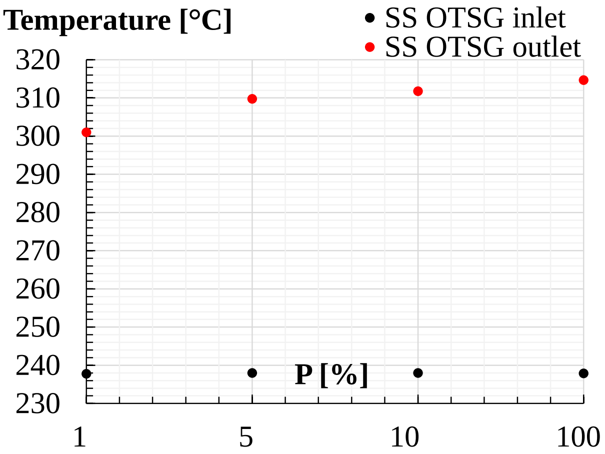

Fig. 90. Secondary side SG inlet and outlet temperatures at the investigated power states.

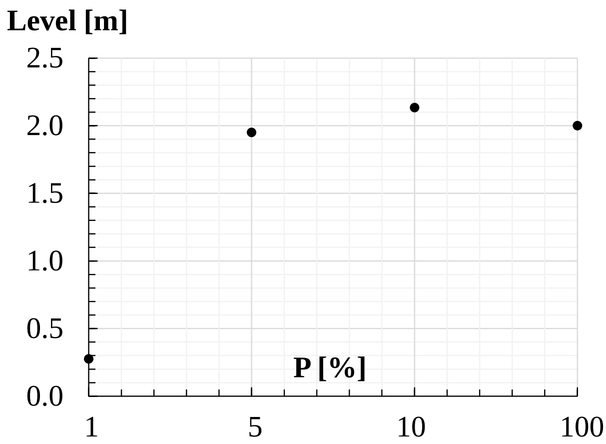

Fig. 91. Condensate tank level at the investigated power states.

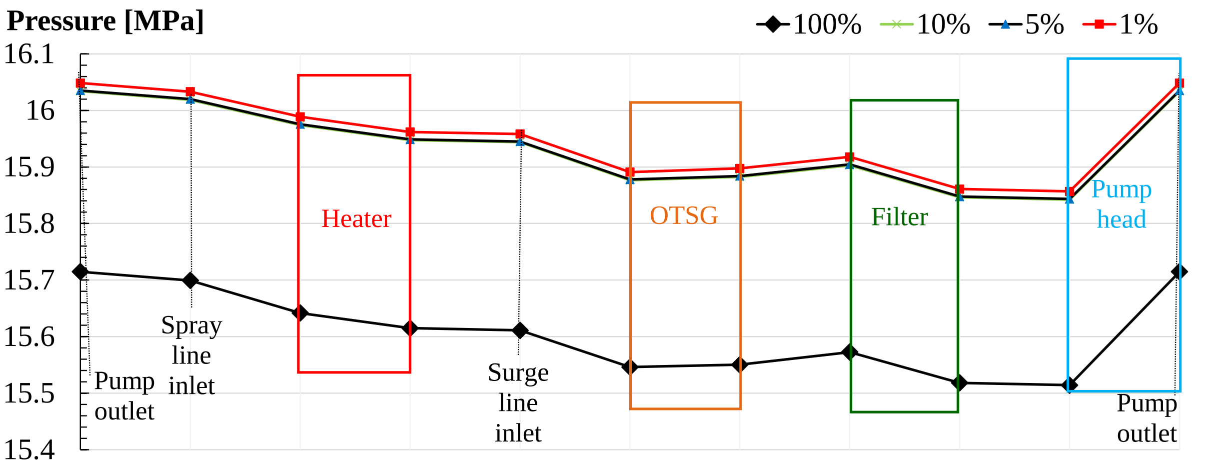

Fig. 92. Pressure profile along the primary loop piping and components

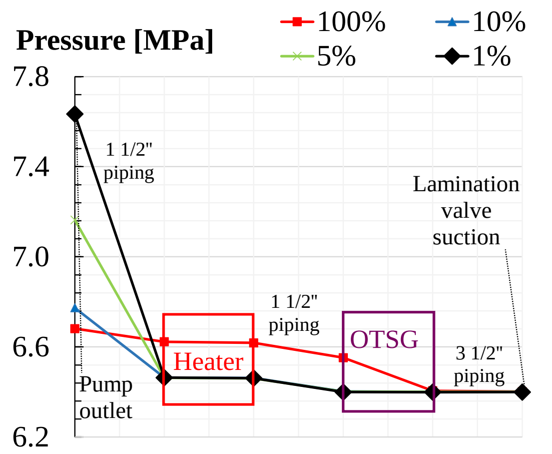

Fig. 93. Pressure profile along the part of the secondary loop piping and component of the section at 6.4 MPa

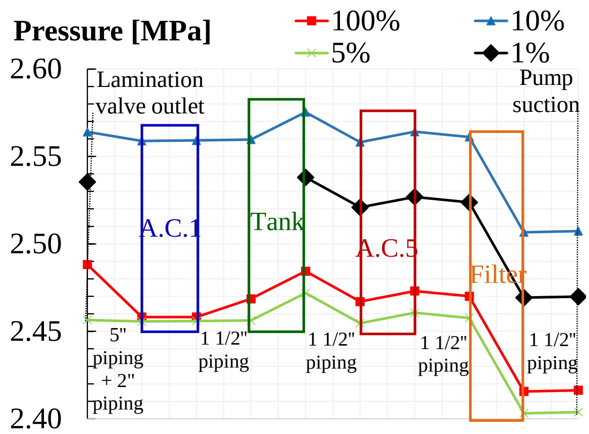

Fig. 94. Pressure profile along the part of the secondary loop piping and component of the section at 2.5 MPa

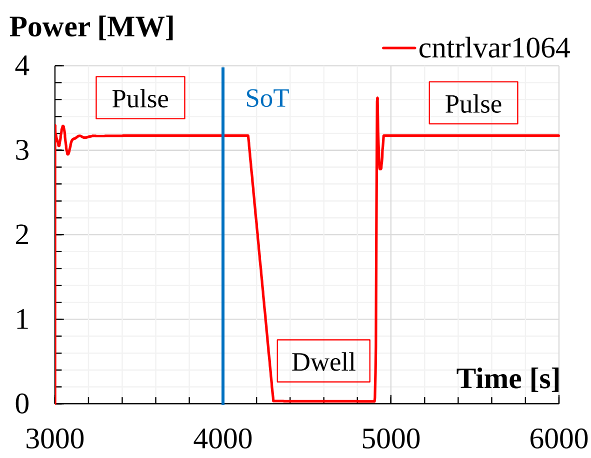

Fig. 95. Power provided to the electrical heater during the pulse-dwell-pulse transition

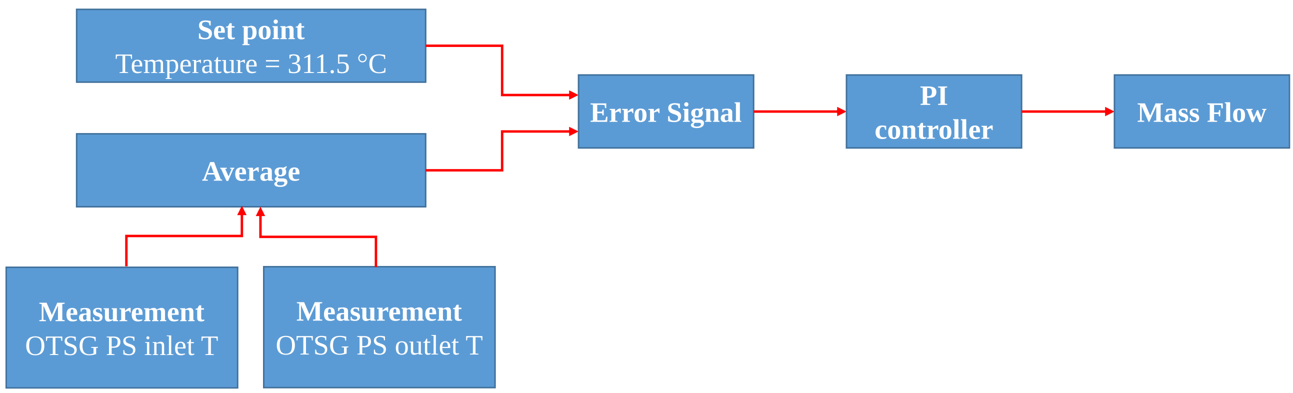

Fig. 96. FW mass flow regulation controlling PS average temperature

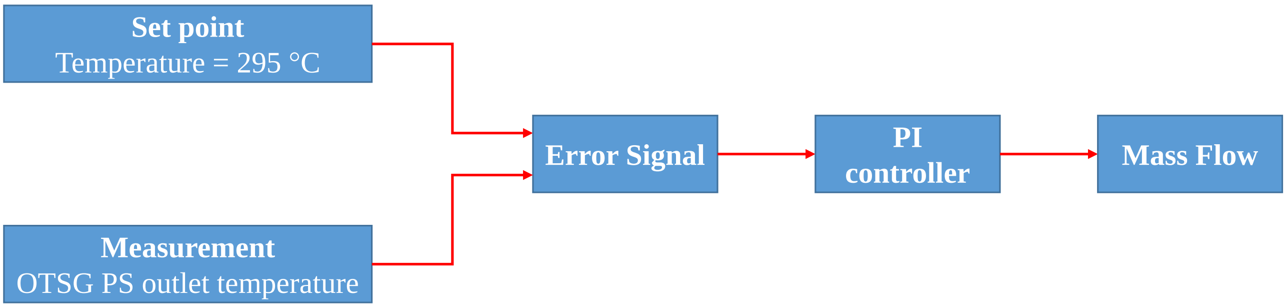

Fig. 97. FW mass flow regulation controlling PS minimum temperature

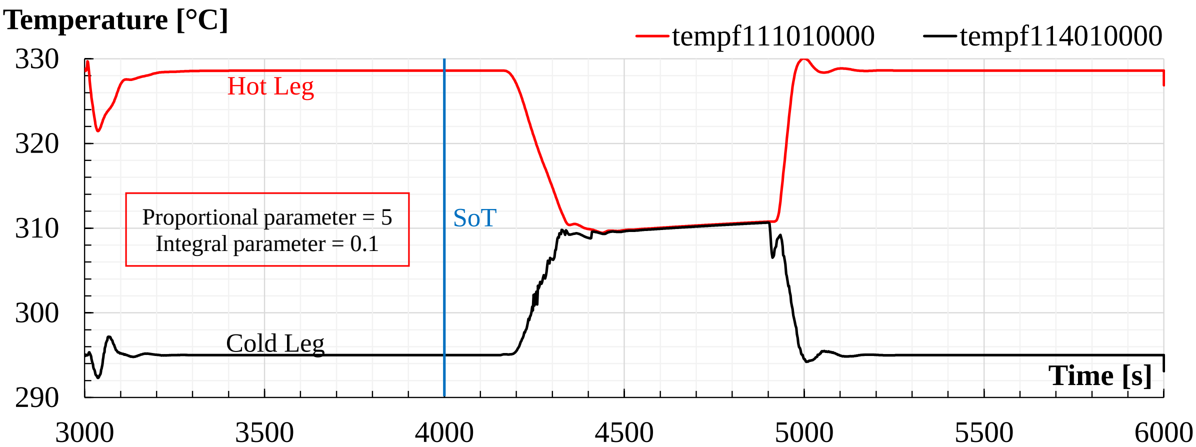

Fig. 98. CL and HL temperatures variation during pulse-dwell-pulse transition with the average temperature PI controller

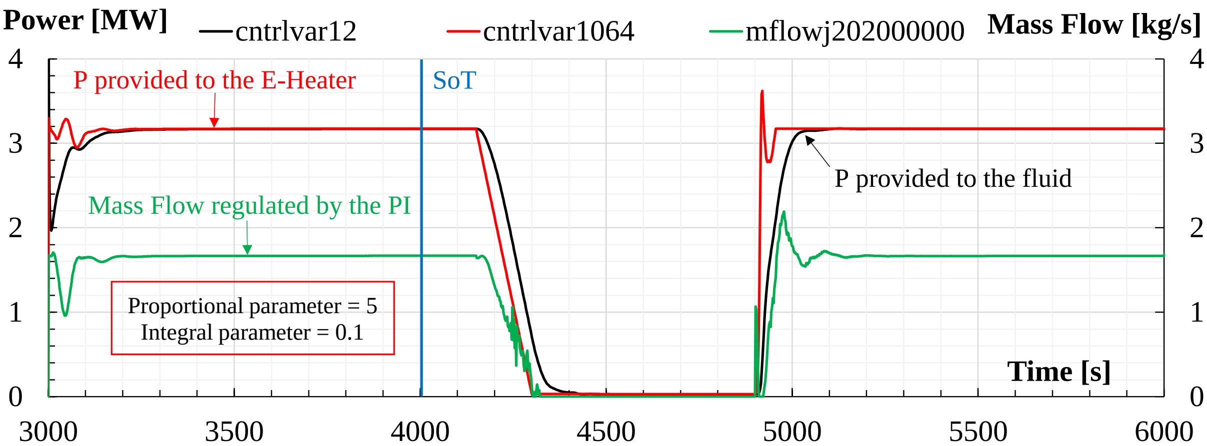

Fig. 99. Power and feedwater variation during pulse-dwell-pulse transition with the average temperature PI controller

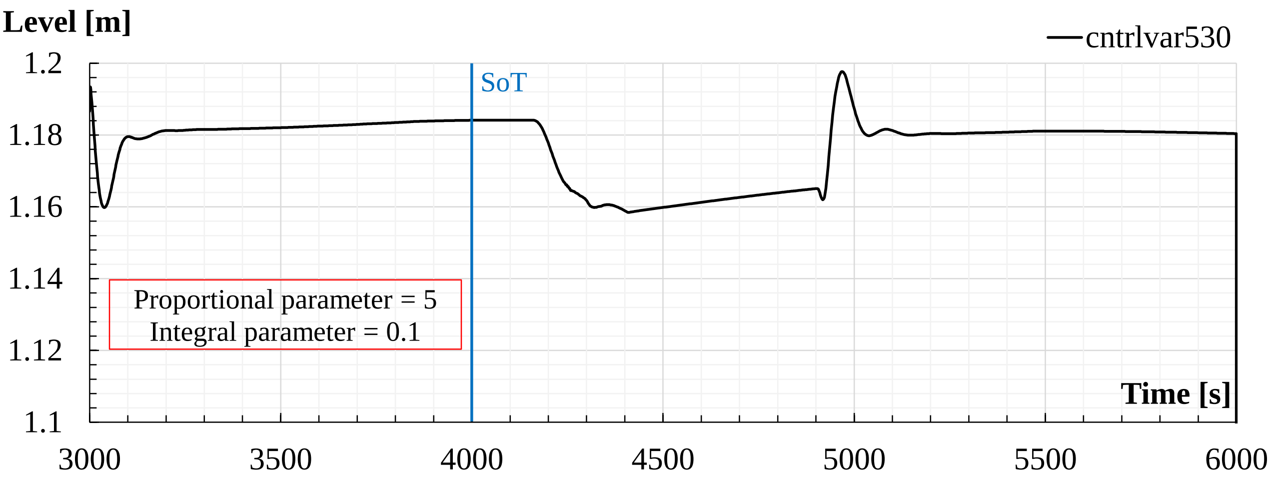

Fig. 100. Pressurizer level variation during pulse-dwell-pulse transition with the average temperature PI controller

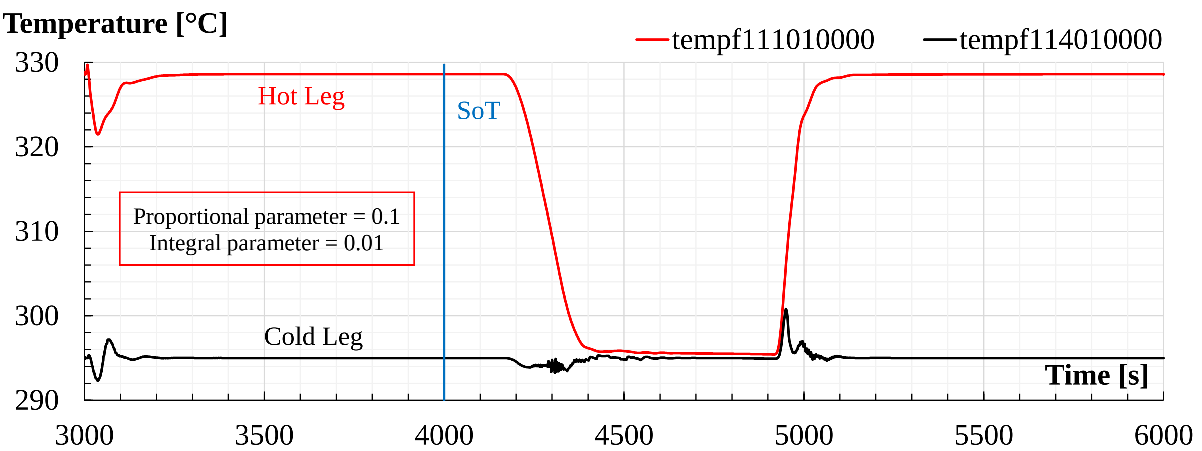

Fig. 101. Primary side temperatures variation during pulse-dwell-pulse transition with the PS minimum temperature PI controller

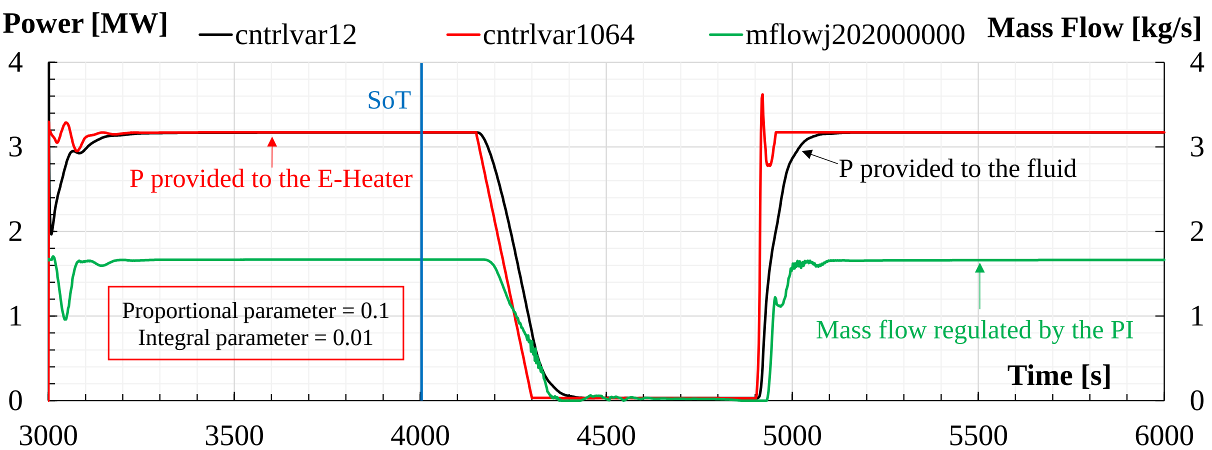

Fig. 102. Power variation during pulse-dwell-pulse transition with the PS minimum temperature PI controller

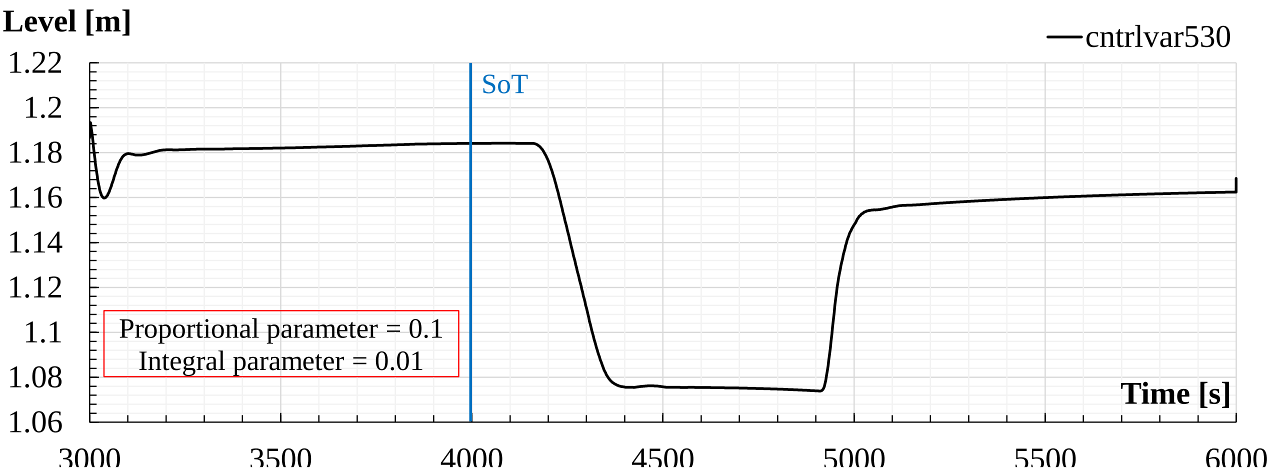

Fig. 103. Pressurizer level variation during pulse-dwell-pulse transition with the PS minimum temperature PI reference controller

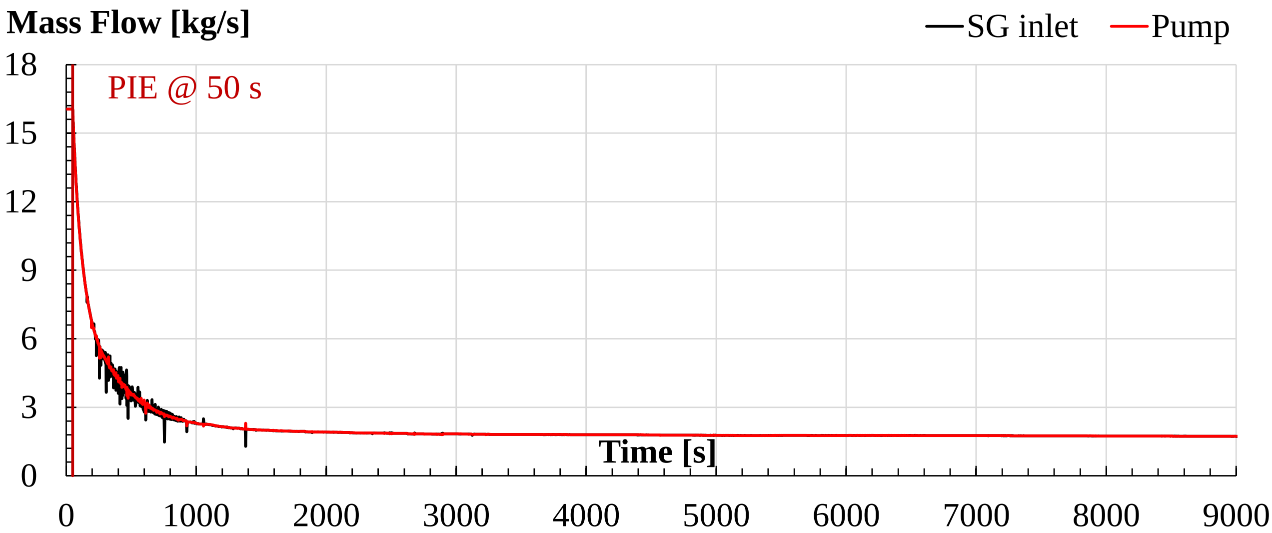

Fig. 104. PS mass flow rate during a LOFA

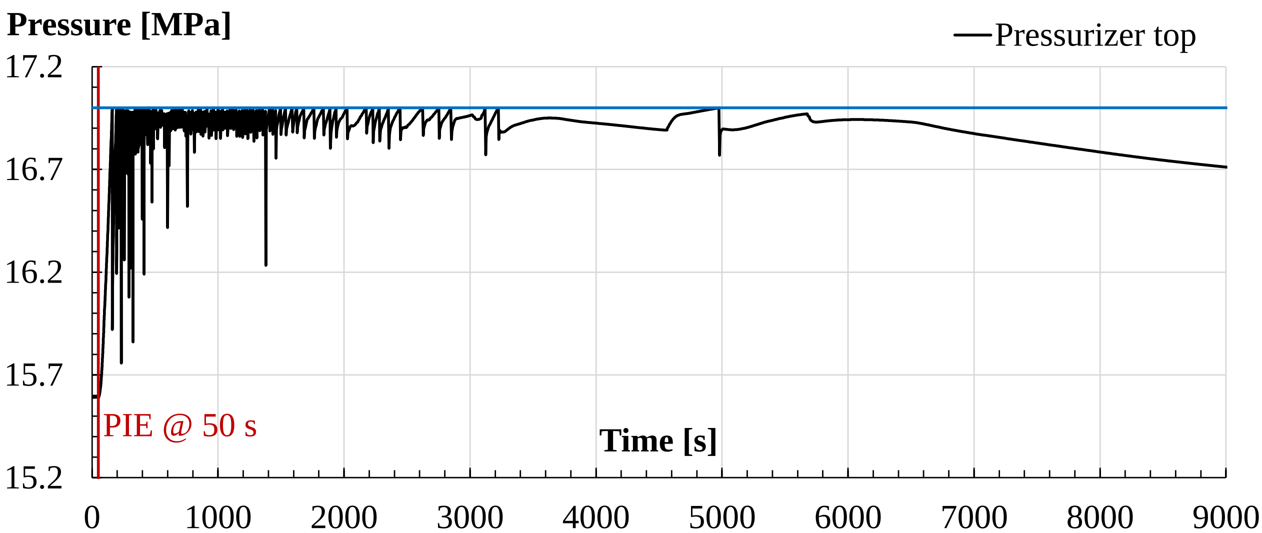

Fig. 105. Pressurizer pressure during a LOFA

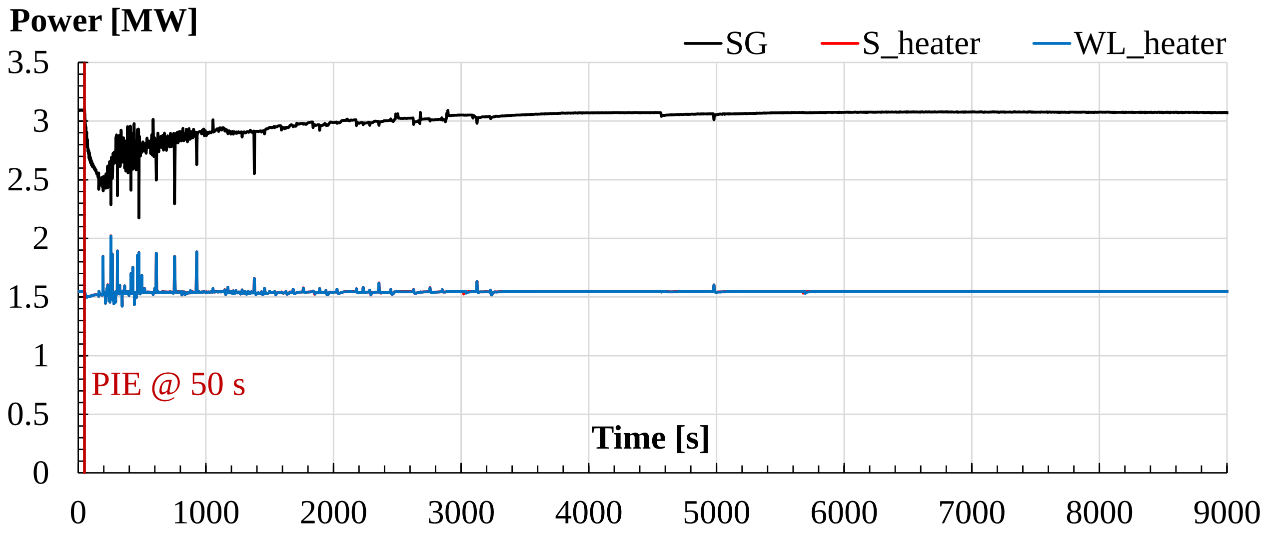

Fig. 106. SG and electric heaters power during a LOFA

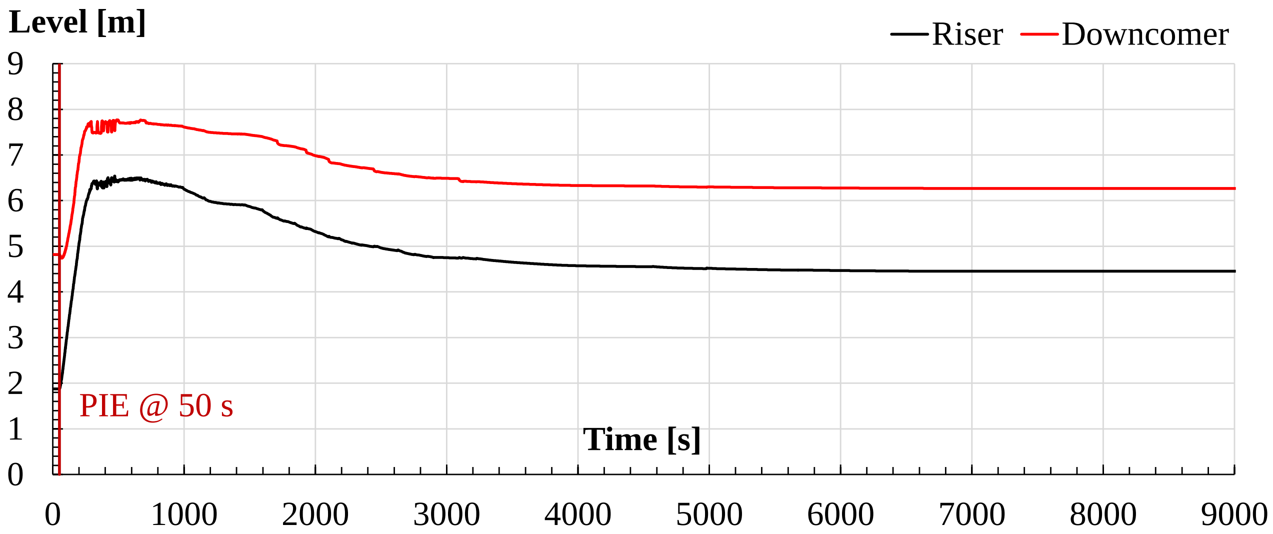

Fig. 107. Riser and Downcomer level during a LOFA

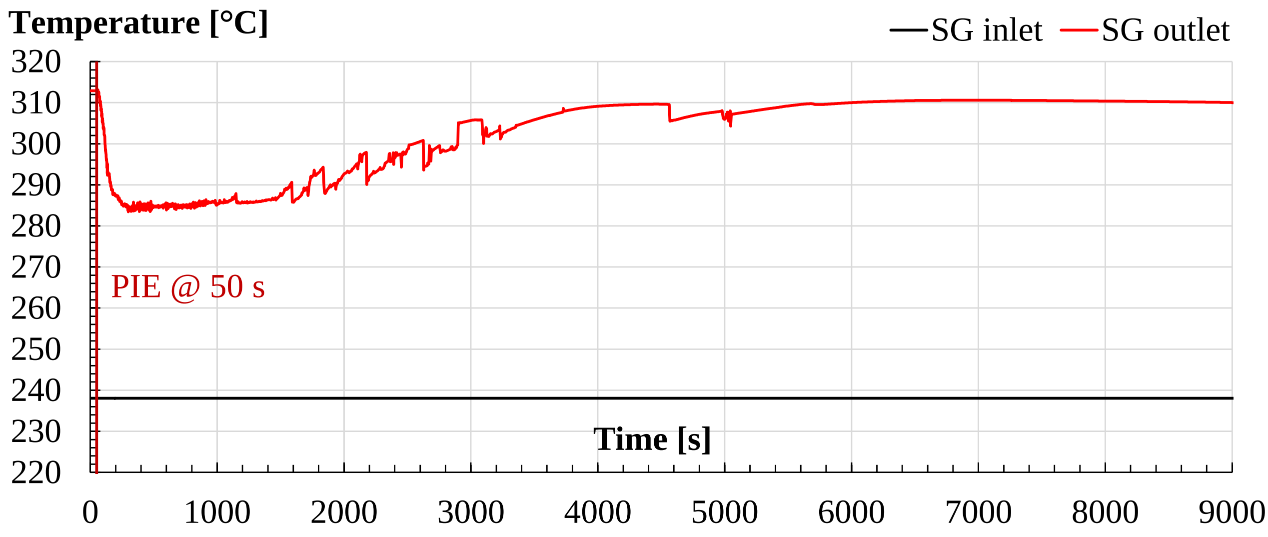

Fig. 108. Secondary side SG inlet and outlet temperature during a LOFA

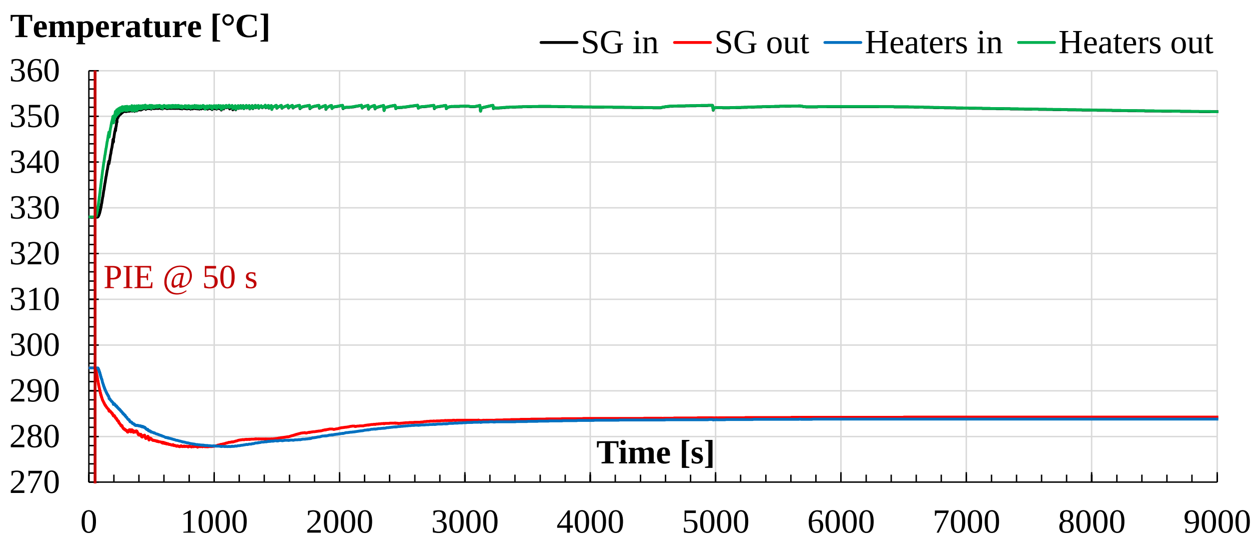

Fig. 109. Primary side SG inlet and outlet temperatures during a LOFA

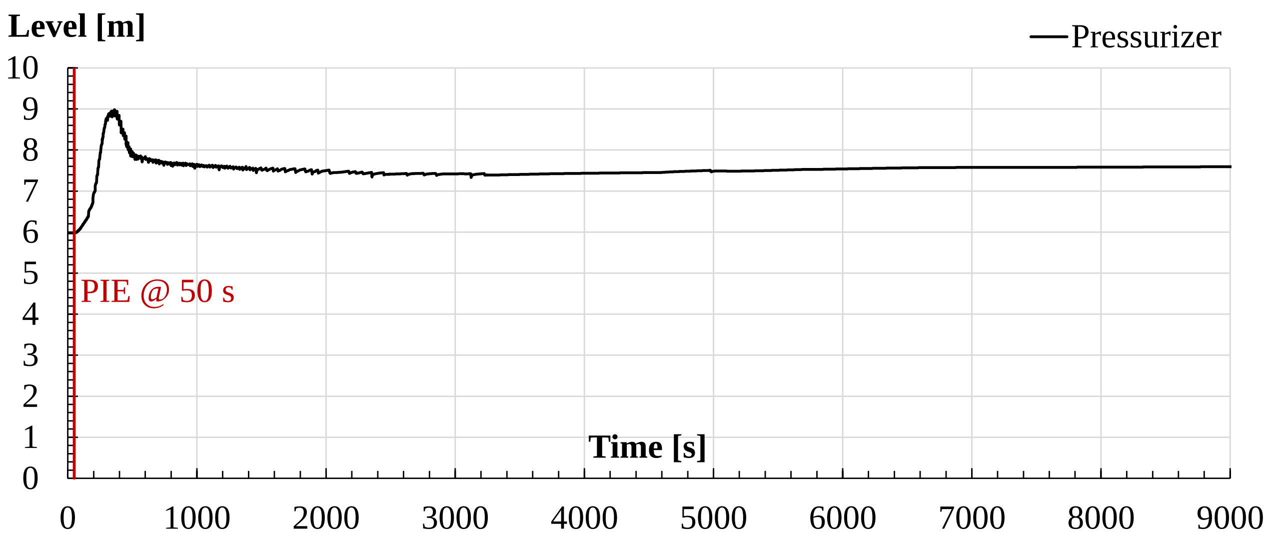

Fig. 110. Pressurizer level during a LOFA

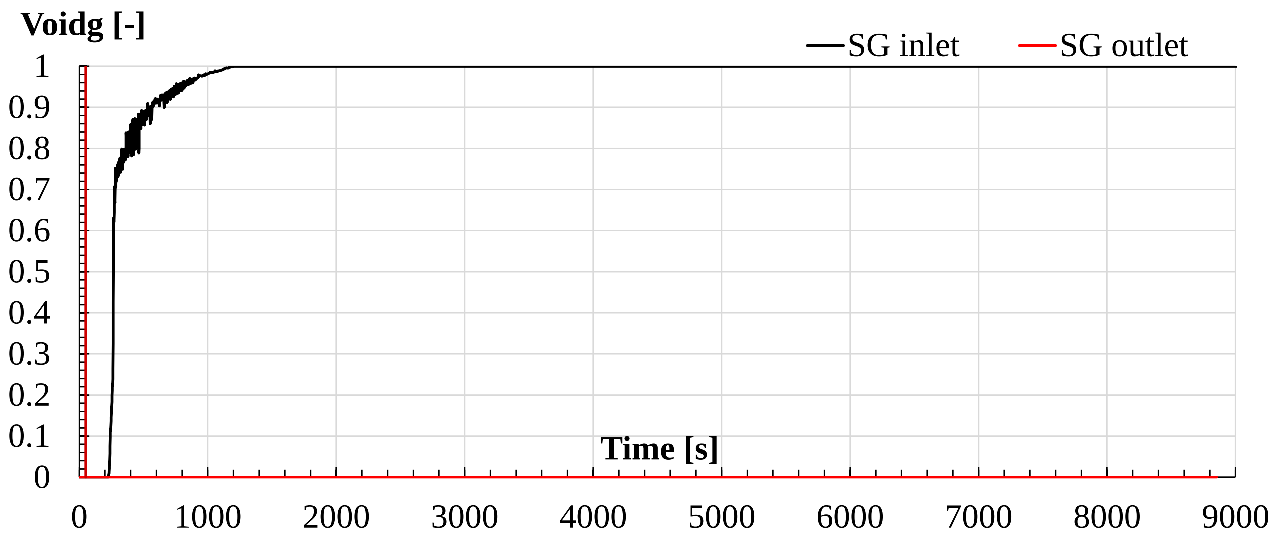

Fig. 111. SG inlet and outlet void fractions during a LOFA

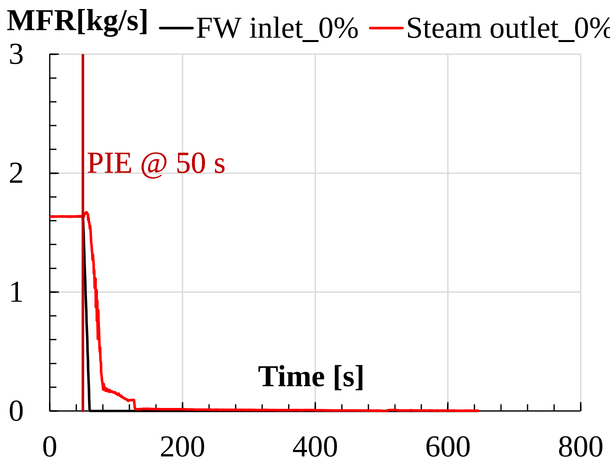

Fig. 112. Feedwater mass flow during unprotected LOHS scenarios in case 0%

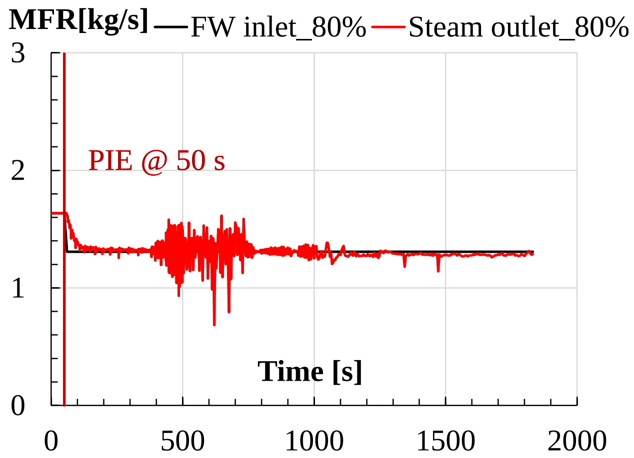

Fig. 113. Feedwater mass flow during unprotected LOHS scenarios in case 80%

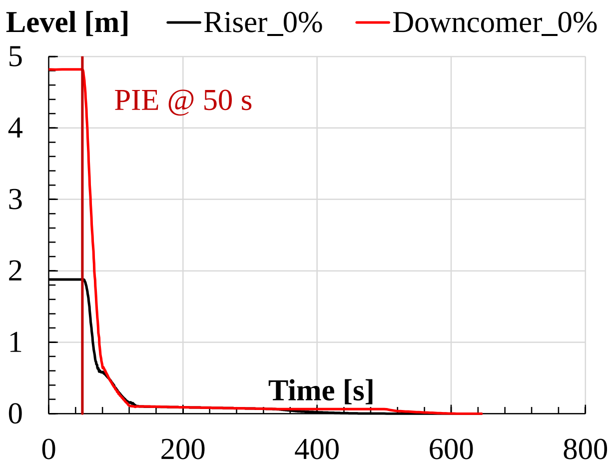

Fig. 114. Riser and downcomer levels during unprotected LOHS scenarios in case 0%

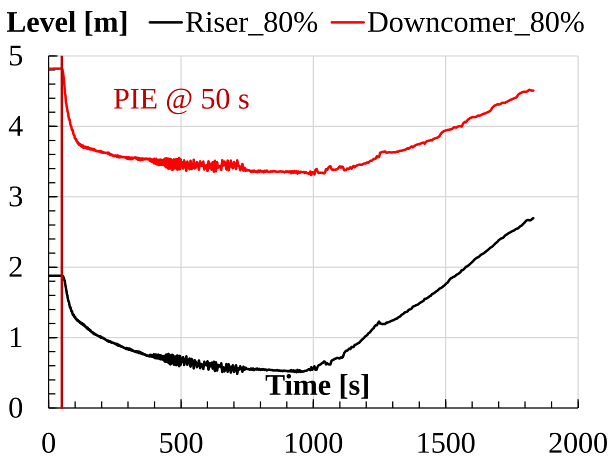

Fig. 115. Riser and downcomer levels during unprotected LOHS scenarios in case 80%

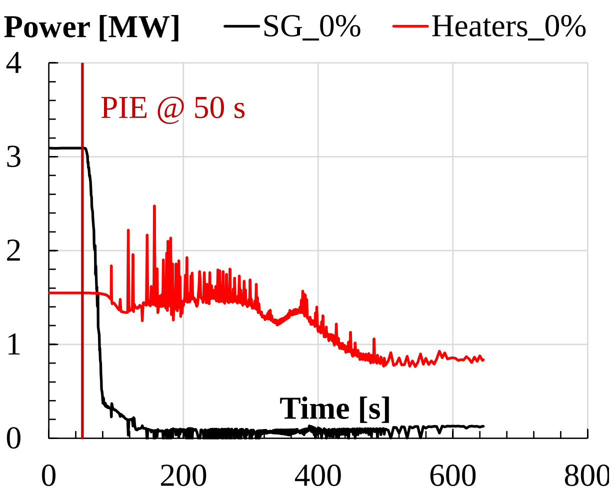

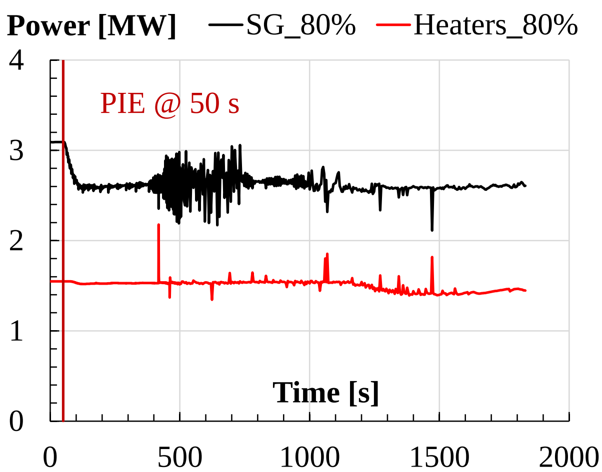

Fig. 116. SG and heaters power during unprotected LOHS scenarios in case 0%

Fig. 117. SG and heaters power during unprotected LOHS scenarios in case 80%

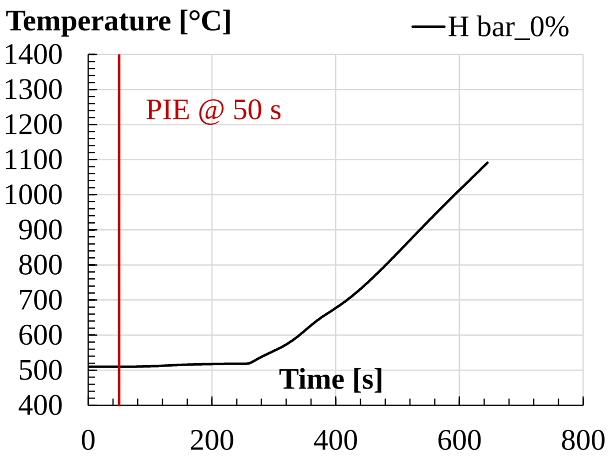

Fig. 118. SG and heaters power during unprotected LOHS scenarios in case 0%

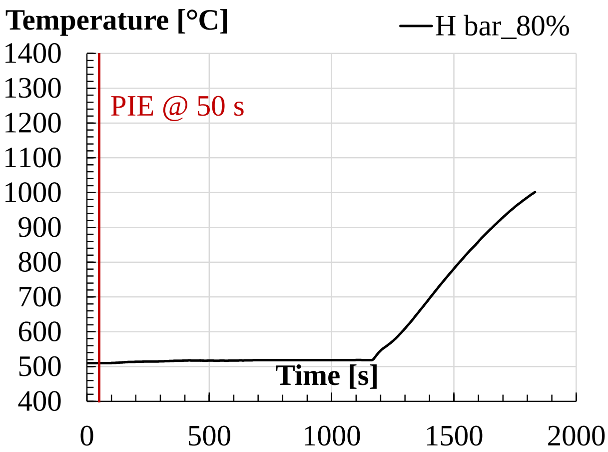

Fig. 119. Heating bar temperature during unprotected LOHS scenarios in case 80%

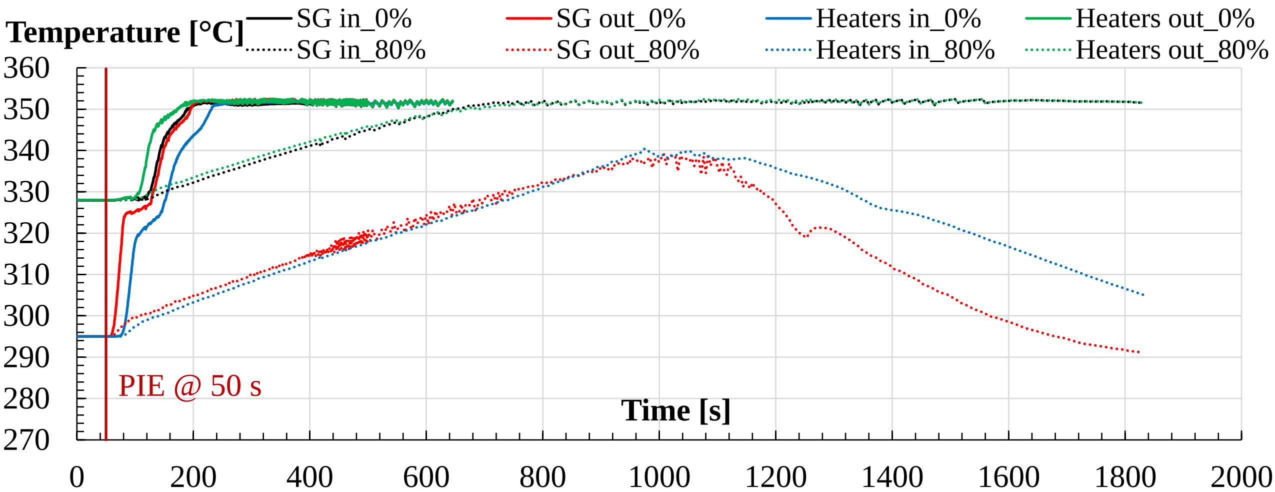

Fig. 120. Primary side temperatures during unprotected LOHS scenarios

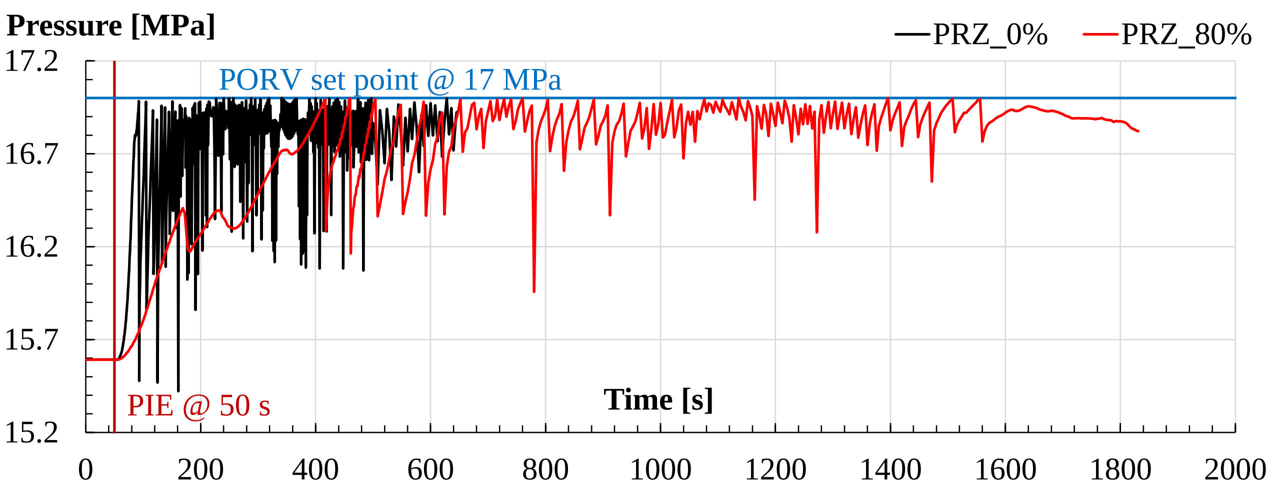

Fig. 121. Pressurizer pressure during unprotected LOHS scenarios

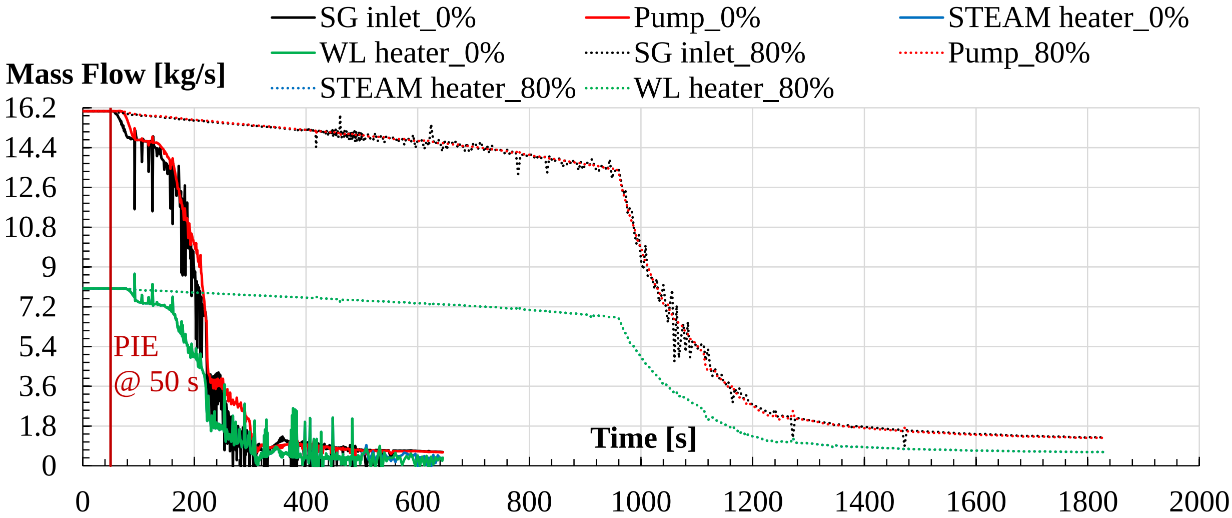

Fig. 122. Primary side mass flow rate during unprotected LOHS scenarios

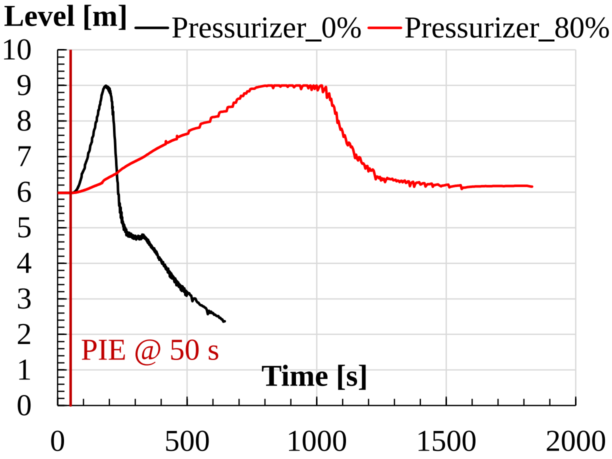

Fig. 123. Pressurizer level during unprotected LOHS scenarios

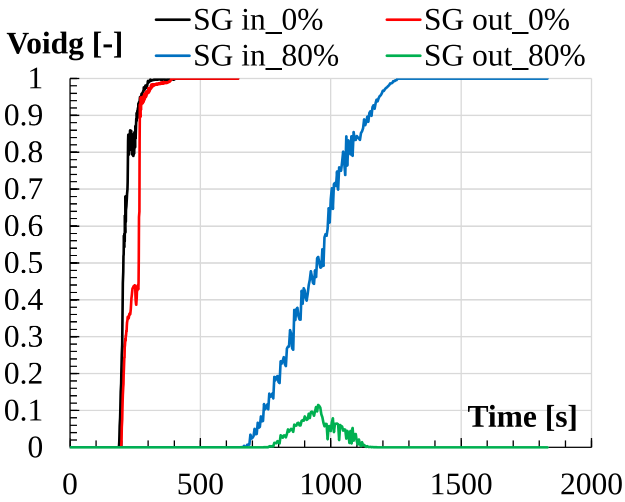

Fig. 124. SG inlet and outlet void fraction during unprotected LOHS scenarios

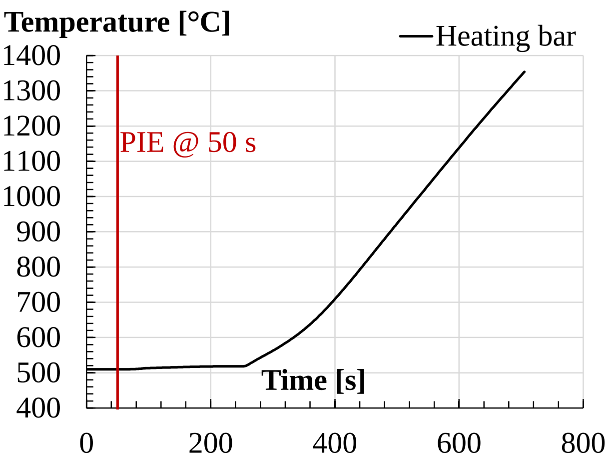

Fig. 125. Heating bar temperature during unprotected LOFA+LOHS scenario

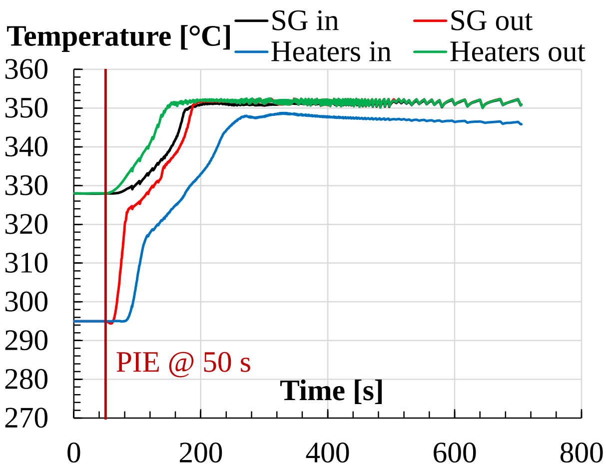

Fig. 126. Primary side temperatures during unprotected LOFA+LOHS scenario

6 WATER LOOP DESIGN AND ANALYSES

The design of the Water Loop facility was originally sized to meticulously reproduce the ITER TBM cooling system [71], respecting the main geometrical parameters such as relative elevation, mass inventories and curves number. It was designed with a nominal power duty of 1 MW. However, Water Loop design was recently distanced from the ITER one, due to modifications on the ITER TBM cooling system, whose design will be finalized after the WL construction. The absence of the previously adopted constraints led to sensitivity analyses performed with the aim of optimizing the design while integrating it into the STEAM one, reducing in such way the redundancy of many components and consequently the costs, without modifying the facilities main features.

This new layout envisions merging the primary loops of both the facilities into the W-HYDRA primary loop (see Sect. 3.1). While the STEAM configuration PS aims at characterizing the Steam Generator (Test Section 1), the WL PS presents flanges to which different Test Sections can be attached. Many of these test sections (i.e, the FW and the TBM) are placed inside a vacuum chamber, where they are exposed to the heat flux produced by an 800 kW-electron-bean gun simulating the plasma generated power. Other test sections (i.e., the BB manifold) are placed outside the vacuum chamber and are foreseen to be operated in isothermal conditions.

6.1 Preliminary analyses in support of the WL design

6.1.1 Initial configuration

Before the merging of WL and STEAM primary loops, WL primary system (red solid line in Fig. 127) was a 15.5 MPa eight-shaped water circuit with a hairpin heat exchanger acting as economizer (HX1) located at the center of the loop. In particular, the fluid purified by a filter was routed by a centrifugal pump towards the economizer for preheating (111-295°C) and then towards an electrical heater for being furtherly heated, if necessary, up to the design temperature of 295°C. At this point the fluid was directed towards the test section. Water returning from the test section (typically at higher temperatures, e.g. 328°C in the case of TBM) passed through two tanks (T1 and T2) designed to replicate the ITER WCS delay tanks, and it was then cooled down to 110 °C by the cold side of the economizer (HX1 shell side), and through another hairpin cooler (HX2) thermally connecting primary and secondary water circuits. The fluid, cooled down to 110 °C, is then redirected towards the pump. The pressurizer (PRZ 1), common with the STEAM facility, was connected to the hot leg between the second delay tank (T2) and the economizer (HX1).

The secondary loop was initially designed to operate at the pressure of 4.0 MPa, with water temperatures ranging from 65 C to 128°C. it was composed of the shell-side of the HX1, a pressurizer, the HX3 and the pump (see blue solid line in Fig. 127).

The tertiary loop, represented by the green solid lines in Fig. 127, served as the ultimate heat sink of the W-HYDRA platform and works at 0.1 MPa. Thermal power was transferred to this loop via the heat exchanger HX3 (30-40°C), and it was subsequently dissipated into the environment through a cooling tower (Tower). Circulation within the loop is ensured by a pump and a regulation valve is envisaged to regulate the mass flow rate. Since the cooling tower was designed to operate with an open cycle, water was going to be continuously integrated with the support of a water treatment system.

6.1.2 WL configuration design and feasibility analysis

The integration of the WL and STEAM primary circuits initially led to a simplified configuration, as depicted in Fig. 128. This configuration involved the elimination of the economizer component in the WL primary loop, an increase in the facility power duty from 1 MW to 3.1 MW, a reduction in the primary side temperature difference from 111-328°C to 295-328°C, the elimination of the delay tanks, and modifications to the secondary and tertiary thermodynamic conditions.

Numerical analyses were conducted on this configuration to assess its feasibility and to size the heat exchangers, focusing on the preliminary design and characterization of the heat exchangers, starting with the P-S HX. The preliminary sizing and characterization were based on design requirements such as comparable velocities on the HXs primary (tube-side) and secondary (shell-side) sides, similar dimensions for P-S and S-T HXs, limited ΔT on the tube sheets to avoid thermal stresses, ensuring that tube external wall temperatures do not exceed the saturation point at the shell-side pressure, and distributing the thermal resistances as evenly as possible among the tube-side, the tubes, and the shell-side.

Regarding geometrical features, several considerations were made. A pitch to outer diameter ratio higher than 1.4 (i.e., P/OD > 1.4) was chosen to avoid manufacturing problems and facilitate assembly, though this limited the secondary fluid velocity and its corresponding heat transfer coefficient, disadvantaging the shell-side compared to the tube-side. Larger tube dimensions (i.e., 5/8”) were preferred over smaller sizes, though less-standard dimensions (i.e., ½” and ¾”) were also considered to compare the effects of this parameter variation on the results. Additionally, it was determined that the tube bundle must have full ranks to avoid side effects.

A compromise was identified in a counter-current (F=1) geometrical bundle equipped with 61 tubes (5/8’’ BWG18) enclosed in a 10” schedule 160 shell. Following a preliminary analytical procedure based on the adoption of the Logarithmic Mean Temperature Difference (LMTD) design approach, the length of the component was calculated and conservatively incremented by the 5%, resulting in a total tube bundle length of 2.6m. The same minimum pipe length was also found for the S-T HX using an identical shell-bundle geometry.

The primary challenge was ensuring that the system could exchange variable amounts of power, depending on the test section being investigated. To address this, calculations were performed with thermal power ranging from 100% to 10% of the nominal value (3100 kW).

To facilitate these calculations, a simple RELAP5 input deck was developed, as shown in Fig. 129. The primary loop model begins with time-dependent volume 116, which sets the fluid inlet temperature. Time-dependent junction 117 fix the fluid mass flow rate, which is directed into pipe 118 that simulates the heat exchanger inlet piping. Valve 119 is responsible for balancing pressure drops and distributing the fluid between the heat exchanger and the bypass line. In the heat exchanger, pipe 120 represents the tube bundle, condensing the flow area of all tubes but maintaining the hydraulic diameter of a single tube. The fluid exits the heat exchanger through single junction 121 into pipe 122, which simulates the outlet piping. Single junction 123 then connects this outlet piping to the outlet time-dependent volume 124, which imposes the outlet pressure. For bypass operations, valve 151 allows part of the mass flow to circumvent the heat exchanger via pipe 152, single junction 153, pipe 154, and single junction 155, which collectively simulate the bypass line.

In the secondary loop, the fluid journey inlet temperature is imposed by time-dependent volume 200. Time-dependent junction 201 sets the mass flow rate as the fluid enters pipe 202, simulating the heat exchanger inlet piping. The fluid then passes through single junction 203 into the heat exchanger shell side, represented by pipe 204. After heat exchange, the fluid exits via single junction 205 into pipe 206, simulating the outlet piping, and finally reaches single junction 207, connecting to the outlet time-dependent volume 208 that imposes the outlet pressure.

The bundle tubes are modeled using an active heat structure (red in Fig. 129) that couples the primary side (pipe 120) to the secondary side (pipe 204) of the heat exchanger. A passive heat structure (grey in Fig. 129) simulates the shell, in contact with ambient air, assumed to have a temperature of 10°C and a heat transfer coefficient of 8 W/mK.

The regulation capability of the P-S HX was investigated by performing a series of RELAP5/Mod3.3 simulations with the aim of characterizing its thermal hydraulic behavior while identifying the range of power variability in which the system parameters are acceptable. In particular, the power decrement is imposed reducing both primary and secondary mass flow rates of the same percentual amount. Furthermore, the primary fluid is partially bypassed by the control system shown in Fig. 130.

The adopted control strategy envisages the installation of an inverter for the pump speed variation and the presence of a HX bypass line for the fluid flowing tube-side. The flow in both the main and the bypass line is regulated thanks to valves that keep a temperature set point at the HX outlet.

The need to bypass part of the mass flow is due to the adoption of a conservative length, capable of guaranteeing the exchange of the required power even in case of plugging or fouling. The bypass is also needed to allow the correct operation of the system at different loads, since the required mass flow rate reduction is not linear with power, due to the heat transfer coefficient variation. The system monitors the temperature resulting from the mixture of the heat exchanger mass flow and the bypassed mass flow.

Simulations main results collected in Tab. 32 show that the percentage of bypassed mass flow rate increases as the power to be exchanged decreases (e.g.., 18% of the total mass flow is bypassed in nominal conditions, while approximately 65% is bypassed at 10% of the nominal power). Tab. 32 also indicates that both primary and secondary side outlet temperatures align with the design specifications.

An important drawback to be underlined is the fluid mixing downstream the HX, due to the significant temperature gradient between the two fluids. This can induce stress that will be considered during the thermo-mechanical analyses. Specifically, the bypass flow is kept at the hot leg temperature (i.e. 328°C), while the temperature of the fluid at the outlet section of the HX drops below the nominal cold leg temperature. Such "subcooling" is inversely proportional to the HX power rating and can reach approximately 106°C at 10% power for the P-S HX (see Tab. 32).

The proposed design and regulation strategy suffers a remarkable weakness due to the high temperatures reached on the pipe bundle surface in the shell side. Specifically, Fig. 131 shows that this temperature is higher than the saturation temperature at the nominal working conditions and can therefore compromise both the heat exchange capabilities and the transient behavior during the power regulation. As a direct result, in fact, the heat transfer regime switches from single phase to subcooled nucleate boiling in proximity of the secondary fluid outlet (Fig. 132). The combined effect of lowering the exchanged power (and therefore reducing the mass flow rates and consequently the fluid velocities) and bypassing an increasing amount of primary fluid, result in a decrement in the primary side heat transfer coefficient that determines the reduction of the wall temperature (Fig. 131) and a delayed passage from single phase to subcooled nucleate boiling heat transfer regime.

To address these issues, several design improvements were considered. These include installing intercoolers in the secondary loop to reduce the logarithmic mean temperature difference in the P-S and S-T HXs, increasing the nominal pressure of the secondary loop to 7.0 MPa to avoid saturation conditions in the P-S HX shell side, and increasing the tertiary loop nominal pressure to 1.0 MPa to avoid saturation conditions in the S-T HX shell side.

These modifications were implemented leading to a new layout, shown in Fig. 19. that foresees the adoption of an 8-shaped secondary circuit with a nominal operating pressure of 7.0 MPa. This configuration adopts an 8-shaped secondary circuit with a nominal operating pressure of 7.0 MPa and is characterized by three heat exchangers: the Primary-Secondary Heat Exchanger (P-S HX), thermally coupling the primary to the secondary side; the Secondary-Tertiary Heat Exchanger (S-T HX), thermally coupling the secondary to the tertiary side; and the Economizer (ECO), which reduces the fluid temperatures within the P-S and S-T HXs.

Desing and sizing activities were then performed to establish the facility power and consequently determine components main dimensions. Specifically, facility powers of 3.1 MW and 0.8MW were investigated.

6.1.3 WL final configuration

A preliminary sizing procedure for 3.1MW of power duty was performed for all the Heat Exchangers, considering various combinations of shells (from 5" to 10" both Sch. 160 and Sch. 80) and tube sizes (½", 5/8" and ¾"). The reference thermal cycle of the facility is shown in Fig. 133. Configurations with tube velocities above 4 m/s or secondary side velocities below 0.9 m/s were discarded. The optimal geometrical configurations of the three HXs are reported in Tab. 33. For the economizer, two optimal configurations are eligible.

The subsequent optimization activities aimed to refine the obtained sizing and address concerns, particularly the economizer length, which posed space constraint issues. To optimize the configuration, sensitivity analyses on the main parameters of the thermal cycle were performed.

The Primary Side thermal cycle is fixed at 328-295°C to emulate the Primary Side of the ITER WCLL TBM, thus no relevant parameters were identified for sensitivity analysis on the PS side.

In contrast, the SS thermal cycle exhibits more variability, allowing for a flexible range of conditions. The ECO length depends on the selected configuration, the sizing power, the overall heat transfer coefficient, and the LMTD, all influenced by the SS mass flow rate and temperature difference. Thus, the key parameters for sensitivity analysis on the SS side are the SS mass flow rate and the temperature difference across the ECO.

The TS thermal cycle is dictated by the operating constraints of the evaporating tower, with a maximum mass flow rate of 94 m^3/h and a maximum inlet temperature of 80°C. To minimize thermal stresses on the S-T HX tube sheet, the TS higher temperature should be kept as high as possible. Consequently, the only variable parameter on the TS side is the mass flow rate, which, with a fixed sizing power of 3.1 MW, uniquely determines the TS lower temperature.

The SS mass flow rate was adjusted while maintaining an outlet temperature of 240°C. This adjustment led to an inlet temperature variation between 200 and 220°C, as determined by the enthalpy balance. As the SS mass flow rate decreased, the temperature difference on the shell-side of the P-S HX increased, along with the tube-side temperature difference in the S-T HX. The combined effect of these trends resulted in an increase in both the P-S and ECO LMTD and a decrease in the S-T HX LMTD (Fig. 134).

Fig. 135 illustrates the impact of the SS mass flow rate on the sizing of the heat exchangers, particularly on the tube lengths. A reduction in SS mass flow rate led to a reduction in the tube length of the P-S HX, as the positive effect of the LMTD increase outweighed the negative effect of the reduced shell-side fluid velocity (and consequently, the heat transfer coefficient). Conversely, the S-T HX tube length increased due to the combined negative effects of both the reduced LMTD and the decreased tube-side fluid velocity. Additionally, there was a significant reduction in the ECO tube length, primarily due to the beneficial impact of the LMTD increase, which more than compensated for the reduction in velocity on both the tube and shell sides.

Being the shell-side characterized by higher flow areas and consequent lower velocities (due to the adoption of easier manufacturable pitches), shell-side velocity analyses were conducted, highlighting potential issues with laminar flow at low velocities (Fig. 136).

Considering a SS MFR of 22.4kg/s and a consequent P-S HX shell-side temperature difference of 210-240°C, the influence of the ECO ΔT on the sizing was investigated, keeping constant its average temperature. This variation determines the reduction of the P-S HX shell-side temperatures (and the consequent P-S HX LMTD increment) as well as the increment of the S-T HX tube-side temperatures (and the correspondent S-T HX LMTD increment). On the contrary, the LMTD of the economizer is decreased.

Therefore, both P-S and S-T HXs sizing is improved (i.e., lower tube lengths in Fig. 137), but their reduction is negligible when compared to the decrement in the ECO reduction: even if its LMTD is reduced, the reduction of the ΔT with fixed MFR determine a reduction of the power to be exchanged by the component reducing its size.

The main drawback of reducing the ECO ΔT is the uneven distribution of thermal stresses, which are concentrated mostly on the other components (i.e., P-S and S-T HXs), thus increasing the temperature difference inside the tubes (Fig. 138).

Finally, the TS mass flow rate primarily affects the S-T HX. An increase in TS mass flow rate decreases the S-T HX shell-side temperature difference and LMTD, but increases the shell-side heat transfer coefficient, resulting in a positive overall effect on tube length.

Safety margins to saturation conditions were maintained in all the simulations.

As a result of the performed sensitivity analyses, an optimization of the thermal cycle was proposed and shown in Fig. 139.

The possibility of downgrading the WL HXs exchangeable power was also investigated to facilitate operations with low-power test sections. Specifically, 800 kW of nominal power was considered, being it the maximum beam gun power (that is never completely transferred to the target due to reflection phenomena that depends on the target material). As a result, any experimental phase characterized by a thermal load higher than 800 kW must be managed in STEAM configuration. Considering the thermal cycle of Fig. 139, the results of the HXs sizing at 800 kW are listed in Tab. 34

6.2 Regulation strategies

The versatility required from the WL facility, in terms of both power dissipation and temperature management, necessitates the implementation of various regulation strategies.

6.2.1 HXs tube-side bypass

Heat exchangers regulation should be performed by scaling fluid mass flow rates in proportion to the desired power. However, with a fixed geometry, the relationship between power and mass flow rate is non-linear. This non-linearity arises because the heat transfer coefficient decreases as fluid velocity decreases in both primary and secondary circuits.

To account for this nonlinearity, the mass flow rate must be adjusted due to the effects that influence nominal flow rates. These effects include power reduction, conservative design considerations, and HTC reduction:

Power reduction means that the mass flow rate should be adjusted proportionally to the reduction in power, ensuring a consistent scaling factor. Additionally, conservative design considerations suggest that having extended heat exchanger lengths by 5% increases the exchange area, allowing the system to handle more power at the same mass flow rate. Finally, HTC reduction due to lower fluid velocities further complicates the relationship between power output and mass flow rate.

The proposed regulation strategy incorporates two control mechanisms to compensate for these effects. The first mechanism is pump speed regulation via an inverter, which maintains the same scaling factor for both power and mass flow rates. The second mechanism is the implementation of a tube-side bypass line, which selectively diverts a portion of the total mass flow, thereby regulating the mixing outlet temperature and effectively managing the mass flow rate through the heat exchanger.

The installation of the bypass on the tube side is based on two key considerations. Firstly, the tube side generally exhibits lower thermal resistance. Reducing the mass flow here leads to a significant decrease in velocity and an increase in thermal resistance compared to the shell side. Furthermore, for heat exchangers where the shell side carries the cold fluid, installing the bypass there could reduce the mass flow excessively, risking fluid overheating and potential saturation. Conversely, reducing mass flow on the tube side, which typically handles the hot fluid, leads to overcooling without causing steam formation. For economizers (ECOs) where the shell side is traversed by hot fluid, design considerations ensure that saturation does not occur.

6.2.2 Total bypass of the Economizer

The second regulation strategy involves fully bypassing the mass flow rate to the tube-side of the Economizer (ECO). This approach is applied to scenarios with thermal cycles differing from the reference cycle, particularly when primary side temperatures are below 328-295 °C.

When the primary loop temperature is reduced, the minimum tertiary loop temperature, limited by the cooling tower and slightly above ambient, narrows the temperature gap between the primary and tertiary loops. This narrowing reduces the Logarithmic Mean Temperature Differences (LMTD) in the P-S HX, ECO, and S-T HX, thereby decreasing the performance of these components. The lower the primary loop temperatures, the more the HX performance deteriorates, leading to a reduction in the power the system can handle using the tube-side bypass regulation.

To manage higher power levels, an alternative strategy is required, which includes several key solutions. The first is the complete tube-side bypass of the ECO. By entirely bypassing the ECO, the temperature gap is redistributed over only two heat exchangers instead of three, thereby increasing the LMTD for the P-S HX and S-T HX and enhancing their performance.

Secondly, bypass lines not used and mass flow rate scaling is non-linear. To further enhance the power exchange capabilities of the P-S HX and S-T HX, the bypass lines are not utilized, and the mass flow rates in the three loops are not scaled linearly with power. Unlike the previous regulation strategy, the proportionality between power and pump mass flow rates is not maintained for applications with the reference thermal cycle. Instead, the mass flow rates are set arbitrarily, within system limits, to increase the velocity on the tube and shell sides of the HXs, thereby improving the overall heat transfer coefficient.

Lastly, a test section bypass line is installed for cases where the loop mass flow rate exceeds the scaled value. Equipped with a regulation valve, this bypass line ensures that only the scaled mass flow enters the test section. By diverting excess flow, the bypass line helps maintain the correct temperature and velocity fields within the test section, preserving the accuracy and reliability of the experiment.

6.2.3 Total bypass of the WL secondary side

The third regulation strategy involves the complete exclusion of the secondary loop by directly connecting the tertiary loop to the P-S HX shell. This method is employed for scenarios with thermal cycles that significantly deviate from the reference cycle, with primary side temperatures much lower than 328-295 °C, when a full ECO bypass is inadequate for proper system operation.

As with the previous strategies, lowering the primary loop temperature while maintaining the tertiary loop temperature slightly above ambient—set by the cooling tower—narrows the temperature gap between the primary and tertiary loops. This narrowing affects the performance of the P-S HX, ECO, and S-T HX by reducing their Logarithmic Mean Temperature Difference (LMTD), thereby decreasing their overall efficiency. As primary loop temperatures decrease, the effectiveness of the heat exchangers declines, limiting the system's capacity to discharge power. When the required primary circuit temperatures fall substantially below the reference temperatures and the power to be dissipated exceeds the capacity of the previously mentioned strategies, a new approach must be implemented.

In this scenario, blind flanges are installed on the secondary loop, both upstream and downstream of the P-S HX. These blind flanges are then connected to the tertiary loop downstream and upstream of the cooling tower, respectively. This configuration is feasible because the secondary loop design pressure is higher than the tertiary loop operating pressure, so it does not pose any structural issues.

Additionally, the bypass line for the P-S HX tube is not utilized. Instead, the mass flow rates of the primary and tertiary loops are adjusted according to system limits to increase the velocities on both the tube and shell sides of the P-S HX, which is now configured as the P-T HX. This adjustment aims to improve the overall heat transfer coefficient.

Finally, a test section bypass line equipped with a regulation valve is installed for scenarios where the loop mass flow rate exceeds the scaled value. This setup ensures that only the scaled mass flow enters the test section, thereby maintaining the correct temperature and velocity fields within it.

The system configuration for the primary loop remains the same as in the ECO full bypass scenario, while the secondary loop is completely bypassed except for the P-S HX shell side.

6.2.4 Regulation strategy in the Manifold configuration

The manifold operates with a mass flow rate of 16 kg/s, significantly higher than the nominal mass flow rate of the Water Loop facility, which is 4.14 kg/s at 800 kW. The WL components, particularly the heat exchanger, are designed for the nominal flow rate of 4.14 kg/s. Exceeding this rate would result in excessive velocities and pressure drops, potentially causing system inefficiencies and damage. To accommodate the higher flow rate in the manifold configuration, the WL heat exchanger is bypassed, and the loop is instead closed using the STEAM facility Steam Generator, which is designed to handle up to 20 kg/s.

The steam generator tubes are designed to withstand a nominal pressure difference of approximately 91 bar (with 155 bar on the primary side and 64 bar on the secondary side). This specification necessitates that the pressure in the secondary loop cannot be reduced without compromising the structural integrity of the tubes, requiring the STEAM secondary loop to be filled with pressurized water.

In this configuration, the primary and secondary sides exchange power based on the set temperature difference. This exchanged power must be replenished by the PS electrical heaters. The regulation of this process involves varying the heater power based on the temperature measured at the heater outlet, which must be maintained at the value required by the test section.

6.2.5 HXs regulation at different power levels

HXs regulations at different power levels were therefore performed analyzing test sections of Tab. 7, distinguishing the regulation strategy based on the primary thermal cycle. The regulation with the reference thermal cycle was analyzed for both 3.1MW and 800kW of facility power size, allowing the selection of the most suitable option.

Primary thermal cycle 295-328°C (TS 1 to TS 5)

The WL capability to operate at various power levels with the DEMO primary side reference thermal cycle (i.e., 295-328°C) was assessed, focusing on the versatility of the loops concerning exchanged power. The investigation included examining flow regimes to evaluate the loop performance and delineate the operational range. For both facility size (3.1 MW and 800 kW), power levels were varied from 100% down to 1%, identifying the corresponding flow regimes adopting the HXs tube-side regulation strategy described in Sect. 6.2.1. Additionally, the heat exchangers (HXs) were tested under the specific power conditions of the test section operating with this thermal cycle (i.e., equatorial and non-equatorial FW and TBM), aiming to identify the flow regimes under these operational conditions.

Regimes were categorized as turbulent (Re > 10,000), transitional (1,000 < Re < 10,000), and laminar (Re < 1,000). The onset of the different regimes was associated with both the percentage of power and the percentage of tube-side mass flow rate at which they occur. In fact, due to the reduction of tube-side mass flow rate by the bypass line, the mass flow rate percentage at which transitions occur is lower than the corresponding power percentage (i.e., the mass flow rate decreases proportionally more than the power).

The repartition of the mass flow among the main and the bypass line is shown in Fig. 140, Fig. 141 and Fig. 142 for the HXs designed for 3.1MW. The three HXs exhibit similar behavior, increasing the bypass mass flow while decreasing the total mass flow rate. At approximately 60% of power, the trends inverts and bypass mfr decreases accordingly with the total one. Tab. 35 shows that the mixing temperature between the bypass and the main flow rises as the total mass flow reduces, making it mandatory the installation of a reinforced joint capable of withstanding the thermal stress.

Tab. 36 summarizes the results for the HXs designed for 3.1 MW. The S-T HX consistently exhibits the least favorable regulation capabilities. P-S and ECO shell-side performance are also suboptimal due to the onset of the transition flow regime at non-negligible power values.

Tab. 37 specifies the operative flow regimes of the main test sections. It shows that the TBM, requiring high operational power, results in fully turbulent flow on both sides of the HXs. In contrast, the S-T HX under the equatorial and non-equatorial conditions exhibits transition regime on both sides.

These observations indicate that while the system can operate across a wide range of power levels, certain components like the S-T HX present challenges in maintaining efficient regulation, especially as flow conditions shift from turbulent to transitional. For this reason, the power downgrade was considered.

The 800 kW facility was introduced to reduce component sizing and enhance regulation performance. Mass flow rate distributions are illustrated in Fig. 143, Fig. 144 and Fig. 145 for all the HXs. Mixing temperature differences are highlighted in Tab. 38. The onset of transition and laminar regimes for this smaller facility size is detailed in Tab. 39. Compared to the 3.1 MW setup, the percentage values for power and mass flow rates at which these regimes occur are generally higher but are relatively smaller in absolute terms due to the lower nominal power. The S-T HX remains the limiting component in terms of regulation capability.

The regulation capabilities under test section conditions for the 800 kW facility are shown in Tab. 40. The TBM test section, operating at 90% of the facility nominal power (722 kW), ensured fully turbulent conditions across all HXs. The equatorial and non-equatorial first wall test sections, operating at lower powers (see Tab. 7), exhibit a fully turbulent regime in all HXs as well, marking an improvement over the 3.1 MW facility.

The 800 kW facility design was therefore selected as reference, since it offers superior regulation capabilities, and allows for precise control even at lower power levels, optimizing the overall performances.

Primary thermal cycle 130-149.9°C (TS 6 and TS 6 bis)

The feasibility study for integrating different test sections into the WL facility began with the adoption of a thermal cycle characterized by a pressure of 7 MPa and temperature ranging from 130°C to 149.9°C. Additionally, power levels of 400 kW and 500 kW were considered for this test section.

The significant reduction in primary loop temperatures, combined with the relatively high-power levels, would preclude the use of the HXs tube-side bypass regulation strategy due to the deterioration of HX performance caused by the contraction in the primary to tertiary loop temperature difference. Therefore, a complete bypass of the Economizer, as described in Section 6.2.2, is required. This approach involves a dedicated bypass line for the Eco tube-side, which increases the P-S HX and S-T HX log mean temperature differences (LMTDs) and raises mass flow rates to ensure higher heat transfer coefficients in the HXs.

The optimization of these configurations was conducted based on several considerations. The tertiary loop temperatures were set slightly above ambient temperature provided by the cooling tower. With an ambient temperature of 15°C, minimum tertiary loop temperatures of 30°C and 35°C were chosen for the 400 kW and 500 kW DEMO DIV test sections, respectively, with a lower temperature for the higher power to enhance the LMTD. The primary loop mass flow rate was adjusted according to the requirements of the test sections for each configuration, considering the temperature difference of 130-149.9°C and power levels of 400 kW and 500 kW. The secondary and tertiary loop mass flow rates were adjusted to ensure that the P-S HX and S-T HX exchanged the required power, aiming for comparable percentage increments relative to the reference case.

The thermal cycles resulting from this optimization process are shown in Fig. 146 and Fig. 147 for test section powers of 400 kW and 500 kW, respectively. Tab. 41 compares the mass flow rates and pressures between TS 6 (and 6 bis) operation with nominal operation (at 800 kW).

Primary thermal cycle 60-80°C (TS 7 to TS 15)
Two potential regulation strategies were considered for very low primary loop temperatures: the total bypass of the economizer (Sect. 6.2.2) and the total bypass of the secondary loop (Sect. 6.2.3). Both strategies were evaluated to determine the optimal configuration for each considered power value.

Regarding the total economizer bypass, the influence of the independent variation of each loop mass flow rate was investigated at first, then the best achievable conditions were assessed based on the maximum velocity to be reached within the loop piping. Results were expressed in terms of tertiary side thermal cycle (i.e., S-T bundle inlet and outlet temperatures): being the power source at low temperature, the feasibility of the whole system lies in maintaining appreciable LMTD between the loops, keeping a tertiary loop maximum temperature higher than the ambient air temperature.

Increasing all the loops mass flow rates determines a positive effect on the tertiary side thermal cycle. Specifically, the secondary side mass flow rate is the parameter that mostly influences the system performances, as it increases the overall heat transfer coefficient of both the P-S HX and S-T HX. However, the positive effect of the increase in the mass flow rates suffers a saturation process, diminishing in efficiency as mass flow rates continue to rise.

The best performance achievable with this regulation strategy was therefore found increasing the loops mass flow rates until a maximum velocity of 4 m/s is obtained (further increase would determine excessive pressure drops). These limits were established based on the maximum velocities observed in the three loops. Specifically, the highest velocities were recorded in the tubes of the P-S HX and S-T HX on the primary and secondary sides, respectively. In the tertiary loop, the greatest velocity was noted within the piping.

While the test section thermal cycle, mass flow rate and pressure drops are preserved, the HXs work with higher mass flow rates and different thermal cycle, with the restraint of keeping the primary loop minimum temperature consistent with the test section inlet one. The test section outlet temperature (i.e., P-S HX inlet temperature) is determined by the mixing of the test section mfr and the bypass mfr.

Results of the analysis are detailed in Tab. 42 and show that the loops mass flow rates are generally consistent across different test sections, as they are primarily determined by the set velocities. Minor variations observed are due to changes in temperature, which affect the density of the fluid.

Additionally, the mock-ups share the same thermal cycle but operate at different power levels. As a result, the distribution of the primary side mass flow rate between the test section and its bypass varies, affecting the mixing temperature. At higher power levels, the bypassed mass flow rate decreases, resulting in a higher mixing temperature.

Furthermore, as the test section power increases, maintaining a constant velocity (and thus a constant overall heat transfer coefficient for the heat exchangers) leads to higher logarithmic mean temperature differences in the heat exchangers. This results in lower temperatures on the tertiary side.

As a result, no thermal cycle compatible with the cooling tower requirements was found for TS 15 due to its high-power output. Furthermore, considering a preliminary minimum tertiary temperature of 25°C to ensure the proper operation of the cooling tower, the table indicates that this regulation strategy can be applied only for the TS 7, TS 8, and TS 10.

The total bypass of the economizer, therefore, proved to be nonsufficient as a regulation strategy to guarantee the operation of all the test sections from 7 to 15. For this reason, the total bypass of the secondary loop was considered to eliminate the interposition of a loop between the primary side (containing the heat source) and tertiary side (containing the heat sink). According to this strategy, the primary and tertiary side mass flow rates are the independent variables that uniquely determine the tertiary side thermal cycle; thus, the system has two degrees of freedom.

To investigate the performance of this configuration, two different approaches were followed. The first approach involved setting a maximum velocity of 4 m/s in both loops and obtaining the tertiary loop thermal cycle. The second approach required imposing a minimum tertiary side temperature of 25°C and evaluating the velocity value (equal for both loops) that meets this condition.

Results of the total bypass of the secondary loop and maximum velocity of 4 m/s in the primary and tertiary sides are collected in Tab. 43. Comparing the results from the total bypass of the secondary loop (Tab. 43) and the economizer bypass (Tab. 42) under the same maximum velocity shows that excluding the secondary loop leads to a significant increase in tertiary loop temperatures, thereby justifying the use of this configuration. Considering a minimum tertiary side temperature of 25°C, this approach is viable for all mock-ups except the TS 15, which has the highest power.

The second approach involves setting 25°C as tertiary side lower temperature to determine the corresponding system configuration for each test section. Given that the system has two degrees of freedom (namely, the primary and tertiary mass flow rates), the same maximum velocity in both loops was maintained as second constraint, to ensure uniform stress distribution. Tab. 44 indicates that achieving a higher tertiary side temperature at constant power requires higher velocities, and consequently, higher mass flow rates. Moreover, at a fixed minimum tertiary temperature, the velocities increase with rising power levels. For a minimum temperature of 25°C, the required velocities remain below 3 m/s for all test sections, except for the TS 15, which requires a maximum velocity of 4.63 m/s in both loops.

6.3 RELAP5/Mod3.3 model of the Water Loop facility

RELAP5 mono-dimensional nodalization of all the three loops was performed, allowing for the thermal-hydraulic analysis of the whole facility. Sensitivity analysis on the time step was performed, varying the maximum time step from $5\cdot10^{-4}$ and $5\cdot10^{-3}$. Since no variations were detected in the results, the maximum time step was adopted.

6.3.1 Primary loop

Hydraulic components

The RELAP5/Mod3.3 nodalization of the W-HYDRA primary loop is shown in Fig. 33. The fluid path in the WL configuration is presented below. Gray-marked components refer to part of the loops that are closedduring the WL operation.

- WL test section (i.e., power source)
    - Pipe 187 simulates the test section

- WL hot leg:
    - Components from 188 to 193 reproduce the section of the loop that connects the test section to the branch where the reunification of the WL test section line and its bypass rejoin. Component 192 is the manual valve that intercepts the test section hot side: it is closed in STEAM operation and opened in WL configuration.
    - In branch 194, the WL test section line and its bypass line reconnect.
    - Pipe 195, branch 196 and pipe 197 reproduce the section of the loop that can be considered hot leg for both STEAM and WL.
    - In branch 198 the bifurcation between the steam generator line and the WL heat exchanger is placed.
    - Components from 100 to 108 are not involved in WL operation. Valves 102 and 107 are closed.
    - Components from 109 to 111 reproduce the WL HX line upstream the bypass bifurcation. Valve 110 is the WL HX hot side manual valve. It is opened in WL configuration and closed if STEAM is operating.

- In branch 112 the bifurcation between the HX main line and the HX bypass is realized.
- Components from 113 to 115 are the main HX line hot side. Manual valve 114 is opened in WL configuration and closed in STEAM operation.

➢ WL HX:
- Branch 116 is the inlet nozzle.
- Pipe 117 simulates the HX tube bundle.
- Branch 118 reproduces the HX outlet nozzle.

➢ WL HX bypass line:
- Components from 120 to 122 simulate the HX bypass line. Valve 121 allows fluid regulation during WL operation. It is always closed in STEAM configuration.

➢ WL cold leg:
- Pipe 119 reproduces the main WL HX line cold side.
- Branch 123 is where the HX main line and the HX bypass line reconnect.
- Components from 124 to 126 simulate the part of the loop connecting the WL HX line to the main cold leg.
- Branch 127 is the point where the WL and the STEAM cold leg rejoin.
- Pipe 128, branch 129 and pipe 130 reproduce the part of the cold leg upstream the filter, common to both loops.
- Branch 131 stands for the filter.
- Pipe 132 simulate the part of the cold leg downstream the filter and upstream the pumps bifurcation branch, common to both the configurations.
- Branch 133 is the bifurcation branch, where the cold leg splits into two parallel pipes reaching the two pumps.
- Components from 134 to 140 are not involved in WL operation. Valves 135 and 139 are closed.
- Components 141 to 147 simulate the low-mass flow pump line. Component 144 simulates the high-mass flow rate pump. Valves 142 and 144 represent the manual valve for the interception of this loop: they are opened for mass flow rates lower than 5 kg/s and closed for mass flow rates within 5 and 20 kg/s. They are both closed in STEAM configuration,
- In branch 148, the reconnection of the pump lines occurs.
- Pipe 149, branch 150 and pipe 151 stand for the part of the cold leg downstream the pump lines connection and the heater lines bifurcation.
- Branch 152 simulates the bifurcation point for the two parallel small cold lines.
- Components from 153 to 163 are not involved in WL operation. Valves 155 and 161 are closed.
- Components from 164 to 174 represent the WL heater line. Valves 166 and 172 are the manual valves for the heater interception. They are open in both STEAM and WL operations. Pipe 169 is the STEAM electric heater, that in WL configuration is only used to compensate for the heat losses.
- In branch 175, the reconnection of the heater lines is realized.
- Pipe 176 constitute the section of the loop that connects the heater lines with the branch where the bifurcation between the WL test section line and its bypass line (that would be part of the STEAM hot leg) are placed.
- Branch 177 realize the bifurcation between the WL test section and its bypass line.
- Components from 178 to 180 are not involved in WL operation. Specifically, valve 179 is closed.
- Components from 181 to 186 reproduce the section of the loop that connects the bifurcation branch for the WL TS line and its bypass to the test section itself. Component 182 is the manual valve that

intercepts the test section cold side: it is closed in STEAM operation and opened in WL configuration.

- Surge line
  - Branch 601, pipe 602 and branch 603 simulate the surge line;

- Spray line
  - Components from 6015 to 619 represent the part of the spray line connected to the cold leg;
  - Component 620 is the spray valve;
  - Pipe 621 and branch 622 simulate the part of the steam line from the spray valve to the upper part of the pressurizer;

- Pressurizer
  - Pipe 605 and pipe 607, connected by multiple junction 606 realize the pressurizer.

- Pressurizer safety valves
  - Component 610 is the PORV (Pressure Operating Relief Valve);
  - Component 612 is the SRV (Safety Relief Valve);
  - Time-dependent volumes 613 and 611 simulate the draining tank where the steam is discharged in case of PORV and SRV opening.

Heat structures

Heat exchanges within the simulated systems and between these systems and the surrounding environment were modeled using heat structures (HS). These heat structures, as illustrated in Fig. 37, are categorized into three types.

Active heat structures are those where power is generated. This category includes the test section walls exposed to the EBG heat flux (HS 187-1), the WL electric heater (HS 169-1), and the pressurizer heaters (HS 607-5).

Coupling heat structures facilitate the thermal coupling of different systems and components. For instance, HS 117-1 models the Inconel tubes within the P-S HX, enabling the coupling of the WL primary circuit with the secondary or tertiary loop, depending on the test section configuration.

Insulated heat structures encompass all other HS that are directly connected to the external environment. The external environment is considered at 10 °C with a heat transfer coefficient (HTC) of 8 W/m^2K for calculating heat losses.

Control systems

The implemented nodalization includes control systems that operate based on the acquisition of key parameters. The sensors referenced in this section are depicted in Fig. 12. The controllers operate according to the scheme shown in Fig. 35. The Water Loop heat exchangers regulation valves, however, follow distinct control logics. Specifically, the valves installed on the HXs main lines adhere to the control scheme in Fig. 148, while those on the HXs bypass line follow the scheme in Fig. 149.

Pump Velocity Control System

The Pump Velocity Control System employs a proportional-integral (P-I) controller to maintain the nominal mass flow rate, which is directly related to the pump velocity. The measured variable is the pump mass flow rate, recorded by the flow meter MF-WCP-001 (Fig. 12). The set point is the nominal mass flow value, which varies depending on the test section being examined. The error is the difference between the set point and the measured variable. The regulated variable is the pump velocity, measured in revolutions per minute (rpm). If the mass flow rate measured by the sensor exceeds the set point (resulting in a negative error), the pump velocity is reduced, thereby decreasing the mass flow rate.

<u>Electric Heater Power Control System</u>
The Electric Heater Power Control System regulates the WL heater (HT-WHP-001) to compensate for heat losses downstream of the test section until the electric heater. The measured variable is the temperature at the electric heater outlet, recorded by TC-WHP-020 (Fig. 12). The set point is the nominal test section inlet temperature, which depends on the test section being studied (refer to Tab. 7). The error is the difference between the set point and the measured temperature. The regulated variable is the heater power provided to HS 169-1 (Fig. 34).

<u>Pressurizer Heater Power Control System</u>
The Pressurizer Heater Power Control System is designed to prevent system depressurization by regulating the power of the electrical heaters in the pressurizer. The measured variable is the pressure at the pressurizer top, with a set point of 15.0 MPa. The error is the difference between the measured pressure and the set point. The regulated variable is the pressurizer heater power provided to HS 607-5 (Fig. 34). This system uses a general table to associate pressure differences with power values. A smaller error results in higher power supplied to the electrical heater. A null error, however, does not result in zero power, as heat losses must be compensated

<u>P-S HX Main Valve Control System</u>
The P-S HX Main Valve Control System adjusts the P-S HX main valve area based on a split range regulation strategy, implemented in the RELAP5 model according to the scheme in Fig. 148. The control system responds to the output of the power calculation, which uses the mass flow rate measured by MF-WCP-001 and the test section inlet and outlet temperatures obtained with TC-WHP-030 and TC-WHP-040. If the power exceeds 60% of the nominal value (i.e., power > 480 kW), the valve is fully opened. Conversely, when the power is less than 60% (i.e., power < 480 kW), the valve area is regulated by a P-I controller. In this range, if the measured mixing temperature between the main line and the bypass line is lower than the set point, the mass flow rate in the heat exchanger is overcooled. To increase the mixing temperature, the main valve area is reduced to allow a higher mass flow through the bypass line, which is hotter.

<u>P-S HX Bypass Valve Control System</u>
The P-S HX Bypass Valve Control System operates based on a similar split range regulation strategy with inverted power ranges (refer to Fig. 149). When the power is below 60% of the nominal value (i.e., power < 480 kW), the bypass valve is fully opened. When the power exceeds 60% (i.e., power > 480 kW), a P-I control system regulates the flow area, following the same logic as the main valve (i.e., using the same measured variable and set point). Specifically, if the measured mixing temperature is lower than the set point, the bypass flow area increases to allow higher mass flow through the hotter branch.

6.3.2 Secondary loop

Hydraulic components

The RELAP5/Mod3.3 nodalization of the 8-shaped Water Loop secondary circuit is shown in Fig. 150 and it is mainly composed of:

- P-S HX cold leg (i.e., the part of the loop downstream the ECO tube side and upstream the P-S HX shell side):
  - Pipe 445, branch 453, pipe 454, branch 458 and pipe 459 constitute the S-T HX cold leg. Specifically, branch 453 is where the ECO bypass line joins the main line, while branch 458 is where the reunification of the ECO total bypass line and the main line occur.

- P-S HX shell-side:
  - Branch 403 is the P-S HX shell-side inlet nozzle;

- Pipe 404 simulates the P-S HX shell side, composed of two passages;
- Branch 405 reproduces the P-S HX shell-side outlet nozzle;

➢ P-S HX hot leg (i.e., the section of the loop downstream the P-S HX tube side and upstream the ECO shell side):
  - Pipe 406, branch 407 and pipe 408 constitute the hot leg of the P-S HX;

➢ ECO shell side:
  - Branch 409 is the ECO shell side inlet nozzle;
  - Pipe 410 replicates the economizer shell, composed of four passages;
  - Branch 411 simulates the ECO shell side outlet nozzle;

➢ S-T HX hot leg (i.e., the part of the loop downstream the ECO shell side and upstream the S-T HX tube side):
  - Components from 412 to 418 reproduce the S-T HX hot leg. Specifically, in branch 413 the bifurcation between the S-T HX main line and the corresponding bypass line is realized.

➢ S-T HX tube side:
  - Branch 419 is the S-T HX tube side inlet nozzle;
  - Pipe 420 replicates the S-T HX tube bundle, composed of two passages;
  - Branch 421 simulates the S-T HX tube side outlet nozzle;

➢ S-T HX bypass line:
  - Components from 423 to 427 constitute the S-T HX tube side bypass line. Specifically, component 423 is a check valve, while component 426 is a regulation valve;

➢ S-T HX cold leg (i.e., the part of the loop downstream the S-T HX tube side and upstream the ECO tube side):
  - Pipe 422, branch 428 and pipe 429 reproduce the section of the loop downstream the S-T HX and upstream the filter;
  - Branch 430 is the filter;
  - Pipe 431 is the part of the loop from the filter to the pump;
  - Component 432 simulate the pump;
  - Components from 433 to 441 replicate the part of the circuit downstream the pump and upstream the ECO tube side. Specifically, ECO tube side main line and the bypass lines bifurcate in correspondence of branch 436.

➢ ECO tube side:
  - Branch 442 is the ECO tube side inlet nozzle;
  - Pipe 443 replicates the ECO tube bundle, composed of two passages;
  - Branch 444 simulates the ECO shell side outlet nozzle;

➢ ECO bypass lines:
  - Pipe 446 constitutes the part of the bypass line common to both the total and the regulation bypass;
  - Branch 447 is where the bifurcation between the total and the regulation bypass occur;
  - Components from 448 to 452 realize the regulation bypass. Specifically, component 449 is a check valve, while component 451 is a regulation valve.

- Components from 455 to 457 reproduce the total bypass line. Specifically, component 456 is a manual valve.

➢ Surge line
- Components from 465 to 467 simulate the surge line. Component 466 is the manual valve that allows the pressurizer interception for eventual low-pressure operations of the loop;

➢ Spray line
- Components from 476 to 478 represent the part of the spray line connected to the colder leg of the loop (i.e., the piping connecting the S-T HX tube side and the ECO tube side);
- Component 479 is the spray valve;
- Pipe 480 and branch 481 simulate the part of the spray line from the spray valve to the upper part of the pressurizer;

➢ Pressurizer
- Pipe 468 and pipe 470, connected by multiple junction 469 realize the pressurizer.

➢ Pressurizer safety valves
- Component 472 is the PORV (Pressure Operating Relief Valve);
- Component 474 is the SRV (Safety Relief Valve);
- Time-dependent volumes 473 and 475 simulate the draining tank where the steam is discharged in case of PORV and SRV opening.

Heat structures
Heat exchanges involving the WL secondary loop were simulated using specific heat structures, as illustrated in Fig. 151. These structures are divided into three categories.

<u>Active heat structure</u> includes the pressurizer heaters (HS 470-5), which are the only power source for the WL secondary side.

<u>Coupling heat structures</u> enable thermal interaction between different systems. The WL secondary loop is thermally coupled with the primary side through the P-S HX (HS 117-0) and with the tertiary side via the S-T HX (HS 420-0). Additionally, a heat structure (HS 433-1) facilitates thermal coupling between the hottest and coldest legs of the loop through the economizer.

<u>Insulated heat structures</u> encompass all other heat structures connected to the external environment. This environment is simulated with a temperature of 10°C and a heat transfer coefficient (HTC) of 8 W/m²K.

Control systems
Secondary loop is equipped with control systems that rely on data acquisition from various sensors. The names of the sensors referred to in this section are shown in Fig. 16. Pump and pressurizer control scheme follows the logic illustrated in Fig. 35, while the HXs regulation valves follows Fig. 148 if installed on the main line or Fig. 149 if placed on the bypass line.

<u>Pump Velocity Control System</u>
Secondary loop mass flow rate is maintained by a PI controller regulating the pump speed according to Fig. 35. he measured variable is the pump mass flow rate, recorded by the flow meter FM-WCS-001 (Fig. 16). The set point is the nominal mass flow value, which depends on the test section being. The error is the difference between the set point and the measured variable, while the regulated variable is the pump velocity

(rpm). If the measured mass flow rate exceeds the set point (negative error), the pump velocity is reduced to decrease the mass flow rate.

Pressurizer Heater Power Control System

The pressurizer heaters are regulated to prevent system depressurization. The control system uses a PI controller that adjusts the heater power based on the pressure at the pressurizer top. The measured variable is this pressure, and the set point is 7.0 MPa. The error is the difference between the measured pressure and the set point, while the regulated variable is the pressurizer heater power, provided to HS 407-5 (Fig. 151). The control system uses a general table to correlate pressure differences with power values, with higher power supplied for smaller errors.

ECO HX main valve Control System

The economizer main valve, WP-WCS-R01 in Fig. 15, is installed on the HX tube side and it works according to a split range regulation strategy whose implementation in the RELAP5 code follows the scheme of Fig. 148. The control system calculates the primary loop power using the mass flow rate measured by the MF-WCP-001 flow meter and the TS inlet and outlet temperatures obtained with TC-WHP-030 and TC-WHP-040. If power is higher than 60% of the nominal value (i.e., power > 480kW), the valve is fully opened. In the opposite case (i.e., power < 480kW), the valve area is regulated by a P-I controller based on the mixing temperature between the main line and the bypass line, measured by TC-WHS-060 (Fig. 16). The set point for this temperature is typically 200°C but may vary for specific test sections. A lower measured temperature indicates overcooling, prompting an increase in the valve area to allow a lower mass flow through the bypass line, thus raising the mixing temperature.

ECO HX Bypass Valve Control System

A regulation valve, WP-WCS-R02 in Fig. 15, is installed on the economizer bypass line, operating in split range with the WP-WCS-R01 according to Fig. 149. The bypass valve has inverted power ranges: when power is < 480 kW it is fully opened, while its area is varied by the same PI controller when power is > 480kW. If the mixing measured temperature is lower than the set point, the bypass flow area decreases to allow the passage of a lower cold mass flow.

S-T HX Main Valve Control System

Similarly to the main regulation valve installed on the economizer tube side, another main regulation valve, VP-WHS-R01 in Fig. 15, is placed on the S-T HX tube side. If power is less than 480 kW, the valve area is regulated by a PI controller according to the mixing temperature between the main line and the bypass line, measured by TC-WCS-100 (Fig. 16). The set point for this temperature is typically 132.4°C but may vary for specific test sections. If the measured temperature is lower than the set point, the main valve area is reduced to allow higher mass flow through the hotter bypass line.

S-T HX Bypass Valve Control System

VP-WHS-R02 in Fig. 15 is the regulation valve that operates according to a split range with VP-WHS-R01. It is situated on the S-T HX bypass line and is regulated by a control system that follows Fig. 149. It is characterized by inverted power ranges w.r.t. the main valve: it is fully opened for power < 480kW and its area is regulated in the other case. Specifically, the same PI controller based on the measurement of TC-WCS-100 is adopted. If the mixing temperature is lower than the set point, the bypass valve flow area is increased to allow the passage of higher hot mass flow.

6.3.3 Tertiary loop

Hydraulic components

The RELAP5 nodalization of the WL tertiary circuit is shown in Fig. 152. Boundary conditions were introduced to avoid the reproduction of the cooling tower, whose operation and control is in charge of the manufacturer. The nodalization is composed of:

- Cold leg:
  - Time-dependent volume 500 fix the fluid inlet temperature;
  - Components from 501 to 305 simulate the part of the loop from the cooling tower outlet to the filter;
  - Branch 306 stands for the filter;
  - Pipe 307 reproduces the section of the circuit from the filter to the pump;
  - Component 308 is the pump, imposing the mass flow rate;
  - Components from 309 to 313 represent the part of the loop from the pump to the S-T HX shell side. Specifically, component 312 is a manual valve: considering the future refurbishment of the facility, this valve will allow the interception of the S-T HX and the direct connection of the tertiary fluid with the primary loop through the P-S HX shell side.

- S-T HX shell side:
  - Branch 314 is the heat exchanger inlet nozzle;
  - Pipe 315 simulates the S-T HX shell side, composed of two passages;
  - Branch 316 represents the heat S-T HX outlet nozzle;

- Hot leg:
  - Components from 317 to 326 reproduce the WL tertiary side hot leg. Specifically, component 318 is the manual valve that is envisaged to allow the S-T HX interception for future refurbishment;
  - Time-dependent volume 600 fixes the outlet pressure.

Heat structures

Fig. 153 lists the loop heat structures and their main characteristics. Specifically, they are categorized according to their role in providing, exchanging or dissipating power.

There are no power sources in the loop, therefore no active structures are reproduced. The coupling heat structure would be the S-T HX bundle (HS 420-0), that couples the tertiary loop with the secondary loop. Finally, the remaining heat structures operate as insulated heat structures, providing insulation to pipes and components that are connected to the external environment, which is set at a temperature of 10 °C and a heat transfer coefficient (HTC) of 8 W/m²K.

Control systems

The nodalization of the tertiary loop is equipped with only one control system regulating the pump speed.

Pump control system:

Tertiary loop nominal mass flow is obtained adopting a PI controller that regulates the pump speed according to the scheme of Fig. 35. The pump mass flow rate, monitored by the flow meter FM-WCT-100 (illustrated in Fig. 18), is the measured variable, with the set point being the nominal mass flow rate specific to the test section under examination. The error, calculated as the difference between the set point and the measured value, governs the adjustment of the pump velocity (measured in revolutions per minute, rpm). If the measured flow rate surpasses the set point, indicating a negative error, the system responds by reducing the pump velocity to decrease the mass flow rate, thereby maintaining the operational parameters within the desired range.

6.4 WL Steady-state characterization at different TS powers

Thermal-hydraulic steady-state simulations using the nodalization of the coupled three loops (Fig. 33, Fig. 150 and Fig. 152) were performed to investigate the system behavior under the power conditions of the envisaged test sections, namely the TBM, the Eq. FW and the Non-Eq. FW (see Tab. 7). Three null transient calculations, each lasting 10000s, were carried out to ensure that the main parameter trends are stable and compliant with design values. The calculations referenced each of the quantities listed in Tab. 45, ensuring that the solution maintained stability with an inherent drift of less than 1% per 100 seconds.

Specifically, Tab. 45 lists and compares the main T/H parameters across different power configurations, providing valuable data and feedback of the efficiency of the adopted control systems. Fig. 154, Fig. 155 and Fig. 156 illustrate the power evolution of the test section and the main HXs over time, demonstrating the stability of the results.

It is observed that the power levels of the test sections do not correspond precisely with the power exchanged by the HXs. This discrepancy arises primarily due to the presence of heat losses. The heater power plays a crucial role in compensating for these heat losses, which remain approximately constant across various scenarios. HL mainly depends on the loop temperature, constant in the three simulations, with the assumption of ambient temperature and HTC being constant too). Proper compensation for these heat losses is essential for maintaining thermal balance and ensuring stable system operation.

As heat losses are relatively steady, they effectively reduce the power exchanged by the heat exchangers. This reduction becomes more pronounced with increasing distance from the heat source (i.e., the test section in the primary loop), leading to a progressive decrease in power transfer. In the primary circuit, the P-S HX transfers less power to the secondary loop than the test section generates, due to heat losses in the primary loop. Similarly, in the secondary circuit, the power transferred through the S-T HX to the tertiary loop is further diminished, reflecting the thermal losses in the secondary loop. It is important to note that the reduction in power is not exactly proportional to the heat losses, as there are additional small sources of power, such as the heaters in the PRZ and the thermal power from the pump.

Due to the reduction in power, the significance of the constant heat losses becomes more pronounced, thus increasing the error in the power exchanged by the HXs. This dynamic highlight the sensitivity of the system to heat loss as power levels diminish.

In parallel, the thermal power of the pumps decreases with the reduction in the flow rate that needs to be processed. This behavior aligns with the expected performance characteristics of the pumps under varying flow conditions and demonstrates the system responsiveness to changes in flow rate.
The regulation valves of the HXs function effectively, with the split range logic operating correctly. The temperatures controlled by these regulation valves remain accurate, whereas other temperatures deviate slightly from the design values due to thermal losses along the lines. This indicates that while the control mechanisms are effective, there is a minor impact from heat losses that needs to be considered.

The mass inventory, which depends on the size of the components and the density of the fluid, remains relatively constant since both parameters are stable. Therefore, significant variations in mass inventory are not observed. This stability in mass inventory simplifies the system analysis and helps maintain consistent performance.

Conversely, pressure drops, influenced by the flow rate, decrease as the flow rate diminishes. This observation aligns with theoretical expectations and confirms that the system behaves as anticipated under varying flow conditions. The reduction in pressure drops with decreasing flow rate further validates the design and operational assumptions.

In conclusion, the steady-state simulations confirm that the system maintains stability under different power configurations. The control systems effectively manage the thermal-hydraulic parameters, ensuring compliance with design specifications. The results provide a comprehensive understanding of the system behavior, highlighting the effective performance of the control mechanisms and the minor impacts of thermal losses and flow rate variations. This detailed analysis is crucial for optimizing the design and operation of thermal-hydraulic systems, ensuring they can handle specified power conditions while maintaining stability and efficiency.

6.5 RELAP5 analyses for optimizing of the operation during pulse-dwell-pulse transitions

The pressurizer component objective to maintain the pressure within the primary loop during the pulsed operation is a critical aspect that requires thorough assessment. Its performance, in fact, are significantly influenced by the rapid change in thermal conditions associated with the pulse-dwell-pulse cycles, which are characteristic of burning plasma scenarios (Sect. 2.2). For this reason, thermal-hydraulic analyses were conducted to investigate the effect of this rapid power variation on the main pressurizer parameters.

The analysis was carried out considering the operational cycle of ITER, which features a shorter pulse period [27] with respect to the one expected for the DEMO reactor. This shorter pulse period poses greater challenges as the system has less time to reach steady-state conditions. The rapid transitions between different power levels exacerbate the pressure fluctuations, making it more difficult for the pressurizer to stabilize the system. By examining these dynamic scenarios, the analyses aim to optimize the pressurizer response to mitigate the impact of the transient conditions, thereby enhancing the overall stability and performance of the Water Loop facility during pulsed plasma operations.

The ITER pulsed plasma regime is characterized by a flat-top full-power state (100%; pulse phase) lasting 450 seconds, followed by a 200-second linear ramp down to 1% power, maintained for 1090 seconds (dwell phase). The power then ramps back up to 100% over 60 seconds. These power fluctuations result in significant temperature variations, imposing high thermal stress on the components and challenging the facility regulation.

RELAP5/Mod3.3 simulation timing is reported in Tab. 46, with bold rows indicating the specific intervals depicted in the figures (initial steady state and first ramp down are excluded).

During the pulse phase, the Test Sections receive fluid at a temperature of 295°C, maintained by the heater set point, and heat it up to 328°C. During the dwell phase, with only 1% nominal power, the test section outlet temperature closely aligns with the inlet temperature, resulting in a minor temperature differential (ΔT) of approximately 0.33°C (instead of 33°C). This causes an increase in Hot Leg (HL) density and consequent decrease in specific volume, leading to fluid contraction. Consequently, the pressurizer liquid level drops, causing the pressure to fall below the pressurizer heater set point of 15.4 MPa.

Sensitivity analyses were performed to evaluate the transient behavior of the pressurizer by varying the prz installed heater power (10 kW, 20 kW, and 40 kW), with the primary goal of mitigating pressure fluctuations resulting from the alternating pulse and dwell phases. A low-pressure signal activates the pressurizer heater, increasing their power to prevent system depressurization (Fig. 157). Higher heater power allows for quicker pressure restoration within acceptable limits (Fig. 158), leading to faster heater shutdown.

Although, the occurrence of the pulse leads to an increase in the test section outlet temperature, accompanied by fluid expansion (density decreases). This makes the PRZ level rise and increases the pressure above the spray set point (15.7 MPa). Higher PRZ heater power determines higher pressure established in the loop at the end of the dwell phase and faster pressurization. The pressure peak is limited by the spray intervention, which takes longer for higher PRZ heater power.

Additional sensitivity analyses with a 10 kW heater were conducted to explore safer operational strategies during rapid power fluctuations, aiming to prevent system depressurization during the pulse phase. In "case 0" (black in Fig. 159, Fig. 160 and Fig. 161), the heater set point was adjusted from 295°C to 311.5°C (the test section average temperature) during the dwell phase to minimize fluid density reduction. Consequently, both cold and hot leg temperatures tend towards 311.5°C during the dwell phase, meaning that the temperature gradient that the hot leg should experience is halved be-tween cold and hot leg. With the power ramp-up, the heater set point reverted to 295°C, causing the cold leg temperature to drop to 295°C (Fig. 159). The hot leg, instead, experiences a temperature peak of approximately 333°C (Fig. 160), resulting in overpressure, limited by the spray intervention (Fig. 161).

To avoid temperature peaks, further analyses were performed by reverting the heater set point from 311.5°C to 295°C before the dwell phase ended. Specifically, this adjustment is implemented 90, 190, 290, 390, and 490 seconds before the pulse (b.p.) to allow the HL temperature to return to its nominal value. Results show that the cold leg temperature (Fig. 159) undergoes thermal cycling of approximately half the nominal ΔT (16.5°C). The hot leg (Fig. 160) experiences an increasing ΔT with longer heater anticipation times, reaching the nominal ΔT (33°C) for adjustments made more than 290 seconds before the pulse. Therefore, this correction effectively limits HL overtemperatures. Loop pressure analysis indicates that maintaining the 311.5°C set point for longer periods reduces depressurization. However, switching to 295°C only 90 seconds before the pulse contains pressure above 15.2 MPa, yet still triggering spray intervention due to a pressure peak (Fig. 161).

Regardless of the operational strategy, pressure fluctuations triggering spray activation appear to be unavoidable. The most viable solution would be to install an electric heater at the test section outlet to maintain a fixed hot leg temperature of 328°C, thus avoiding pressure variations due to density changes. However, this would significantly increase facility complexity and cost. Therefore, among the strategies considered, using 40 kW electric heaters in the pressurizer is preferred as it results in lower pressure cycling, with comparable overpressure but less significant depressurization.

6.6 Accidental scenarios

LOFA and LOHS scenarios were simulated also in WL conditions, considering the TBM test section which is characterized by the higher power. These transients proved to be less severe than those conducted in the STEAM (Sect. 5.4), which has a much higher nominal power, even though in both cases the PIE conservatively occurs during a steady state full power pulse.

6.6.1 LOFA

LOFA in WL conditions was investigated to understand the system response when operating under these specific circumstances. This scenario was analyzed using the RELAP5/Mod3.3 code, performing a 9000-second transient to simulate the thermal-hydraulic behavior of the system. The PIE is the failure of the MCP, occurring at 50 seconds after steady-state conditions at full power. Throughout the transient, the power in the Test Section is maintained at its nominal pulse value. It is also assumed that the control valves of the P-S HX continue to operate as intended and that the feedwater mass flow rate and inlet temperature remain constant.

Fig. 162 and Fig. 163 shows that upon the MCP failure, the primary coolant flow rate decreases significantly. Given that the secondary flow rate remains constant as boundary condition, this reduction leads to a slight HX power reduction (Fig. 164) and to the overcooling of the primary side HX outlet and mixing temperature (Fig. 165). In response, the control logic of the bypass valve reacts by fully opening the valve (Fig. 166) to increase the bypassed flow rate, thereby raising the mixing temperature. Once the overcooled fluid reaches the electric heater (delayed by the reduced flow velocity), its power output starts to increase to maintain the setpoint outlet temperature at 295°C (Fig. 167).

As the primary coolant flow decreases, the primary system temperature (Fig. 165) and pressure (Fig. 168) begin to rise due to reduced heat removal. The increase in temperature leads to a reduction in fluid density, causing the pressurizer level to rise initially (Fig. 169). This rise in pressure is managed by the spray system and primarily by PORV, ensuring the pressure remains within safe limits.

Despite the bypass valve being fully open to allow higher bypass mass flow rates and increase the mixing temperature, the bypass flow rate continues to decline. This happens because the Test Section, operating at full power with reduced flow, reaches saturation and begins to produce steam (non-null void fraction, as shown in Fig. 170). The presence of steam, characterized by higher pressure losses, causes the fluid to be drawn from the heat exchanger, leading to a further reduction in the bypass flow rate until it eventually drops to zero. Consequently, the mixing temperature becomes equivalent to the outlet temperature of the heat exchanger (Fig. 165).

The increase of the average primary system temperature facilitates natural circulation, and the system stabilizes at a new operating point where the primary flow rate and temperature difference among HL and CL are both reduced. Steam produced within the Test Section is condensed in the P-S HX (null void fraction at the HX outlet, as shown in Fig. 170), where feedwater operation allows the exchange of the nominal power. The cold leg downstream the heat exchanger operates at a temperature higher than the mixing temperature setpoint, causing the bypass valve to close. Consequently, the control system loses its effectiveness because, with the main valve fully open and the bypass valve closed, it can no longer reduce the mixing temperature. However, the transient does not pose a significant danger, as the pressure is effectively managed and maintained below critical values.

The sequence of main events and the corresponding timing is reported in Tab. 48

Further calculations were performed assuming the control systems of the P-S HX valves were non-functional, leaving the valves stuck in their pre-PIE positions. The results remained essentially the same. As noted, the opening of the bypass valve following the PIE does not result in an increased bypass flow due to the overall reduction in total flow and partial vaporization in the Test Section. Therefore, it can be concluded that the control logic of the HX valves has no significant effect on this transient

6.6.2 LOHS

To understand the system behavior during a LOHS scenario occurring while W-HYDRA primary system is operating in WL configuration with the TBM test section, a transient analysis was conducted using the RELAP5/Mod3.3 code. A 9000-second transient was simulated with the PIE being the failure of the feedwater pump, which occurs after 50s of steady-state conditions at full power. Within the subsequent 10 seconds, the feedwater flow rate drops to zero.

The boundary conditions for this simulation include a constant pulse output for the test section power and a functional control system for the P-S HX regulation valves. The primary pump (MCP) is shut down when the primary fluid temperature reaches the setpoint of Tsat - 5°C to avoid cavitation.

The abrupt reduction in feedwater flow rate to zero within 10 seconds (Fig. 171) causes a dramatic loss of the system heat removal capacity. This effectively nullifies the heat sink, leading to a significant reduction in the heat exchanged between the primary and secondary sides in the P-S HX. Despite this, the power output of the Test Section remains constant (BC), causing the feedwater temperature at the HX inlet to rise rapidly (Fig. 172), reaching saturation. As a result, a two-phase mixture fills the PS HX shell side (void fraction higher than zero, as shown in Fig. 173), furtherly reducing the system heat transfer capability. A higher average temperature fluid with lower temperature difference (ΔT) is present, as well as superheated vapor at the SS HX outlet.

The lack of effective heat removal leads to a rapid increase in the temperature at the PS HX outlet to rise (Fig. 174), increasing the mixing temperature of the main and bypass flows. This rise triggers the closure of the bypass valve (Fig. 175), thereby reducing the bypass flow rate that drops to 0. As a result, the mixing temperature matches the HX outlet temperature.

The overall increase in primary temperatures results in a decrease in fluid density, which raises the pressurizer pressure and liquid collapsed level (Fig. 176). Consequently, the MCP, operating at a constant speed and head, processes a progressively lower flow rate until the flow curve alters its slope (Fig. 177). This change occurs when the fluid temperature at the pump reaches 5°C below saturation, indicating a critical point in the transient evolution.

With both primary and secondary side heat removal capacity compromised and a constant TS power output, the simulation was stopped when the system reached a critical temperature threshold, indicating that the integrity of the system would be compromised beyond this point.

The sequence of main events is collected in Tab. 49.

The calculations were also performed with the P-S HX regulation valves stuck in their pre-PIE positions (during steady-state conditions). The transient evolution remains practically unchanged, reinforcing the observation that their control logic does not impact the outcome of this accidental scenario.

An unprotected LOHS transient scenario can only be used to evaluate Grace Time for the system. Compared to the STEAM case analyzed in 5.4.2, the WL system exhibits a longer Grace Time due to a higher ratio between system inertia and power source. The WL system benefits from a lower power source while sharing the same pressurizer (that constitutes the greater portion of system volume) with the STEAM system, thus extending the Grace Time before reaching critical conditions.

Tab. 30. Main design data and properties of P-S HX.

Parameter	Unit	Value	Description
		Primary loop	
W	kW	3100	Nominal thermal power
$p_{H2O,1}$	MPa	15.5	H_2O pressure in the primary side
$T_{H2O,in,1}$	°C	328.0	H_2O temperature at the TS inlet
$T_{H2O,out,1}$	°C	295.0	H_2O temperature at the TS outlet
$\Gamma_{H2O,1}$	kg/s	16.05	H_2O nominal mass flow rate
$\rho_{H2O,ave}$	kg/m^3	697.1	H_2O average density inside the HX
$\mu_{H2O,ave}$	Pa s	8.376E-05	H_2O average dynamic viscosity inside the HX
$C_{pH2O,ave}$	J/kg K	5976.9	H_2O average specific heat inside the HX
$k_{H2O,ave}$	W/m K	0.534	H_2O average thermal conductivity
N_{tubes}	-	61	Number of tubes in the bundle
D_{in}	mm	13.38	Tube inside diameter
D_{out}	mm	15.87	Tube outside diameter
v_1	m/s	2.68	Average water velocity
Re	-	2.99E+05	Average Reynolds number
Pr	-	0.935	Average Prandtl number
Nu	-	541.3	Average Nusselt number
HTC_1	W/m^2 K	21603.0	Average heat transfer coefficient
R_i /L	K m /W	1.10E-03	Thermal resistance on 1 m length of pipe
		Secondary loop	
$p_{H2O,2}$	MPa	4	H_2O pressure
$T_{H2O,in,2}$	°C	190.0	H_2O temperature upstream the HX
$T_{H2O,out,2}$	°C	225.0	H_2O temperature downstream the HX
$\Gamma_{H2O,2}$	kg/s	19.57	H_2O nominal mass flow rate
$\rho_{H2O,ave}$	kg/m^3	878	H_2O average density inside the HX
$\mu_{H2O,ave}$	Pa s	1.308E-04	H_2O average dynamic viscosity inside the HX
$Cp_{H2O,ave}$	J/kg K	4533.0	H_2O average specific heat inside the HX
$k_{H2O,ave}$	W/m K	0.659	H_2O average thermal conductivity
D_{in}	mm	215.91	Shell inside diameter
D_{out}	mm	273.05	Shell outside diameter
D_h	mm	26	Hydraulic diameter
P/D	-	1.5	Pitch to diameter ratio
v_2	m/s	0.91	Average water velocity

Re	-	1.61E+05	Average Reynolds number
Pr	-	0.897	Average Prandtl number
Nu	-	322.4	Average Nusselt number
HTC_2	W/m^2 K	8043.0	Average heat transfer coefficient
R_o /L	K m / W	2.49E-03	Thermal resistance on 1 m length of shell
Pipe			
k	W/m K	18.86	Steel thermal conductivity
R_s /L	K m /W	1.44E-03	Thermal resistance on 1 m length of steel
Results			
ΔT_1	K	103	Temperature difference on one side of the HX
ΔT_2	K	105	Temperature difference on the other side of the HX
ΔT_{ml}	K	104	Logarithmic mean temperature difference
UA	W/K	29809	Global thermal conductance
F	-	1	Correction factor
L	m	150.1	Equivalent total length of the pipe
L_{pipe}	m	2.46	Pipe bundle length
L_{real}	m	2.6	Real pipe length of the bundle (with fouling)

Tab. 31. Main design data and properties of S-T HX.

Parameter	**Unit**	**Value**	**Description**
Secondary loop			
W	kW	3100	Nominal thermal power
$p_{H2O,2}$	MPa	4	H_2O pressure
$T_{H2O,in,2}$	°C	190.0	H_2O temperature upstream the HX
$T_{H2O,out,2}$	°C	225.0	H_2O temperature downstream the HX
$\Gamma_{H2O,2}$	kg/s	19.57	H_2O nominal mass flow rate
$\rho_{H2O,ave}$	kg/m^3	878	H_2O average density inside the HX
$\mu_{H2O,ave}$	Pa s	1.308E-04	H_2O average dynamic viscosity inside the HX
$Cp_{H2O,ave}$	J/kg K	4533.0	H_2O average specific heat inside the HX
$k_{H2O,ave}$	W/m K	0.659	H_2O average thermal conductivity
N_{tubes}	-	61	Number of tubes in the bundle
D_{in}	mm	13.38	Tube inside diameter
D_{out}	mm	15.87	Tube outside diameter
v_2	m/s	2.60	Average water velocity
Re	-	2.34E+05	Average Reynolds number
Pr	-	0.897	Average Prandtl number
Nu	-	438.9	Average Nusselt number
HTC_2	W/m^2 K	21600.4	Average heat transfer coefficient
R_i /L	K m /W	1.10E-03	Thermal resistance on 1 m length of pipe
Tertiary loop			
$p_{H2O,3}$	MPa	0.6	H_2O pressure
$T_{H2O,in,3}$	°C	40.0	H_2O temperature upstream the HX
$T_{H2O,out,3}$	°C	80.0	H_2O temperature downstream the HX
$\Gamma_{H2O,3}$	kg/s	18.52	H_2O nominal mass flow rate
$\rho_{H2O,ave}$	kg/m^3	982.2	H_2O average density inside the HX

$\mu_{H2O,ave}$	Pa s	5.038E-04	H_2O average dynamic viscosity inside the HX
$Cp_{H2O,ave}$	J/kg K	4185.9	H_2O average specific heat inside the HX
$k_{H2O,ave}$	W/m K	0.659	H_2O average thermal conductivity
D_{in}	mm	215.91	Shell inside diameter
D_{out}	mm	273.05	Shell outside diameter
D_h	mm	26	Hydraulic diameter
P/D	-	1.5	Pitch to diameter ratio
V_3	m/s	0.77	Average water velocity
Re	-	3.96E+04	Average Reynolds number
Pr	-	3.283	Average Prandtl number
Nu	-	176.2	Average Nusselt number
HTC_3	W/m^2 K	4325.3	Average heat transfer coefficient
R_o /L	K m / W	4.64E-03	Thermal resistance on 1 m length of shell
Pipe			
k	W/m K	18.86	Steel thermal conductivity
R_s /L	K m /W	1.44E-03	Thermal resistance on 1 m length of steel
Results			
ΔT_1	K	145.0	Temperature difference on one side of the HX
ΔT_2	K	150.0	Temperature difference on the other side of the HX
ΔT_{ml}	K	147.5	Logarithmic mean temperature difference
UA	W/K	21019	Global thermal conductance
F	-	1	Correction factor
L	m	150.89	Equivalent total length of the pipe
L_{pipe}	m	2.474	Pipe bundle length
L_{real}	m	2.6	Real pipe length of the bundle (with fouling)

Tab. 32. RELAP5 results of P-S HX at different power values

Parameter	**Power**										
	100%	**90%**	**80%**	**70%**	**60%**	**50%**	**40%**	**30%**	**20%**	**15%**	**10%**
Power [MW]											
HX power	3.10	2.79	2.48	2.17	1.86	1.55	1.24	0.93	0.62	0.47	0.31
Mass Flow [kg/s]											
PS total MF	16.05	14.44	12.84	11.23	9.63	8.02	6.42	4.81	3.21	2.41	1.60
PS MF HX	13.08	10.60	8.51	6.77	5.31	4.05	3.03	2.05	1.25	0.90	0.56
PS bypass MF	2.97	3.84	4.33	4.46	4.32	3.97	3.39	2.76	1.96	1.51	1.04
SS HX MF	19.58	17.56	15.67	13.70	11.75	9.79	7.48	5.88	3.92	2.93	1.96
Temperature [°C]											
PS inlet T	328.0	328.0	328.0	328.0	328.0	328.0	328.0	328.0	328.0	328.0	328.0
PS HX outlet T	286.7	281.6	276.0	270.2	264.1	257.5	251.9	242.5	233.5	228.3	221.8
PS outlet T	295.0	295.0	295.0	295.0	295.0	295.0	295.0	295.0	295.0	295.0	295.0
SS inlet T	190.0	190.0	190.0	190.0	190.0	190.0	190.0	190.0	190.0	190.0	190.0
SS outlet HX T	225.0	225.1	224.9	225.0	225.0	224.9	226.6	224.9	224.9	225.1	224.8
Pressure [MPa]											
PS inlet p	15.53	15.52	15.51	15.51	15.51	15.50	15.50	15.50	15.50	15.50	15.50
PS outlet p	15.52	15.51	15.51	15.51	15.50	15.50	15.50	15.50	15.50	15.50	15.50
SS inlet p	4.00	4.00	4.00	4.00	4.00	4.00	4.00	4.00	4.00	4.00	4.00
SS outlet p	4.00	4.00	4.00	4.00	4.00	4.00	4.00	4.00	4.00	4.00	4.00
Velocity [m/s]											
PS liquid velocity	2.32	1.88	1.51	1.20	0.94	0.72	0.54	0.36	0.22	0.16	0.10
SS liquid velocity	0.91	0.82	0.73	0.64	0.55	0.46	0.35	0.27	0.18	0.14	0.09
PS bypass liq vel	0.33	0.43	0.48	0.50	0.48	0.44	0.38	0.31	0.22	0.17	0.12

Tab. 33. Geometry and dimensions selected for the three HXs with a sizing power of 3.1 MW.

Component	Configuration		Length[m]	ΔT [°C]	V [m/s]
P-S HX	Shell	8’’ Sch.80	3.6	30	1,40
	Tube	37 ¾’’ 18 BWG		33	2,89
ECO	Shell	10’’ Sch.160	19.7	74.2	1,06
	Tube	61 ⅝’’ 18 BWG		72	2,92
	Shell	8’’ Sch.80	24.4	74.2	1,36
	Tube	37 ¾’’ 18 BWG		72	3,14
S-T HX	Shell	8’’ Sch.80	5.3	40	0,99
	Tube	37 ¾’’ 18 BWG		32.2	3,06

Tab. 34. Geometry and dimensions selected for the three HXs with a sizing power of 800 kW.

Component	Configuration		Length[m]	ΔT [°C]	V [m/s]
P-S HX	Shell	5’’ Sch.80	2.9	40	0.65
	Tube	19 ⅝’’ 18 BWG		33	2.22
ECO	Shell	6’’ Sch.160	7.8	67	0.57
	Tube	37 ½’’ 18 BWG		69.7	1.60
S-T HX	Shell	5’’ Sch.80	3.8	30	0.81
	Tube	19 ⅝’’ 18 BWG		42.7	2.22

Tab. 35. Temperature difference at the mixing point for the 3.1 MW HXs

Power [%]	ΔT mixing [°C]		
	P-S HX	ECO HX	S-T HX
100	38.07	74.0	47.2
90.3	42.37	76.5	50.9
90	46.90	79.1	54.8
80	51.70	81.7	58.8
70	56.84	84.4	63.1
60	62.39	87.2	67.7
50	68.51	90.2	72.6
40	75.45	93.3	78.2
30.5	80.80	95.7	82.5
30	83.76	96.9	84.8
25.3	94.99	101.2	93.9
20	98.78	102.6	97.0
10	101.06	103.3	98.8
5	103.57	104.1	100.9
1	116.79	107.8	112.2

Tab. 36. Power and MFR in correspondence of which transition and laminar regimes occur for the WL HXs designed for 3.1 MW

Component	Configuration		Power [%]		MFR [%]	
			TRANS.	LAM.	TRANS.	LAM.
P-S	Shell	8’’ Sch.80	5	0.5	5	0.5
	Tube	37 ¾’’ 18 BWG	7	0.9	3	0.3
ECO	Shell	10’’ Sch.160	7	0.7	7	0.7
	Tube	61 ⅝’’ 18 BWG	9	0.9	6	0.6
	Shell	8’’ Sch.80	5	0.5	5	0.5
	Tube	37 ¾’’ 18 BWG	7	0.7	5	0.4
S-T	Shell	8’’ Sch.80	12	1	12	1
	Tube	37 ¾’’ 18 BWG	14	2	7	0.8

Tab. 37. WL HXs flow regimes at the test sections power levels with a facility power of 3.1 MW

Component	Configuration		Eq FW	Non-eq FW	TBM
P-S	Shell	8’’ Sch.80	TURB	TURB	TURB
	Tube	37 ¾’’ 18 BWG	TRAN	TRAN	TURB
ECO	Shell	10’’ Sch.160	TURB	TRAN	TURB
	Tube	61 ⅝’’ 18 BWG	TRAN	TRAN	TURB
	Shell	8’’ Sch.80	TURB	TURB	TURB
	Tube	37 ¾’’ 18 BWG	TURB	TRAN	TURB
S-T	Shell	8’’ Sch.80	TRAN	TRAN	TURB
	Tube	37 ¾’’ 18 BWG	TRAN	TRAN	TURB

Tab. 38. MFR repartition and temperature difference at the mixing point for the 800 kW HXs

Power [%]	ΔT mixing [°C]		
	P-S HX	ECO HX	S-T HX
100	43.1	74.8	50.9
90.3	46.8	76.9	54.2
90	47.0	77.0	54.3
80	51.0	79.2	57.8
70	55.4	81.6	61.5
60	60.0	84.0	65.5
50	65.1	86.5	69.7
40	70.7	89.2	74.4
30.5	76.8	92.0	79.4
30	77.2	92.1	79.7
25.3	80.6	93.6	82.6
20	85.0	95.4	86.2
10	95.7	99.5	95.1
5	104.0	102.3	102.2
1	117.0	105.8	113.8

Tab. 39. Power and MFR in correspondence of which transition and laminar regimes occur for the WL HXs designed for 800 kW

Co.	Configuration		Power [%]		MFR [%]	
			TRA	LAM	TRA	LAM
P-S	Shell	5" Sch.80	9	0.9	9	0.9
	Tube	19 5/8" 18 BWG	11	1	5.1	0.38
ECO	Shell	6" Sch.STD	14	1	14	1
	Tube	37 1/2" 18 BWG	15	1	11	0.66
S-T	Shell	5" Sch.80	23	2	23	2
	Tube	19 5/8" 18 BWG	20	3	11.3	1.35

Tab. 40. WL HXs flow regimes at the test sections power levels with a facility power of 800 kW

Co.	Configuration		Eq FW	Non-eq FW	TBM
P-S	Shell	5" Sch.80	TURB	TURB	TURB
	Tube	19 5/8" 18 BWG	TURB	TURB	TURB
ECO	Shell	6" Sch.STD	TURB	TURB	TURB
	Tube	37 1/2" 18 BWG	TURB	TURB	TURB
	Shell	5" Sch.80	TURB	TURB	TURB
	Tube	19 5/8" 18 BWG	TURB	TURB	TURB
S-T	Shell	5" Sch.80	TURB	TURB	TURB
	Tube	19 5/8" 18 BWG	TURB	TURB	TURB

Tab. 41. TS 6 and TS 6 bis thermodynamic conditions and comparison wrt the reference thermal cycle

Loop	Reference (800 kW)		TS 6 (400 kW)		TS 6 bis (500 kW)	
	Mfr [kg/s]	p [MPa]	Mfr [kg/s]	p [MPa]	Mfr [kg/s]	p [MPa]
PS	4.14	15.5	4.79 (+15.7%)	7.5	5.98 (+44.4%)	7.5
SS	4.37	7	5.24 (+19.9%)	4.0	6.98 (+59.7%)	4.0
TS	6.37	0.6	7.37 (+15.7%)	0.6	10.50 (+64.8%)	0.6

Tab. 42. WL Configurations for TS 7 to TS 15 with 4 m/s maximum loop velocity and total economizer bypass regulation

TS	Power [kW]	PS MFR [kg/s]	SS MFR [kg/s]	TS MFR [kg/s]	PS T max [°C]	PS T min [°C]	SS T max [°C]	SS T min [°C]	TS T max [°C]	TS T min [°C]
TS 7	132.2	10.52	10.59	19.03	63.0	60.0	48.9	45.9	38.6	36.9
TS 7	182.35	10.51	10.61	18.94	64.2	60.0	44.2	40.1	29.2	26.9
TS 9	196.8	10.51	10.61	19.00	64.5	60.0	42.8	38.4	26.4	23.9
TS 10	139.75	10.52	10.59	18.95	63.2	60.0	48.2	45.0	37.2	35.4
TS 11	212.5	10.51	10.63	19.03	64.8	60.0	41.3	36.5	23.2	20.5
TS 12	220.65	10.51	10.63	19.04	65.0	60.0	40.5	35.5	21.5	18.7
TS 13	259.7	10.51	10.65	19.07	65.9	60.0	36.4	30.5	12.7	9.4
TS 14	268.8	10.51	10.65	19.07	66.1	60.0	35.4	29.3	10.5	7.1
TS 14bis	279.363	10.51	10.65	19.08	66.4	60.0	34.2	27.9	7.7	4.2
TS 15	432.95	-	-	-	-	-	-	-	-	-

Tab. 43. WL Configurations for TS 7 to TS 15 with 4 m/s maximum loop velocity and total secondary loop bypass regulation

TS	Power [kW]	PS MFR [kg/s]	TS MFR [kg/s]	PS T max [°C]	PS T min [°C]	TS T max [°C]	TS T min [°C]
TS 7	132.2	10.52	18.84	63.0	60.0	51.0	49.4
TS 7	182.35	10.51	18.87	64.2	60.0	47.5	45.2
TS 9	196.8	10.51	18.88	64.5	60.0	46.4	43.9
TS 10	139.75	10.52	18.85	63.2	60.0	50.5	48.7
TS 11	212.5	10.51	18.89	64.8	60.0	45.3	42,6
TS 12	220.65	10.51	18.89	65.0	60.0	44.7	41.9
TS 13	259.7	10.51	18.92	65.9	60.0	41.7	38.4
TS 14	268.8	10.51	18.92	66.1	60.0	41.0	37.6
TS 14bis	279.363	10.51	18.93	66.4	60.0	40.2	36.7
TS 15	432.95	10.50	19.01	69.9	60.0	27.0	21.6

Tab. 44. WL Configurations for TS 7 to TS 15 with 25°C as minimum tertiary loop temperature and total secondary loop bypass regulation

TS	Power [kW]	PS MFR [kg/s]	TS MFR [kg/s]	HX tubes V [m/s]	TS pipes V [m/s]	PS T max [°C]	PS T min [°C]	TS T max [°C]	TS T min [°C]
TS 7	132.2	1.78	3.22	0.68	0.68	77.8	60.0	34.8	25.0
TS 7	182.35	2.87	5.20	1.10	1.10	75.2	60.0	33.4	25.0
TS 9	196.8	3.23	5.84	1.23	1.23	74.6	60.0	33.1	25.0
TS 10	139.75	1.93	3.50	0.74	0.74	77.3	60.0	34.6	25.0
TS 11	212.5	3.63	6.57	1.38	1.38	74.0	60.0	32.8	25.0
TS 12	220.65	3.85	6.96	1.47	1.47	73.7	60.0	32.6	25.0
TS 13	259.7	4.99	9.02	1.90	1.90	72.5	60.0	31.9	25.0
TS 14	268.8	5.27	9.54	2.01	2.01	72.2	60.0	31.8	25.0
TS 14bis	279.363	5,62	10.17	2.14	2.14	71.9	60.0	31.6	25.0
TS 15	432.95	12.15	21.98	4.63	4,63	68.5	60.0	29.7	25.0

Tab. 45. RELAP5 results of WL operation in TBM, Eq. FW and Non-Eq. FW configurations

Parameter	TBM			Eq. FW			Non-eq. FW		
	R5	**Ref.**	**±ε**	**R5**	**Ref.**	**±ε**	**R5**	**Ref.**	**±ε**
Powers [kW]									
PS - Test Section	+722.27	722.39	-0.02%	+244.12	244.16	-0.02%	202.37	202.40	-0.01%
PS - P-S HX	-708.42	-722.39	-1.93%	-230.19	-244.16	-5.72%	-188.43	-202.40	-6.90%
PS - electrical heater	+3.37	N/A	-	+4.74	N/A	-	+4.75	N/A	-
PS - prz heaters	+1.77	N/A	-	+1.76	N/A	-	+1.76	N/A	-
PS - pump thermal power	+1.57	N/A	-	+0.073	N/A	-	+0.031	N/A	-
PS - heat losses	-22.3	N/A	-	-22.21	N/A	-	-22.19	N/A	-
SS - ECO	±1158	±1155	±0.26%	±392.68	±390.59	±0.54%	±325.76	±323.79	±0.61%
SS - S-T HX	-706.83	-722.39	-2.15%	-227.21	-244.21	-6.96%	-185.36	-202.40	-8.42%
SS - pump thermal power	+1.79	N/A	-	+0.07	N/A	-	+0.042	N/A	-
SS - prz heater	+0.17	N/A	-	+0.16	N/A	-	+0.16	N/A	-
SS - heat losses	-3.57	N/A	-	-3.58	N/A	-	-3.58	N/A	-
TS - pump thermal power	+1.5	N/A	-	+1.94	N/A	-	+0.75	N/A	-
Mass Flow Rates [kg/s]									
PS - pump	3.74	3.4	0	1.26	1.26	0	1.05	1.05	0
PS - TS	3.74	3.74	0	1.26	1.26	0	1.05	1.05	0
PS - P-S HX tube-side main line	2.55	N/A	-	0.52	N/A	-	0.41	N/A	-
PS - P-S HX tube side bypass line	1.19	N/A	-	0.74	N/A	-	0.64	N/A	-
PS - SRV	0	0	0	0	0	0	0	0	0
PS - PORV	0	0	0	0	0	0	0	0	0
PS - Surge line	0	0	0	0	0	0	0	0	0
PS - Spray line	0	0	0	0	0	0	0	0	0
SS - pump	3.95	3.95	0	1.33	1.33	0	1.11	1.11	0
SS - ECO HX main line	3.60	N/A	-	1.00	N/A	-	0.82	N/A	-
SS - ECO HX bypass	0.35	N/A	-	0.33	N/A	-	0.29	N/A	-
SS - ECO HX total bypass	0	N/A	-	0.00	N/A	-	0.00	N/A	-
SS – S-T HX main line	2.93	N/A	-	0.63	N/A	-	0.50	N/A	-
SS – S-T HX bypass	1.02	N/A	-	0.70	N/A	-	0.61	N/A	-
SS - SRV	0	0	0	0	0	0	0	0	0
SS - PORV	0	0	0	0	0	0	0	0	0

SS - Surge line	0	0	0	0	0	0	0	0	0
SS - Spray line	0	0	0	0	0	0	0	0	0
TS – pump	5.75	5.75	0	1.94	1.94	0	1.61	1.61	0
Pressures [MPa]									
PS - pressurizer top	15.60	15.55	0.32%	15.60	15.55	0.32%	15.60	15.55	0.32%
PS - pump	15.71	-	-	15.68	-	-	15.68	-	-
SS - pressurizer top	7.10	7.00	1.43%	7.10	7.00	1.43%	7.10	7.00	1.43%
SS - pump	7.19	-	-	7.16	-	-	7.16	-	-
TS - pump	0.66	0.6	10%	0.65	0.6	10%	0.65	0.6	10%
Temperatures [°C]									
PS - PRZ	345.3	344.8	0.5 °C	345.3	344.8	0.5 °C	345.3	344.8	0.5 °C
PS - upstream TS	294.8	295.0	-0.2 °C	294.3	295	-0.7 °C	294.1	295	-0.9 °C
PS - downstream TS	327.9	328.0	-0.1 °C	327.5	328	-0.5 °C	327.4	328	-0.6 °C
PS - upstream P-S HX	327.5	328.0	-0.5 °C	326.4	328	-1.6 °C	326.1	328	-1.9 °C
PS - downstream P-S HX	278.0	-	N/A	242.8	-	N/A	238.4	-	N/A
PS - mixing downstream P-S HX	295.0	295.0	0 °C	295.0	295	0 °C	295.0	295	0 °C
SS - PRZ	286.8	285.8	1 °C	286.8	285.8	1 °C	286.8	285.8	1 °C
SS - upstream P-S HX	200.0	200.0	0 °C	200.0	200	0 °C	200.0	200	0 °C
SS - downstream P-S HX	239.2	240.0	-0.8 °C	237.7	240	-2.3 °C	237.2	240	-2.8 °C
SS - upstream ECO shell side	239.1	240.0	-0.9 °C	237.6	240	-2.4 °C	237.1	240	-2.9 °C
SS - downstream ECO shell side	174.1	175.0	-0.9 °C	172.1	175	-2.9 °C	171.5	175	-3.5 °C
SS - upstream S-T HX	174.1	175.0	-0.9 °C	172.1	175	-2.9 °C	171.4	175	-3.6 °C
SS - downstream S-T HX	117.7	-	N/A	87.4	-	N/A	83.7	-	N/A
SS - mixing downstream S-T HX	132.4	132.4	0 °C	132.4	132.4	0 °C	132.4	132.4	0 °C
SS - upstream ECO tube side	132.5	132.4	0.1 °C	132.3	132.4	-0.1 °C	132.3	132.4	-0.1 °C
SS - downstream ECO tube side	206.2	-	N/A	221.8	-	N/A	222.9	-	N/A
SS - mixing downstream ECO tube side	200.0	200.0	0 °C	200.0	200	0 °C	200.0	200	0 °C
TS – upstream the S-T HX	50.0	50	0 °C	49.9	50	-0.1 °C	49.9	50	-0.1 °C
TS - downstream the S-T HX	79.37	80	-0.63 °C	77.8	80	-2.2 °C	77.3	80	-2.7 °C
Levels [m]									
PS – pressurizer	5.55	N/A	-	5.49	N/A	-	5.47	N/A	-
SS - pressurizer	0.59	N/A	-	0.59	N/A	-	0.59	N/A	-
Heat Losses [kW]									
PS - P-S HX hot leg	-1.75	N/A	-	-1.74	N/A	-	-1.74	N/A	-

PS - P-S HX	-0.26	N/A	-	-0.25	N/A	-	-0.25	N/A	-
PS - P-S HX cold leg	-1.07	N/A	-	-1.01	N/A	-	-1.01	N/A	-
PS - P-S HX bypass line	-0.45	N/A	-	-0.45	N/A	-	-0.45	N/A	-
PS - CL from HX reconnection point to heater lines bifurcation	-2.33	N/A	-	-2.32	N/A	-	-2.32	N/A	-
PS - E-heater cold leg	-0.43	N/A	-	-0.43	N/A	-	-0.43	N/A	-
PS - E-heater	-1.18	N/A	-	-1.18	N/A	-	-1.18	N/A	-
PS - E-heater hot leg	-0.27	N/A	-	-0.27	N/A	-	-0.27	N/A	-
PS - Test Section cold leg	-4.24	N/A	-	-4.23	N/A	-	-4.23	N/A	-
PS - Test Section hot leg	-5.80	N/A	-	-5.78	N/A	-	-5.78	N/A	-
PS - Hot leg from TS reconnection to HX bifurcation	-0.81	N/A	-	-0.80	N/A	-	-0.80	N/A	-
PS - Surge line	-0.22	N/A	-	-0.21	N/A	-	-0.21	N/A	-
PS - Pressurizer	-3.42	N/A	-	-3.43	N/A	-	-3.43	N/A	-
PS - Spray line	-0.11	N/A	-	-0.10	N/A	-	-0.10	N/A	-
SS - P-S HX Shell (no nozzles)	-0.255	N/A	-	-0.251	N/A	-	-0.250	N/A	-
SS - WL P-S HX HOT LEG	-0.501	N/A	-	-0.498	N/A	-	-0.497	N/A	-
SS - ECO HX Shell + tubes nozzles	-0.68	N/A	-	-0.70	N/A	-	-0.70	N/A	-
SS - WL S-T HX hot leg	-0.33	N/A	-	-0.33	N/A	-	-0.33	N/A	-
SS - WL S-T HX cold leg	-0.58	N/A	-	-0.57	N/A	-	-0.57	N/A	-
SS - S-T HX bypass	-0.07	N/A	-	-0.07	N/A	-	-0.07	N/A	-
SS - WL P-S HX cold leg	-0.41	N/A	-	-0.45	N/A	-	-0.45	N/A	-
SS - ECO HX bypass common line	-0.12	N/A	-	-0.12	N/A	-	-0.12	N/A	-
SS - ECO HX total bypass	-0.03	N/A	-	-0.03	N/A	-	-0.03	N/A	-
SS - ECO HX regulation bypass	-0.04	N/A	-	-0.04	N/A	-	-0.04	N/A	-
SS - Surge line	-0.09	N/A	-	-0.07	N/A	-	-0.07	N/A	-
SS - Pressurizer	-0.27	N/A	-	-0.27	N/A	-	-0.27	N/A	-
SS - Spray line	-0.19	N/A	-	-0.19	N/A	-	-0.19	N/A	-
TS - Cold leg	-0.75	N/A	-	-0.74	N/A	-	-0.73	N/A	-
TS - S-T HX shell	-0.06	N/A	-	-0.06	N/A	-	-0.07	N/A	-
TS - Hot leg	-0.91	N/A	-	-0.89	N/A	-	-0.88	N/A	-
Mass Inventories [kg]									
PS – P-S HX hot leg	33.02	N/A	-	33.17	N/A	-	33.21	N/A	-
PS – P-S HX (including nozzles)	8.75	N/A	-	9.20	N/A	-	9.26	N/A	-
PS - P-S HX cold leg	27.07	N/A	-	27.56	N/A	-	27.61	N/A	-

PS - P-S HX bypass line	4.44	N/A	-	4.46	N/A	-	4.46	N/A	-
PS - CL from HX reconnection point to heater lines bifurcation (including filter and pump)	124.19	N/A	-	124.26	N/A	-	124.28	N/A	-
PS - E-heater cold leg	15.28	N/A	-	15.30	N/A	-	15.30	N/A	-
PS - E-heater	213.53	N/A	-	213.65	N/A	-	213.68	N/A	-
PS - E-heater hot leg	11.81	N/A	-	11.81	N/A	-	11.81	N/A	-
PS - From heater HL to TS CL	32.60	N/A	-	32.60	N/A	-	32.60	N/A	-
PS - Test Section cold leg	280.18	N/A	-	280.38	N/A	-	280.45	N/A	-
PS - Test Section hot leg	290.31	N/A	-	291.15	N/A	-	291.38	N/A	-
PS - Hot leg from TS reconnection to HX bifurcation	40.47	N/A	-	40.64	N/A	-	40.68	N/A	-
PS - Surge line	5.92	N/A	-	6.05	N/A	-	6.08	N/A	-
PS - Pressurizer	303.04	N/A	-	300.39	N/A	-	299.73	N/A	-
PS - Spray line	4.24	N/A	-	4.21	N/A	-	4.21	N/A	-
SS - P-S HX Shell with nozzles	20.53	N/A	-	20.61	N/A	-	20.63	N/A	-
SS - P-S HX hot leg	17.84	N/A	-	17.89	N/A	-	17.91	N/A	-
SS - ECO HX Shell with nozzles	59.22	N/A	-	59.08	N/A	-	59.08	N/A	-
SS - S-T HX hot leg before bifurcation	9.69	N/A	-	9.72	N/A	-	9.72	N/A	-
SS - S-T HX hot leg after bifurcation	10.37	N/A	-	10.39	N/A	-	10.40	N/A	-
SS - S-T HX tubes with plenums	13.27	N/A	-	13.50	N/A	-	13.53	N/A	-
SS - S-T HX cold leg before reunification	2.64	N/A	-	2.70	N/A	-	2.70	N/A	-
SS - S-T HX bypass line	1.95	N/A	-	1.96	N/A	-	1.96	N/A	-
SS - S-T HX cold leg after reunification and before filter	29.41	N/A	-	29.41	N/A	-	29.41	N/A	-
SS - Filter	0.58	N/A	-	0.58	N/A	-	0.58	N/A	-
SS - HX S-T cold leg after filter before pump	2.89	N/A	-	2.89	N/A	-	2.89	N/A	-
SS - Pump	9.36	N/A	-	9.36	N/A	-	9.36	N/A	-
SS - HX S-T cold leg after pump	4.05	N/A	-	4.05	N/A	-	4.05	N/A	-
SS - HX ECO tube side cold leg after bifurcation	16.00	N/A	-	16.00	N/A	-	16.00	N/A	-
SS - HX ECO tubes with plenums	27.44	N/A	-	27.04	N/A	-	27.00	N/A	-
SS - HX ECO tube hot leg before first reunification	13.82	N/A	-	13.51	N/A	-	13.49	N/A	-
SS - HX ECO bypass - common line	11.83	N/A	-	11.83	N/A	-	11.83	N/A	-
SS - HX ECO regulation bypass	0.63	N/A	-	0.63	N/A	-	0.63	N/A	-
SS - HX ECO tube hot leg between the two reunifications	1.61	N/A	-	1.61	N/A	-	1.61	N/A	-
SS - HX ECO total bypass	3.70	N/A	-	3.70	N/A	-	3.70	N/A	-

SS - HX P-S shell cold leg	3.24	N/A	-	3.24	N/A	-	3.24	N/A	-
SS - Surge Line	0.65	N/A	-	0.82	N/A	-	0.81	N/A	-
SS - Pressurizer	35.52	N/A	-	35.72	N/A	-	35.70	N/A	-
SS - Spray Line	10.71	N/A	-	10.71	N/A	-	10.71	N/A	-
TS - Cold leg before filter	404.93	N/A	-	404.93	N/A	-	364.93	N/A	-
TS - Filter	1.75	N/A	-	1.75	N/A	-	1.75	N/A	-
TS - Cold leg from filter to pump	9.74	N/A	-	9.74	N/A	-	9.74	N/A	-
TS - Pump	9.88	N/A	-	9.88	N/A	-	9.88	N/A	-
TS - Cold leg after pump before bifurcation	75.36	N/A	-	75.36	N/A	-	75.36	N/A	-
TS - Cold leg after bifurcation	68.86	N/A	-	68.86	N/A	-	68.86	N/A	-
TS - S-T HX shell with nozzles	32.04	N/A	-	32.07	N/A	-	32.08	N/A	-
TS - Hot leg before reunification	22.09	N/A	-	22.11	N/A	-	22.12	N/A	-
TS - Hot leg after reunification	466.52	N/A	-	466.99	N/A	-	467.14	N/A	-
Dynamic pressure drops [kPa]									
PS - P-S HX line before the main line-bypass bifurcation	4.31	N/A	-	0.52	N/A	-	0.37	N/A	-
PS - P-S HX main hot leg upstream the regulation valve	0.28	N/A	-	0.01	N/A	-	0.00	N/A	-
PS - main P-S HX valve	4.11	N/A	-	3.32	N/A	-	2.99	N/A	-
PS - P-S HX main hot leg downstream the regulation valve	0.23	N/A	-	0.01	N/A	-	0.01	N/A	-
PS - P-S HX (including inlet & outlet nozzles)	6.48	N/A	-	0.28	N/A	-	0.18	N/A	-
PS - P-S HX main cold leg before the bypass reunification	0.50	N/A	-	0.04	N/A	-	0.03	N/A	-
PS - P-S HX bypass line upstream the regulation valve	2.50	N/A	-	0.37	N/A	-	0.26	N/A	-
PS - Bypass P-S HX valve	7.15	N/A	-	1.04	N/A	-	0.77	N/A	-
PS - P-S HX bypass line downstream the regulation valve	0.94	N/A	-	0.56	N/A	-	0.42	N/A	-
PS - P-S HX cold leg after the reunification of the bypass	2.53	N/A	-	0.33	N/A	-	0.23	N/A	-
PS - Cold leg (common to both STEAM and WL) before filter	0.02	N/A	-	0.01	N/A	-	0.00	N/A	-
PS - Filter	3.55	N/A	-	0.43	N/A	-	0.30	N/A	-

PS - Cold leg (common to both STEAM and WL) after filter	0.01	N/A	-	0.00	N/A	-	0.00	N/A	-
PS - WL pump line - before the pump	1.36	N/A	-	0.15	N/A	-	0.10	N/A	-
PS - WL Pump dp	-46.82	N/A	-	-2.09	N/A	-	-0.09	N/A	-
PS - pump line - after the pump	1.73	N/A	-	0.20	N/A	-	0.14	N/A	-
PS - Cold leg (both STEAM and WL) from pump to heaters line	0.06	N/A	-	0.00	N/A	-	0.00	N/A	-
PS - E-heater cold leg	2.41	N/A	-	0.28	N/A	-	0.19	N/A	-
PS – E-heater	0.43	N/A	-	0.04	N/A	-	0.03	N/A	-
PS - E-heater hot leg	0.27	N/A	-	0.03	N/A	-	0.02	N/A	-
PS - HL from heater lines to TS line	0.08	N/A	-	0.01	N/A	-	0.01	N/A	-
PS - TS cold leg	0.33	N/A	-	0.01	N/A	-	0.01	N/A	-
PS - Test Section	22.94	N/A	-	2.687	N/A	-	1.84	N/A	-
PS - TS hot leg	0.33	N/A	-	0.03	N/A	-	0.03	N/A	-
PS - Hot leg (common to both STEAM and WL) after TS bypass	32.38	N/A	-	32.47	N/A	-	32.50	N/A	-
SS - P-S HX shell side with nozzles	1.50	N/A	-	0.18	N/A	-	0.12	N/A	-
SS - P-S HX hot leg	2.94	N/A	-	0.34	N/A	-	0.24	N/A	-
SS - ECO HX shell side with nozzles	3.02	N/A	-	0.37	N/A	-	0.26	N/A	-
SS - S-T HX hot leg before bifyrcation	1.08	N/A	-	0.13	N/A	-	0.09	N/A	-
SS - S-T HX hot leg after bifurcation, before reg.valve	0.62	N/A	-	0.00	N/A	-	0.00	N/A	-
SS - S-T HX main line reg.valve	5.09	N/A	-	3.66	N/A	-	2.83	N/A	-
SS - S-T HX hot leg after reg.valve	0.28	N/A	-	0.01	N/A	-	0.01	N/A	-
SS - S-T HX tube side with plenums	7.86	N/A	-	0.41	N/A	-	0.26	N/A	-
SS - S-T HX cold leg before reunification	0.88	N/A	-	0.13	N/A	-	0.09	N/A	-
SS - S-T HX bypass before reg.valve	2.43	N/A	-	0.57	N/A	-	0.42	N/A	-
SS - S-T HX bypass reg.valve	11.39	N/A	-	2.99	N/A	-	2.25	N/A	-
SS - S-T HX bypass after reg.valve	0.83	N/A	-	0.53	N/A	-	0.40	N/A	-
SS - S-T HX cold after reunification, before filter	3.37	N/A	-	0.43	N/A	-	0.30	N/A	-
SS - Filter	59.55	N/A	-	6.90	N/A	-	4.77	N/A	-
SS - pipe line from filter to pump	0.20	N/A	-	0.02	N/A	-	0.02	N/A	-
SS - pump dp	-121.52	N/A	-	-18.75	N/A	-	-13.11	N/A	-
SS - pipe line after the pump, before the bifurcation	0.31	N/A	-	0.03	N/A	-	0.02	N/A	-

SS - ECO HX tube side cold leg, after the bifurcation	1.31	N/A	-	0.08	N/A	-	0.06	N/A	-
SS - ECO main line reg.valve	7.37	N/A	-	4.70	N/A	-	3.46	N/A	-
SS - ECO HX tube side cold leg, after the reg.valve	1.02	N/A	-	0.08	N/A	-	0.05	N/A	-
SS - ECO HX tube side with plenums	21.38	N/A	-	1.84	N/A	-	1.28	N/A	-
SS - ECO HX tube side hot leg, before first reunification	2.02	N/A	-	0.24	N/A	-	0.17	N/A	-
SS - ECO HX bypass common line	0.56	N/A	-	0.10	N/A	-	0.07	N/A	-
SS - ECO HX regulation bypass before reg. valve	1.07	N/A	-	1.02	N/A	-	0.76	N/A	-
SS - ECO HX bypass reg. valve	31.11	N/A	-	5.25	N/A	-	3.88	N/A	-
SS - ECO HX regulation bypass after reg. valve	0.71	N/A	-	1.01	N/A	-	0.74	N/A	-
SS - ECO HX tube side hot leg between the two reconnections	2.53	N/A	-	0.29	N/A	-	0.20	N/A	-
SS - ECO HX total bypass	36.75	N/A	-	8.07	N/A	-	6.06	N/A	-
SS - P-S HX shell side hot leg	0.47	N/A	-	0.06	N/A	-	0.04	N/A	-
TS - cold leg before the filter	2.85	N/A	-	0.39	N/A	-	-1.61	N/A	-
TS – filter	17.07	N/A	-	2.00	N/A	-	1.39	N/A	-
TS - cold leg from the filter to the pump	0.05	N/A	-	0.01	N/A	-	0.00	N/A	-
TS - Tertiary side pump	-36.33	N/A	-	-12.92	N/A	-	-600.98	N/A	-
TS - cold leg after the pump before bifurcation	0.61	N/A	-	0.07	N/A	-	0.04	N/A	-
TS - cold leg after the bifurcation	0.64	N/A	-	0.07	N/A	-	0.04	N/A	-
TS - S-T HX shell side with nozzles	1.53	N/A	-	0.20	N/A	-	0.14	N/A	-
TS - hot leg before the reunification	0.47	N/A	-	0.07	N/A	-	0.05	N/A	-
TS - hot leg after the reunification	-41.84	N/A	-	-44.83	N/A	-	-44.96	N/A	-

Tab. 46. Timing adopted for calculation purposes.

Primary System	
Initial steady state	From 0 s to 1000 s
Ramp down	From 1000 s to 1200 s
Dwell phase	From 1200 s to 2290 s
Ramp up	From 2290 s to 2350 s
Pulse phase	**From 2350 s to 2800 s**
Ramp down	**From 2800 s to 3000 s**
Dwell phase	**From 3000 s to 4090 s**
Ramp up	**From 4090 s to 4150 s**
Pulse phase	**From 4150 s to 4600 s**
Ramp down	**From 4600 s to 4800 s**
Dwell phase	**From 4800 s to 5890 s**
Ramp up	**From 5890 s to 5950 s**

Tab. 47. Test matrix of the accidental analyzed scenarios in WL TBM configuration.

Accident	**MCP**	**Feedwater pump**	**Simul. time**	**Comments**
LOFA	OFF @ 50s (PIE)	ON	9000s	- Transition from forced to natural circulation. - Higher ΔT between hot and cold leg. - PORV is triggered multiple times in the first part of the transient. - Steam production in the Test Section. - Effective condensation in the P-S HX. - Control logic of HX valves has no significant effect on the transient.
LOHS	ON (until $T_{pump}< T_{sat}$-5°C)	OFF @ 50s (PIE	1941s	- Severe scenario used to evaluate the system grace time. - W.r.t. the LOHS during STEAM operation, the grace time is higher due to a higher ratio between system inertia and power source.

Tab. 48. Sequence of main events for a LOFA occurring during WL TBM operation.

#	**Event**	**LOFA**
1	PIE: MCP failure	50s
2	Spray first intervention @16MPa	148s
3	PS MF < 80%	80s
4	PS MF < 50%	177s
5	Saturation conditions at the heater outlet	Not occurring
6	Saturation conditions at the TS outlet	210s
7	PORV first intervention	212s
9	PRZ maximum level	9m @ 544s
11	PS MF < 20%	940s
12	FW < 50%	Not occurring
13	FW < 20%	Not occurring

Tab. 49. Sequence of main events for a LOHS occurring during WL TBM operation.

#	Event	LOHS_0
1	PIE: FW pump failure	50s
2	FW < 80%	53s
3	FW < 50%	56s
4	FW < 20%	59s
5	Spray first intervention @16MPa	113ss
6	PORV first intervention	456ss
7	Saturation conditions at the heater outlet	Not occurring
8	MCP pump OFF (Tpump > Tsat – 5°C)	592s
9	PS MF < 80%	600s
10	Saturation conditions at the TS outlet	652s
11	PRZ maximum level	9m @ 684s
12	PS MF < 50%	688s
13	PS MF < 20%	1056s

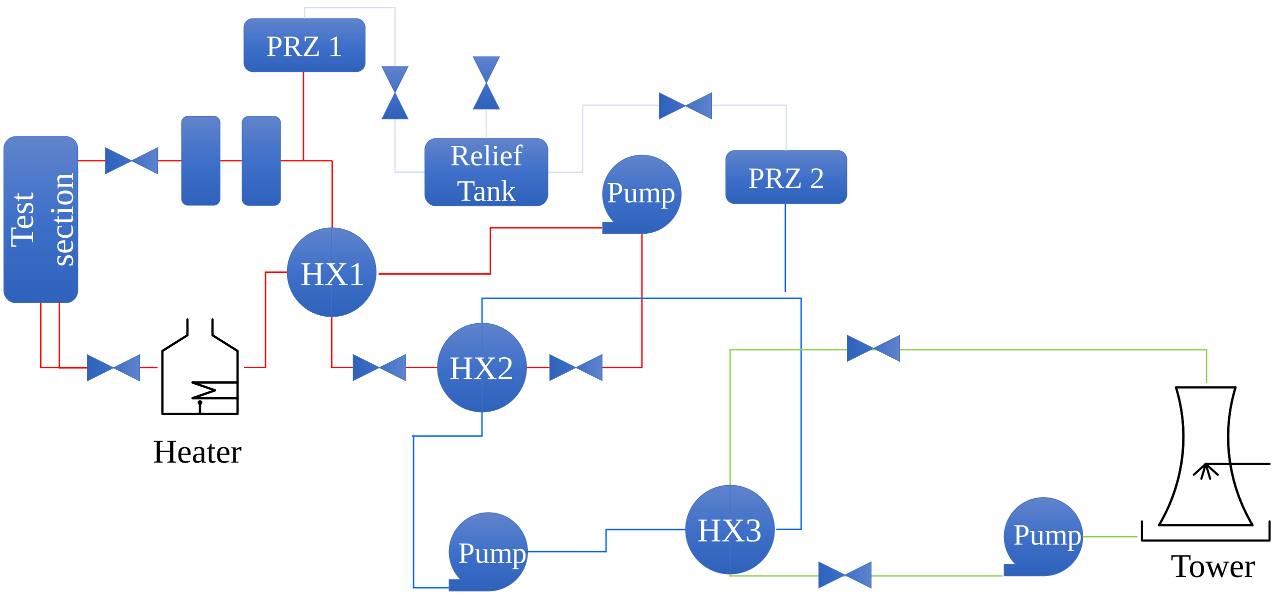

Fig. 127. Water Loop old layout schematization

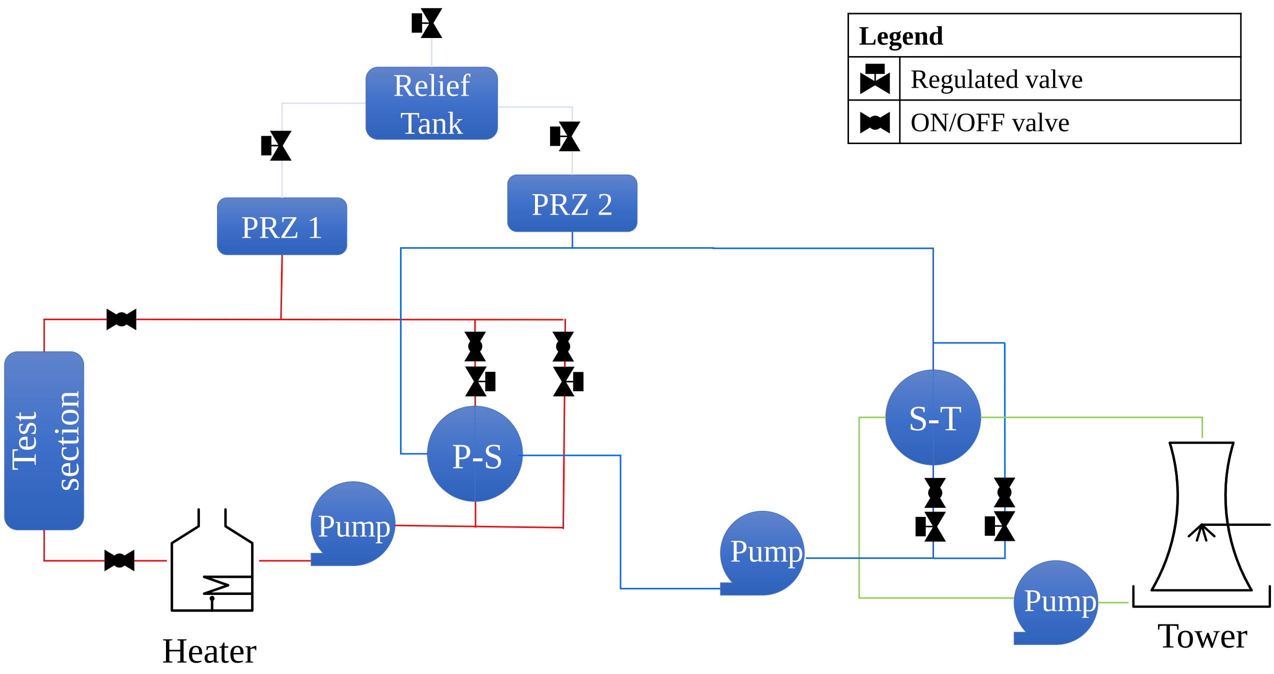

Fig. 128. First analyzed WL configuration after the merging of the STEAM and WL primary circuits: primary (red), secondary (blue) and tertiary (green) loops

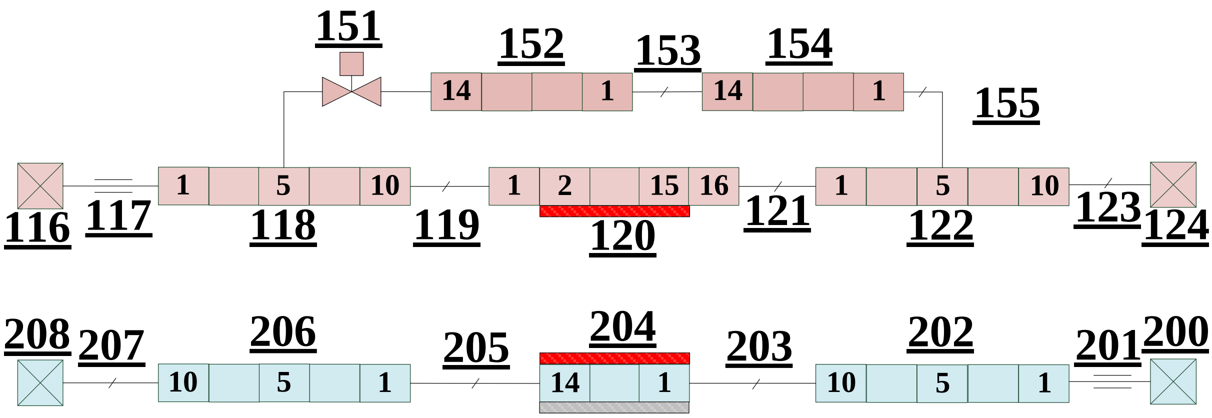

Fig. 129. RELAP5/Mod3.3 nodalization of the primary-secondary Water Loop heat exchanger.

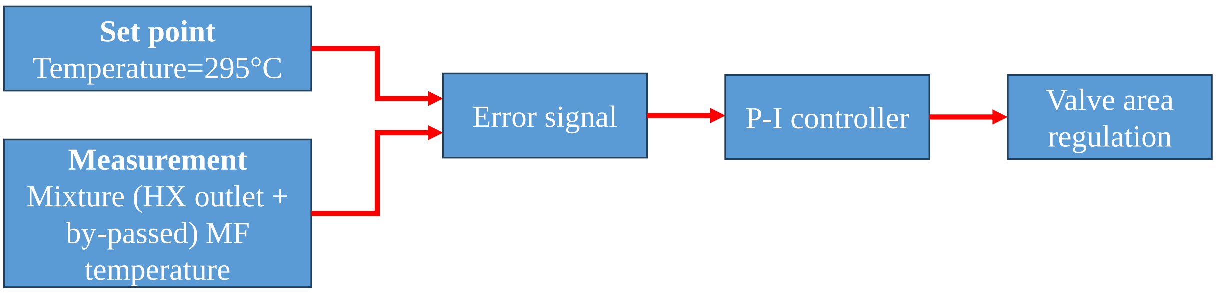

Fig. 130. Control logic implemented for the primary side mass flow bypass.

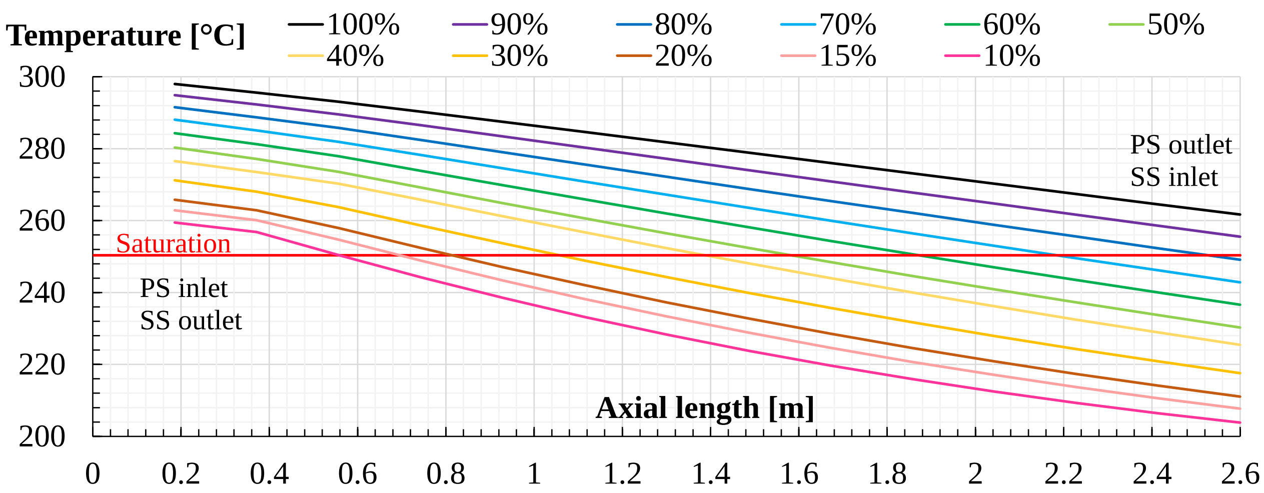

Fig. 131. Shell-side wall temperature profile along the axial length for different power loads.

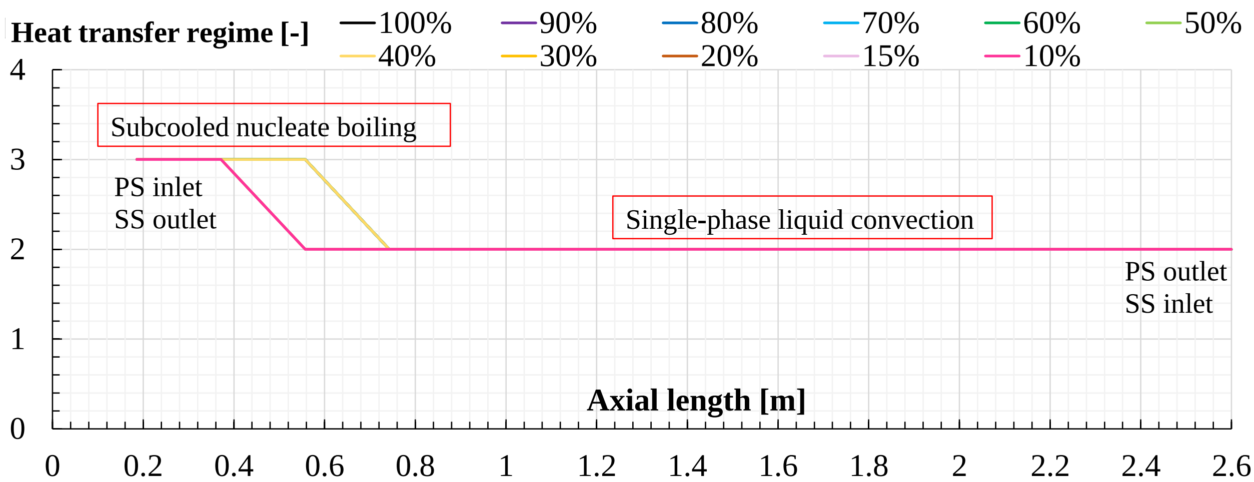

Fig. 132. Heat transfer regime along the heat exchanger axial length for different power loads.

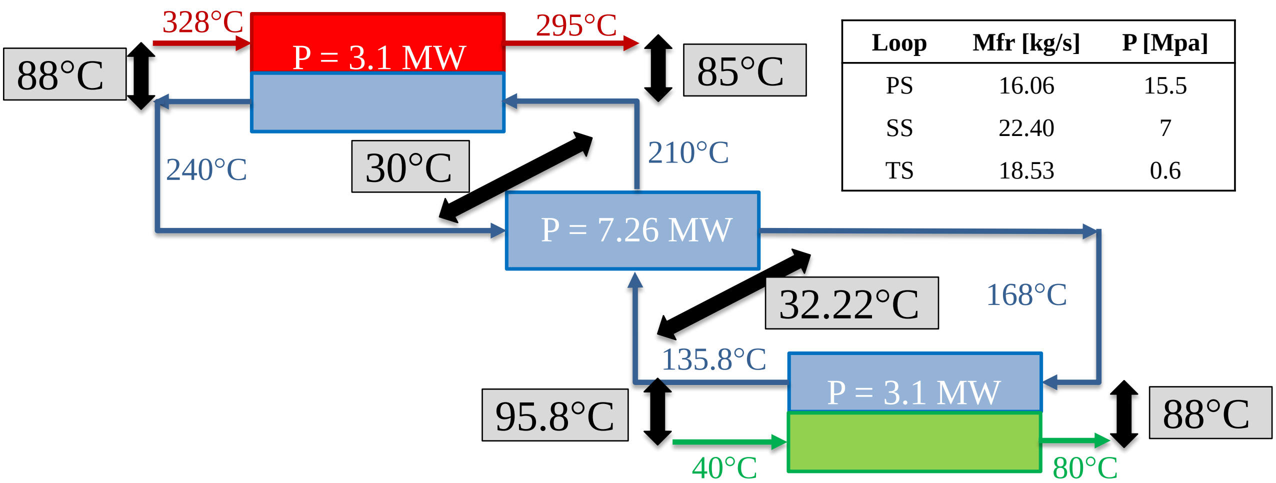

Loop	Mfr [kg/s]	P [Mpa]
PS	16.06	15.5
SS	22.40	7
TS	18.53	0.6

Fig. 133. Water Loop preliminary reference thermal cycle and thermal-hydraulic parameters

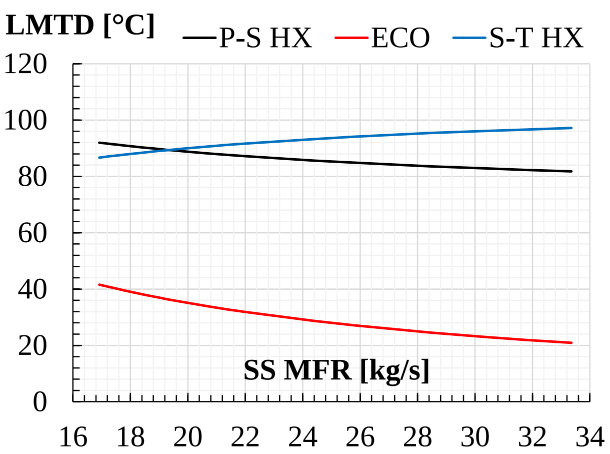

Fig. 134. SS MFR influence on the HXs LMTD

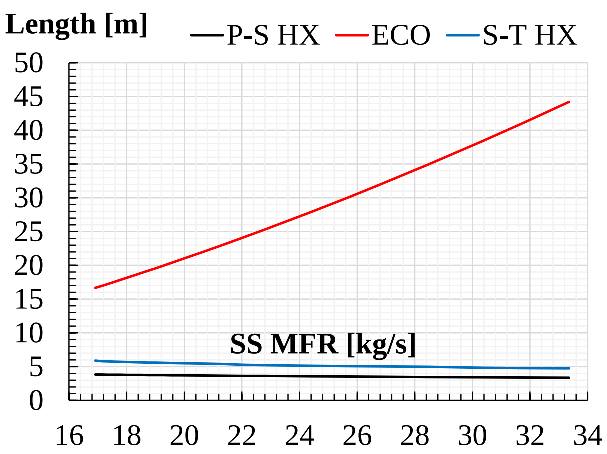

Fig. 135. SS MFR influence on the HXs tubes length

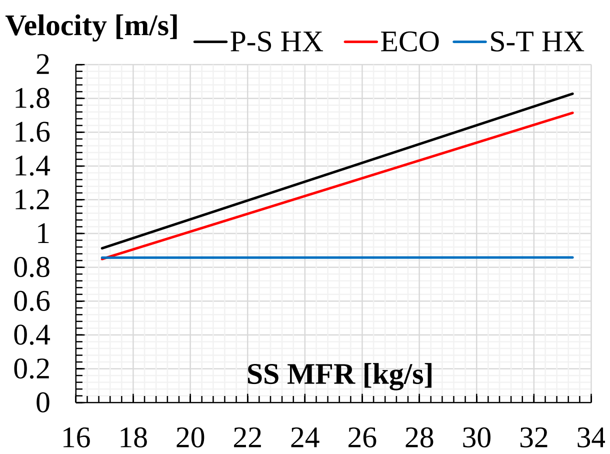

Fig. 136. Shell side velocity of the HXs with different SS MFR

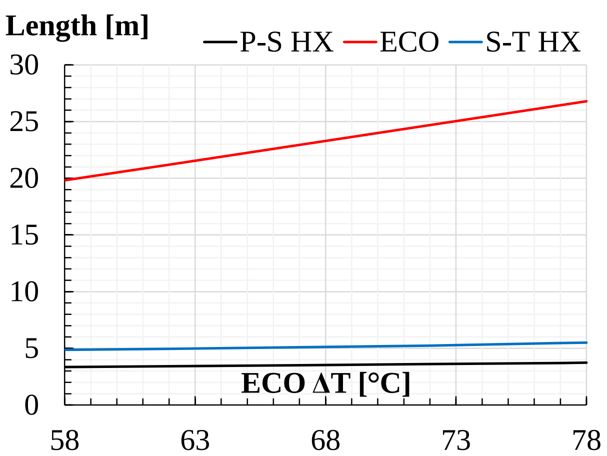

Fig. 137. ECO ΔT influence on the HXs tubes length

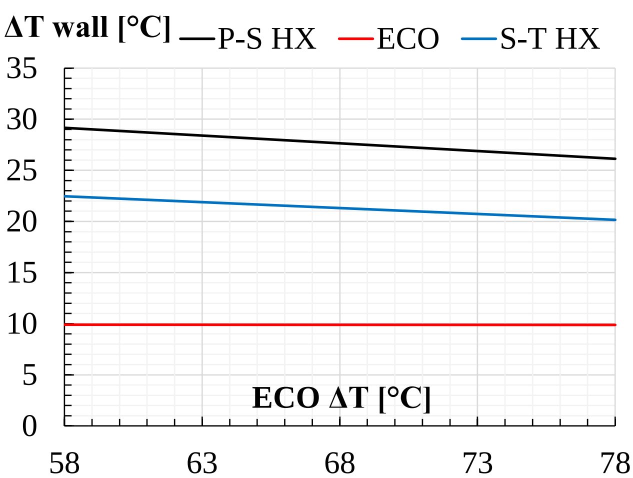

Fig. 138. ECO ΔT influence on the average wall ΔT of the HXs

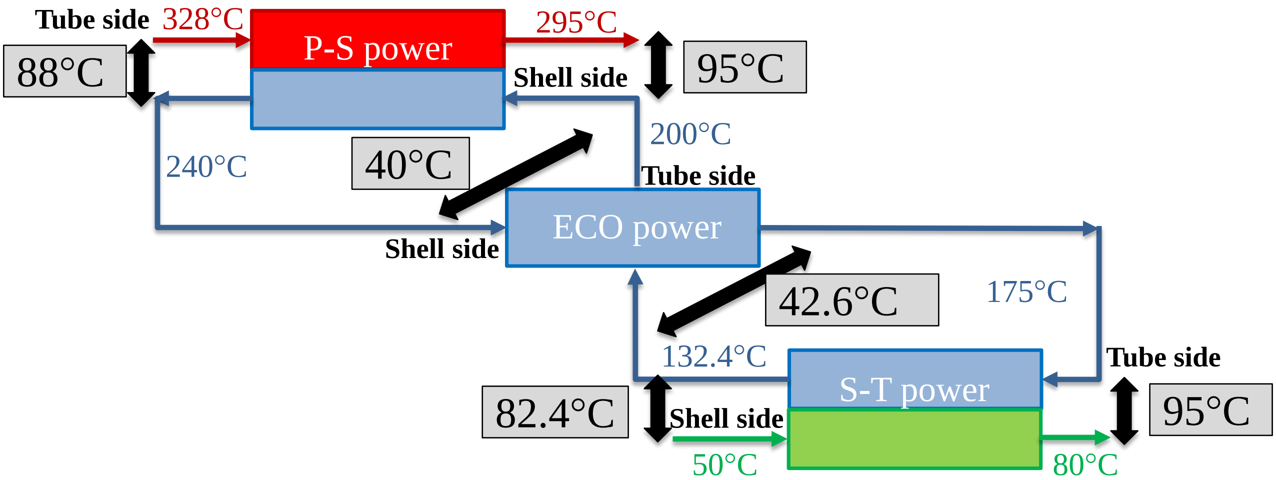

HX	Power [kW]	Loop	Mfr [kg/s]	P [Mpa]
P-S	3100	PS	16.06	15.5
ECO	5110	SS	16.92	7.0
S-T	3100	TS	24.96	0.6

HX	Power [kW]	Loop	Mfr [kg/s]	P [Mpa]
P-S	800	PS	4.14	15.5
ECO	1280	SS	4.37	7.0
S-T	800	TS	6.37	0.6

Fig. 139. WL optimized thermal cycle and thermo-dynamic parameters for power levels of 3.1 MW and 800 kW

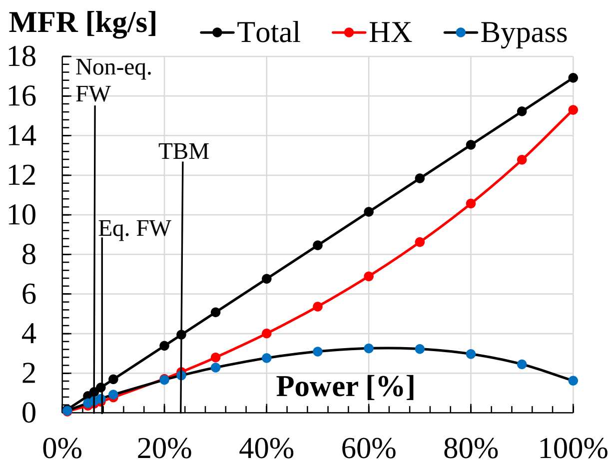

Fig. 140. P-S HX MFR distribution for the 3.1 MW WL

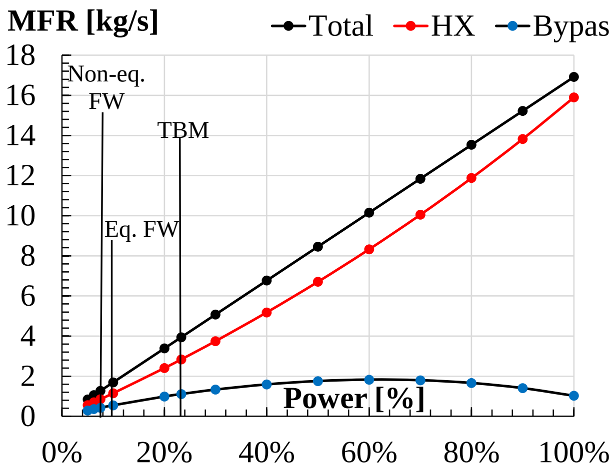

Fig. 141. ECO MFR distribution for the 3.1 MW WL

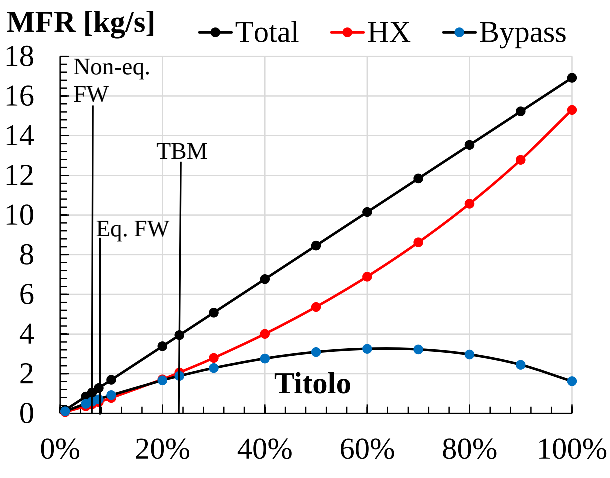

Fig. 142. S-T HX MFR distribution for the 3.1 MW WL

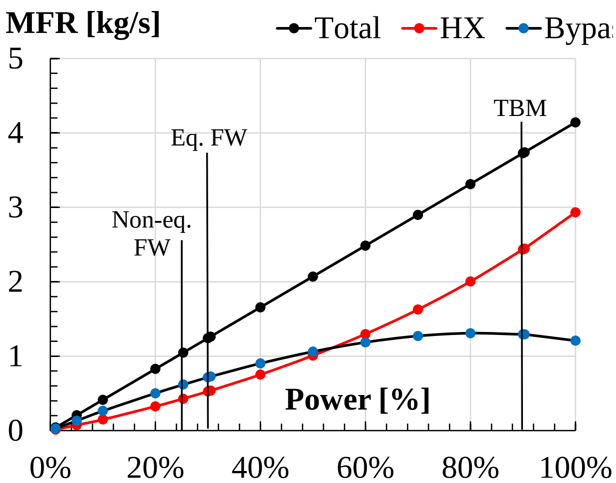

Fig. 143. P-S HX MFR distribution for the 800 kW WL

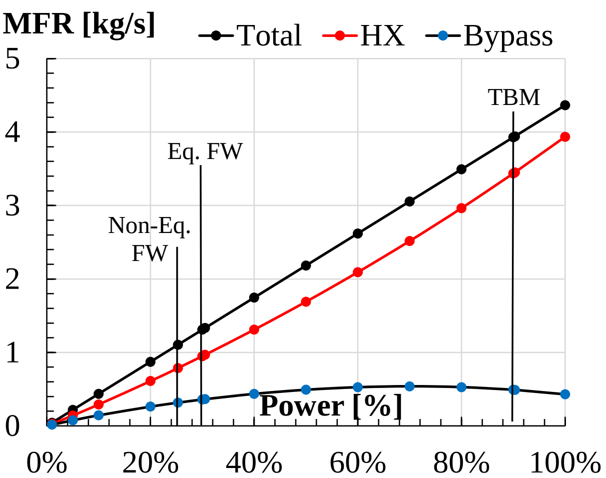

Fig. 144. ECO MFR distribution for the 800 kW WL

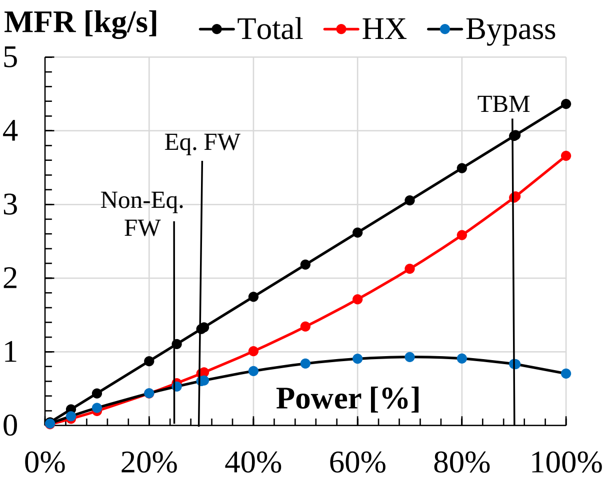

Fig. 145. S-T HX MFR distribution for the 800 kW WL

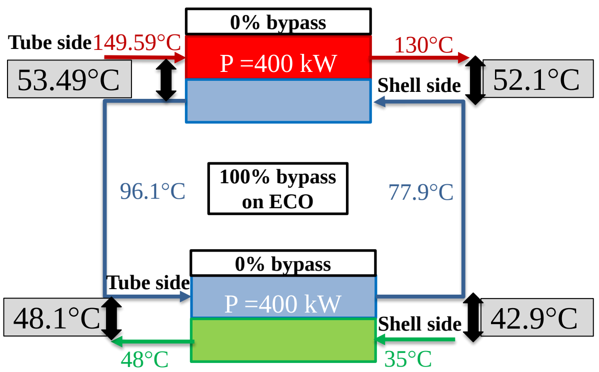

Fig. 146. TS 6 thermal cycle

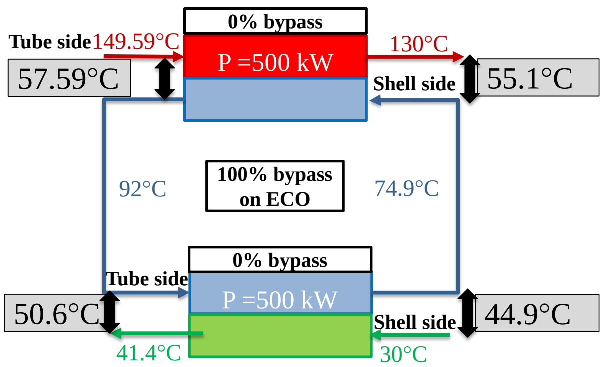

Fig. 147. TS 6 bis thermal cycle

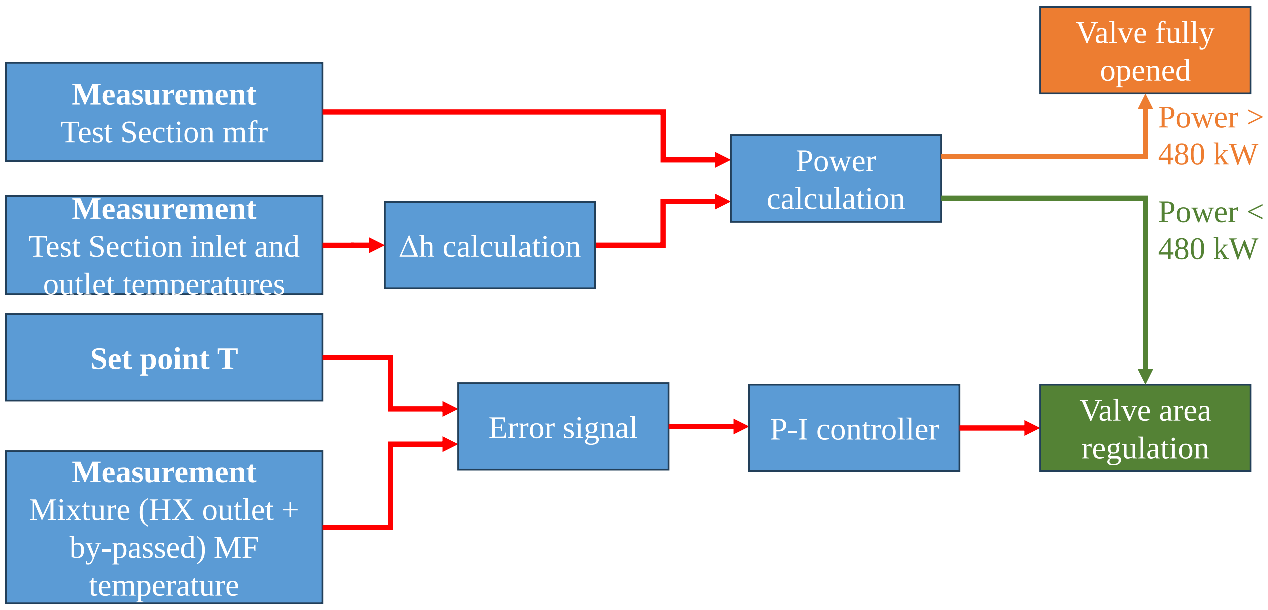

Fig. 148. Main valve regulation control logic

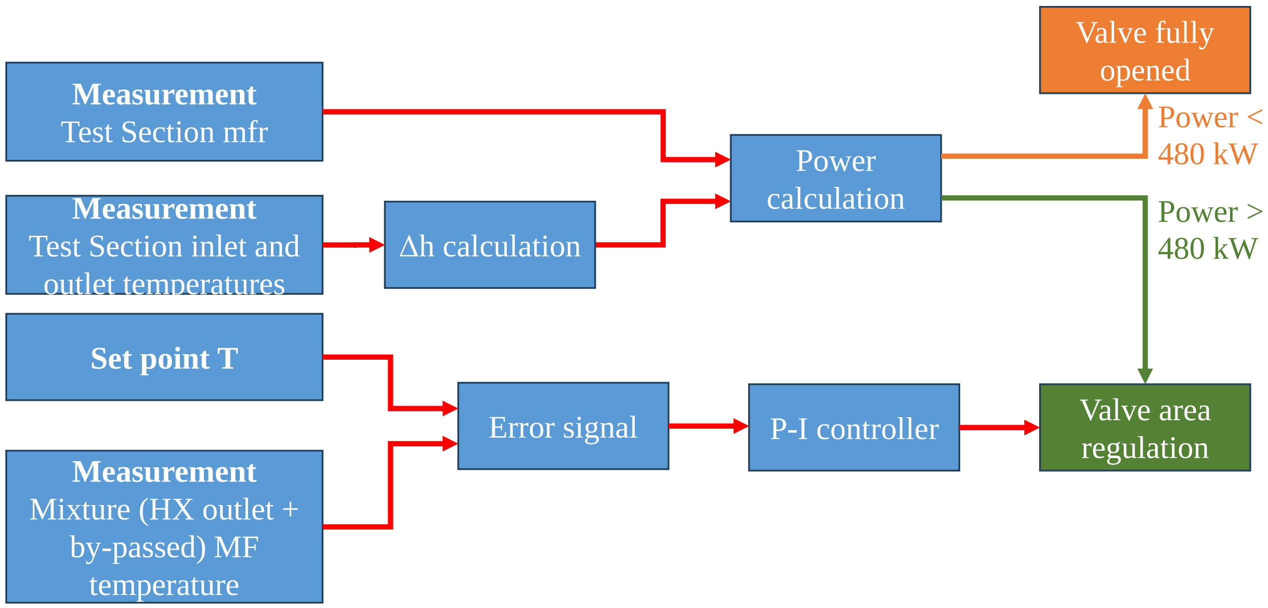

Fig. 149. Bypass valve regulation control logic

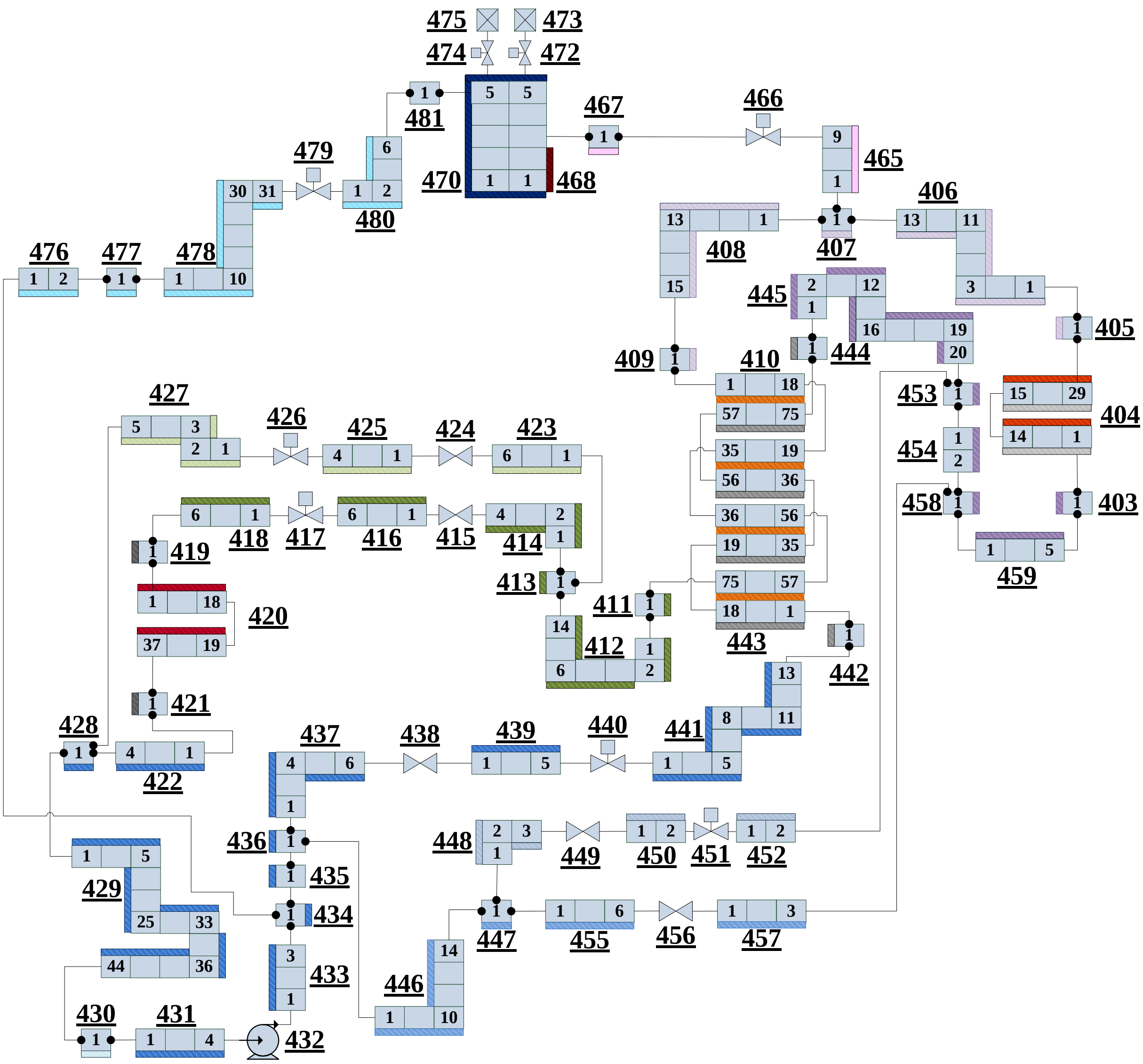

Fig. 150. Water Loop secondary side RELAP5/Mod3.3 nodalization

#	HS	Components*	Symbol	Size	Description
1	117-0	(117) – (404)		19 x 5/8" 18BWG	P-S HX tube bundle (active HS)
2	404-0	404		5" Sch. 80	P-S HX shell insulation
3	405-0	405, 406, 407, 408, 409		2 1/2" sch. STD	From P-S shell to ECO shell insulation
4	410-0	410 442, 444		6" Sch. 160	ECO HX shell insulation ECO inlet & outlet plena insulation
5	411-0	411, 412, 413, 414, 416, 418		2 1/2" sch. STD	From ECO shell to S-T shell insulation
6	419-0	419, 421 304		6" Sch. 160	S-T HX inlet & outlet plena insulation S-T HX shell insulation (tertiary side)
10	420-0	(420) – (304)		19 x 5/8" 18BWG	S-T HX tube bundle (active HS)
11	422-0	422, 428, 429, 431, 433, 434, 435, 436, 437, 439, 441 430		2 1/2" Sch. STD	From S-T shell to ECO tube insulation Filter insulation
12	423-0	423, 425, 427		1 1/4" Sch. STD	S-T HX by-pass insulation
13	433-1	(433) – (417)		37 x 1/2" 18BWG	ECO HX tube side (active HS)
14	445-0	445, 453, 454, 458, 459, 403		2 1/2" Sch. STD	From ECO tube to P-S shell insulation
15	446-0	446, 447, 455, 457		2 1/2" Sch. STD	ECO HX total bypass
16	448-0	448, 450, 452		1" Sch. STD	ECO HX regulation bypass
17	465-0	465, 467		1" Sch. STD	Surge Line insulation
18	470-0 470-1 470-2	470		14" Sch. 80	Body pressurizer insulation Bottom head pressurizer insulation Upper head pressurizer insulation
19	470-5	470		3 x OD=16mm	Pressurizer heating bars (active HS)
20	476-0 477-0	476 477, 478, 480, 481		1" Sch. STD 1 1/2" Sch. STD	Spray line insulation

* Indicated as 'ccc' or 'ccc, CCC, …' if passive HS (insulation).
Indicated as '(ccc, xxx) – (CCC, XXX)' if active HS (ccc and xxx left boundary, CCC and XXX right boundary)
In the components, 1xx refers to STEAM-WL primary loop, 2xx refers to STEAM secondary loop, 3xx refers to WL tertiary loop and 4xx refers to WL secondary loop

Fig. 151. Water Loop secondary side heat structures

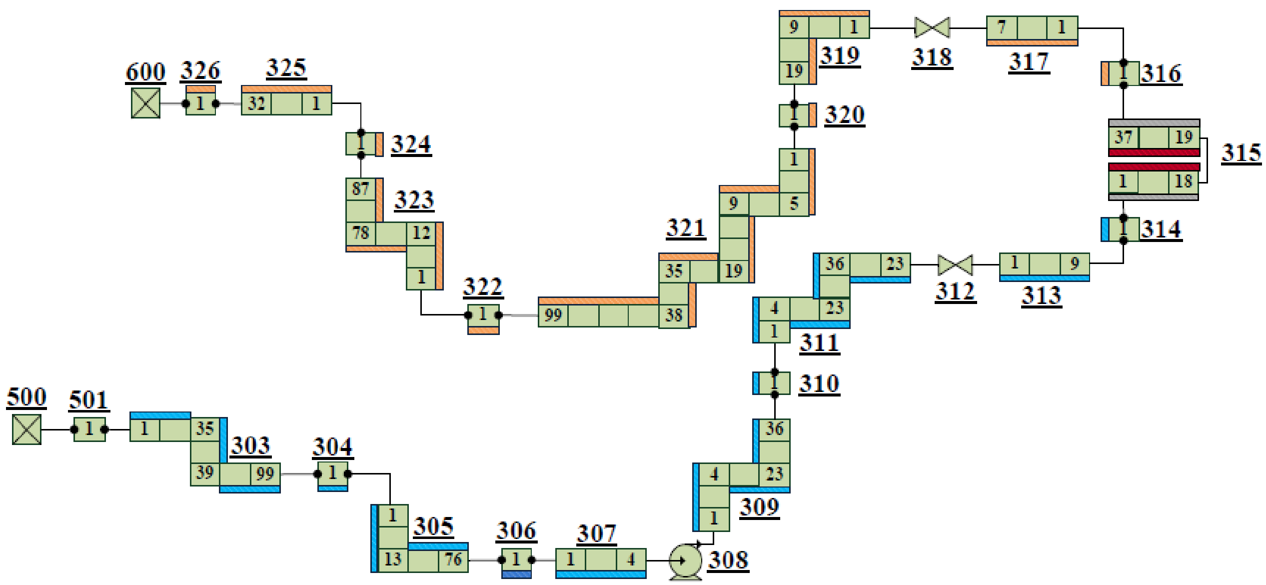

Fig. 152. Water Loop tertiary side RELAP5/Mod3.3 nodalization

#	HS	Components*	Symbol	Size	Description
1	303-1 304-0 309-0	303 304, 305, 307 309, 310, 311, 313, 314		4" Sch STD	Cold Leg insulation pt.1 Cold Leg insulation pt.2 Cold Leg insulation pt.3
2	306-0	306		4" Sch STD	Filter insulatiom
3	420-0	(420) – (304)		19 x 5/8" 18BWG	S-T HX tube bundle (active HS)
4	315-0	315		5" Sch. 80	S-T HX tube bundle insulation
5	316-0 323-0	316, 317, 319, 320, 321 323, 324, 325		4" Sch STD	Hot Leg insulation pt 1 Hot Leg insulation pt 2

* Indicated as 'ccc' or 'ccc, CCC, …' if passive HS (insulation).
Indicated as '(ccc, xxx) – (CCC, XXX)' if active HS (ccc and xxx left boundary, CCC and XXX right boundary)
In the components, 3xx refers to WL tertiary loop and 4xx refers to WL secondary loop

Fig. 153. Water Loop tertiary side heat structures

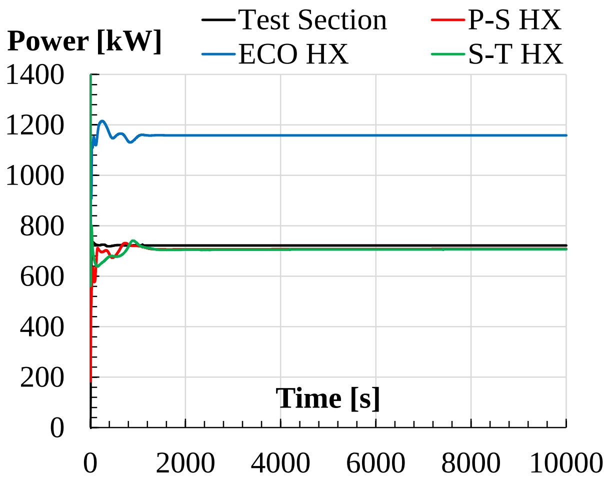

Fig. 154. TBM powers evolution with time

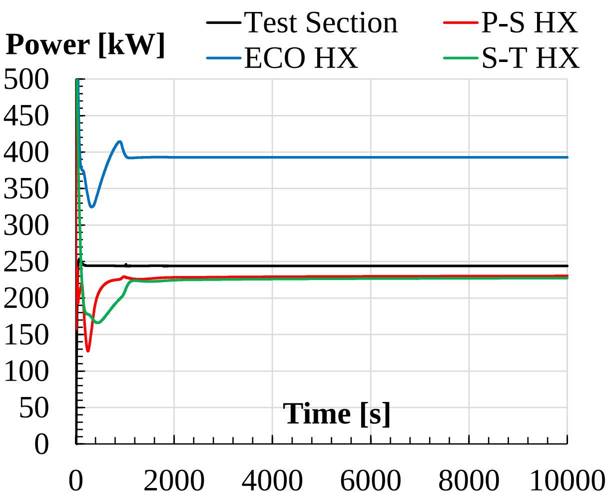

Fig. 155. Eq. FW powers evolution with time

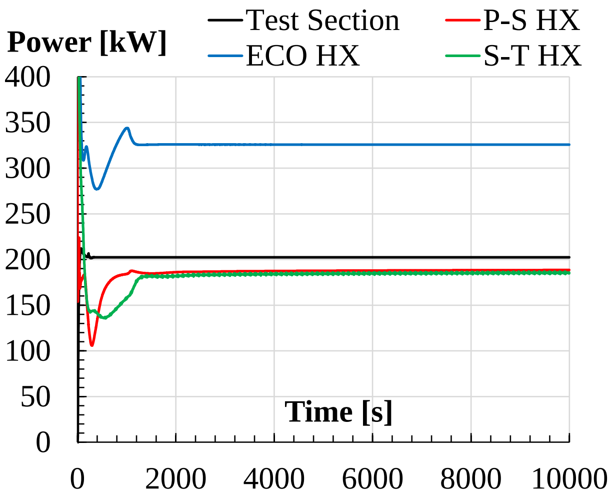

Fig. 156. Non-Eq. FW powers evolution with time

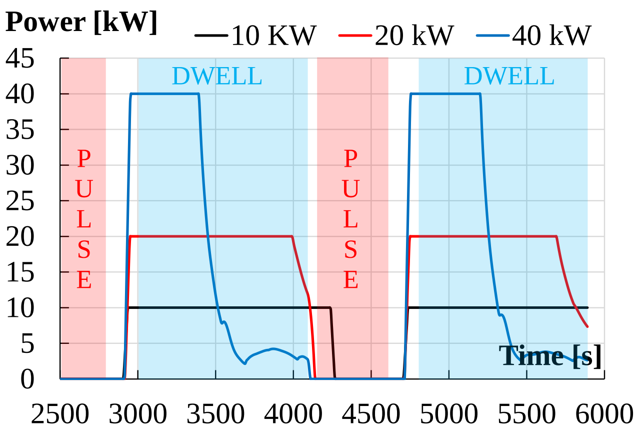

Fig. 157. PRZ heater power evolution in pulsed operation at different PRZ heater maximum powers.

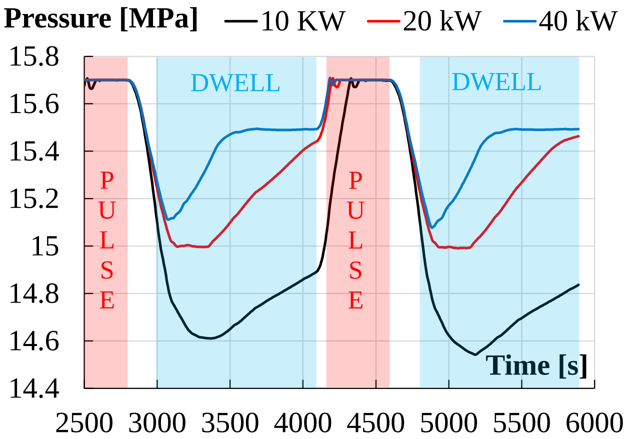

Fig. 158. Pressurizer pressure evolution in pulsed evolution at different PRZ heater maximum powers.

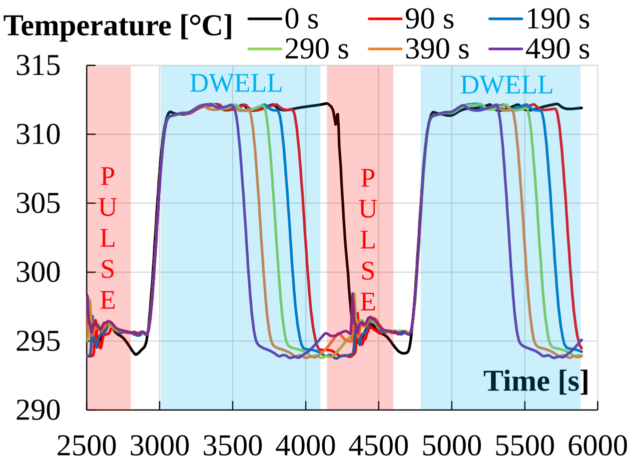

Fig. 159. TS inlet temperature evolution in pulsed operation. Legend refers to the time before pulse (b.p) in correspondence to which the heater set point is switched from 311.5 °C to 295 °C.

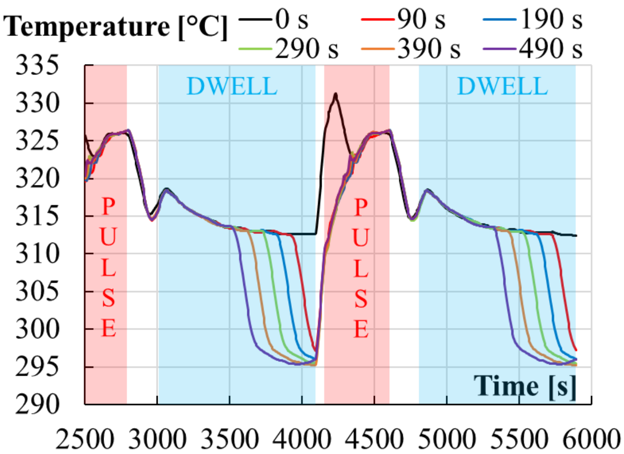

Fig. 160. TS outlet temperature evolution in pulsed operation. Legend refers to the time before pulse (b.p.) in correspondence to which the heater set point is switched from 311.5 °C to 295 °C.

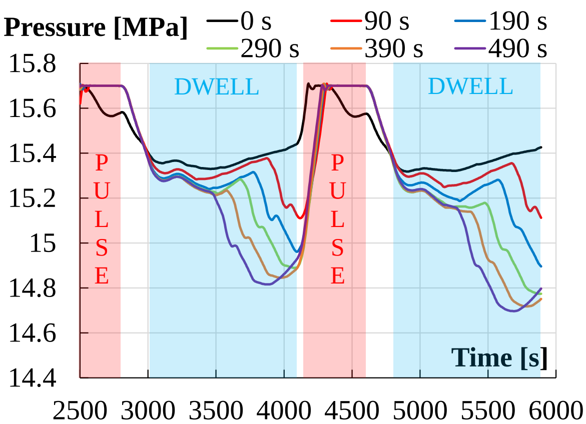

Fig. 161. Pressurizer pressure evolution in pulsed operation. Legend refers to the time before pulse in correspondence to which the heater set point is switched from 311.5 °C to 295 °C.

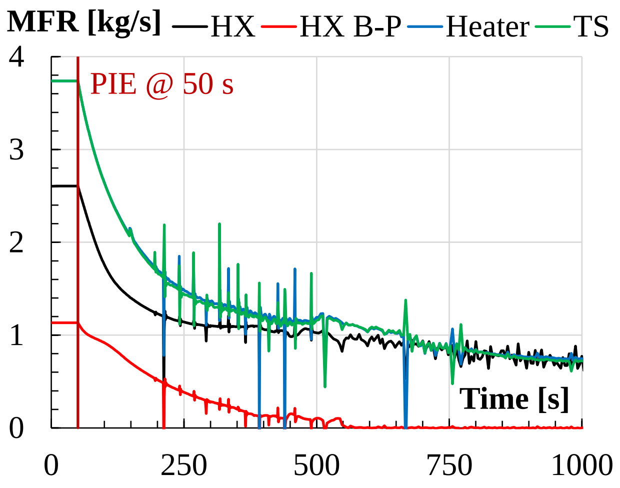

Fig. 162. Short-time PS MFR during a LOFA

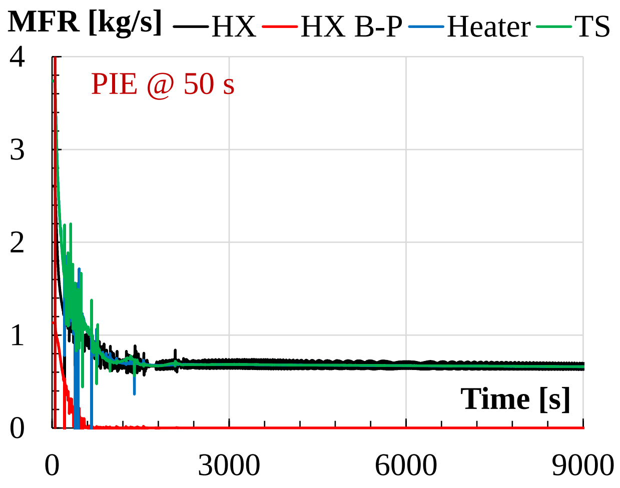

Fig. 163. Long-time PS MFR during a LOFA

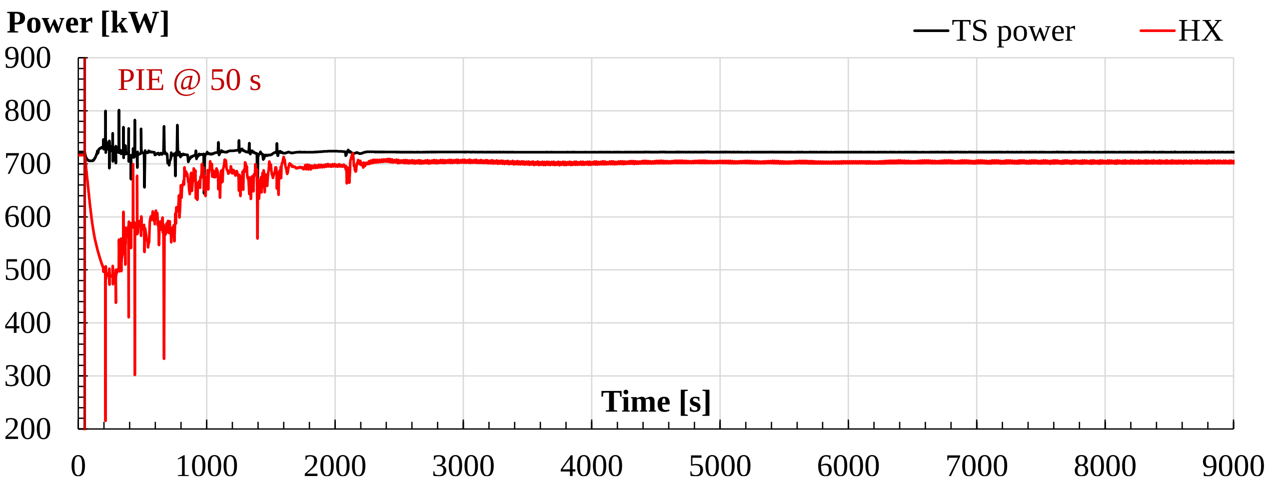

Fig. 164. TS and HX power during a LOFA

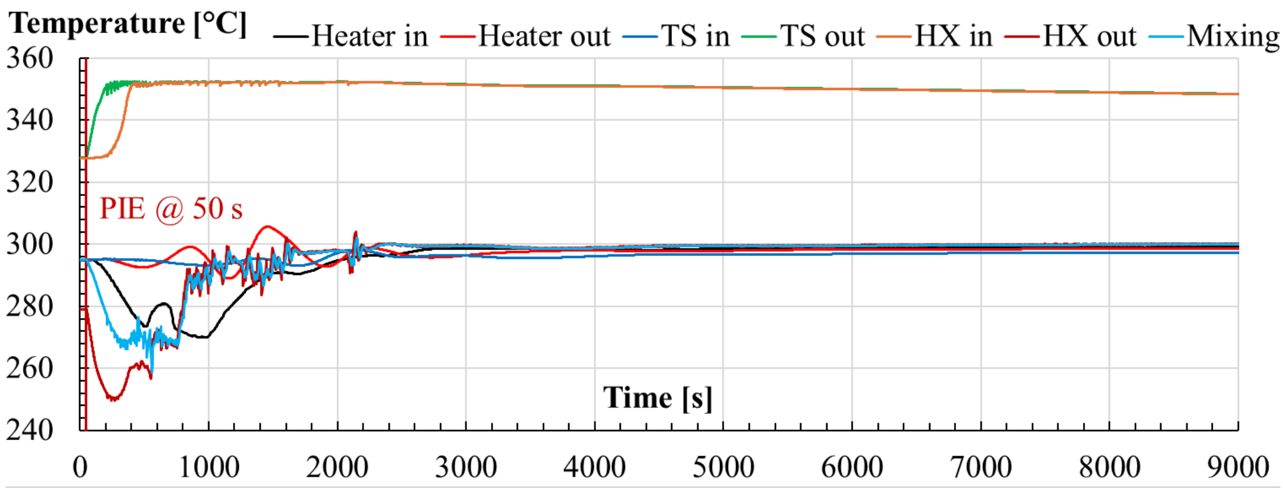

Fig. 165. Primary side temperatures during a LOFA

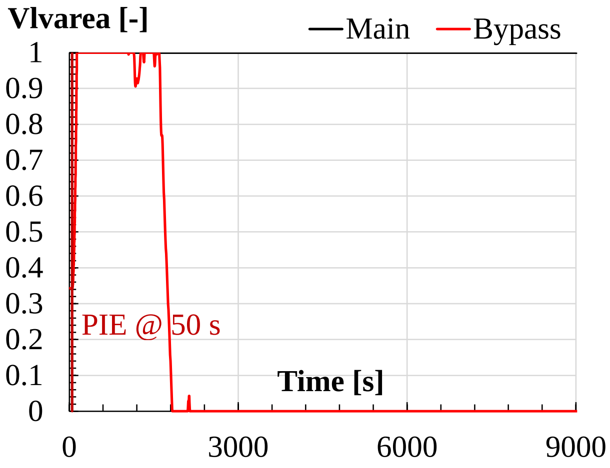

Fig. 166. P-S HX main and bypass line during a LOFA

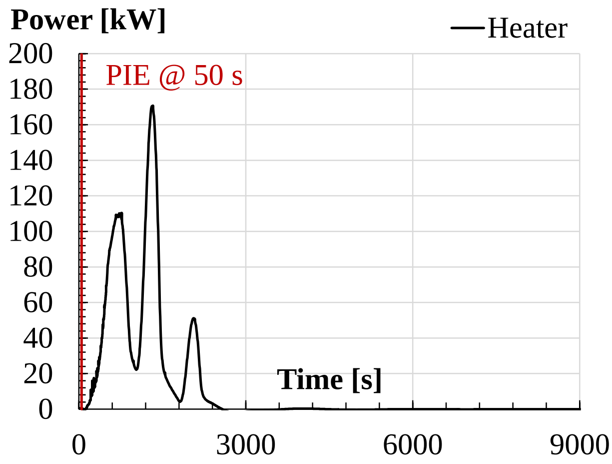

Fig. 167. Electric heater power during a LOFA

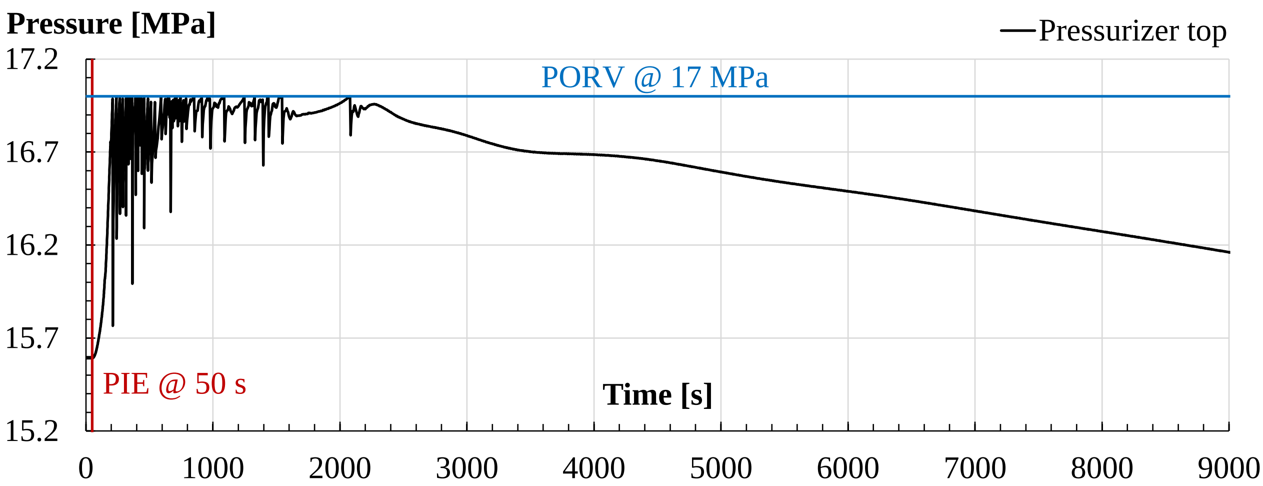

Fig. 168. Pressurizer pressure during a LOFA

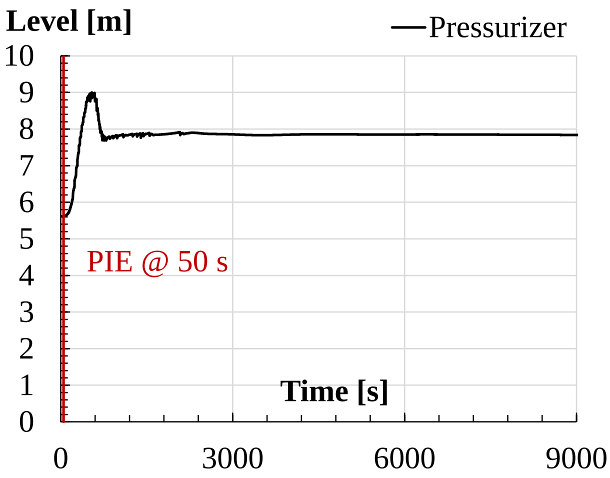

Fig. 169. Pressurizer level during a LOFA

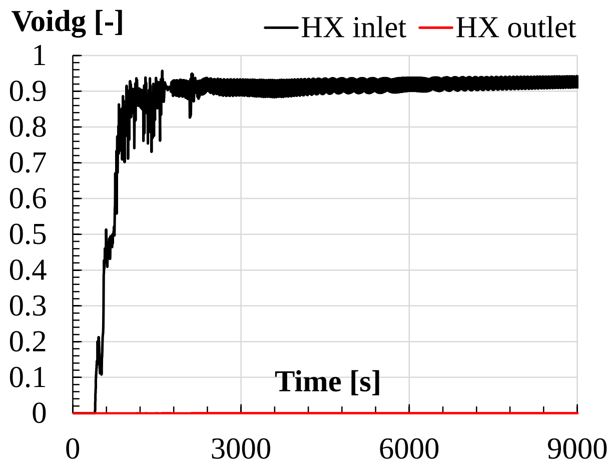

Fig. 170 P-S HX inlet and outlet void fraction during a LOFA

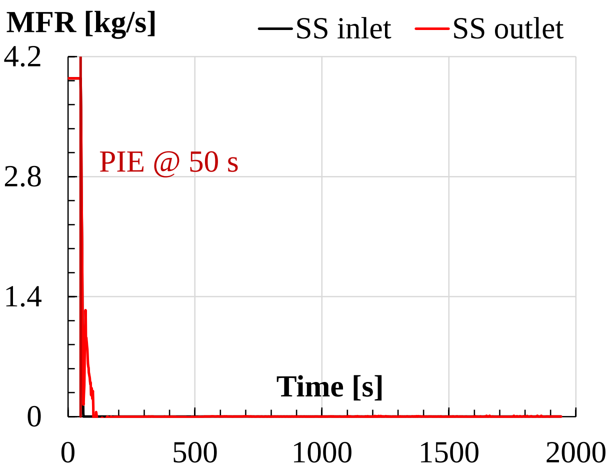

Fig. 171. Secondary side mass flow rate during a LOHS

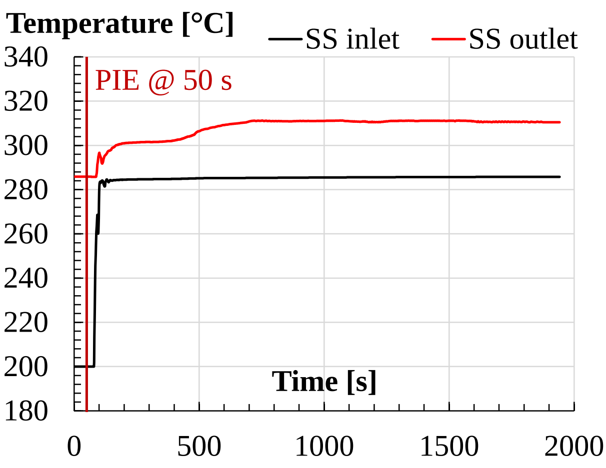

Fig. 172. P-S HX inlet and outlet temperature on the secondary side during a LOHS

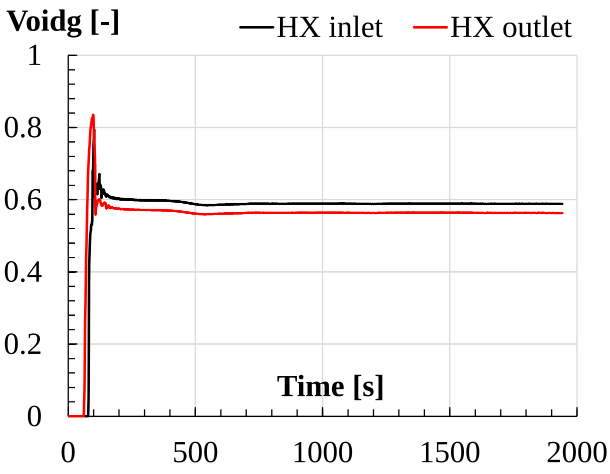

Fig. 173. P-S HX inlet and outlet void fraction during a LOHS

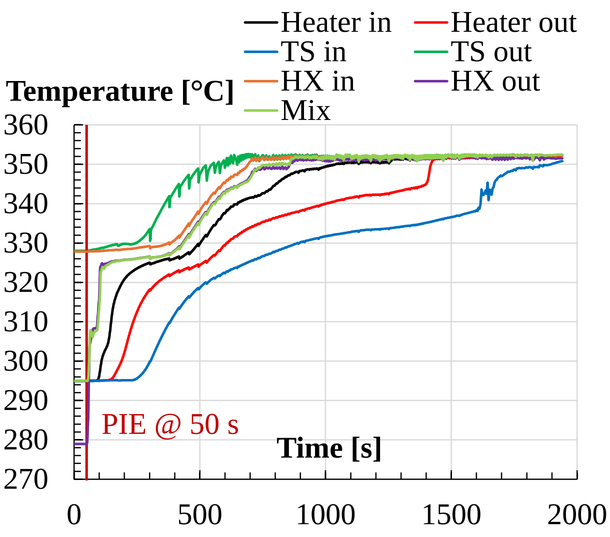

Fig. 174. PS temperatures during a LOHS

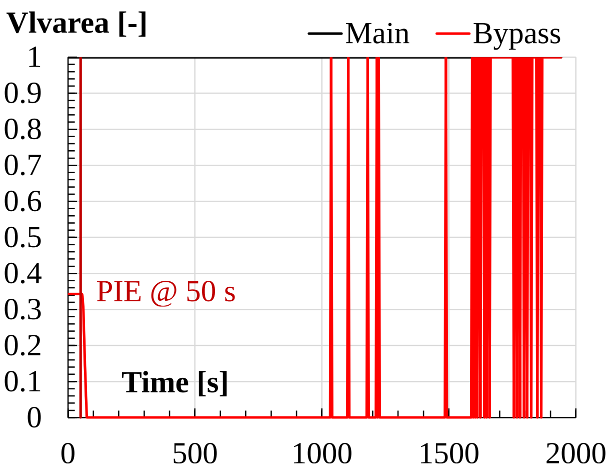

Fig. 175. P-S HX regulation valves area during a LOHS

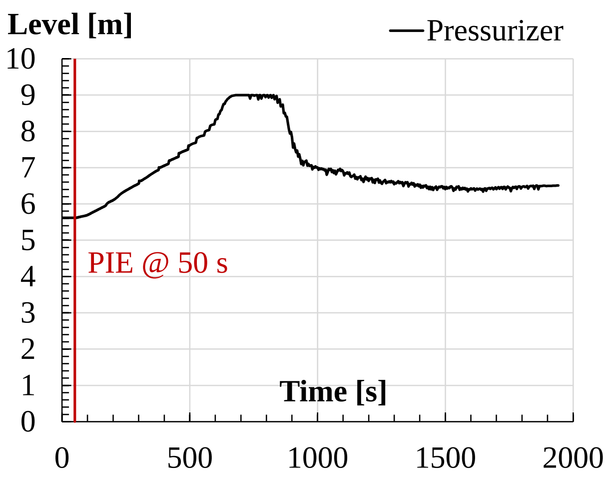

Fig. 176. Pressurizer level during a LOHS

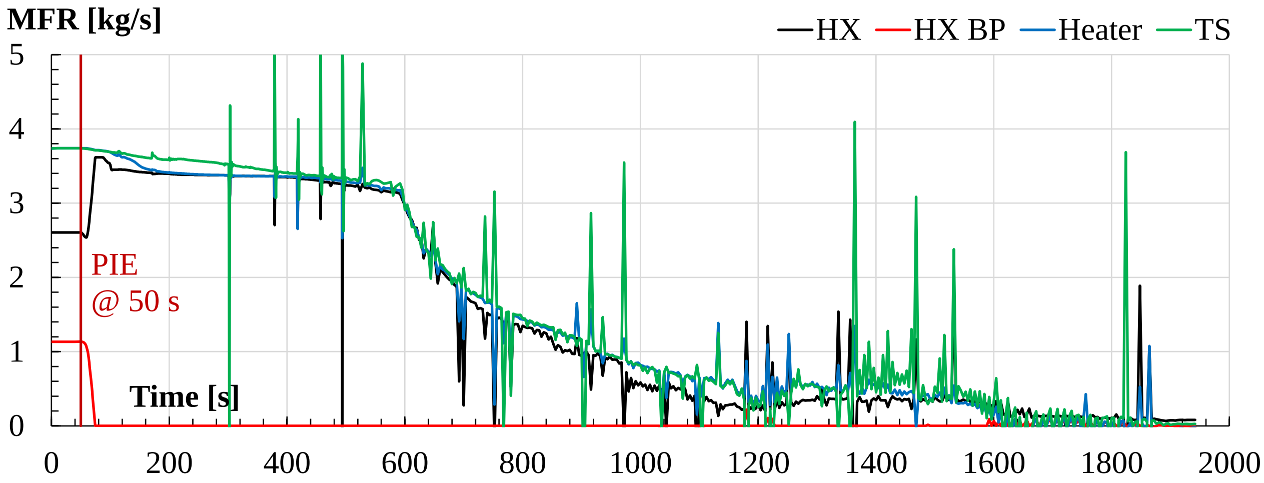

Fig. 177. PS mass flow rates during a LOHS

7 CONCLUSIONS

Under the EUROfusion Consortium, which coordinates and funds R&D within a roadmap toward commercial nuclear fusion power plants, the path to achieving fusion energy entails the construction and operation of ITER and DEMO, the technological and economic demonstrators, respectively. The tokamak configuration, selected as the reference machine type, utilizes magnetic fields to confine the plasma. A distinctive aspect of tokamak operation is its pulsed mode, resulting from the inability of the central solenoid to indefinitely sustain the variable current needed to generate the toroidal magnetic field. This pulsed nature requires all systems to withstand variable loads and operate in response to these fluctuations. Thermal-hydraulic design plays a crucial role, demanding heat removal systems with components capable of managing such conditions.

In this framework, the ENEA Division of Experimental Engineering (Nuclear Department) and the Department of Astronautical, Electrical and Energy Engineering of Sapienza University of Rome are conducting joint thermal-hydraulic analyses to support the ITER and DEMO development efforts. The work primarily focuses on designing the WCLL BB concept and its associated Bop. Pulsed operation in fusion reactors introduces new and complex challenges for components and systems, impacting design, reliability, and safety, particularly for critical elements like the First Wall and the Steam Generator. To facilitate rapid power transitions dictated by the pulsed plasma generated power, the OTSG has been selected because of its lower thermal inertia with respect to other commercial solutions available in the nuclear field (e.g., U-tube SGs).

The main objective of this thesis is the thermal-hydraulic design of the DEMO steam generator mock-up, of the STEAM experimental facility that allows for the testing of the component and will address the specific challenges related to its operation. STEAM is part of the larger W-HYDRA experimental platform, which includes the Water Loop facility for testing DEMO BB components and ITER TBM. Together, these facilities provide a versatile infrastructure for exploring thermal-hydraulic behaviors under various operating conditions, contributing both to the fusion research field and to experimental engineering advancements. Since these facilities share the primary circuit, Water Loop design and analysis in steady state and transient scenarios were objectives of the thesis as well.

Although STEAM and the Water Loop share the primary loop, their purposes are fundamentally different. STEAM focuses on a component-level investigation, specifically characterizing the performance and reliability of the steam generator mock-up under various operational and accidental scenarios. The facility itself does not represent the DEMO plant in its entirety but aims to replicate its thermodynamic boundary conditions in correspondence of the test section. To ensure these boundary conditions are accurately reproduced, proportional-integral control systems were implemented. In contrast, the Water Loop facility is designed for system-level analyses, where the thermal-hydraulic response of the entire system is as critical as that of the test section.

The main objective (i.e., the design and thermal-hydraulic characterization of the DEMO steam generator mock-up) was achieved following the power-to-volume scaling method from the DEMO WCLL BB SG keeping the full-length of the tubes. The sizing procedure was guided by a balance between incorporating a complete set of tube rows and achieving a relatively contained power output (i.e., below 4 MW). The final design resulted in a component with 37 tubes and a power of 3.1 MW. Given the reduced radial size of the unit, the adoption of an external downcomer was preferred to avoid tolerance issues during construction of an annular component. The consequent distortions in the thermal-hydraulic behavior of the fluid were assessed, showing good representativeness of the mock-up. Optimization analyses further led to the adoption of a hexagonally shaped riser to reduce bypass effects.

The following step was the conceptual design of the STEAM facility, aimed at hosting the SG mock-up, to ensure that it could replicate the thermal-hydraulic conditions expected for the DEMO WCLL BB SG, while providing a heat dissipation system as the final heat sink. A particular focus was placed on designing and optimizing systems and components (e.g., air coolers and the low-pressure section of the secondary loop) with detailed numerical analyses carried out to assess their performance across various operating scenarios. RELAP5/Mod3.3 analyses supported the design, analysis and optimization phase. Steady state conditions were simulated, and pre-test analyses were performed to support the design of the experimental campaign. The pre-test analyses confirmed the ability of the OTSG to effectively follow the rapid power oscillations characteristic of pulsed operation, without exhibiting any critical deviations or instabilities in its thermal-hydraulic parameters. These findings not only validated the robustness of the OTSG design but also highlighted its suitability for integration into fusion reactor systems, demonstrating its capability to sustain dynamic operational conditions with reliability.

Furthermore, facility dynamics were evaluated under accidental scenarios, such as pump failures, including both Loss of Flow Accident (LOFA) and Loss of Heat Sink (LOHS) conditions, to verify the system response and resilience in handling potential operational anomalies. These analyses supported the design of STEAM and verified its functionality, but they do not directly contribute to DEMO reactor safety, since STEAM primary purpose is to demonstrate the viability of the steam generator and characterize its behavior under pulsed operation.

The design of the Water Loop facility faced not only the challenges associated with pulsed operation, but also the complexity of enabling the testing of various mock-ups and components with diverse power and flow requirements. Being tasked with ensuring heat removal across a broad range of thermal-hydraulic conditions, its design necessitated thorough optimization analyses to define alternative layouts that could accommodate the varying demands of different test scenarios. This approach allowed for enhancing its versatility and effectiveness in conducting a wide range of experiments. The RELAP5/Mod3.3 code was adopted for supporting the design phase and to conduct steady-state and transient analyses at different power levels. Analyses in accidental conditions were performed too, not only to support the facility design and pre-test phase, but also to contribute to safety aspects of ITER design by investigating the integrated behavior of components under various scenarios.

Through the design of the STEAM and Water Loop facilities within the W-HYDRA platform, this research has contributed to the development of a pioneering experimental infrastructure for testing and validating SG and plasma facing components performance under pulsed operation conditions. It allows for comprehensive investigations into the thermal-hydraulic dynamics of components that have not previously been engineered for such variable regimes, providing an experimental pathway to the demonstration of their feasibility. By facilitating a range of testing scenarios, including the simulation of transient accidents, the facilities significantly contribute to the international landscape of fusion research. The outcomes of this PhD activity represent a major milestone in advancing the technologies relevant to ITER TBM and DEMO BB, laying the groundwork for future developments in fusion energy systems. The platform designed in this work will generate valuable experimental data that will enrich the literature on SG and plasma facing components performance under pulsed operation conditions.

Future activities include the realization of the designed experimental campaigns and the related post-test analysis. Therefore, the RELAP5/Mod3.3 models and correlations adopted for the design and pre-test analyses will be validated also for the pulsed operation. At this point, the RELAP5/Mod3.3 code could be used to conduct design and safety analysis for the full-scale systems.

LIST OF REFERENCES

[1] International Energy Agency (IEA), **Global Energy & CO2 Status Report**, 2021, https://www.iea.org/reports/global-energy-co2-status-report-2019

[2] IPCC, **Climate Change 2021: The Physical Science Basis. Contribution of Working Group I to the Sixth Assessment Report of the Intergovernmental Panel on Climate Change,** 2021, https://www.ipcc.ch/report/ar6/wg1/

[3] International Atomic Energy Agency (IAEA), **Nuclear Power Reactors in the World**" 2020, https://www-pub.iaea.org/MTCD/Publications/PDF/RDS-2-40_web.pdf

[4] J. P. Freidberg, **Plasma Physics and Fusion Energy**, Cambridge University Press, 2007, https://doi.org/10.1017/CBO9780511755705

[5] A. H. Boozer, **Physics of magnetically confined plasmas** Reviews of Modern Physics, vol. 76, no. 4, pp. 1071-1141, 2004.

[6] F. Romanelli, et al., **Fusion Electricity – A Roadmap to the Realization of Fusion Energy**, EFDA Report, ISBN 978-3-00-040720-8T, 2012.

[7] https://web.uniroma1.it/diaee/

[8] https://euro-fusion.org/

[9] INTERNATIONAL ATOMIC ENERGY AGENCY, Fusion Physics, Non-serial Publications , IAEA, Vienna (2012)

[10] Wesson, J. (2004). **Tokamaks** (3rd ed.). Oxford University Press.

[11] Chen, F. F., **Introduction to Plasma Physics and Controlled Fusion**, Springer, 2016.

[12] Harms, A. A., et al., **Principles Of Fusion Energy: An Introduction To Fusion Energy For Students Of Science And Engineering**, World Scientific Publishing Company, 2000.

[13] Pearson, R. J., **Tritium supply and use: a key issue for the development of nuclear fusion energy**, Fusion Engineering and Design, 136 Part B, pages 1140-1148, 2018, https://doi.org/10.1016/j.fusengdes.2018.04.090

[14] INTERNATIONAL ATOMIC ENERGY AGENCY, Plasma Physics and Technology Aspects of the Deuterium–Tritium Fuel Cycle for Fusion Energy, IAEA-TECDOC-2049, IAEA, Vienna (2024)

[15] Tosti, S., Ghirelli, N., **Tritium in fusion: production, uses and environmental impact**, Environmental Science, Physics, Engineering, 2013, https://api.semanticscholar.org/CorpusID:127843689

[16] Atzeni, S., Meyer-ter-Vehn, J., **The physics of inertial fusion - Hydrodynamics, dense plasma physics, beam-plasma interaction**, Physics, 2004, https://10.1093/ACPROF:OSO/9780198562641.001.0001

[17] Chen, F. F., **Introduction to Plasma Physics and Controlled Fusion**, Springer, 2013.

[18] INTERNATIONAL ATOMIC ENERGY AGENCY, Fundamentals of Magnetic Fusion Technology, Non-serial Publications , IAEA, Vienna (2023)

[19] Helander, P. (2014). Theory of Plasma Confinement in Non-Axisymmetric Magnetic Fields. Reports on Progress in Physics, 77(8), 087001, https://10.1088/0034-4885/77/8/087001

[20] De Tommasi, G., **Plasma Magnetic Control in Tokamak Devices**. J Fusion Energy 38, 406–436, 2019. https://doi.org/10.1007/s10894-018-0162-5

[21] Federici, G., et al., **An overview of the EU breeding blanket design strategy as an integral part of the DEMO design effor**t, Fusion Engineering and Design, 141, 2019, https://doi.org/10.1016/j.fusengdes.2019.01.141

[22] Hatler, C., **The path towards plasma facing components: A review of state-of-the-art in W-based refractory high-entropy alloys**, Current Opinion in Solid State and Materials Science, 34, 2025, https://doi.org/10.1016/j.cossms.2024.101201

[23] D'Andrea, D., **Cryogenics in Fusion: Industrial Approach of Cryogenics Applied to Fusion Plants**, J Fusion Energ 38, 499–502 (2019). https://doi.org/10.1007/s10894-018-0196-8

[24] INTERNATIONAL ATOMIC ENERGY AGENCY, Experiences for Consideration in Fusion Power Plant Design Safety and Safety Assessment, IAEA-TECDOC-2076, IAEA, Vienna (2024), https://doi.org/10.61092/iaea.yx3s-dsv2

[25] L. Barucca et al., **Status of EU DEMO heat transport and power conversion systems**, Fusion Eng. Des., 136 (2018), pp. 1557-1566, https://doi.org/10.1016/j.fusengdes.2018.05.057.

[26] Muratov, V.P.; et al., **ITER – International Thermonuclear Experimental Reactor, Fundamentals of Magnetic Thermonuclear Reactor Design**, Woodhead Publishing Series in Energy, 2018, Pages 39-67, https://doi.org/10.1016/B978-0-08-102470-6.00003-2

[27] Ciurluini, C.; Narcisi, V.; Tincani, A.; Ferrer, C.O.; Giannetti, F., **Conceptual design overview of the ITER WCLL Water Cooling System and supporting thermal-hydraulic analysis**, Fusion Eng. Des. 2021, 171, 112598. https://doi.org/10.1016/j.fusengdes.2021.112598

[28] L. V. Boccaccini et al., **Status of maturation of critical technologies and systems design: Breeding blanket**, Fusion Eng. Des., 179 (2022) 113116.

[29] F. Cismondi, et al., **Progress of the conceptual design of the European DEMO breeding blanket, tritium extraction and coolant purification systems**, Fusion Eng. Des., 157 (2020), Article 111640, 10.1016/j.fusengdes.2020.111640

[30] T. Giegerich, et al., **Development of a viable route for lithium-6 supply of DEMO and future fusion power plants**, Fusion Engineering and Design, 149, 111339, https://doi.org/10.1016/j.fusengdes.2019.111339

[31] T. Ihli, et al**., Review of blanket designs for advanced fusion reactors**, Fusion Engineering and Design, 83, Pages 912-919, 2008, https://doi.org/10.1016/j.fusengdes.2008.07.039

[32] A.R. Raffray, M. Akiba, V. Chuyanov, L. Giancarli, S. Malang**, Breeding blanket concepts for fusion and material requirements**, Journal of Nuclear Materials, Volume 307-311/21-30, (2002)

[33] L. Giancarli, M. Ferrari, M.A. Futterer, S. Malang, **Candidate blanket concepts for a European fusion power plant study**, Fusion Engineering and Design, Volume 49- 50/445-456, (2000)

[34] A. Del Nevo, et al., **WCLL breeding blanket design and integration for DEMO 2015: status and perspectives**, Fusion Engineering and Design, Volume 124, pages 682-686, (2017), https://doi.org/10.1016/j.fusengdes.2017.03.020

[35] A. Del Nevo, et al., **WCLL BB design and Integration studies 2020 activities**, IDM Ref. EFDA_D_2NTP7J, Dec. 2020.

[36] C. Gliss, June-2017 **DEMO Reference Configuration model**, IDM Ref. EFDA_D_2MUNPL, July 2017.

[37] Barucca, L.; et al., **Pre-conceptual design of EU DEMO balance of plant systems: objectives and challenges**, Fusion Engineering and Design 169 (2021) 112504.

[38] R. Mozzillo, et al., **Design of the European DEMO vacuum vessel inboard wall**, Fusion Eng. Des., 160 (2020), Article 111967, https://doi.org/10.1016/j.fusengdes.2020.111967

[39] F. M. Castrovinci et al., **Thermal-hydraulic study of the Primary Heat Transport System of the DEMO Divertor Cassette Body**, Fusion Engineering and Design, 192, 2023, https://doi.org/10.1016/j.fusengdes.2023.113733

[40] Tincani A., Ciurluini C., Del Nevo A., Giannetti F., Tarallo A., Tripodo C., Cammi A., Vannoni A., Eboli M., Del Moro T., Lorusso P., Barucca L., **Conceptual Design of the Steam Generators for the EU-DEMO WCLL Reactor**, Energies, 16 (6), 2601, 2023, https://doi.org/10.3390/en16062601

[41] C. Ciurluini, A. Vannoni et al., **Thermal-hydraulic assessment of Once-Through Steam Generators for EU-DEMO WCLLBreeding Blanket primary cooling system application**, Fusion Engineering and Design, 193, 113688, 2023, https://doi.org/10.1016/j.fusengdes.2023.113688.

[42] J.B. Kitto, S.C. Stultz, Steam, its Generation and Use, (41st ed.), **The Babcock & Wilcox Company**, Barberton, Ohio, U.S.A. (2005).

[43] L. Barucca et al**., Maturation of critical technologies for the DEMO balance of plant systems**. Fusion Eng. Des. 179 (2022) 113096, https://doi.org/10.1016/j.fusengdes.2022.113096.

[44] Information Systems Laboratories, **RELAP5/Mod3.3 code manual volume I: code structure, system models, and solution methods**, July 2003.

[45] Information Systems Laboratories, **RELAP5/Mod3.3 code manual volume II: user's guide and input requirements**, January 2003.

[46] Information Systems Laboratories, **RELAP5/Mod3.3 code manual volume II: appendix A input requirements**, June 2004.

[47] Information Systems Laboratories, **RELAP5/Mod3.3 code manual volume VII: summaries and reviews of independent code assessment reports**, December 2001.

[48] Information Systems Laboratories, **RELAP5/Mod3.3 code manual volume IV: models and correlations**, December 2001.

[49] The US Nuclear Regulatory Commission (USNRC), RELAP5/MOD3.3 code manual volume 2, appendix A: input requirements, NUREG/CR-5535; USNRC: Washington, DC, USA, 1995.

[50] F. P. Incropera et al., **Fundamentals of Heat and Mass Transfer**, 7th Ed., John Wiley & Sons Inc., Hoboken, New Jersey, USA, (2011)

[51] F. Giannetti, et al., BOP-2.2-T035-D002 WCLL BB PHTS Data Sheets (Direct Coupling Option with Small ESS), EUROfusion internal Deliverable, (2020) IDM Ref. EFDA_D_ 2NPBJW v1.2, April 2020.

[52] L. Barucca, WP-BoP meeting between CREATE and Ansaldo Nucleare to define a preliminary methodology for HCPB BB and WCLL BB PHTS piping thickness evaluation and material selection, EUROfusion Internal Deliverable, IDM Ref. EFDA_D_2NAU6V v1.1, 30 May 2018.

[53] **The American Society of Mechanical Engineers (ASME), Boiler and Pressure Vessel Code**, Section II, Part D, Properties (Metric), 2015 Edition, New York, New York, USA.

[54] J. G. Ziegler and N. B. Nichols, **Optimum settings for automatic controllers**, Transaction of the American. Society of Mechanical Engineers (ASME), vol. 64, pp. 759-768, November 1942.

[55] J. G. Ziegler and N.B. Nichols, **Process lags in automatic control circuits**, Transaction of the American. Society of Mechanical Engineers (ASME), vol. 65, pp. 433-444, July 1943.

[56] P. Arena, A. Del Nevo, M. Eboli, B. Gonfiotti. P. Maccari, R. Marinari, A. Tincani, N. Badodi, G. Biongiovì, I. Catanzaro, F. Galleni, C. Risi, L.L. Sanasi, A. Tarallo and A. Vannoni, **W-HYDRA: a new experimental platform for the Water-Cooler Lead Lithium Breeding Blanket**, Nuclear Fusion, https://doi.org/10.1088/1741-4326/ad50r9

[57] P. Lorusso, A. Del Nevo, P. Arena, M. Eboli, R. Marinari, A. Tincani, P. Agostini, N. Badodi, A: Cammi, T. Del Moro, A. Vannoni, C. Ciurluini, F. Giannetti, L. Barucca, **STEAM: A novel experimental infrastructure for the development of the DEMO BoP water coolant technology**, 19th International Topical Meeting on Nuclear Reactor Thermal Hydraulics (NURETH-19), Brussels, Belgium, March 6-11, 2022.

[58] A. Vannoni et al., **STEAM Experimental Facility: A Step Forward for the Development of the EU DEMP BoP Water Coolant Technology**, Energies 2023, 16 (23), 7811 https://doi.org/10.3390/en16237811

[59] I. Moscato, et al., **Tokamak cooling systems and power conversion system options**, Fusion Engineering and Design 178 (2022) 113093.

[60] https://www.oecd-nea.org/jcms/pl_19744

[61] A. Vannoni, **Development of a Steam Generator Mock-Up for EU DEMO Fusion Reactor: Conceptual Design and Code Assessment**, Energies, 16 (9), 3729. https://doi.org/10.3390/en16093729

[62] D. Caterino, A. Del Nevo, M. Eboli, A. Froio, R. Marinari, A. Vannoni, A. Zappatore, **Thermal-hydraulic assessment of the Steam Generator mock-up for the EU DEMO WCLL using CFD co-simulation**, Fusion Engineering and Design (201), April 2024, https://doi.org/10.1016/j.fusengdes.2024.114237

[63] Vannoni A., Lorusso P., Arena P., Eboli M., Marinari R., Tincani A., Ciurluini C., Giannetti F., Badodi N., Tripodo C., Cammi A., Barucca L., Tarallo A., Agostini P., Del Nevo A., **STEAM Experimental Facility: A Step Forward for the Development of the EU DEMO BoP Water Coolant Technology**, Energies 2023, 16 (23), 7811 https://doi.org/10.3390/en16237811

[64] A. Vannoni et al., **RELAP5-based thermal-hydraulic assessment of the STEAM facility for DEMO WCLL balance of plant analysis**, Fusion Engineering and Design (202), May 2024, https://doi.org/10.1016/j.fusengdes.2024.114397

[65] A. Vannoni et al., **Status, design and thermal-hydraulic analyses of the STEAM facility for DEMO WCLL Balance of Plant system**, 30th International Conference on Nuclear Engineering (ICONE-30), Kyoto, Japan, May 21-26, 2023.

[66] Vannoni A., Eboli M., Lorusso P., Ciurluini C., Giannetti F., TIncani A., Del Nevo A., **Pre-test analysis of low power operations of STEAM, the EU-DEMO steam generator mock-up facility**, Fusion Engineering and Design (201), April 2024, https://doi.org/10.1016/j.fusengdes.2024.114239

[67] A. Vannoni, M. Eboli, P. Lorusso, C. Ciurluini, F. Giannetti, A. Tincani, A. Del Nevo, **RELAP5/Mod3.3 thermal-hydraulics characterization of the steam generator mock-up during operational transients in STEAM facility in support of the design of the DEMO WCLL BoP**, Fusion Engineering and Design 200, march 2024, https://doi.org/10.1016/j.fusengdes.2024.114165

[68] D. Papini, A: Cammi, **Modelling of Heat Transfer Phenomena for Vertical and Horizontal Configurations of In-Pool Condenser and Comparison with Experimental Findings, Science and Technology of Nuclear Installation**, Volume 2010, https://doi.org/10.1155/2010/815751

[69] Palermo, E. Fable, **Reference Ramp-Up and Ramp-Down trajectories for EU-DEMO and database of plasma perturbations**, EC H2020 EUROfusion Project, WPPMI-5.2.1-T052, IDM Ref. 2NJ85C v1.0, 06 Jul 2020.

[70] F. Palermo, E. Fable, **Ramp-Up and Ramp-Down investigation**, EC H2020 EUROfusion Project, WPPMI-5.2.1-T046, IDM Ref. 2NB66G v1.0, 11 Feb 2020.

[71] Vannoni, A.; et al., **The Design of Water Loop Facility for Supporting the WCLL Breeding Blanket Technology and Safety**, Energies 2023, 16, 7746, https://doi.org/10.3390/en16237746